Heteroatom Containing Polycyclic Aromatic Hydrocarbons with Positive Charge - Synthesis and Characterization

Dissertation

zur Erlangung des Grades
"Doktor der Naturwissenschaften"

dem Fachbereich Chemie und Pharmazie der
Johannes Gutenberg-Universität Mainz
vorgelegt von

Dongqing Wu
geboren in Henan Province / P. R. China

Mainz, 2008

Decan: Herr Prof. Dr.

1. Berichterstatter: Herr Prof. Dr.

2. Berichterstatter: Herr Prof. Dr.

Tag der mündlichen Prüfung:

Die vorliegende Arbeit wurde in der Zeit von August 2004 bis Mai 2008 im Max-Planck-Institut für Polymerforschung in Mainz unter Anleitung von Herrn Prof. Dr. Müllen ausgeführt.

Ich danke Herrn Prof. Dr. K. Müllen für seine wissenschaftliche und persönliche Unterstützung sowie für sein ständige Diskussionsbereitschaft.

Content

Index of Abbreviations

BNAX	benzo[5,6]naphthaceno[1,12,11,10-*jklmna*]xanthylium
BNATX	benzo[5,6]naphthaceno[1,12,11,10-*jklmna*]thioxanthylium
DBNT	dibenzo[*jk,mn*]naphtho[2,1,8-*fgh*]- thebenidinium
DBPQP	2-phenyl-naphthacene[1,2]quinolizino- [3,4,5,6-*def*]benzo[*i*]-phenanthridinium
DCM	dichloromethane
DSC	differential scanning calorimetry
EA	elemental analysis
ESR	electron spin resonance
FD MS	field desorption mass spectroscopy
FET	field effect transistor
g	gram
HBC	hexa-peri-hexabenzocoronene
HPAH	heteroatom containing polycyclic aromatic hydrocarbons
h	hour
ISA	Ionic self-assembly
LED	light emitting diode
MS	mass spectroscopy
min	minute
m.p.	melting point
MALDI-TOF	matrix-assisted laser desorption ionization –time of flight
NIR	near infrared
NMR	nuclear magnetic resonance
PE	petroleum ether
PAH	polycyclic aromatic hydrocarbons
PQP	2-phenyl-benzo[8,9]quinolizino[4,5,6,7-*fed*]phenanthridinylium
RT	room temperature
STM	scanning tunneling microscopy
TCNQ	7,7,8,8-tetracyanoquinodimethane
THF	tetrahydrofuran
TLC	thin layer chromatography
UV-vis	ultraviolet/visible

Chapter 1

Introduction

1.1 Aromaticty and aromatic compounds

Aromaticity is a chemical property in which a conjugated ring of unsaturated bonds, lone pairs, or empty orbitals exhibits a stabilization stronger than would be expected by the stabilization of conjugation alone. It can also be considered as a manifestation of cyclic delocalization and of resonance.[1-7]

The first known use of the word "aromatic" as a *chemical* term - namely, applied to compounds that contain the benzene groups – occurred in an article by A. W. Hofmann in 1855.[8] Nevertheless, it is curious that Hofmann said nothing about why he introduced an adjective indicating olfactory character to a group of chemical substances, only some of which have notable aromas.

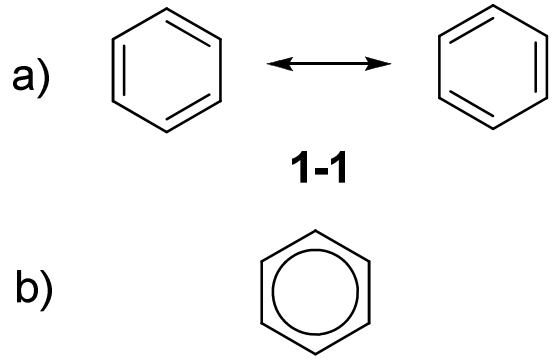

Figure 1-1. a) Kekulé and b) Robinson structures of benzene.

First discovered by M. Faraday in 1825[9], the simplest, yet the most important aromatic compound is benzene **1-1**. The structure of benzene remained for a long time a centre of dispute in the scientific community until its cyclohexatriene structure (Figure 1.1a) was first proposed by A. Kekulé in 1865. Over the next few decades,

most chemists readily accepted this structure, since it accounted for most of the known isomeric relationships of aromatic chemistry. However, it was always puzzling that the purportedly highly unsaturated molecule was so unreactive toward addition reactions. An explanation for the exceptional stability of benzene was conventionally attributed to Sir R. Robinson[10], who was the first to coin the term aromatic sextet as a group of six electrons that resists disruption (Figure 1.1b). In 1931 the quantum mechanical origins of this stability, or aromaticity, were first modelled by E. Hückel who was the first to separate the bonding electrons into σ and π electrons.[11]

An aromatic compound is an organic molecule which contains a set of covalently-bound atoms with specific characteristics:

a). A delocalized conjugated π-system, most commonly an arrangement of alternating single and double bonds;

b). Coplanar structure, with all the contributing atoms in the same plane;

c). Contributing atoms arranged in one or more rings;

d). The number of π delocalized electrons that is even, but not a multiple of 4. This is known as Hückel's rule. Permissible numbers of π electrons include 2, 6, 10, 14, and so on;

e). Special reactivity in organic reactions such as electrophilic aromatic substitution and nucleophilic aromatic substitution.

The key aromatic compounds of commercial interest are benzene, toluene, *ortho*-xylene and *para*-xylene. About 35 million tons of these compounds are produced worldwide every year. They are extracted from complex mixtures obtained by the refining of oil or by distillation of coal tar, and are used to produce a range of important chemicals and polymers, including styrene, phenol, aniline, polyester and nylon[12]. Aromatic compounds can usually be classified into three types:

a). Substituted benzenes:

Many chemical compounds contain simple benzene rings in their structure.

Examples include trinitrotoluene (TNT), acetylsalicylic acid (aspirin), 1,3-benzodioxole (methylenedioxybenzene) and paracetamol.

b). Heterocyclics:

In heterocyclic aromatics, one or more of the atoms in the aromatic ring is of an element other than carbon. This can alter the ring's aromaticity, and thus (as in the case of furan) change its reactivity. Other examples include pyridine, imidazole, pyrazole, oxazole, thiophene, and their benzannulated analogs.

c). Polycyclic aromatic hydrocarbons:

Polycyclic aromatic hydrocarbons (PAHs) are molecules containing two or more simple aromatic rings fused together by sharing two neighboring carbon atoms such as naphthalene, anthracene and phenanthrene.

1.2 Polycyclic aromatic hydrocarbon

Polycyclic aromatic hydrocarbons (PAHs), which were first discovered in coal tar in the 19th century, have become one of the most widely investigated compounds in medical sciences, biology, organic chemistry, physics and material sciences in recent years.[1, 5, 6, 13-15]

PAHs are the first chemical carcinogens to be discovered. In 1775, the English surgeon P. Pott found an association between exposure to soot and a high incidence of scrotal cancers in chimney sweepers. The famous description of chemically induced carcinogenesis found the experimental counterpart in the coal tar tumors induced in rabbits by Yamagiwa and Ichikawa in 1915. Later research indicated that it was PAHs in the residue of combustion such as soot and coal tar which caused skin cancers of human and animals. PAHs were regarded as the main carcinogens before 1950s. Nowadays, PAHs are still one of the most important classes of carcinogens due to their abundance in the environment.[16, 17]

PAHs are also found in the interstellar medium, comets and meteorites. A team led by A. Witt of the University of Toledo, Ohio studied ultraviolet light emitted by

the Red Rectangle nebula and found the spectral signatures of anthracene and pyrene. This discovery was considered as the confirmation of the *PAH world hypothesis*. This biological hypothesis proposes that PAHs served as basis for the origin of life in a pre-RNA world.[18]

To the interest of organic chemists and material scientists, the most attractive property of PAHs is their aromaticity.[19-25] The electron delocalization along the polycyclic aromatic structures gives rise to interesting electronic and optical properties of these PAH materials. The breakthrough discovery of conducting and semiconducting organic polymers in 1970s leads to promising applications in the field of organic electronics nowadays.[26-28] The intrinsic electronic properties and the versatile functionalization qualified PAHs also are promising semiconducting materials in organic devices such as light-emitting diodes (LED), field effect transistors (FET), liquid crystal display (LCD) and solar cells.[29, 30] On the other hand, these polycyclic aromatic molecules can form stable columnar mesophase after attaching flexible chains, which are desirable for device processing due to their self-assembly and self-healing capability.[19, 31, 32]

Furthermore, two-dimensional all-benzenoid PAHs can be viewed as model compounds for graphite. Therefore, PAHs are also of special interest in theoretical problems like the scope, limitation and effects of electron delocalization in aromatic materials.[33]

1.2.1 Synthesis of PAHs

The natural and industrial sources of PAHs are coal tar, oil shale and the side-products of the catalytic hydrocracking of petroleum. Due to the industrial scale of the process, some PAHs which only exist in very small amounts in the crude material are able to be collected in reasonable amounts. First contributions in the area of direct synthesis and characterization of PAHs were pioneered by R. Scholl, E. Clar and M. Zander.[13, 34-38] However, the classical synthetic methods involved poor selectivity and relatively vigorous reaction conditions such as high temperatures and

pressures (Scheme 1-1).

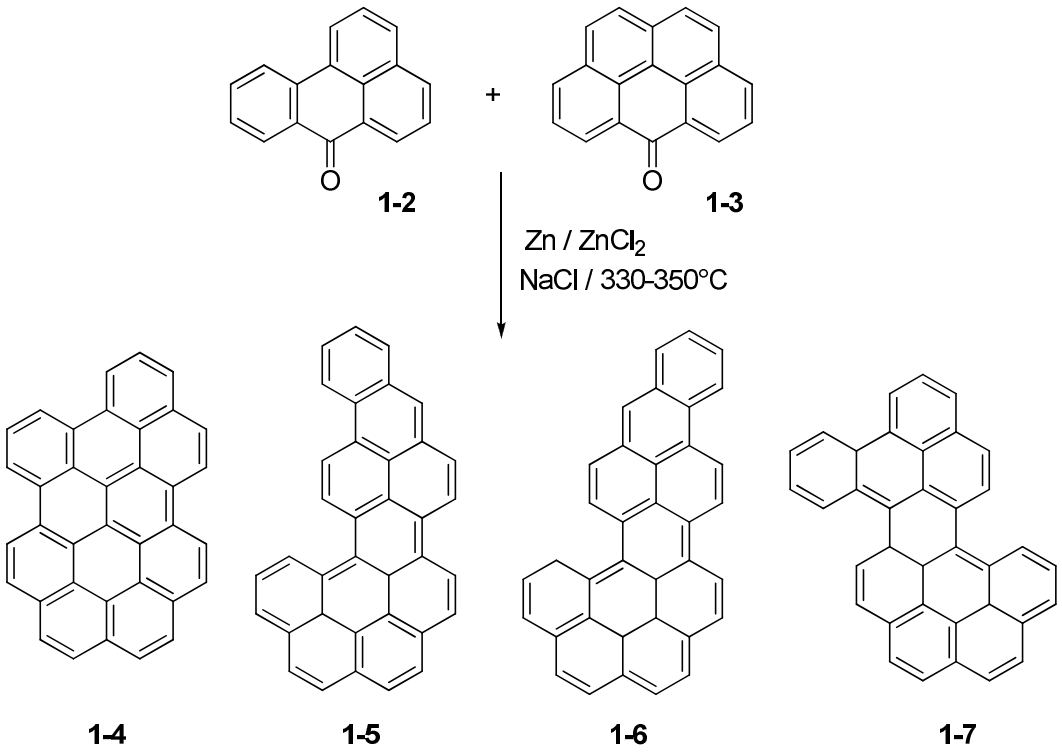

Scheme 1-1. Unselective Synthesis of PAHs.

Nowadays, research towards the synthesis of PAHs focuses on much milder methods, with better regioselectivity and higher yields. Several widely used modern synthetic methods are listed below:

1.2.1.1 Flash vacuum pyrolysis (Thermolysis)

The classic strategy toward pure PAHs is the conversion of appropriate precursors to target PAHs at elevated temperature. A typical experimental process is flash vacuum pyrolysis (FVP), in which high temperature gas-phase pyrolysis of precursors with short contact time (tens of ms to several seconds) in the hot zone result in electrocyclization with loss or migration of hydrogens (or hydrogen halide).

Key point of FVP is to design the precursors, which should have a good thermal stability and proper reactive sites. Appropriate planar precursors with halogen substituents in the fjord regions or at *ortho*-positions have been applied to synthesize strained geodesic PAH in significantly higher yields because the C_{aryl}-X (X =

halogens) bonds have lower dissociation enthalpies than C_{aryl}-H bonds. A most successful example is the rational chemical synthesis of the Buckminster fullerene C_{60} **1-9**, in which the key step was accomplished by FVP (Scheme 1-2).[39, 40]

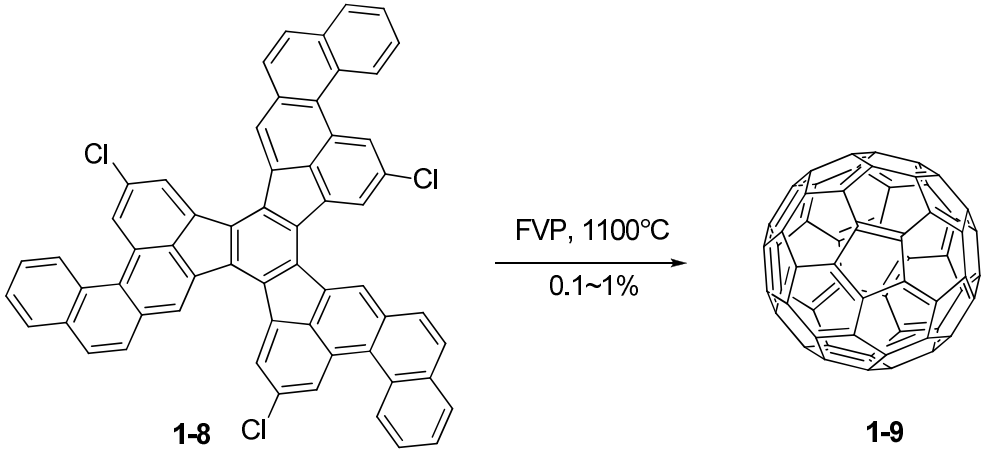

Scheme 1-2. Synthesis of fullerene C_{60} by FVP method.

Intramolecular carbene insertion during the pyrolysis process is another new synthetic method to prepare curved PAHs. This method was firstly reported by R. F. C. Brown, which is based on the reversible rearrangement of terminal acetylenes to vinylidenes under the conditions of FVP (Figure 1-2).[41, 42]

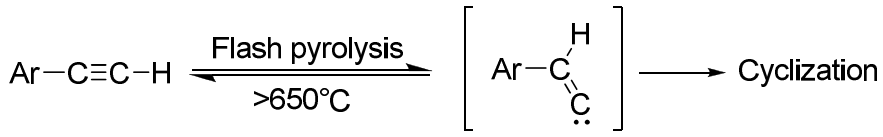

Figure 1-2. The reversible rearrangement of terminal acetylenes to vinylidenes.

One example is the gram-scale three-step synthesis of the bowl-shaped 20-carbon fullerene fragment corannulene **1-14** (Scheme 1-3) from commercially available starting materials, which was developed by L. T. Scott *et al*.[43, 44]

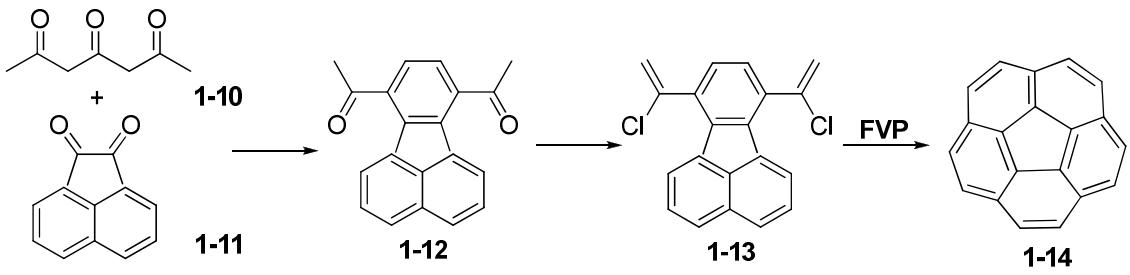

Scheme 1-3. Three-step synthesis of corannulene.

1.2.1.2 Friedel-Crafts condensation (Haworth phenanthrene synthesis)

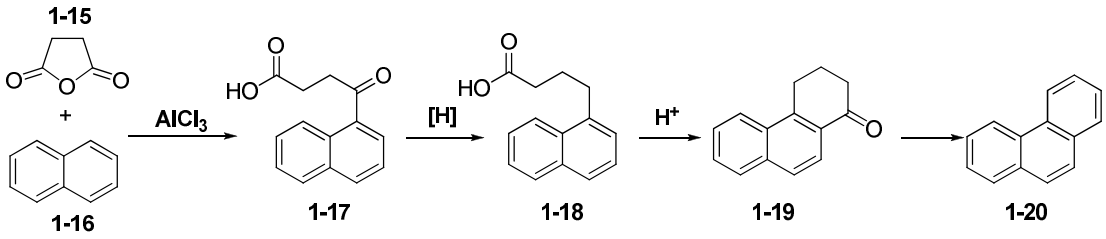

Scheme 1-4. Haworth phenanthrene synthesis.

Haworth synthesis provides a rational route to PAHs, as first illustrated by the synthesis of alkylphenanthrene.[45] The classic Haworth synthesis starts from Friedel-Crafts condensation of succinic anhydrides **1-15** with a polyarene **1-16** to give a keto-acid product **1-17**, followed by reduction of the keto group to form the butanoic acid **1-18**. And the essential transformation in this synthesis is the intramolecular Friedel-Crafts acylation of **1-18** to yield the ketone product **1-19,** which can be aromatized to the corresponding PAH **1-20** (Scheme 1-4).

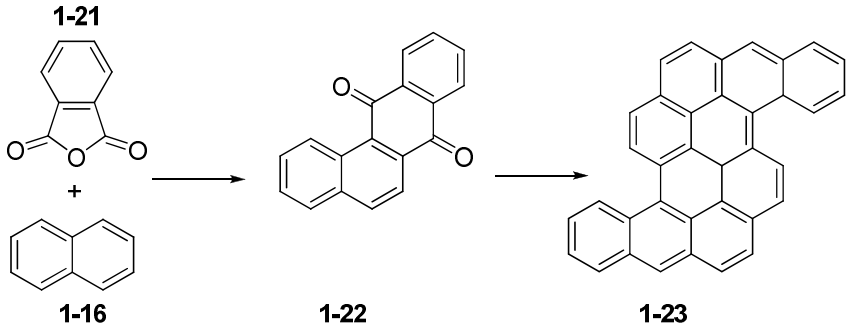

Scheme 1-5. Modified Haworth synthesis to larger PAHs

In order to construct PAHs larger than phenanthrene, Haworth synthesis could be modified by using different polyarene or aromatic anhydrides, thereby allowing fusion of two or more benzenoid rings to an existing aromatic system (Scheme 1-5).[46-48]

1.2.1.3 Acidic cyclodehydration and dehydrogenation of alkylated enamines

Alkylation of enamines **1-24** and enamine salts followed by acidic cyclodehydration and dehydrogenation provides an efficient synthetic approach to a wide range of polycyclic aromatic compounds.[49] It utilizes readily available reagents and mild conditions, entails relatively few synthetic steps, is readily adaptable to synthesis on a large scale, and provides generally good overall yields. This method with appropriate modifications establishes a convenient synthetic access to a wide range of PAHs.

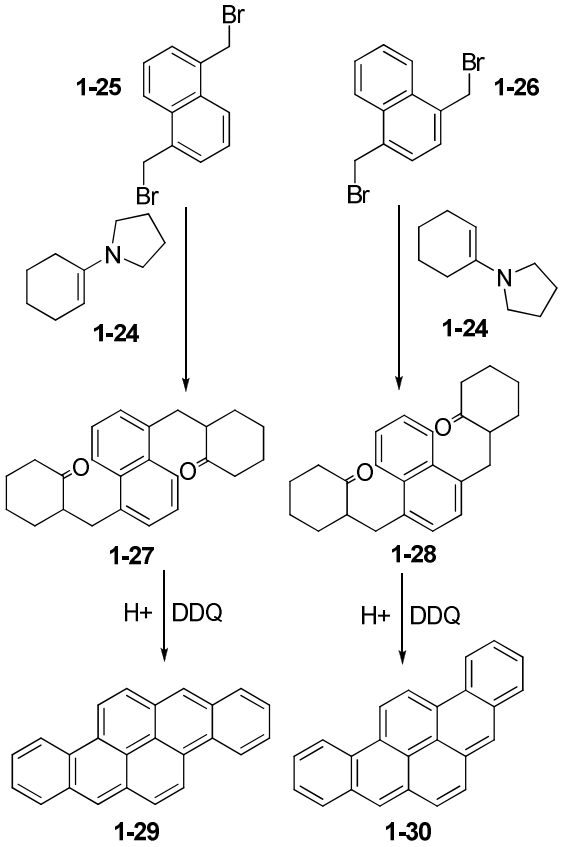

Scheme 1-6. Acid-catalyzed cyclohehydration of diketones as synthetic access to PAHs.

For example, the reaction of two equiv of enamine **1-24** with 1,5-bis(bromomethyl)naphthalene (**1-25**) and 1,4-bis(bromomethyl)naphthalene (**1-26**) gave the expected diketones **1-27** and **1-28** respectively, which underwent double cyclodehydration in both cases to the adjacent aromatic ring. Subsequent dehydrogenation yielded corresponding dibenzo[*b,def*]chrysene (**1-29**) and benzo[*rst*]pentaphene (**1-30**) containing six benzenoid rings (Scheme 1-6). It is worth to note that both reactions occurred strictly regiospecifically and only a single major isomeric cyclization product was isolated.[49]

1.2.1.4 Photocyclization

The photo-induced ring closure of stilbene type compounds in the presence of an oxidant, such as iodine or iron(III) chloride, has been widely used in the preparation of condensed PAHs.[50-54] These reactions allow to obtain cyclohexadienenes from 1,3,5-hexatrienes, and the oxidant serves to dehydrogenate the unstable primary dihydroaromatic products. Since the symmetrical and unsymmetrical stilbenes can be conveniently prepared employing Wittig, Heck as well as McMurry coupling reactions, various PAHs can be easily made.[55-58] A typical example of photocyclization is the irradiation of 2,2'-(1Z)-1,2-ethenediylbis-naphthalene (**1-31**) afforded 10b,10c-dihydro-dibenzo[*c,g*]phenanthrene (**1-32**).[59]

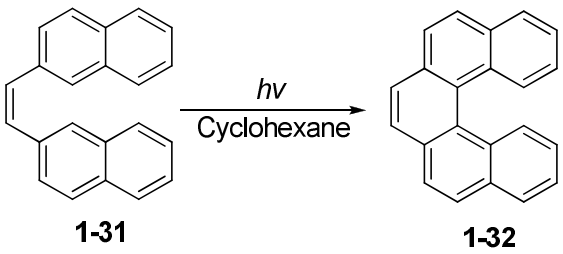

Scheme 1-7. Synthesis of 10b,10c-dihydro-dibenzo[*c,g*]phenanthrene by photocyclization.

Recently, C. Nuckolls *et al*. reported a novel synthetic route towards hexa-*cata*-hexabenzocoronene **1-34** and its derivatives by photocyclization of the adequate precursor, bisolefins **1-33** (Scheme 1-8). The yields of the final steps were usually more than 80%, therefore allowing large-scale preparation of the non-planar

PAH molecules.[60]

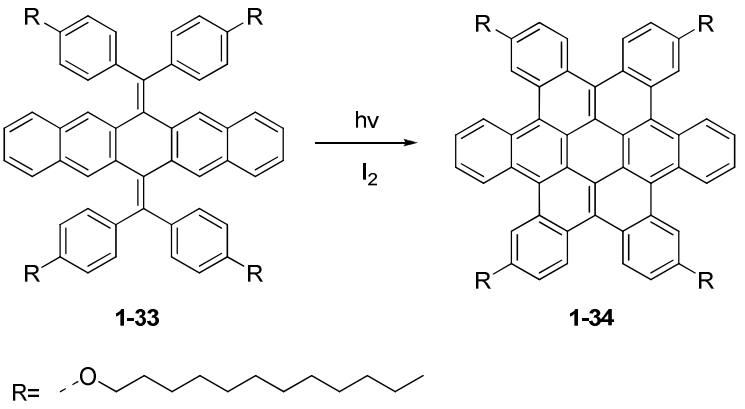

Scheme 1-8. Photochemical cyclization as an approach to obtain non-planar HBC.

1.2.1.5 Intermolecular and intramolecular Diels-Alder cycloaddition

The Diels-Alder cycloaddition is a versatile synthetic approach towards large PAH molecules.[61-64] To extend the aromatic skeleton, maleic anhydride and quinones are often used as dienophiles in the intermolecular Diels-Alder cycloaddition. For example, this strategy was used by E. Clar and M. Zander to synthesize benzo[*ghi*]perylene (**1-37**) and coronene **1-39** from perylene **1-35** (Scheme 1-9).[64]

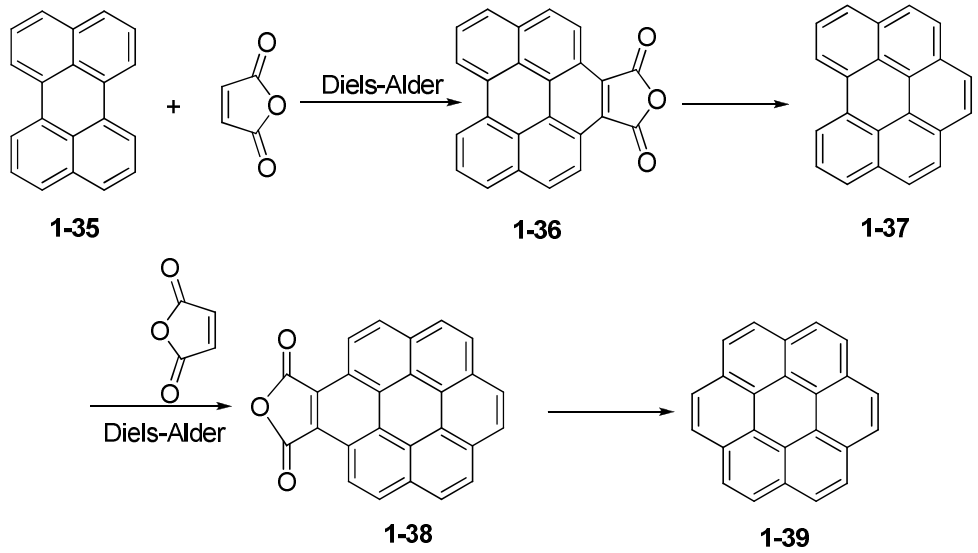

Scheme 1-9. Example of the use of Diels-Alder cycloaddition for the construction of PAHs.

K. Müllen *et al.* presented another elegant method to construct extended PAHs

by utilizing an intramolecular Diels-Alder cycloaddition to build up the precursor for a 54 carbon atoms containing, rhombus-shaped PAH **1-43** (Scheme 1-10).[65]

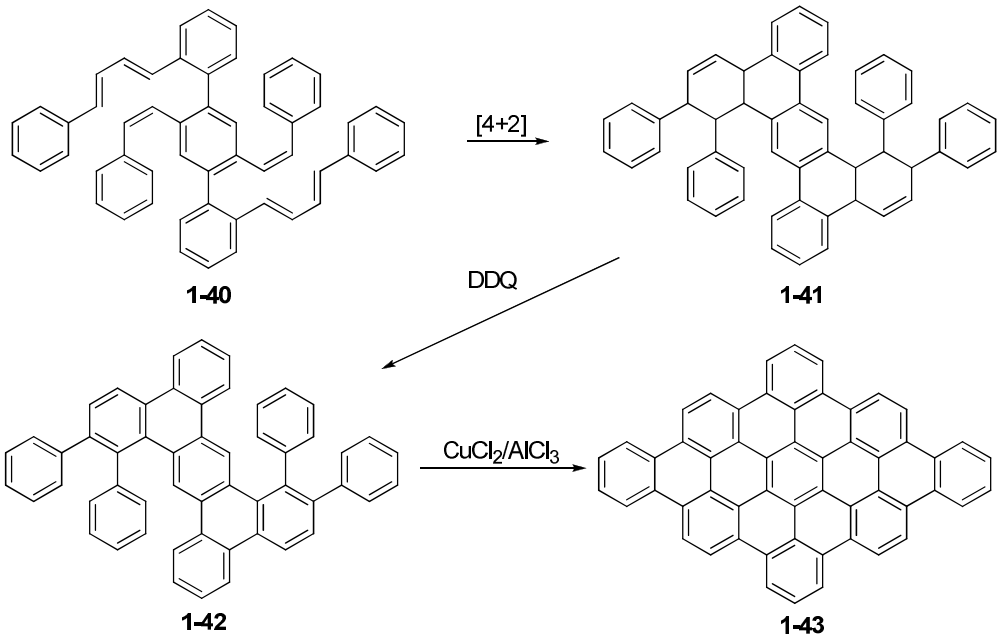

Scheme 1-10. Müllen's synthesis of the rhombus-shaped PAH **1-43**.

In this method, the intramolecular Diels-Alder cycloaddition of the *para*-terphenyl compounds **1-40**, in which the diene- and the dienophile structures were arranged in a way that they could react with each other, produced cyclohexene structures **1-41**. The tetraphenyl-substituted tetrabenzo[*a*,*c*,*h*,*j*]anthracenes (**1-42**) was obtained by subsequent mild aromatization of **1-41**. Further planarization of **1-42** with copper(II) chloride and aluminum(III) chloride afforded the target PAH **1-43**.

1.2.1.6 Oxidative cyclodehydrogenation

Intramolecular oxidative cyclodehydrogenation of appropriate oligophenylene precursors in the presence of Lewis acid catalysts have been developed as a powerful tool to make various all benzenoid discotic PAHs in the Müllen group.[1, 5, 6] The synthesis of the branched oligophenylenes is mainly based on the Diels-Alder cycloaddition between tetraphenylcyclopentadienones (CP) and arylethynylenes or *via* cobalt catalyzed cyclotrimerization of substituted diphenylacetylenes. A typical example is the synthesis of hexa-*peri*-hexabenzocoronenes (HBCs) **1-45** and their

derivatives from hexaphenylbenzene precursors **1-44** by an intramolecular cyclodehydrogenation with iron (III) chloride or $AlCl_3$-$Cu(OTf)_2$ in quantitative yields.

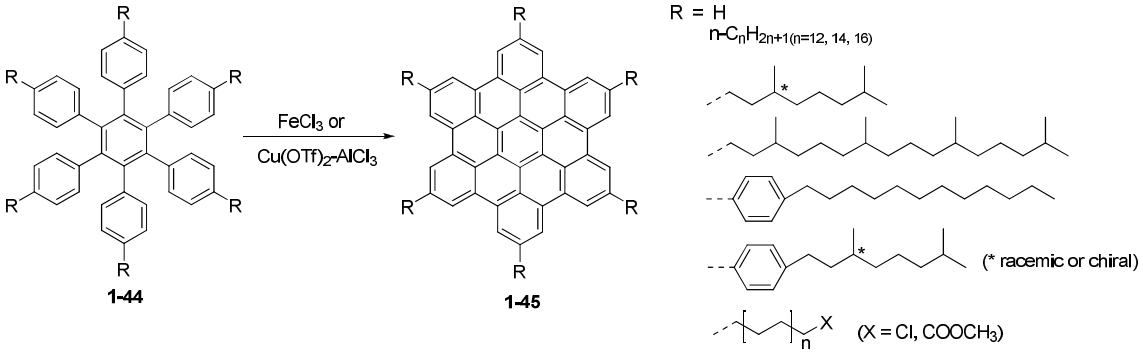

Scheme 1-11. General synthesis of six-fold symmetric HBC derivatives.

1.2.1.7 Other synthetic methods towards PAHs

Other synthetic methods such as extrusion of heteroatoms[66-68], cyclotrimerization reactions of alkynes and arylenes[69, 70], and electrophilic cyclization reactions[71-73], are also very useful for the synthesis of PAHs, and the details can be found in the references.

1.2.2 Supramolecular chemistry of PAHs

Supramolecular chemistry refers to the area of chemistry that focuses on the non-covalent bonding interactions between molecules. While traditional chemistry aims at the construction of the covalent bond, supramolecular chemistry examines the weaker and reversible non-covalent interactions between molecules including hydrogen bonding, metal coordination, hydrophobic forces, van der Waals forces, π-π interactions and electrostatic effects.[74-77] Therefore various substituted PAHs bearing flexible alkyl (or alkyl ether) chains become excellent candidates for research into supramolecular chemistry due to their phase separation between aromatic units and flexible alkyl chains as well as strong π-π interactions in one-dimensional stacking.[1, 5, 7]

1.2.2.1 Discotic liquid crystals from PAHs

Liquid crystalline (LC) phases are typical systems which self-assemble on a microscopic scale. They possess unusual material characteristics, by combining properties of a crystalline solid (optical and electric anisotropy) with those of a liquid (inability to support a shear stress in static equilibrium, viscosity). Liquid crystals can be divided into thermotropic and lyotropic liquid crystals. Thermotropic liquid crystals exhibit a phase transition into the LC phase as temperature is changed, whereas lyotropic liquid crystals exhibit phase transitions as a function of concentration of the mesogen in a solvent (typically water) as well as temperature.[78, 79]

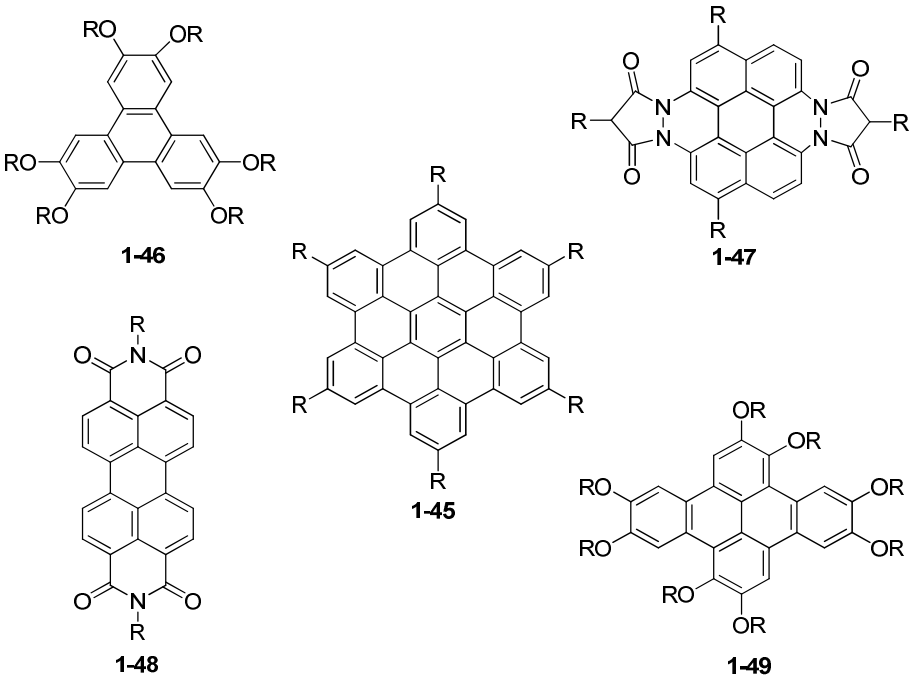

Figure 1-3. Different discotic mesogens.

Discotic (disc-like, columnar) liquid crystals, which were discovered in 1977 by Chandrasekhar *et al*., is *"liquid crystals of disc-like molecules"*.[80, 81] They offer diverse applications as a result of their orientation in the columnar mesophase, making them ideal candidates for molecular wires in various optical and electronic devices such as photocopiers, laser printers, photovoltaic cells, light-emitting diodes (LEDs), field-effect transistors (FETs), and holographic data storage.[32, 79, 81]

As molecular shape is an important factor in determining whether certain molecules will self-assemble into liquid crystalline phases, discotic PAH molecules preferably form columnar mesophases. As shown in Figure 1-3, the most extensively investigated classes of discotic PAH mesogens are triphenylenes, dibenzopyrenes, perylenes and hexa-*peri*-hexabenzocoronenes (HBCs).[5, 7] For example, hexaalkoxytriphenylenes **1-46** are of significant interest as fast photoconductors for applications in xerography and laser printing due to the high photoconductivity of their liquid crystals.[82-84]

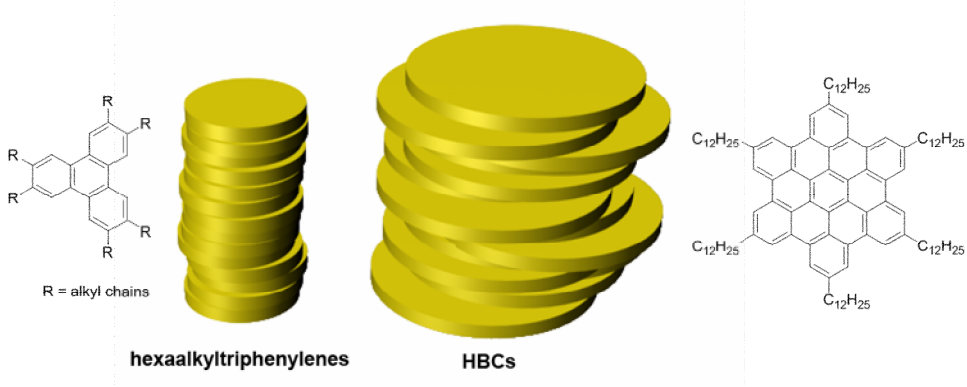

Figure 1-4. Stacks of small and large discs. To obtain strong π-π interactions, the stacking of small discs requires substantially higher orders as compared to large discs.

Another interesting example is the hexadodecyl-substituted HBC derivative **1-45** synthesized by K. Müllen *et al.* which display an extremely broad columnar mesophase with a phase width of 339 °C.[79] The corresponding hexaalkyltriphenylenes, however, are nonmesomorphic.[85] One possible reason might be that larger discs can form columns with substantial overlap of the aromatic areas more easily than the smaller ones. (Figure 1-4).

1.2.2.2 Self-assembly of PAHs in solution

Solution processing such as drop-casting and spin-coating is an economical and efficient method for device fabrication. In order to obtain optimized performance, the construction of pre-organized supramolecular structures in solution by the controllable self-assembly of PAH molecules is crucial.[86] Therefore, one major

challenge for molecular material science is to tune the self-association of the molecules because it translates into the processing behavior and furthermore into the performance of a device. Molecules with a pronounced tendency to self-assemble are suitable for processing from solution, because the required ordered pre-aggregation is given.[87]

One representative example is the controlled self-assembly of the disc-shaped HBCs, which were peripherally substituted by flexible dodecyl chains **1-50** or rigid polyphenylene dendrons **1-51** and **1-52** (Figure 1-5). Steric hindrance arising from the substituents, from less hindered dodecyl to bulky dendrons, was utilized to program the self-assembly of the HBC cores in solution. This study of large discotic PAHs in solution shows how structural and environmental factors can affect the supramolecular behavior and electronic properties of disc-shaped π-systems.[86]

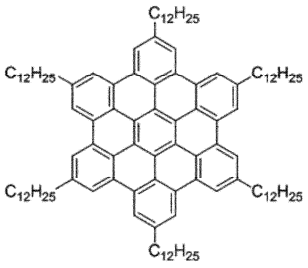

1-50

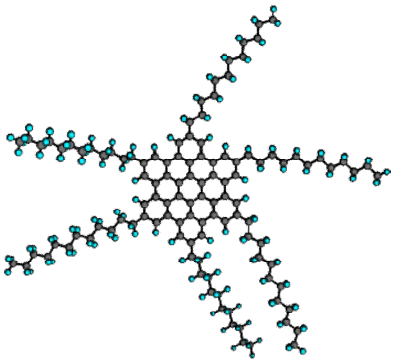

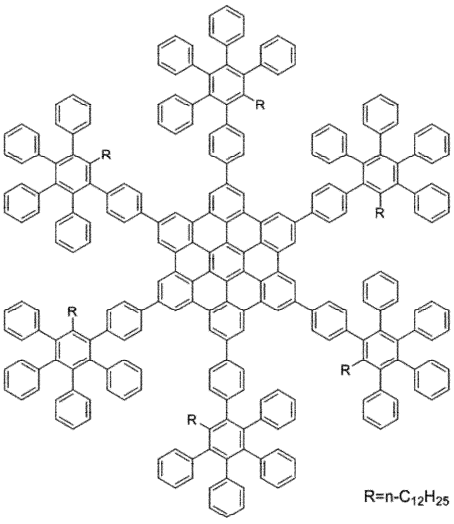

1-51

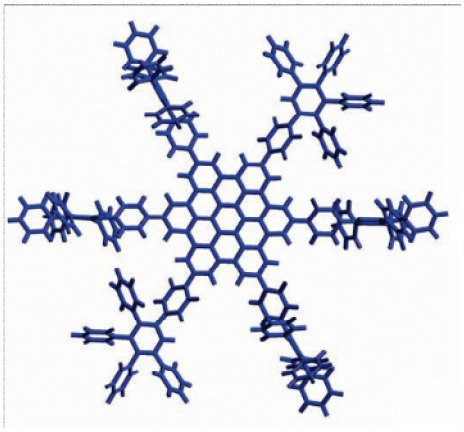

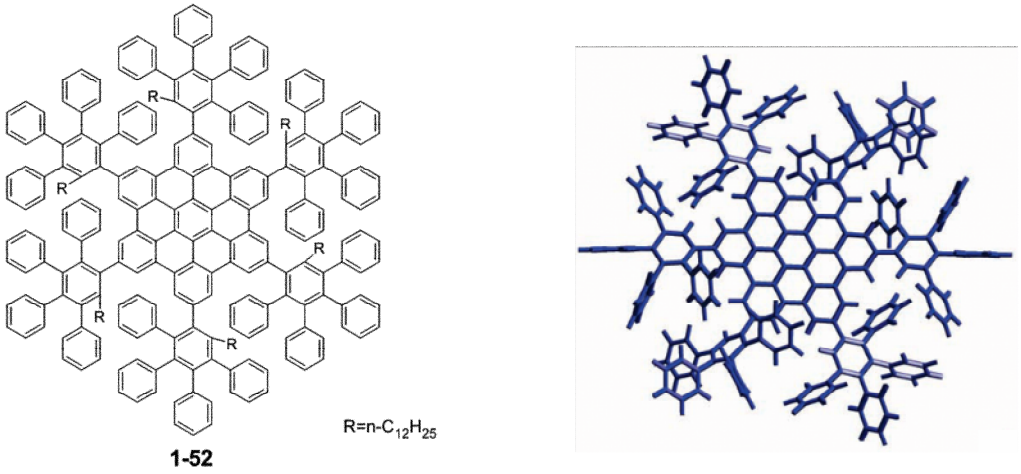

Figure 1-5. Molecular structures and three-dimensional models of the HBC molecules reported by K. Müllen *et al*.

1.2.2.3 Monolayers of PAHs

During the last decade, the supramolecular structures obtained from the self-assembly of nanoscaled building blocks on surface have attracted great interest of physicists, chemists and material scientists, due to their potential applications in the fabrication of electronic devices based on single molecules. Discotic PAHs are regarded as two-dimensional nanostructures and their self-assembly behavior on the surface have been widely studied by using of scanning tunneling microscopy (STM).[88, 89]

For example, the STM images of the HBC derivative and other graphitic discs at the liquid-HOPG interface clearly displayed a molecular resolution of monolayers or multilayers (Figure 1-6).[90-92]

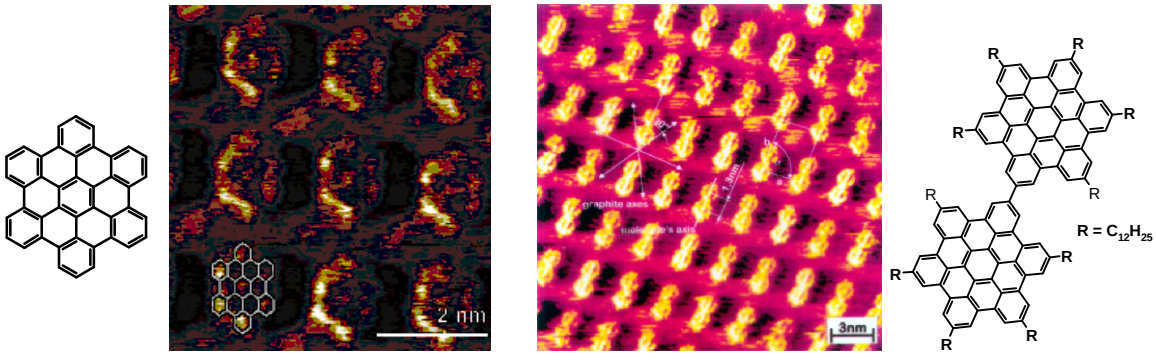

Figure 1-6. Some STM images of graphitic materials on the HOPG surface.

Besides being simply visualized on different surfaces by STM, the HBC functionalized with pyrene **1-53** showed interesting nanoscale phase separation on the HOPG surface, which was stable on the time scale of several minutes. This crystalline arrangement offers intriguing prospects for scanning tunneling spectroscopy (STS) studies on the two coplanar moieties, also upon photoexcitation. Furthermore, the possibility to grow highly ordered 2D and 3D structures of hybrid organic architectures containing PAHs could open perspectives for the development of local scale polarity measurements characterized by higher resolution and better reproducibility (Figure 1-7).[93]

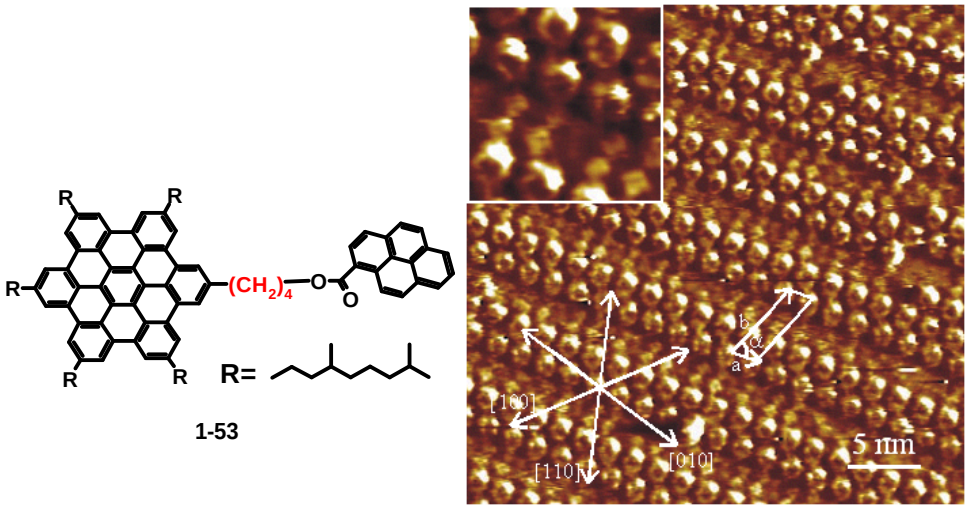

Figure 1-7. Nanoscale phase separation on the HOPG surface.

1.2.3 Electronic device from PAHs

Taking advantages of various available structures, high charge carrier mobility and strong self-assembly behavior of the discotic PAHs such as triphenylene, perylene and HBC *etc.*, a number of organic devices (LEDs, FETs and organic solar cells) with high performances were fabricated:

The first organic light emitting device (OLED) based on triphenylene discs was made by Wendorff *et al*. in 1997 and it was interesting to note that the oriented discs in liquid crystal phase decrease the threshold electric field significantly (from 1.4 x 10^{-6} to 6 x 10^{-5} V/cm).[94]

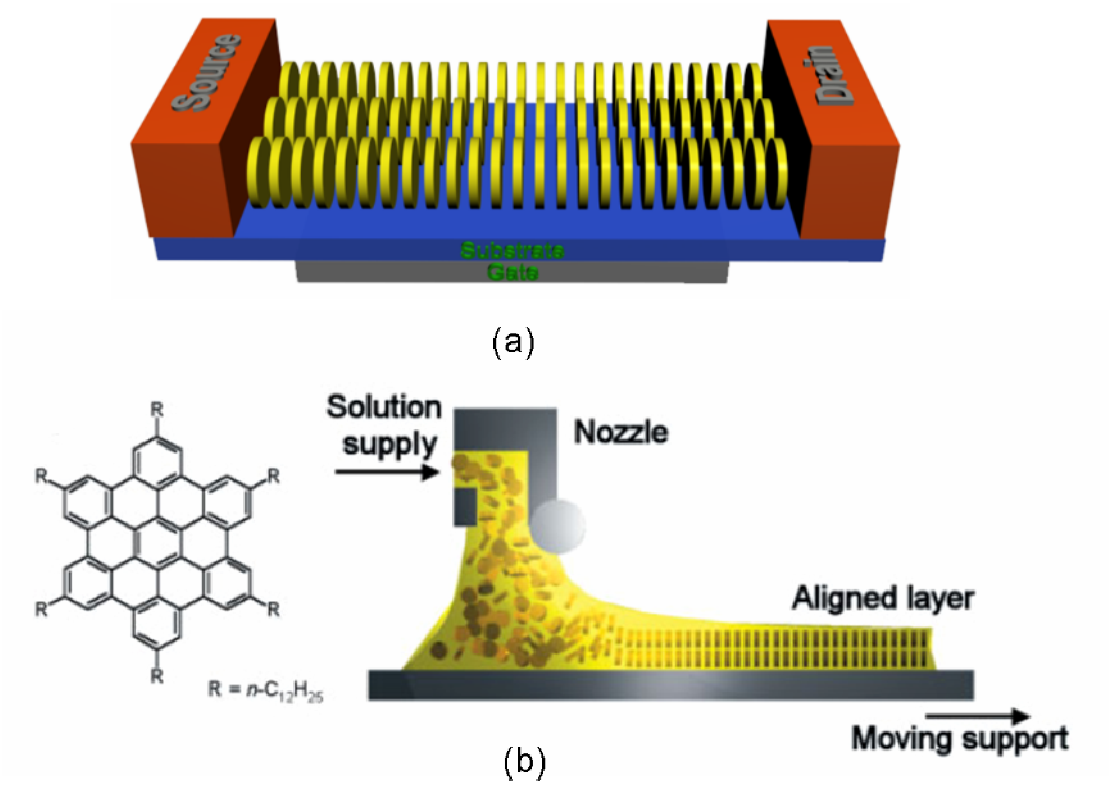

Figure 1-8. (a) Schematic representation of discotic LC materials in FETs; (b) Schematic representation of zone-casting technique. The continuously supplied solution is spread by means of a nozzle onto a moving support. The solution as well as the support are thermally controlled. Under appropriate rates of solvent evaporation and solution supply, a stationary gradient of concentration is formed with the meniscus. This results I directional crystallization.

Recently, W. Pisula and K. Müllen *et al*. employed a novel zone-casting method (Figure 1-8c) to fabricate long-range-oriented hexadodecyl-HBC films on substrates in order to attain highly ordered active layers in FETs. The obtained FET devices exhibited mobility as high as 1×10^{-2} $cm^2V^{-1}s^{-1}$ and on-off ratio of 10^4.[95]

In the area of organic solar cells, progress was made by L. Schmidt-Mende *et al*. in 2001.[96] The mixed solution of the liquid crystalline HBC-PhC12 **1-54** (electronic donor) and crystalline perylene diimide **1-55** (PDI, electronic acceptor) was spin-coated on an ITO substrate (Figure 1-9), and the obtained photodiodes exhibited extremely high external quantum efficiency (EQE = 34% at 490 nm).

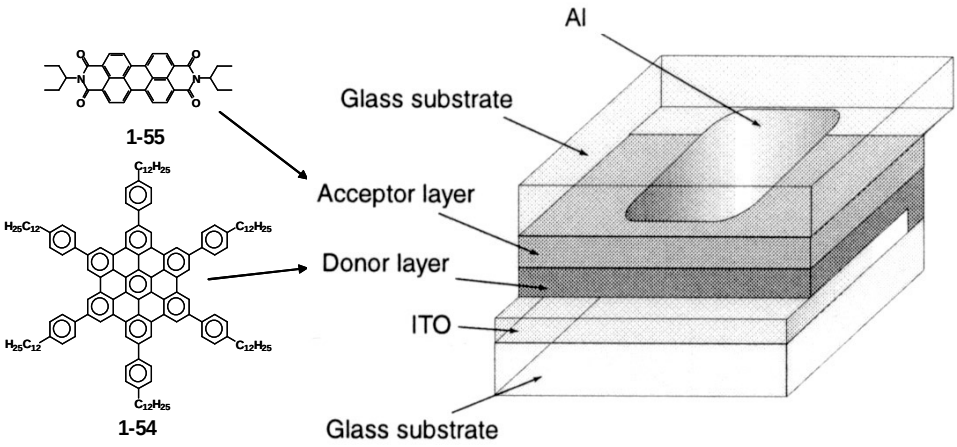

Figure 1-9. Highly efficient photodiodes based on discotic LC (HBC-PhC12) and crystalline (PDI) materials.

1.3 Heteroatom containing polycyclic aromatic hydrocarbons (HPAHs)

Heterocyclic compounds are organic compounds whose molecules contain one or more rings of atoms with at least one atom (the heteroatom) being an element other than carbon, most frequently oxygen, nitrogen, or sulfur. Among the more than 20 million registered chemical compounds nowadays, about one half of them contains heterocyclic systems. Heterocyclic compounds are becoming more and more important in all aspects of biology, chemistry, physics and material sciences, not only because of their abundance, but above all due to their biological, chemical, physical, and technical significance. Heterocyclic compounds can be found in many natural products, such as chlorophyll, vitamins, hormones, antibiotics, and alkaloids and they also constitute a very important part of the products in chemical industry like dyes, pharmaceuticals, and herbicides.[97-99]

As limited by the available synthetic approaches, heteroatom containing polycyclic aromatic hydrocarbons (HPAHs) are outnumbered by their all-hydrocarbon analogs mentioned in section 1.2.1. Apparently, the embedding of heteroatoms, such as nitrogen, oxygen or sulfur, into the graphitic structures will not only change their optoelectronic and electronic properties but also offer the possibility to create novel

PAHs based organometallic or ionic complexes.[5, 99-101] Therefore, HPAHs are expected to provide revolutionary organic functional materials and indeed have attracted great attentions of chemists, physicists and material scientists.

1.3.1 Synthesis of HPAHs

As the result of their unique structures, the synthetic methods of HPAHs are more or less different from the way to obtain all-hydrocarbon PAHs. In the last decades, various approachs were developed to synthesize various HPAHs:

1.3.1.1 Photocyclization

Photocyclization is one of the most widely used synthetic techniques to prepare HPAHs, especially with nitrogen atoms.

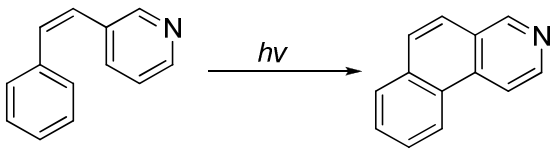

1-56 **1-57**

Scheme 1-12. The photolysis cyclization of stilbazoles.

The first photolysis cyclization to HPAH was reported by C. J. Timmons *et al.*, who found that the aza-analogues of stilbene, stilbazole **1-56** could also be cyclized to afford azaphenanthrene **1-57** upon irradiation under ultraviolet light in cyclohexane solution (Scheme 1-12).[102, 103] Different from their vital role in the photolysis cyclization of stilbenes, iodine had little effect on the reactions in dilute solution, and even appeared to inhibit the dehydrogenation in concentrated solutions of the stilbazoles. Nowadays, this method is applied to construct larger HPAHs such as **1-59** and **1-61** by using different heterocyclic precursors (Scheme 1-13).[104]

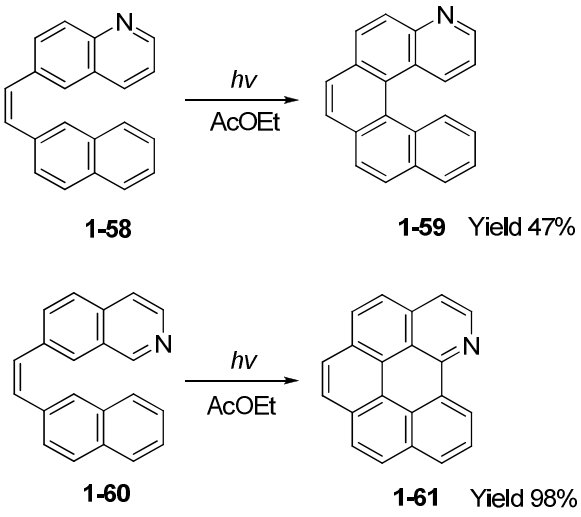

Scheme 1-13. Photocyclization to larger HPAHs.

Very importantly, photocyclization can also be used to access nitrogen containing PAHs with positive charge. For example, A. R. Katritzky *et al.* firstly discovered that the photocyclization of 1,2,6-triarylpyridinium salts **1-62** gave benzo[8,9]quinolizino[4,5,6,7-*fed*]phenanthridinylium salts (**1-63**) in good yield (Scheme 1-14).[105, 106]

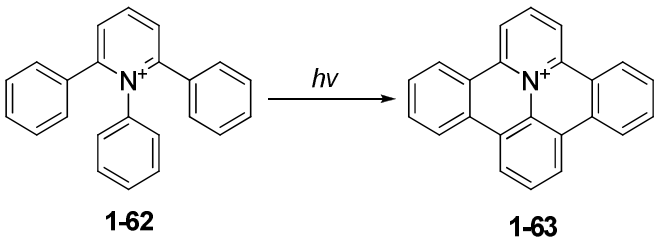

Scheme 1-14. Photocyclization of 1,2,6-triarylpyridinium salts.

1.3.1.2 Intramolecular quaternization

Intramolecular quaternization is a very efficient method to synthesize benzo[*c*]quinolizinium salts (**1-66**) and its derivates. By heating *cis*-2'-chloro-2-stilbazole (**1-65**) or its derivates over 170 °C in the presence of iodine, nitrogen containing **1-66** could be obtained in moderate yields (Scheme 1-15).[107, 108]

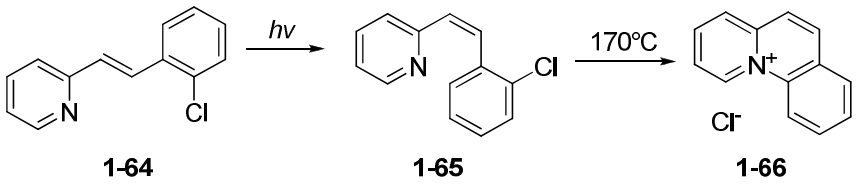

Scheme 1-15. Intramolecular quaternization to HPAHs.

1.3.1.3 Condensation

The condensation reactions between diketon **1-67** and *ortho*-dianimo aromatic molecules **1-68** were often used to produce tetrapyrido-[3,2-*a*:2',3'-*c*:3",2"-*h*:2"3"'-*j*]phenazine (tpphz **1-69**) and its derivates, which are frequently used as rigid ligand for conjugated metallic complexes (Scheme 1-16).[109]

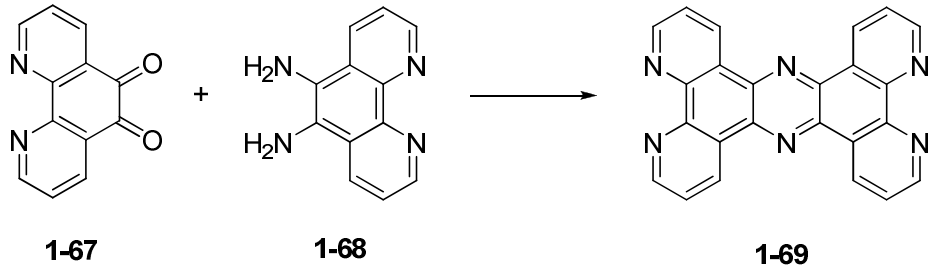

Scheme 1-16. Synthesis of tpphz by condensation.

Another intensively investigated class of discotic material, 5,6,11,12,17,18-hexaazatrinaphthylene (diquinoxalino[3,3-*a*:2',3'-*c*]phenazine or HATNA **1-72**) and its derivates could also be simply synthesized by three-fold condensation reactions of appropriate diamines **1-70** with hexaketocyclohexane **1-71** (Scheme 1-17).[110]

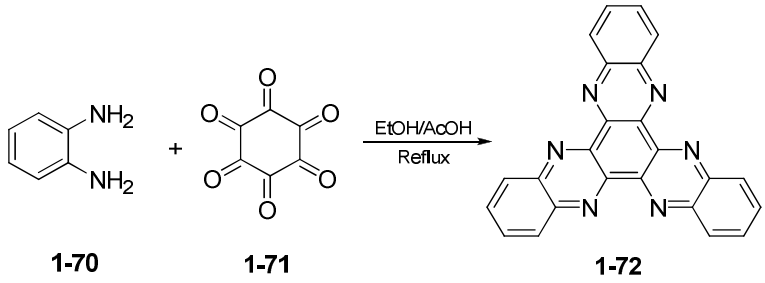

Scheme 1-17. The three-fold condensation of diamines with hexaketocyclohexane

Modified condensations of heterocyclic compounds were also adopted to

construct HPAHs. For example, the nitrogen centered discotic mesogen, tricycloquinazoline (TCQ) **1-75** could be obtained by the cyclotrimerization of 2,1-benzisoxazole derivates **1-74** (Scheme 1-18).[111]

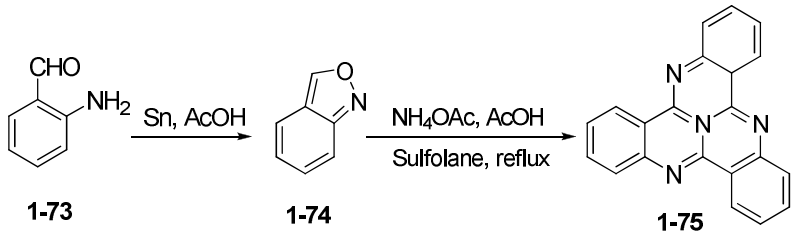

Scheme 1-18. Synthesis of TCQ by the trimerization of 2,1-benzisoxazole.

1.3.1.4 Oxidative cyclodehydrogenation

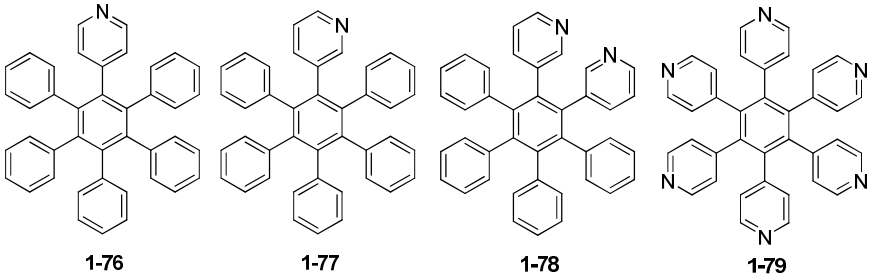

Figure 1-10. Examples of pyridine containing precursors failed to the standard oxidative cyclodehydrogenation.

As mentioned in section 1.2.1.6, oxidative cyclodehydrogenation is a very efficient approach to synthesize all-hydrocarbon PAHs such as HBC and its extended analogues.[1, 5] However, when the benzene ring was substituted by an electron-deficient pyridine ring, the cyclodehydrogenation under the same conditions failed to give the expected HPAHs presumably due to the difficulty of forming radical cations from pyridine rings[112, 113] (Figure 1-10). Therefore, to replace benzene with proper heterocyclic aromatic ring seems to be a crucial factor for the synthesis of HPAHs by oxidative cyclodehydrogenation. One successful example was reported recently by M. Takase and K. Müllen *et al.*, who obtained annularly fused hexapyrrolohexaazacoronenes (HPHACs, **1-82**) by the oxidiation of hexapyrrolylbenzene **1-81** with iron(III) chloride (Scheme 1-19).[100] It should be mentioned that additional electron-withdrawing groups such as bromide,

4-trifluoromethylphenyl on **1-82** were necessary to stabilize the final products under the oxidative conditions.

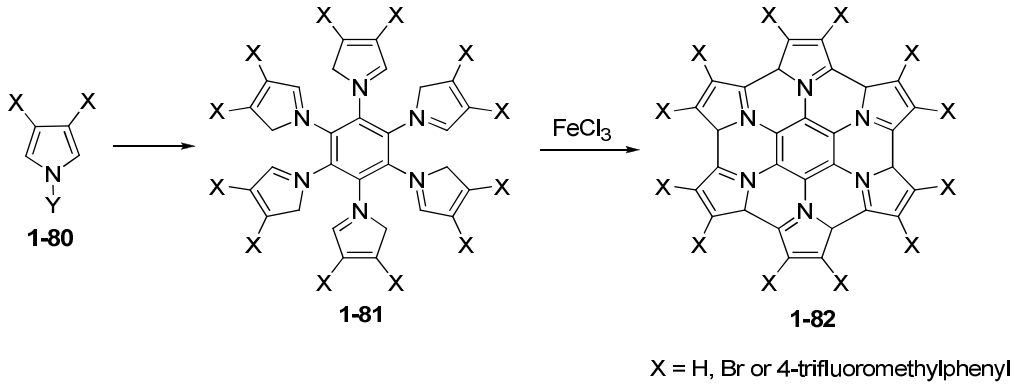

Scheme 1-19. Synthesis of annularly fused hexapyrrolohexaazacoronenes (HPHAC).

Besides nitrogen containing PAHs, thiophene-fused PAHs can also be obtained from appropriate thienyl based oligophenylene precursors through iron(III) chloride mediated oxidative cyclodehydrogenations. A typical example is the synthesis of a series of dibenzo[3,4:5,6]anthra[1,2-*b*:8,7-*b*']dithiophene (**1-85**) and tetrabenzo[*b,b',e,e'*]benzo[1,2-*g*:5,4-*g*']bis[1]benzothiophene (**1-87**) reported by T. M. Swager *et al.* recently (Scheme 1-20).[114]

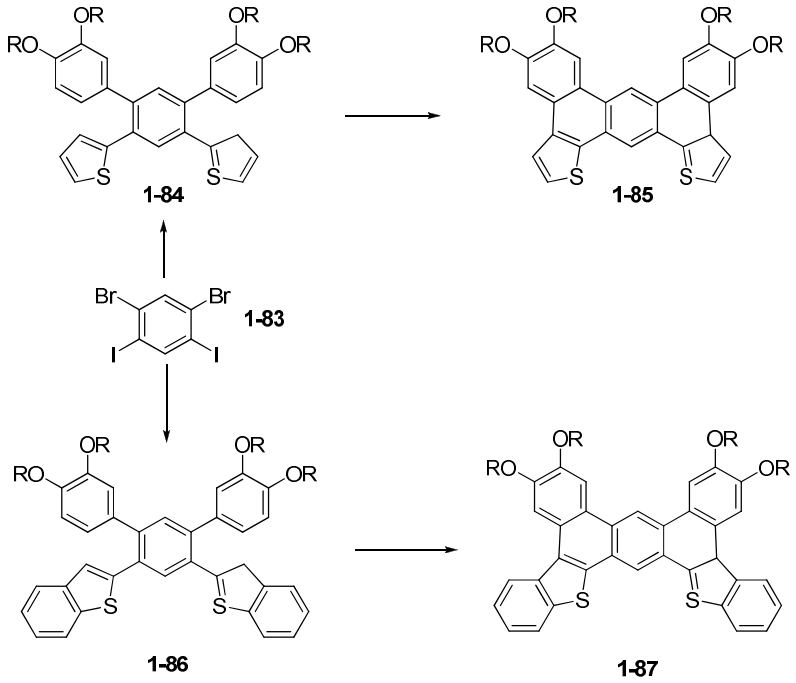

Scheme 1-20. Synthesis of sulfur containing PAHs by oxidative cyclizations.

1.3.2 Properties and application of HPAHs

1.3.2.1 Physical properties and aggregation behavior of HPAHs

Heteroatom containing PAHs are of particular interest in material sciences since such heteroatoms influence the electronic nature without modifying the structure. While an all-hydrocarbon aromatic cores such as triphenylene **1-46** and HBC **1-45** can provide an electron-rich, p-type (donor) semiconducting materials, the use of heteroaromatic cores can provide access to electron-poor, n-type (acceptor) materials. Two typical examples are the hexaazatriphenylenes[115] (N doped) **1-88** and 10a-aza-10b-borapyrenes[116] (B-N doped) **1-89** (Scheme 1-21).

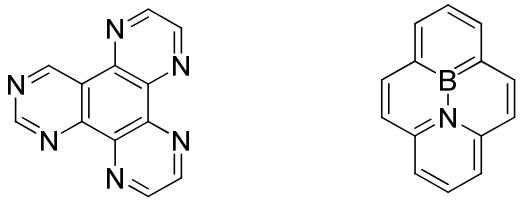

1-88 **1-89**

Scheme 1-21. N-type HPAHs: hexaazatriphenylenes and 10a-aza-10b-borapyrenes.

The intracolumnar self-organization behavior can also be greatly influenced by incorporation of heteroatoms. For example, the wide angle X-ray scattering of the mesophase from tricycloquinazoline (TCQ) **1-75** showed a π-π distance of 3.29 Å, which is one of the smallest core-core separations by far now known in discotic liquid crystal systems[111]. The significance of the small value of π-π distance could be seen in the light of the following: The columnar organization of these materials provides a one-dimensional pathway for charge transport. The efficiency of the transport depends on the extent of the π-π* overlapping of the neighboring discs within a column. For optimization of the charge transport one would like to maximize the overlap by decreasing the core-core separation without a loss of the fluid nature of the phase. Hence materials which exhibit a columnar phase but show a small core-core separation are good candidates for rapid intra-columnar charge migration.

1.3.2.2 HPAH based organometallic complexes

HPAHs with nitrogen atoms on the periphery of aromatic frameworks like tpphz **1-69** are able to construct rigid and conjugated dimetallic complexes with ruthenium and osmium ions.[109, 117] These compounds can be used as molecular light switches for DNA[118, 119] and micellar solutions[120] or for the study of fast electron transfer through DNA[121, 122]. They were also found to be a good DNA cleavage agent with high DNA affinity.[123]

1.3.2.3 FET from HPAHs

Derivates of 5,6,11,12,17,18-hexaazatrinaphthylene (HATNA) **1-72** have recently attracted much attention as n-type semiconducting materials for organic electronic applications, due to their ease of reduction and high environmental stability. When it was suitably decorated, it appeared to self-assemble into columnar superstructures with large bandwidths.[110, 124] By using the pulse-radiolysis time-resolved microwave conductivity (PR-TRMC) technique, the mobilities as high as 0.9 $cm^2\ V^{-1}s^{-1}$ had been achieved in the crystalline phases of hexa-(alkylsulfanyl) derivatives of HATNA.[125] S. R. Marder *et al.* also reported that stable amorphous films fabricated by the isomeric mixture of a tris(pentafluorobenzyl ester) derivative of HATNA showed an effective charge-carrier mobility of 0.02 cm^2/Vs, while the pure 2,8,15-isomer exhibited significantly different morphologies and low carrier mobilities (0.001-0.07 cm^2/Vs).[126]

1.4 Motivation and objective

As reviewed in the above sections, polycyclic aromatic hydrocarbons (PAHs) show excellent electronic and optoelectronic properties, unique supramolecular behavior and promising applications in the organic electronic and molecular scale devices. Furthermore, the incorporation of heteroatoms such as nitrogen, oxygen and sulfur into the aromatic framework of PAHs can not only influence their physical and chemical properties but also modify their supramolecular behavior. Nevertheless,

some more improvements both in organic synthesis, supramolecular chemistry as well as material applications are still desirable:

a). Doping nitrogen atom into the aromatic core is the most widely used strategy to prepare heteroatom containing polycyclic aromatic hydrocarbons (HPAHs). However, most of such cases only used neutral nitrogen atoms,[100, 110, 111] and nitrogen containing PAHs with positive charge were scarcely studied[105, 106, 127] mainly due to synthetic difficulties. One major objective of this work is to develop novel synthetic methods towards various nitrogen containing PAH cations with different aromatic cores and substituents.

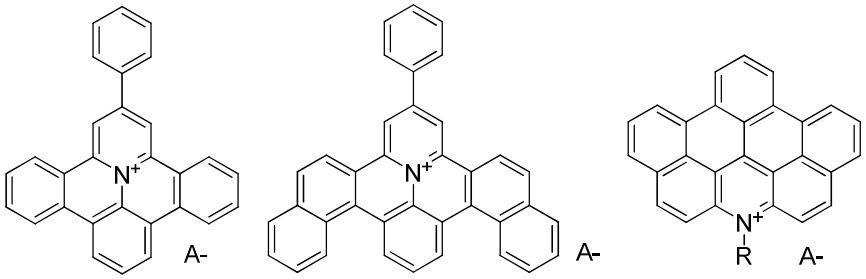

Scheme 1-22. Examples of nitrogen containing PAHs with positive charge.

b). Small oxygen or sulfur containing aromatic compounds with positive charge have received great attention of physicists and chemists in theoretical studies as well as in practical application. For example, pyrylium salts are very important intermediates for the formation of a range of carbocyclic and other heterocyclic molecules.[97] On the other hand, they are also widely used as redox reagents for the basic study of electrochemical processes.[128] However, the synthesis of oxygen or sulfur containing large PAHs with positive charge (including more than six fused aromatic rings)[129-131] has not yet been reported. The second objective in this thesis is to establish a synthetic strategy towards unprecedented oxygen and sulfur containing large PAHs with positive charge.

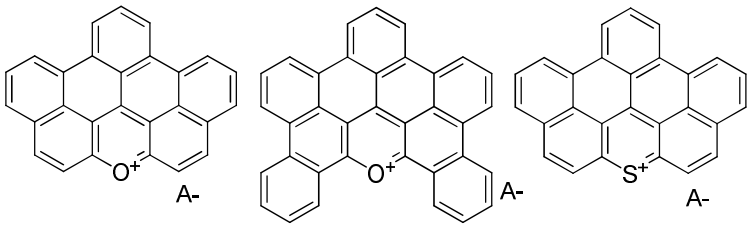

Scheme 1-23. Examples of oxygen and sulfur containing PAHs with positive charge.

c). As discussed in previous sections, supramolecular chemistry of aromatic molecules such as liquid crystal behavior and self-assembly in solution are very crucial for their application in material sciences because large structures with unique properties can be readily accessed by using bottom-up methods with small molecules as building blocks.[6, 7] Nevertheless, to the best of our knowledge, the supramolecular chemistry of heteroatom containing PAHs with positive charge has never been reported so far. In order to use them as organic materials in the future, the study of the supramolecular behavior of these heteroatom containing PAHs with positive charge is urgently required.

It is worthy to note that small nitrogen containing aromatic molecules with positive charge such as alkylpyridinium and imidazolium are belong to the most widely studied molecules in supramolecular research due to their ability to form ordered nanostructures in solution[132-136]. Mono alkylated heteroatom containing PAHs with positive charge are expected to have some novel aggregation behavior in solution because these amphiphilic molecules can be viewed as the combination of PAH and small surfactants. Therefore, one objective in this work is to investigate the self-assembly behavior of such molecules in solution.

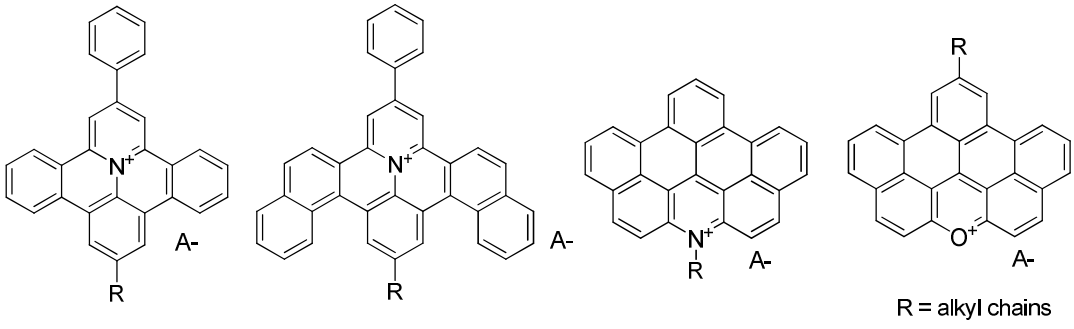

Scheme 1-24. Examples of amphiphilic heteroatom containing PAHs with positive charge.

Furthermore, in the research of discotic liquid crystal based on PAHs, adding other intermolecular forces such as hydrogen bonding and dipolar interaction is an efficient method to modify their stacking in the liquid crystal phase. Ionic interaction is also an important intermolecular force and proved to be an effective approach to adjusting the liquid crystal behavior of PAHs in recent years.[137, 138] Whereas the ionic interactions were usually introduced by the substituents at the periphery of the discs[139, 140], the liquid crystal behavior of heteroatom containing PAHs with positive charge on their aromatic cores has not been report up-to-date. The study of the liquid crystal behavior of multi-alkyl chain substituted heteroatom containing PAHs with positive charge is also one objective in this thesis.

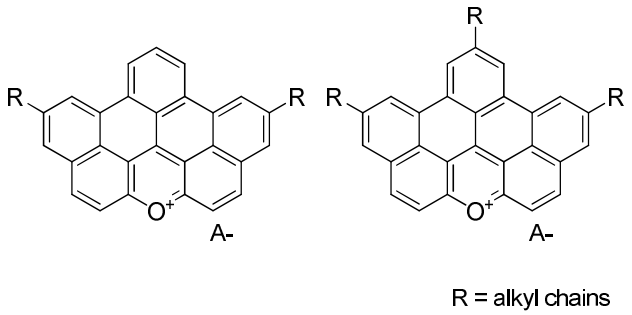

Scheme 1-25. Examples of heteroatom containing polycyclic aromatic mesogens with positive charge.

d). Ionic self-assembly (ISA) is the coupling of structurally different building blocks by electrostatic (Coulombic) interactions. This concept was first brought forward by M. Antonietti *et al.* and became more and more popular in supramolecular research.[137, 138, 141] Various ionic complexes with unique liquid crystal and photophysical properties were conveniently prepared by ISA method recently. Heteroatom containing PAHs with positive charge are ideal building blocks for ISA research because their ionic interaction and π-π interaction can be used together to adjust the stacking of the ionic complexes. Therefore, the investigation of the preparation and the self-assembly behavior of the ionic complexes from heteroatom containing PAHs with positive charge and organic anions is another objective in our work.

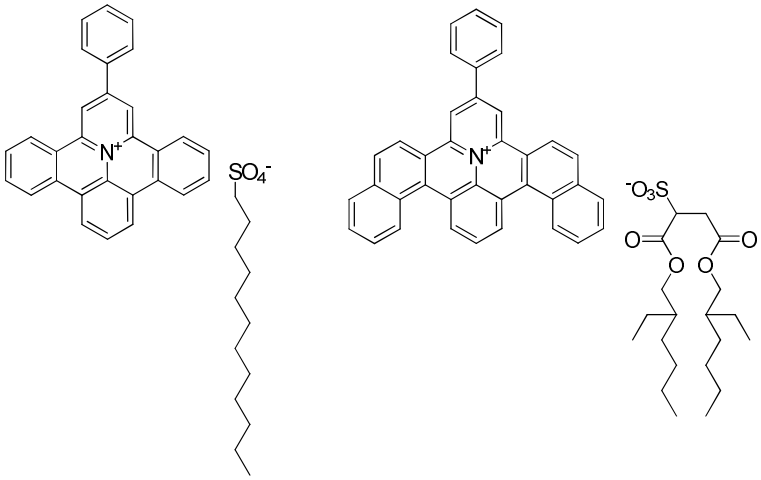

Scheme 1-26. Examples of ionic complexes obtained by ISA method.

References

1. Watson, M. D.; Fechtenkötter, A.; Müllen, K., *Chem. Rev.* **2001,** 101, (5), 1267.
2. Schleyer, P. v. R., *Chem. Rev.* **2001,** 101, (5), 1115.
3. Schleyer, P. v. R., *Chem. Rev.* **2005,** 105, (10), 3433.
4. Balaban, A. T.; Schleyer, P. v. R.; Rzepa, H. S., *Chem. Rev.* **2005,** 105, (10), 3436.
5. Wu, J. S.; Pisula, W.; Müllen, K., *Chem. Rev.* **2007,** 107, (3), 718.
6. Grimsdale, A. C.; Müllen, K., *Angew. Chem. Int. Ed.* **2005,** 44, (35), 5592.
7. Hoeben, F. J. M.; Jonkheijm, P.; Meijer, E. W.; Schenning, A., *Chem. Rev.* **2005,** 105, (4), 1491.
8. Hofmann, A. W., *Proc. of Royal Soc* **1855,** 8, 1.
9. Faraday, M., *Phil. Trans. R. Soc.* **1825**, 440.
10. Armit, J. W.; Robinson, R., *J. Chem. Soc.* **1925,** 127, 1604.
11. Huckel, E.; Huckel, W., *Nature* **1932,** 129, 937.
12. Sainsbury, M., *Aromatic Chemistry*. Oxford University Press: 1992.
13. Clar, E., *Polycyclic Hydrocarbons*. Academic Press: New York, **1964**; Vol. I/II.
14. Dias, J. R., *Handbook of Polycyclic Hydrocarbons*. Elsevier: Amsterdam, **1988**.
15. G.Harvey, R., *Polycyclic Aromatic Hydrocarbons*. Wiley-VCH: New York, 1997.
16. Fetzer, J. C., *The Chemistry and Analysis of the Large Polycyclic Aromatic Hydrocarbons*. Wiley: New York, 2000.
17. Luch, A., *The Carcinogenic Effects of Polycyclic Aromatic Hydrocarbons*. Imperial College Press: London, 2005.
18. Ehrenfreund, P.; Rasmussen, S.; Cleaves, J.; Chen, L. H., *Astrobiology* **2006,** 6, (3), 490.
19. Watson, M. D.; Fechtenkötter, A.; Müllen, K., *Chem. Rev.* **2001,** 101, (5), 1267.
20. Bleeke, J. R., *Chem. Rev.* **2001,** 101, (5), 1205.
21. Nyulaszi, L., *Chem. Rev.* **2001,** 101, (5), 1229.
22. Minkin, V. I.; Minyaev, R. M., *Chem. Rev.* **2001,** 101, (5), 1247.
23. Mitchell, R. H., *Chem. Rev.* **2001,** 101, (5), 1301.
24. Gomes, J. A. N. F.; Mallion, R. B., *Chem. Rev.* **2001,** 101, (5), 1349.

25. Katritzky, A. R.; Jug, K.; Oniciu, D. C., *Chem. Rev.* **2001,** 101, (5), 1421.
26. Heeger, A. J., *Rev. Mod. Phys.* **2001,** 73, (3), 681.
27. Shirakawa, H., *Angew. Chem. Int. Ed.* **2001,** 40, (14), 2575.
28. MacDiarmid, A. G., *Angew. Chem. Int. Ed.* **2001,** 40, (14), 2581.
29. Reynolds, T. A. S. R. L. E. J. R., *Handbook of Conducting Polymers*. 2nd Ed ed.; Marcel Dekker, Inc.: New York, 1998.
30. Hutten, G. H. P. F. v., *Semiconducting Polymers* Wiley-VCH: Weiheim, 2000.
31. Sage, I. C., *Handbook of Liquid Crystals*. Wiley-VCH: Weinheim, 1998; Vol. Vol. 1, p 731.
32. Bushby, R. J.; Lozman, O. R., *Curr. Opin. Solid State Mat. Sci.* **2002,** 6, (6), 569.
33. Dias, J. R., *Thermochim. Acta* **1987,** 122, (2), 313.
34. Clar, E.; Schmidt, W., *Tetrahedron* **1979,** 35, (22), 2673.
35. Clar, E.; Stewart, D. G., *J. Am. Chem. Soc.* **1953,** 75, (11), 2667.
36. Scholl, R.; Seer, C., *Chem. Ber.* **1922,** 55, 330.
37. Scholl, R.; Seer, C., *Liebigs Ann. Chem.* **1912,** 394, (1/3), 111.
38. Scholl, R.; Seer, C.; Weitzenbock, R., *Chem. Ber.* **1910,** 43, 2202.
39. Scott, L. T.; Boorum, M. M.; McMahon, B. J.; Hagen, S.; Mack, J.; Blank, J.; Wegner, H.; de Meijere, A., *Science* **2002,** 295, (5559), 1500.
40. Boorum, M. M.; Vasil'ev, Y. V.; Drewello, T.; Scott, L. T., *Science* **2001,** 294, (5543), 828.
41. Brown, R. F. C.; Harringt.Kj; McMüllen, G. L., *Chem. Commun.* **1974**, (4), 123.
42. Brown, R. F. C.; Eastwood, F. W.; Jackman, G. P., *Aust. J. Chem.* **1977,** 30, (8), 1757.
43. Scott, L. T.; Hashemi, M. M.; Meyer, D. T.; Warren, H. B., *J. Am. Chem. Soc.* **1991,** 113, (18), 7082.
44. Scott, L. T.; Cheng, P. C.; Hashemi, M. M.; Bratcher, M. S.; Meyer, D. T.; Warren, H. B., *J. Am. Chem. Soc.* **1997,** 119, (45), 10963.
45. Haworth, R. D., *J. Chem. Soc.* **1932**, 1125.
46. Tomaszewski, J. E.; Manning, W. B.; Muschik, G. M., *Tetrahedron Lett.* **1977**, (11), 971.

47. Fujisawa, S.; Oonishi, I.; Aoki, J.; Ohashi, Y.; Sasada, Y., *Bull. Chem. Soc. Jpn.* **1985,** 58, (11), 3356.
48. Fujisawa, S.; Takekawa, M.; Nakamura, Y.; Uchida, A.; Ohshima, S.; Oonishi, I., *Polycycl. Aromat. Compd.* **1999,** 14, 99.
49. Harvey, R. G.; Pataki, J.; Cortez, C.; Di Raddo, P.; Yang, C. X., *J. Org. Chem.* **1991,** 56, (3), 1210.
50. Wood, C. S.; Mallory, F. B., *J. Org. Chem.* **1964,** 29, (11), 3373.
51. Mallory, F. B.; Wood, C. S.; Gordon, J. T., *J. Am. Chem. Soc.* **1964,** 86, (15), 3094.
52. Castro, P. P.; Diederich, F., *Tetrahedron Lett.* **1991,** 32, (44), 6277.
53. Broene, R. D.; Diederich, F., *Tetrahedron Lett.* **1991,** 32, (39), 5227.
54. Herbert, M., *Angew. Chem. Int. Ed.* **1992,** 31, (11), 1399.
55. Riadh Elbed, B. B. J.-P. G. M. G. A. M., *Eur. J. Org. Chem.* **2004,** 2004, (7), 1517.
56. Sharma, A. K.; Lin, J. M.; Desai, D.; Amin, S., *J. Org. Chem.* **2005,** 70, (13), 4962.
57. Defay, N., *Organic Magnetic Resonance* **1974,** 6, (4), 221.
58. Flammang.M; Nasielsk.J; Martin, R. H., *Tetrahedron Lett.* **1967**, (8), 743.
59. Somers, J. B. M.; Couture, A.; Lablachecombier, A.; Laarhoven, W. H., *J. Am. Chem. Soc.* **1985,** 107, (5), 1387.
60. Xiao, S. X.; Myers, M.; Miao, Q.; Sanaur, S.; Pang, K. L.; Steigerwald, M. L.; Nuckolls, C., *Angew. Chem. Int. Ed.* **2005,** 44, (45), 7390.
61. Davies, W.; Porter, Q. N., *J. Chem. Soc.* **1957**, (DEC), 4967.
62. Kohnke, F. H.; Slawin, A. M. Z.; Stoddart, J. F.; Williams, D. J., *Angew. Chem. Int. Ed.* **1987,** 26, (9), 892.
63. Schluter, A. D.; Loffler, M.; Enkelmann, V., *Nature* **1994,** 368, (6474), 831.
64. Clar, E.; Zander, M., *J. Chem. Soc.* **1957**, (NOV), 4616.
65. Muller, M.; Kubel, C.; Müllen, K., *Chem.-Eur. J.* **1998,** 4, (11), 2099.
66. Staab, H. A.; Diederich, F., *Chem. Ber.* **1983,** 116, (10), 3487.
67. Krieger, C.; Diederich, F.; Schweitzer, D.; Staab, H. A., *Angew. Chem. Int. Ed.* **1979,** 18, (9), 699.

68. Diederich, F.; Staab, H. A., *Angew. Chem. Int. Ed.* **1978,** 17, (5), 372.
69. Boese, R.; Matzger, A. J.; Mohler, D. L.; Vollhardt, K. P. C., *Angew. Chem. Int. Ed.* **1995,** 34, (13-14), 1478.
70. Nambu, M.; Mohler, D. L.; Hardcastle, K.; Baldridge, K. K.; Siegel, J. S., *J. Am. Chem. Soc.* **1993,** 115, (14), 6138.
71. Goldfinger, M. B.; Crawford, K. B.; Swager, T. M., *J. Am. Chem. Soc.* **1997,** 119, (20), 4578.
72. Cho, B. P.; Harvey, R. G., *J. Org. Chem.* **1987,** 52, (26), 5668.
73. Cho, B. P.; Harvey, R. G., *J. Org. Chem.* **1987,** 52, (26), 5679.
74. Breen, T. L.; Tien, J.; Oliver, S. R. J.; Hadzic, T.; Whitesides, G. M., *Science* **1999,** 284, (5416), 948.
75. Lehn, J. M., *Science* **2002,** 295, (5564), 2400.
76. Whitesides, G. M.; Grzybowski, B., *Science* **2002,** 295, (5564), 2418.
77. Helmer, M., *Nature* **2004,** 427, (6975), 597.
78. Vorlander, D., *Chem. Ber.* **1907,** 40, 1970.
79. Laschat, S.; Baro, A.; Steinke, N.; Giesselmann, F.; Hagele, C.; Scalia, G.; Judele, R.; Kapatsina, E.; Sauer, S.; Schreivogel, A.; Tosoni, M., *Angew. Chem. Int. Ed.* **2007,** 46, (26), 4832.
80. Chandrasekhar, S.; Sadashiva, B. K.; Suresh, K. A., *Pramana* **1977,** 9, (5), 471.
81. Bushby, R. J.; Lozman, O. R., *Curr. Opin. Colloid Interface Sci.* **2002,** 7, (5-6), 343.
82. Breslow, R.; Jaun, B.; Kluttz, R. Q.; Xia, C. Z., *Tetrahedron* **1982,** 38, (6), 863.
83. Fontes, E.; Heiney, P. A.; Dejeu, W. H., *Phys. Rev. Lett.* **1988,** 61, (10), 1202.
84. Mertesdorf, C.; Ringsdorf, H.; Stumpe, J., *Liq. Cryst.* **1991,** 9, (3), 337.
85. Herwig, P.; Kayser, C. W.; Müllen, K.; Spiess, H. W., *Adv. Mater.* **1996,** 8, (6), 510.
86. Wu, J. S.; Fechtenkötter, A.; Gauss, J.; Watson, M. D.; Kastler, M.; Fechtenkötter, C.; Wagner, M.; Müllen, K., *J. Am. Chem. Soc.* **2004,** 126, (36), 11311.
87. El Hamaoui, B.; Zhi, L. J.; Pisula, W.; Kolb, U.; Wu, J. S.; Müllen, K., *Chem. Commun.* **2007**, (23), 2384.

88. Schmitz-Hubsch, T.; Sellam, F.; Staub, R.; Torker, M.; Fritz, T.; Kubel, C.; Müllen, K.; Leo, K., *Surf. Sci.* **2000,** 445, (2-3), 358.
89. Staub, R.; Toerker, M.; Fritz, T.; Schmitz-Hubsch, T.; Sellam, F.; Leo, K., *Surf. Sci.* **2000,** 445, (2-3), 368.
90. Samori, P.; Severin, N.; Simpson, C. D.; Müllen, K.; Rabe, J. P., *J. Am. Chem. Soc.* **2002,** 124, (32), 9454.
91. Samori, P.; Fechtenkötter, A.; Jackel, F.; Bohme, T.; Müllen, K.; Rabe, J. P., *J. Am. Chem. Soc.* **2001,** 123, (46), 11462.
92. Ito, S.; Herwig, P. T.; Bohme, T.; Rabe, J. P.; Rettig, W.; Müllen, K., *J. Am. Chem. Soc.* **2000,** 122, (32), 7698.
93. Tchebotareva, N.; Yin, X. M.; Watson, M. D.; Samori, P.; Rabe, J. P.; Müllen, K., *J. Am. Chem. Soc.* **2003,** 125, (32), 9734.
94. Christ, T.; Glusen, B.; Greiner, A.; Kettner, A.; Sander, R.; Stumpflen, V.; Tsukruk, V.; Wendorff, J. H., *Adv. Mater.* **1997,** 9, (1), 48.
95. Pisula, W.; Menon, A.; Stepputat, M.; Lieberwirth, I.; Kolb, U.; Tracz, A.; Sirringhaus, H.; Pakula, T.; Müllen, K., *Adv. Mater.* **2005,** 17, (6), 684.
96. Schmidt-Mende, L.; Fechtenkötter, A.; Müllen, K.; Moons, E.; Friend, R. H.; MacKenzie, J. D., *Science* **2001,** 293, (5532), 1119.
97. Gilchrist, T. L., *Heterocyclic Chemistry*. 3rd ed.; Prentice Hall: New Jersey, 1997.
98. Eicher, T.; Hauptmann, S., *The Chemistry of Heterocycles: Structure, Reactions, Syntheses, and Applications*. 2nd ed.; Wiley-VCH: 2003.
99. Katritzky, A. R.; Pozharskii, A. F., *Handbook of heterocyclic chemistry*. 2nd ed.; Pergamon: Amsterdam, 2000.
100. Takase, M.; Enkelmann, V.; Sebastiani, D.; Baumgarten, M.; Müllen, K., *Angew. Chem. Int. Ed.* **2007,** 46, (29), 5524.
101. Draper, S. M.; Gregg, D. J.; Schofield, E. R.; Browne, W. R.; Duati, M.; Vos, J. G.; Passaniti, P., *J. Am. Chem. Soc.* **2004,** 126, (28), 8694.
102. Loader, C. E.; Sargent, M. V.; Timmons, C. J., *Chem. Commun.* **1965**, (7), 127.
103. Loader, C. E.; Timmons, C. J., *J. Chem. Soc.* **1966**, (12), 1078.
104. Bazzini, C.; Brovelli, S.; Caronna, T.; Gambarotti, C.; Giannone, M.; Macchi, P.;

Meinardi, F.; Mele, A.; Panzeri, W.; Recupero, F.; Sironi, A.; Tubino, R., *Eur. J. Org. Chem.* **2005**, (7), 1247.

105. Katritzky, A. R.; Zakaria, Z.; Lunt, E., *J. Chem. Soc. Perkin Trans. 1* **1980**, (9), 1879.

106. Katritzky, A. R.; Zakaria, Z.; Lunt, E.; Jones, P. G.; Kennard, O., *Chem. Commun.* **1979**, (6), 268.

107. Fozard, A.; Bradsher, C. K., *J. Org. Chem.* **1966,** 31, (7), 2346.

108. Fozard, A.; Bradsher, C. K., *Chem. Commun.* **1965**, (13), 288.

109. Bolger, J.; Gourdon, A.; Ishow, E.; Launay, J. P., *Chem. Commun.* **1995**, (17), 1799.

110. Barlow, S.; Zhang, Q.; Kaafarani, B. R.; Risko, C.; Amy, F.; Chan, C. K.; Domercq, B.; Starikova, Z. A.; Antipin, M. Y.; Timofeeva, T. V.; Kippelen, B.; Bredas, J. L.; Kahn, A.; Marder, S. R., *Chem.-Eur. J.* **2007,** 13, (12), 3537.

111. Kumar, S.; Rao, D. S. S.; Prasad, S. K., *J. Mater. Chem.* **1999,** 9, (11), 2751.

112. Lambert, C.; Noll, G., *Angew. Chem. Int. Ed.* **1998,** 37, (15), 2107.

113. Lambert, C.; Noll, G., *Chem.-Eur. J.* **2002,** 8, (15), 3467.

114. Tovar, J. D.; Rose, A.; Swager, T. M., *J. Am. Chem. Soc.* **2002,** 124, (26), 7762.

115. Pieterse, K.; van Hal, P. A.; Kleppinger, R.; Vekemans, J.; Janssen, R. A. J.; Meijer, E. W., *Chem. Mat.* **2001,** 13, (8), 2675.

116. Bosdet, M. J. D.; Piers, W. E.; Sorensen, T. S.; Parvez, M., *Angew. Chem. Int. Ed.* **2007,** 46, (26), 4940.

117. Bolger, J.; Gourdon, A.; Ishow, E.; Launay, J. P., *Inorg. Chem.* **1996,** 35, (10), 2937.

118. Friedman, A. E.; Chambron, J. C.; Sauvage, J. P.; Turro, N. J.; Barton, J. K., *J. Am. Chem. Soc.* **1990,** 112, (12), 4960.

119. Turro, C.; Bossmann, S. H.; Jenkins, Y.; Barton, J. K.; Turro, N. J., *J. Am. Chem. Soc.* **1995,** 117, (35), 9026.

120. Chambron, J. C.; Sauvage, J. P., *Chem. Phys. Lett.* **1991,** 182, (6), 603.

121. Murphy, C. J.; Arkin, M. R.; Jenkins, Y.; Ghatlia, N. D.; Bossmann, S. H.; Turro, N. J.; Barton, J. K., *Science* **1993,** 262, (5136), 1025.

122.Murphy, C. J.; Arkin, M. R.; Ghatlia, N. D.; Bossmann, S.; Turro, N. J.; Barton, J. K., *Proc. Natl. Acad. Sci.* **1994,** 91, (12), 5315.

123.Gupta, N.; Grover, N.; Neyhart, G. A.; Liang, W. G.; Singh, P.; Thorp, H. H., *Angew. Chem. Int. Ed.* **1992,** 31, (8), 1048.

124.Lemaur, V.; Da Silva Filho, D. A.; Coropceanu, V.; Lehmann, M.; Geerts, Y.; Piris, J.; Debije, M. G.; Van de Craats, A. M.; Senthilkumar, K.; Siebbeles, L. D. A.; Warman, J. M.; Bredas, J. L.; Cornil, J., *J. Am. Chem. Soc.* **2004,** 126, (10), 3271.

125.Lehmann, M.; Kestemont, G.; Aspe, R. G.; Buess-Herman, C.; Koch, M. H. J.; Debije, M. G.; Piris, J.; de Haas, M. P.; Warman, J. M.; Watson, M. D.; Lemaur, V.; Cornil, J.; Geerts, Y. H.; Gearba, R.; Ivanov, D. A., *Chem.-Eur. J.* **2005,** 11, (11), 3349.

126.Kaafarani, B. R.; Kondo, T.; Yu, J. S.; Zhang, Q.; Dattilo, D.; Risko, C.; Jones, S. C.; Barlow, S.; Domercq, B.; Amy, F.; Kahn, A.; Bredas, J. L.; Kippelen, B.; Marder, S. R., *J. Am. Chem. Soc.* **2005,** 127, (47), 16358.

127.Benniston, A. C.; Rewinska, D. B., *Org. Biomol. Chem.* **2006,** 4, (21), 3886.

128.Saeva, F. D.; Olin, G. R., *J. Am. Chem. Soc.* **1980,** 102, (1), 299.

129.Fetzer, J. C., *Large (C> = 24) Polycyclic Aromatic Hydrocarbons: Chemistry and Analysis*. Wiley-Interscience: New York, 2000.

130.Fetzer, J. C., *Polycyclic Aromatic Compounds* **2002,** 22, (3-4), 321.

131.Fetzer, J. C., *Polycyclic Aromatic Compounds* **2007,** 27, (2), 143.

132.Bijma, K.; Engberts, J., *Langmuir* **1997,** 13, (18), 4843.

133.Lu, W.; Fadeev, A. G.; Qi, B. H.; Smela, E.; Mattes, B. R.; Ding, J.; Spinks, G. M.; Mazurkiewicz, J.; Zhou, D. Z.; Wallace, G. G.; MacFarlane, D. R.; Forsyth, S. A.; Forsyth, M., *Science* **2002,** 297, (5583), 983.

134.Rogers, R. D.; Seddon, K. R., *Science* **2003,** 302, (5646), 792.

135.Cooper, E. R.; Andrews, C. D.; Wheatley, P. S.; Webb, P. B.; Wormald, P.; Morris, R. E., *Nature* **2004,** 430, (7003), 1012.

136.Wasserscheid, P.; Keim, W., *Angew. Chem. Int. Ed.* **2000,** 39, (21), 3773.

137.Faul, C. F. J.; Antonietti, M., *Adv. Mater.* **2003,** 15, (9), 673.

138.Faul, C. F. J., *Mol. Cryst. Liquid Cryst.* **2006,** 450, 255.

139. Guan, Y.; Zakrevskyy, Y.; Stumpe, J.; Antonietti, M.; Faul, C. F. J., *Chem. Commun.* **2003**, (7), 894.

140. Franke, D.; Vos, M.; Antonietti, M.; Sommerdijk, N.; Faul, C. F. J., *Chem. Mat.* **2006,** 18, (7), 1839.

141. Faul, C. F. J.; Antonietti, M.; Massa, W., *Acta Crystallogr. Sect. E.* **2004,** 60, O1769.

Chapter 2

Synthesis and Self-assembly of Centrally Charged Nitrogen Containing Polycyclic Aromatic Hydrocarbons

In the following chapter, the synthesis and characterization of centrally charged nitrogen containing polycyclic aromatic hydrocarbons (PAHs), 2-phenyl-benzo[8,9]quinolizino[4,5,6,7-*fed*]-phenanthridinylium (PQP) salts and its dibenzo derivates 2-phenyl-naphthacene[1,2]quinolizino[3,4,5,6-*def*]benzo[*i*]phenanthridinium (DBPQP) salts will be discussed. The self-assembly behavior of these centrally charged PAHs in solution as well as in the bulk will also be presented.

2.1 Introduction

2-Phenyl-benzo[8,9]quinolizino[4,5,6,7-*fed*]-phenanthridinylium (PQP) salt (**2-3**, Scheme 2-1), which is also called 9-phenyl-2,10b-diazadibenzo[*fg,op*]naphthacenium salt, was first reported by A. R. Katritzky *et al.* in 1979.[1] Its unique structure makes it an ideal candidate for the investigation of heteroatom containing polycyclic aromatic hydrocarbons (HPAHs) with positive charge because it can be viewed as both nitrogen centered dibenzopyrene and as pyridinium salt embedded in one extended polyaromatic system. As the first model compound in our study on HPAHs with positive charge, the synthesis of PQP salts is of significant importance because the conceivable synthetic strategy can not only be applied to developing various PQP derivates but also be used to guide the molecular design of even more complicated HPAHs with positive charge. However, after the first synthesis of PQP salts was

published[2], comprehensive research work on the synthesis of this centrally charged HPAH and its derivates is so far still absent. In this work, the synthesis of various PQP derivates, especially the key step, photocyclization was systematically studied. As the extension of the previous work done by Katritzky, a series of alkylated PQP derivates, 2-phenyl-9-alkylbenzo[8,9]quinolizino[4,5,6,7-*fed*]phenanthridinylium salts were synthesized by us. Furthermore, the synthesis of extended derivates of PQP salts with two additional fused benzene rings, 2-phenyl-11-alkylnaphthacene[1,2]quinolizino[3,4,5,6-*def*]benzo[*i*]phenanthridinium tetrafluoroborates (DBPQPBF_4), were also developed in this work. The UV-vis absorption and fluorescence spectra of these two different centrally charged PAHs were also compared.

As discussed in Chapter 1, the self-assembly of polycyclic aromatic hydrocarbons (PAHs) to form aggregates with different morphologies is attractive for supramolecular electronics.[3-6] The nanoscaled aggregates such as nanotubes and nanofibers obtained from π-π interactions between PAHs can provide charge transporting pathways, and thus can be used as active materials in electronic and optoelectronic devices.[7] The appropriate substituents like amphiphilic functional groups, linear or branched alkyl chains at the periphery of discotic PAHs such as triphenylene, dibenzonaphthacene and hexa-*peri*-hexabenzocoronene (HBC) improves both their processability and self-organization behavior. The latter advantage comes from the presence of additional intermolecular forces, including van der Waals interactions, amphiphilic interactions, hydrogen bonding or other noncovalent forces.[8-15] However, the introduction of substituents such as alkyl chains or polyethylene oxide (PEO) chains can only be preformed at the periphery of the discs. The incorporation of heteroatoms into the aromatic skeleton of such discotic molecules offers additional opportunities to influence strongly their electronic and self-organization properties. For example, hexaazatriphenylenes (HATPs) **1-88** show n-type charge-carrier transport characteristics, whereas all-hydrocarbon PAHs are p-type electronic materials.[16-20] Nevertheless, few centrally charged discotic PAHs

have been synthesized[1, 2], and to the best of our knowledge their aggregation behavior has not been reported. Due to this, the self-assembly behavior of alkylated PQP salts with different anions in solution as well as in the solid-state were investigated in our work. One-dimensional (1D) nanoscaled fibers (continuous threadlike aggregates), ribbons (flexible belt like aggregates) and tubular structures were formed in a defined manner by simply varying the length of the alkyl chains and the counterions of these amphiphilic PQP derivates. In order to further understand the effect of size and shape of aromatic core on the self-assembly behavior of the centrally charged PAHs, alkylated DBPQP salts were studied in a similar manner. Interestingly, two-dimensional (2D) vesicles were obtained conveniently from their methanolic solution which might be due to the unique symmetry and planarity of their aromatic parts. All the results will be discussed in detail in the following sections.

2.2 Synthesis and characterization of PQP derivates

2.2.1 General method to synthesize PQP salts

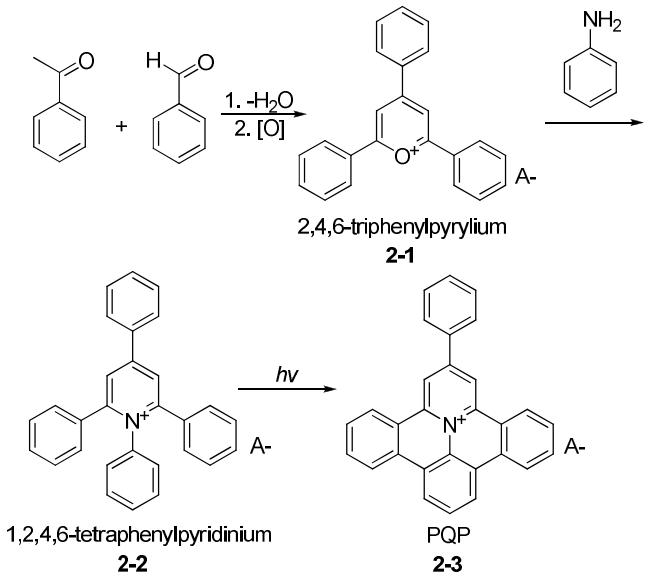

Scheme 2-1. Schematic illustration of the synthesis of PQP salts.

The general synthetic route toward PQP salt is outlined in Scheme 2-1. The first step is the condensation and succeeding oxidization of two equivalent of acetophenone and one equivalent of benzaldehyde which gives the corresponding

2,4,6-triphenylpyrylium salt **2-1**. This step can be done in one-pot[21-24] or multi-steps[25-27] and the yields are ranging from 30 to 40 %.

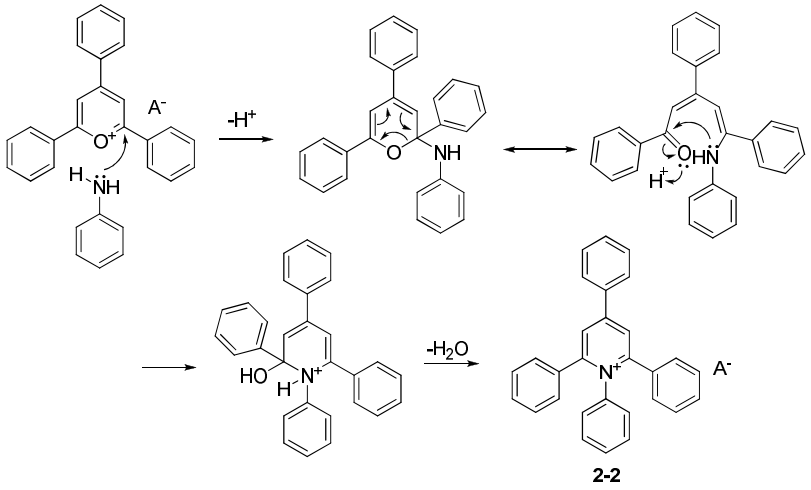

Scheme 2-2. Synthetic mechanism of 1,2,4,6-tetraphenylpyridinium salts

The second step is the synthesis of 1,2,4,6-tetraphenylpyridinium salts **2-2** from corresponding **2-1** and aniline. As shown in Scheme 2-2, it is a typical nucleophilic C-2 opening/recyclization of pyrylium salts.[28] Usually, this reaction can reach quantitative yield. Finally, the dehydrogenation of **2-2** by irradiating with UV light gives the target PQP salt **2-3** (Scheme 2-1). The photocyclization method toward PQP salts was first found by A. R. Katritzky and his co-workers incidentally when they tried to obtain benzyne via a photochemical decarboxylative elimination of the polyarylpyridinium betaines.[2] In our work, after comparing the other different cyclization methods for HPAHs such as intramolecular oxidative cyclodehydrogenation with Lewis acid and catalytic dehydrogenation, it turns out that photocyclization is so far the only effective method to attain PQP derivates and other heteroatom containing PAHs with positive charge. Katritzky *et al.* presumed that the photocyclization occurs in two stages via a monocyclised intermediate **2-4**, but they failed to isolate this intermediate in their work (Scheme 2-3a).[2] Remarkably enough, in our synthetic approach, the monocyclised intermediate **2-4** was successfully isolated through a controlled experiment, additionally its single crystal was obtained by recrystallization from methanolic solution and thus confirmed Katritzky's hypothesis (Scheme 2-3b).

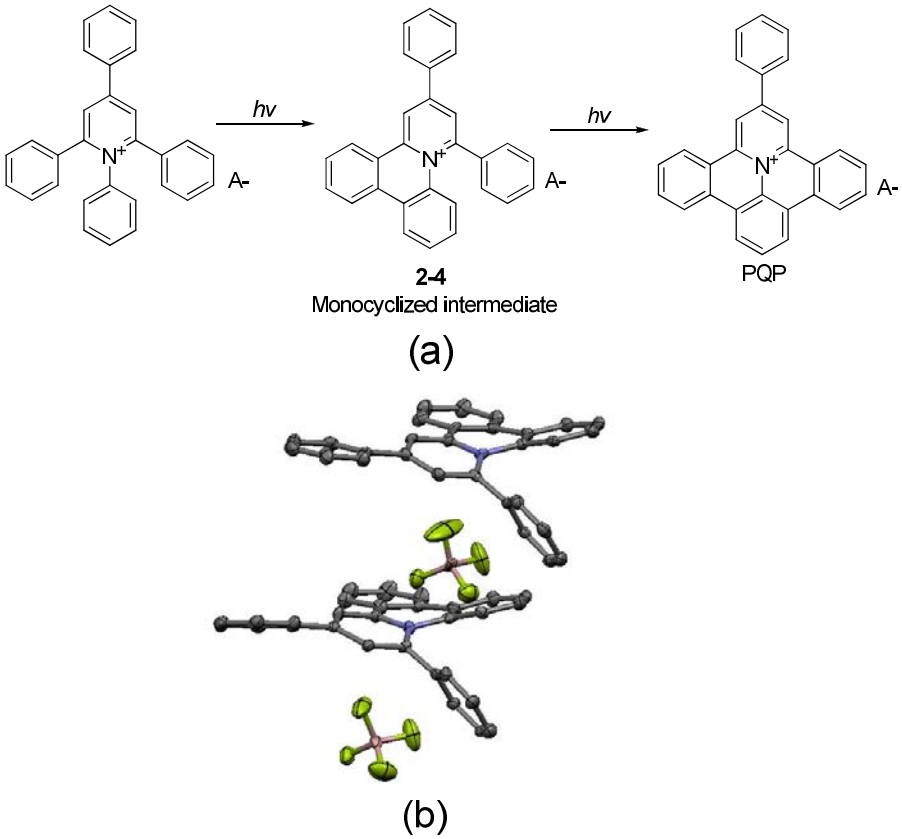

Scheme 2-3. (a) Synthesis of PQP salt via UV irradiation (in solution, 300 nm, r.t); (b) The crystal structure of monocyclised **2-4** with tetrafluoroborate (BF_4-) as anions.

2.2.2 Synthesis of alkylated PQP derivates

In Katritzky's pioneering work on the synthesis of PQP salts, only several methyl substituted PQP salts and their 9-aza analogs were reported.[1, 2] From the point view of material sciences, the synthesis of PQP derivates with more complicated structures is still required. In order to chemically modify a molecule, attaching alkyl chains is one of the most widely used synthetic concepts. Different alkyl chains were often used on ionic amphiphiles like pyridinium and imidazolium salts in order to modify their properties such as phase transition temperature and aggregation behavior in aqueous solution.[29] Recently, large PAH molecules, hexa-*peri*-hexabenzocoronenes (HBCs) with branched, bulky alkyl substituents of different lengths in the periphery of the aromatic core were synthesized to tune their self-assembly behavior both in the solution and in the bulk.[14] Accordingly, the introduction of suitable alkyl substituents

on PQP salts are expected to be remarkably interesting, because the amphiphlic structure can be engendered due to the comprisal of hydrophilic positively charged headgroup and hydrophobic alkyl tails. In general, amphiphilic molecules can self-assemble into aggregates with defined sizes and shapes in selective solvents that may be used in applications such as nanostructured electronics, light-energy conversion and mimicking biomineralization processes. Therefore, a series of novel alkylated PQP salts, 2-phenyl-9-alkylbenzo[8,9]quinolizino[4,5,6,7-*fed*]-phenanthridinylium salts (abbreviated as PQPX-n, where X stands for the anion and n corresponds to the number of methylene units in the alkyl chain) were synthesized in this work. The synthetic route of these molecules is shown in Scheme 2-4: The undehydrogenated precursors, 1-(4-alkylphenyl)-2,4,6-triphenylpyridinium salts were obtained directly from commercially available 2,4,6-triphenylpyrylium salts and 4-alkyl-anilines in nearly quantitative yields (90 - 98%). The photocyclization of these tetraarylpyridinium salts in mixed solvent (hexane : ethanol = 5 : 1) under 300 nm UV light and further recrystallization of the precipitated solids in ethanol gave corresponding PQP derivates (**2-10**, **2-11**, **2-12**, **2-13** and **2-14**) in good yields (41 - 66%). All molecules were characterized by ^{1}H and ^{13}C NMR spectroscopy, MALDI-TOF mass spectrometry as well as elemental analysis.

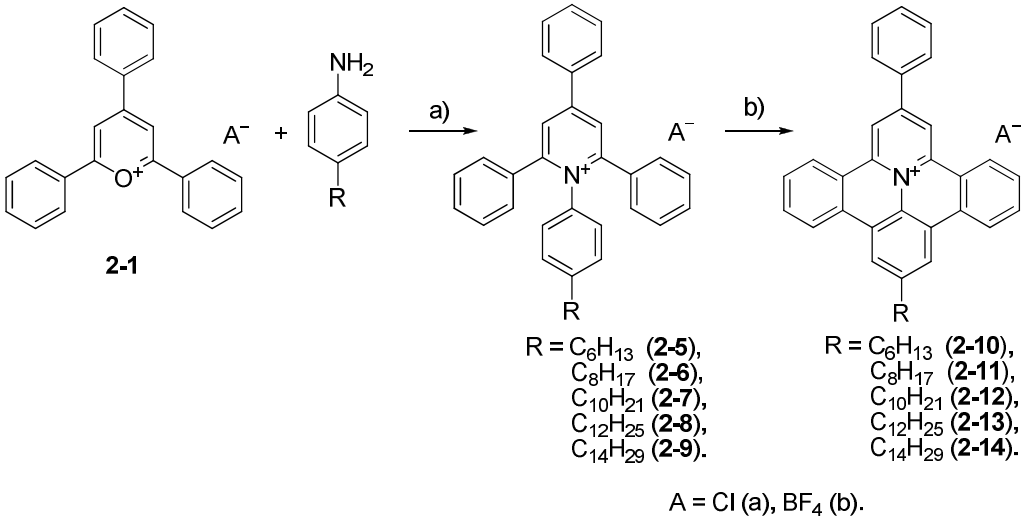

Scheme 2-4. Synthesis of PQPX-n; a) ethanol, refluxing, *c.a.* 6 hours; b) mixed solvent (hexane : ethanol = 5 : 1) , r.t. *hυ* (300 nm), *c.a.* 72 hours,.

It should be mentioned that a co-solvent system was very important for our synthesis of alkylated PQP salts. Usually, methanol was the most common solvent for photocyclization in the literature. However, methanol had good solubility for both starting 1,2,4,6-tetraphenylpyridinium salts and the resulting PQP salts. Large amounts of product would remain dissolved in their methanolic solution and the further irradiation of PQP salts could lead to unnecessary decomposition and decrease the yield. Due to this reason, a mixed solvent of hexane and ethanol was found to be suitable in our experiments. Very interestingly, this kind of co-solvents system bore the only limited solubility of the final PQP salts, thus nearly all the products precipitated during the cyclodehydrogenation, and the yield as well as purity of PQP salts could be improved considerably.

2.2.3 Synthesis and characterization of DBPQP derivates

Besides the attachment of different substituents, increasing the aromatic core size and altering the aromatic core shape are also very important synthetic concepts in developing novel PAH molecules. In our group, the synthesis of various all-hydrocarbon PAHs with different sizes and shapes has been developed in the last years.[30-33] These novel discotic nanographenes not only show interesting chemical and physical properties but also exhibit promising applications in material sciences.[34] In the case of centrally charged discotic PAHs, the molecules larger than PQP are also expected to be interesting as theoretic models, molecular building blocks as well as organic functional materials. It is therefore urgent for us to develop new synthetic concept to more extended nitrogen containing PAHs with positive charge. Herein, we present a class of unprecedented centrally charged PAHs, 2-phenyl-11-alkylnaphthacene[1,2]quinolizino[3,4,5,6-*def*]benzo[*i*]phenanthridinium tetrafluoroborates (DBPQPBF_4-n, where n corresponds to the number of methylene units in the alkyl chain), which can be viewed as the extended derivates of PQP salts with two additional fused benzene rings.

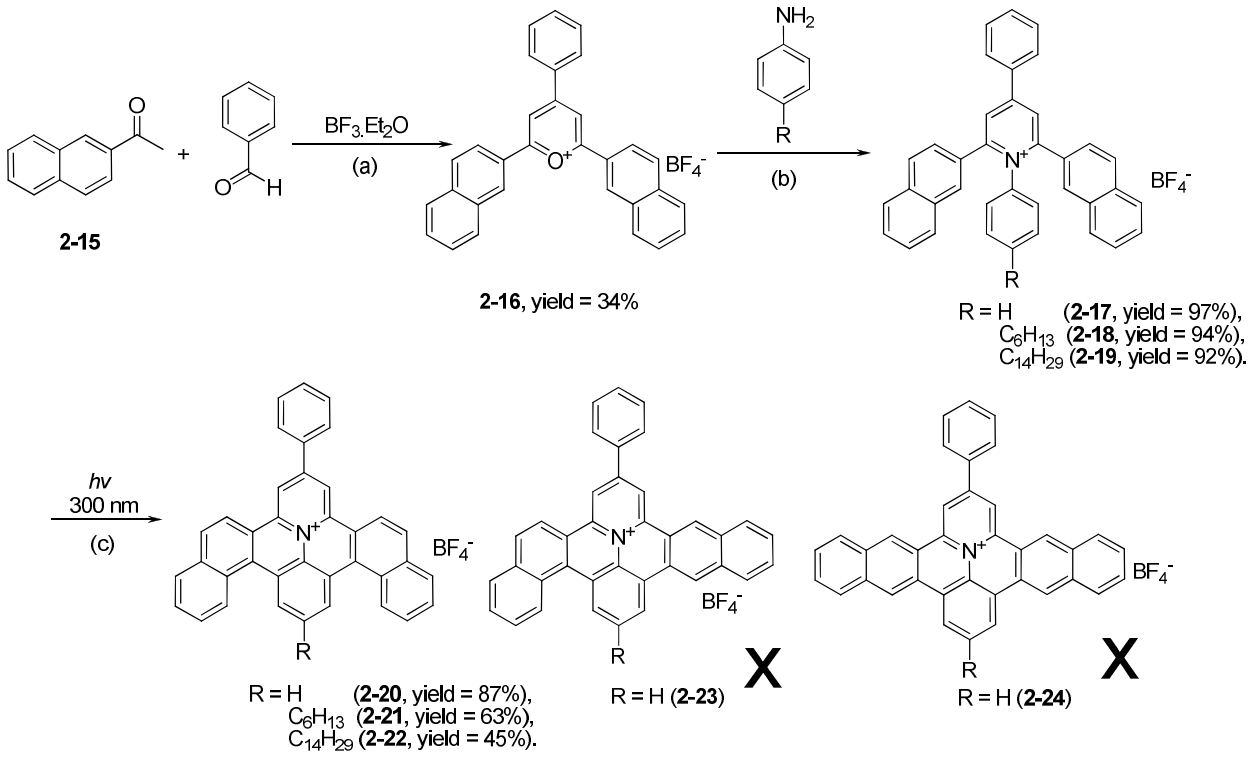

Scheme 2-5. Synthesis of DBPQPBF$_4$-n; (a) toluene, refluxing, 2 hours, yield = 34%; (b) ethanol, refluxing, *c.a.* 6 hours nearly quantitative yields; (c) mixed solvent (hexane : ethanol = 5 : 1), r.t., *hv*, *c.a.* 72 hours, yield = 87% (**2-20**), 63% (**2-21**) and 45% (**2-22**).

The detailed synthetic pathway to DBPQPBF$_4$-n is outlined in Scheme 2-5: The one-pot condensation-oxidization[21-24] of two equivalent of 1-(naphthalen-2-yl)ethanone (**2-15**) and one equivalent of benzaldehyde mediated by the Lewis acid catalyst, boron trifluoride etherate in anhydrous toluene gave 2,6-di(naphthalen-2-yl)-4-phenylpyrylium tetrafluoroborate (**2-16**) as red powder (yield 34%). The subsequent nucleophilic C-2 opening/recyclization of **2-16** and aniline in ethanol produced 1-(4-alkylphenyl)-2,6-di(naphthalen-2-yl)-4-phenylpyridinium tetrafluoroborate (**2-17**, **2-18** and **2-19**) in quantitative yields. The photocyclization of these tetraarylpyridinium precursors in mixed solvent (hexane : ethanol = 5 : 1) and following recrystallization of the precipitated solids in ethanol gave the corresponding 2-phenyl-11-alkylnaphthacene[1,2]quinolizino-[3,4,5,6-*def*]benzo[*i*]phenanthridinium tetrafluoroborates (DBPQPBF$_4$ **2-20**,

DBPQPBF$_4$-6 **2-21** and DBPQPBF$_4$-14 **2-22**) in good yields. All molecules were characterized by ^{1}H and ^{13}C NMR spectroscopy, MALDI-TOF mass spectrometry as well as elemental analysis.

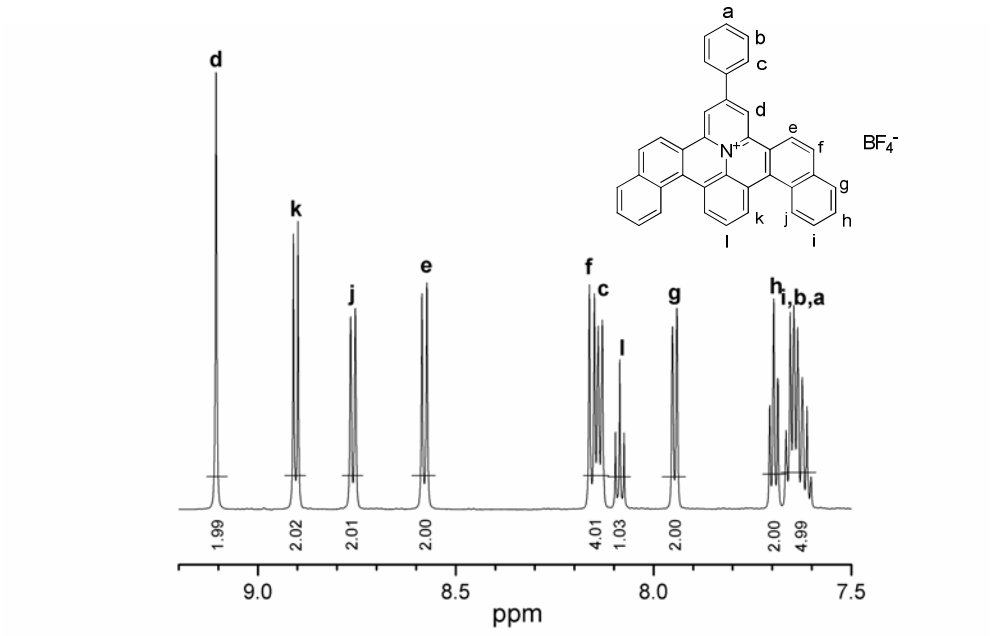

Figure 2-1. The ^{1}H NMR spectra (700MHz, r.t., CD_2Cl_2) of the dehydrogenated product **2-20**.

It is interesting to note that the dehydrogenated product of **2-17** was only compound **2-20** without other isomers such as **2-23** or **2-24**. The structure of **2-20** was unraveled by its ^{1}H NMR spectra. As shown in Figure 2-1, ^{1}H NMR spectrum (700 MHz) of the product clearly exhibited 12 groups of peaks which suggested that the product was not the mixture of several isomers but a pure compound. Compound **2-23** could firstly be excluded because its asymmetric structure would result in 17 groups of different peaks. On the other hand, **2-24** should include three single peaks and four double peaks, and thus could be excluded since there were only one single peak and at least 5 double peaks as indicated in Figure 2-1. Accordingly, compound **2-20**, whose spectrum should contain one singlet, one ab-, one ab_2-, one ab_2c_2- and one abcd-system, was the only possible product after dehydrogenation. Similarly, the ^{1}H NMR spectra of dehydrogenated products of alkylated teterarylpyridinium salts **2-18** and **2-19** also indicated that they were pure products without isomers (compound **2-21** and **2-22**) which had the same aromatic core as **2-20** (The spectra are not shown here.).

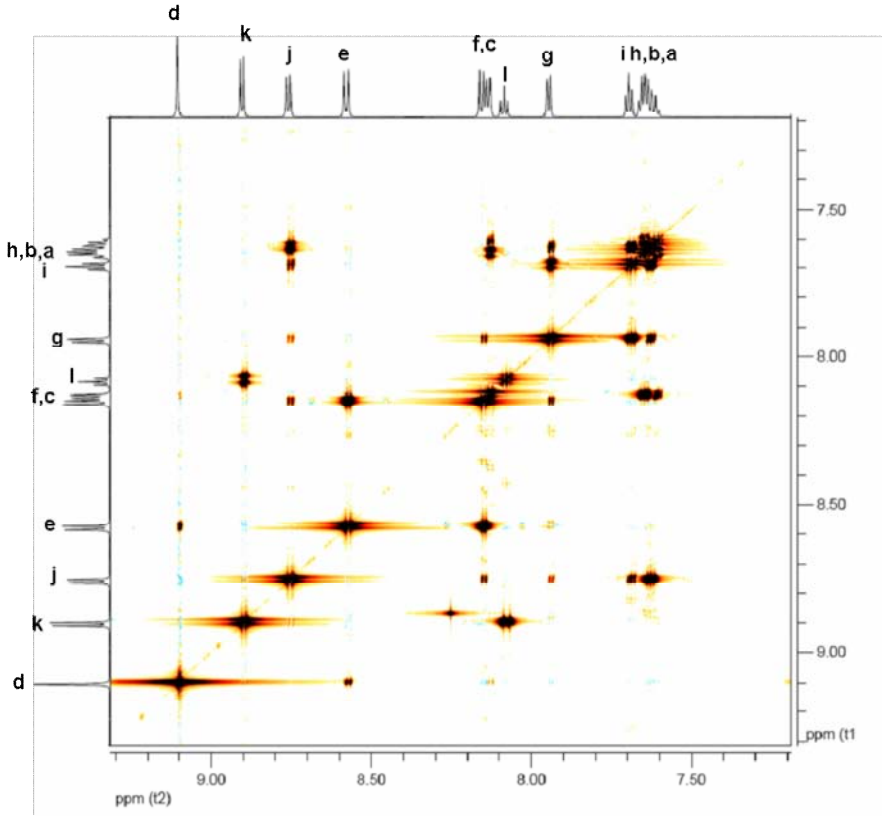

Figure 2-2. The ^{1}H-^{1}H COSY spectra (700MHz, r.t., CD_2Cl_2) of **2-20**.

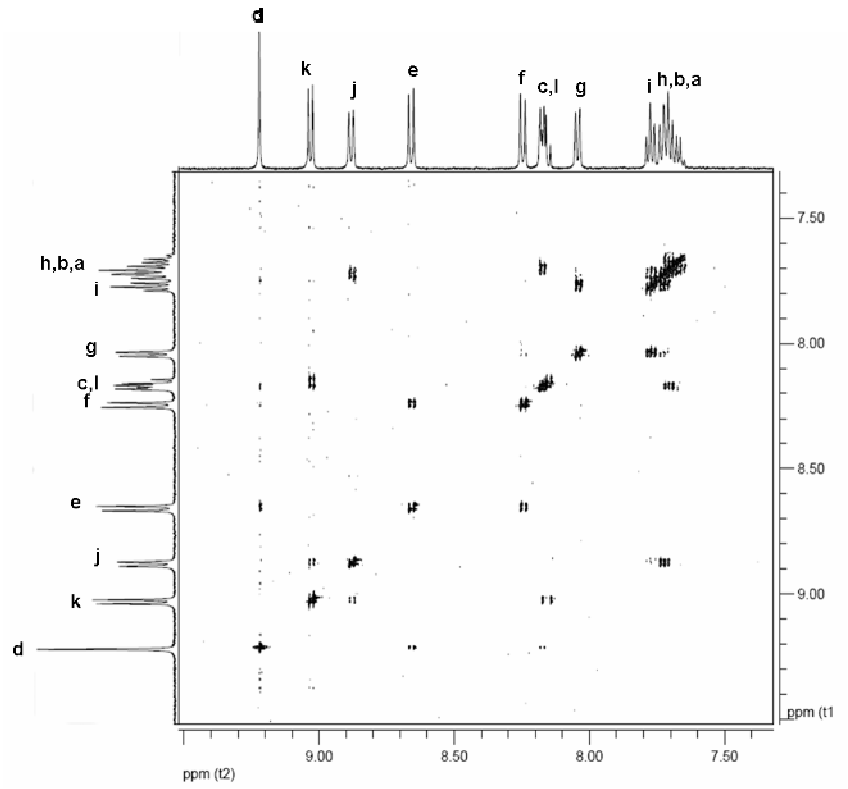

Figure 2-3. The ^{1}H-^{1}H NOESY spectra (500MHz, r.t., CD_2Cl_2) of **2-20**.

The proton signals of **2-20** were further adscripted according to its ^{1}H NMR spectrum together with H,H-COSY and H,H-NOESY spectra (Figure 2-1, 2-2 and 2-3). The proton signal (9.11 ppm, 2H) from proton **d** could be firstly identified as it was the only singlet in the spectra. By using this singlet as starting point, the signal of proton **e** could be assigned to the doublet at 8.58 ppm (2H) due to their correlation in H,H-COSY and H,H-NOESY spectra. Similarly, the coupling between the doublet of proton **e** and another doublet at 8.15 ppm indicated that it was originated from proton **f** (ab-system, Figure 2-2 and 2-3). On the other hand, the doublet at 8.13 ppm (2H) was ascribed to proton **c** due to its weak coupling with the singlet of proton **d** in the H,H-COSY spectrum. As shown in the H,H-NOESY spectrum of **2-20**, the coupling between the doublet of proton **c** and the doublet at 7.64 ppm (2H) indicated that the latter was due to proton **b**. Consequently, the triplet at 7.62 ppm (1H) was assigned to proton **a** in the ab_2c_2-system because it not only coupled with proton **c** (Figure 2-2) but also correlated to proton **b** (Figure 2-3). The other triplet (8.09 ppm) with the intensity of one was then ascribed to proton **l**. This triplet showed coupling with the doublet at 8.90 ppm (2H) in the H,H-NOESY spectrum, which should belong to proton **k** in the ab_2-system. The correlation between the signal of proton **f** and the doublet at 7.94 ppm (2H) proved this doublet was from proton **g**. The NOE cross peak in the H,H-NOESY which was resulted from the triplet at 7.70 ppm (2H) and the doublet of proton **g** indicated that the triplet was the signal of proton **h**. The last doublet at 8.76 ppm (2H) could be consequently assigned to proton **j**. According to the coupling between it and the triplet at 7.66 ppm (2H), the latter was justified as the signal from proton **i** in the abcd-system.

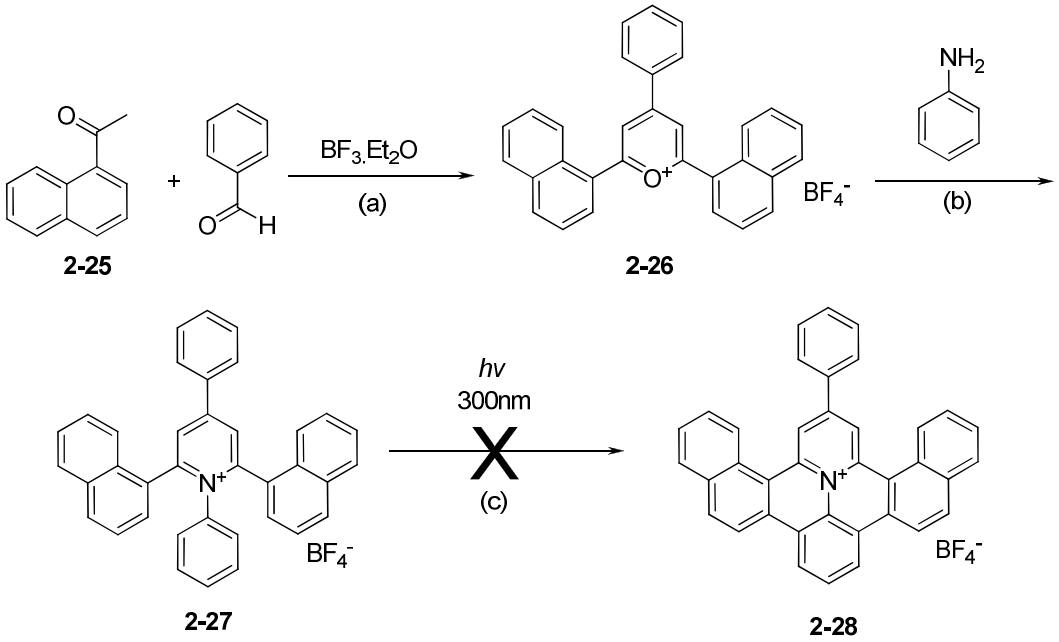

Scheme 2-6. Attemped synthesis of another isomer of DBPQPBF$_4$ **2-28**; (a) toluene, refluxing, 2 hours, yield = 28%; (b) ethanol, refluxing, *c.a.* 6 hours, yield = 94%; (c) mixed solvent (hexane : ethanol = 5 : 1), r.t., *hυ*, 72 hours.

In order to obtain more centrally charged discotic PAHs with varied structures, one isomer of **2-17**, 1-phenyl-2,6-di(naphthalen-1-yl)-4-phenylpyridinium tetrafluoroborate (**2-27**) was synthesized. As shown in Scheme 2-6, 2,6-di(naphthalen-1-yl)-4-phenylpyrylium tetrafluoroborate (**2-26**) could firstly be obtained from the one-pot reaction between two equivalent of 1-(naphthalen-1-yl)ethanone (**2-25**) and one equivalent of benzaldehyde with boron trifluoride etherate as catalyst in a moderate yield. Subsequent reaction between compound **2-26** and aniline results in compound **2-27** (MW = 484 without anion) in a yield of 94%. In the interest of getting an isomer of DBPQP salt **2-20**, the solution of **2-27** was irradiated with 300 nm UV light for 72 hours. However, the expected dehydrogenated product **2-28** (MW = 480 without anion) could not be detected by mass spectroscopy even after long time UV irradiation (Figure 2-4).

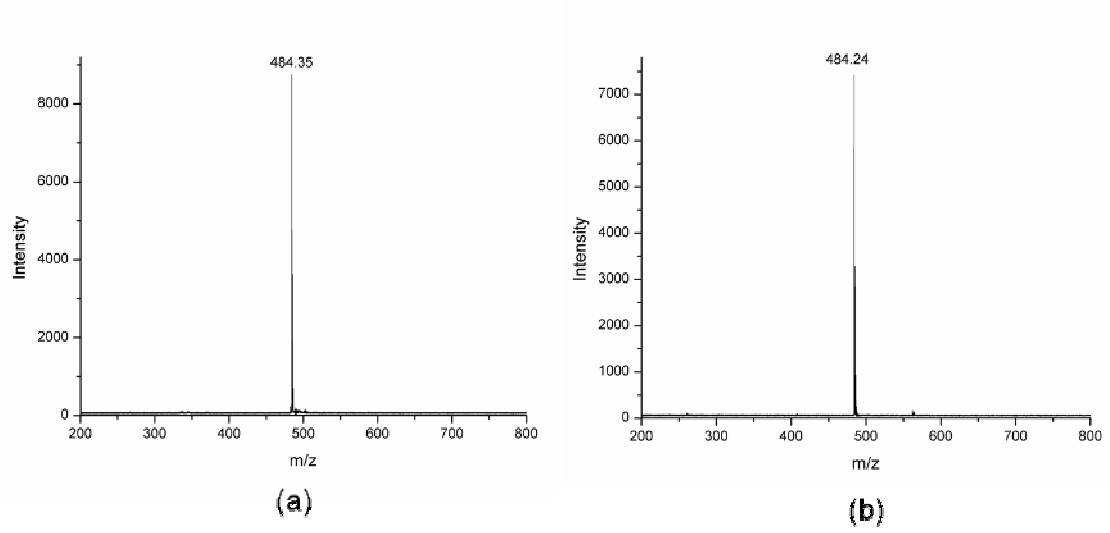

Figure 2-4. MALDI-TOF mass spectra of **2-27** in mixed solvent (hexane : ethanol = 5 : 1): (a) before UV irradiation; (b) after 72 hours' irradiation (300 nm, r.t.).

The successful synthesis of DBPQP salt **2-20** without isomers (Scheme 2-5) and the failure to synthesize compound **2-28** (Scheme 2-6) indicated that the photocyclization of tetraarylpyridinium salts was highly selective. Obviously, in both cases, the ß protons of naphthyl substituents were inert to photochemical dehydrogenation conditions and only the protons at α position were active enough to be eliminated under UV irradiation. This phenomenon is expected to be helpful to direct the future molecular design of similar centrally charged PAHs under UV irradiations.

2.2.4 UV-vis absorption and fluorescence spectra of PQP and DBPQP salts

In the interest of understanding the effect of the shape and size of aromatic core on the physical properties of the centrally charged PAHs, the UV-vis absorption and fluorescence spectra of PQPBF$_4$-14 **2-14b** and DBPQPBF$_4$-14 **2-22** in methanol were compared in Figure 2-5. The absorption spectrum of compound **2-14b** was dominated by a strong band located at 305 nm (log ε = 4.88) followed by two weak absorption bands at longer wavelength region 348 (log ε = 4.43) and 430 nm (log ε = 4.00) (Figure 2-5a). Compared with **2-14b**, compound **2-22** showed similar absorption

bands in which the first main band split to two peaks at 306 (log ε = 4.92) and 328 (log ε = 4.90) nm, and the other two low energy bands were located at 380 (log ε = 4.31), and 479 nm (log ε = 4.03) respectively. On the other hand, both molecules exhibited structureless emission peaks in their fluorescence spectra. Remarkably, the emission maximum at 529 nm for **2-22** was red-shifted by 63 nm compared with **2-14b**. The obvious difference of the absorbance and fluorescence spectra between **2-14b** and **2-22** indicated a strong influence of the extension of the aromatic core size and symmetry[35, 36] for centrally charged PAHs on their photophysical properties.

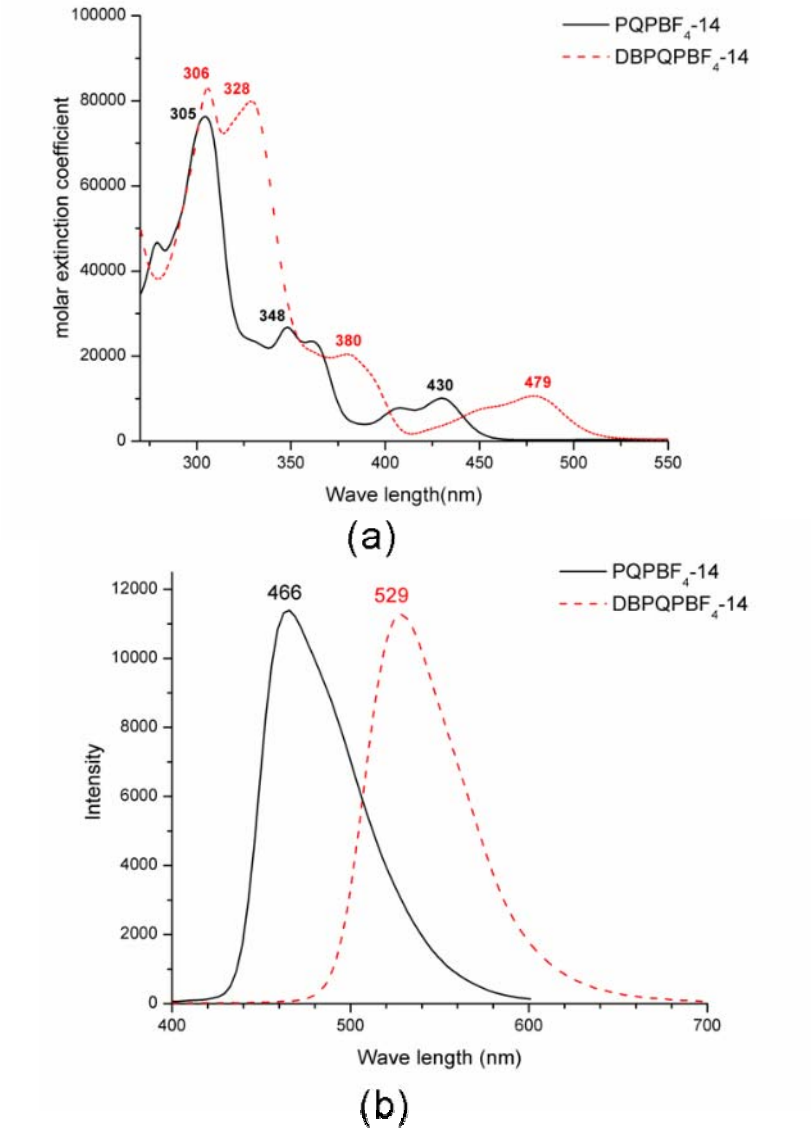

Figure 2-5. (a) UV-vis absorption and (b) fluorescence spectra of the methanolic solution of centrally charged PAHs **2-14b** and **2-22** (methanolic solution, r.t.).

2.3 Self-assembly behavior of PQP and DBPQP salts

As mentioned in Section 2.2.2, centrally charged nitrogen containing PAHs with alkyl chains are amphiphilic molecules and are expected to form ordered aggregates in selective solvent. Due to this, the self-assembly behavior of PQP salts having different anions or alkyl chains (**2-10**, **2-11**, **2-12**, **2-13** and **2-14**) together with DBPQP tetrafluoroborate bearing different alkyl chains (**2-21** and **2-22**) in solution and in the bulk were investigated in this work. One-dimensional (1D) nanoscaled fibers, ribbons, helical and tubular structures as well as two-dimensional (2D) vesicles were formed conveniently and in a defined manner from their methanolic solutions by simply varying the length of the alkyl chains, the size of counterions and the aromatic discs of the centrally charged PAHs. A mechanism of PQP and DBPQP aggregation was also proposed here.

2.3.1 The effect of alkyl chains

As the most widely used technique to detect the aggregates in solution[37], dynamic light scattering (DLS) experiments were first used to investigate the self-assembly behavior of PQP salts in solution. Methanol was chosen as the solvent in this work because it had good solubility for centrally charged aromatic core of PQP salts and poor solubility for their alkyl chains. In order to find out their critical aggregation concentration (CAC), the DLS experiments of methanolic solutions of PQPCl-6 **2-10a** and PQPCl-14 **2-14a** at different concentrations were preformed. According to their autocorrelation functions (not shown), PQPCl-6 and PQPCl-14 exhibited aggregation behavior at 7.3×10^{-4} mol/L (0.4 g/L) and 3.6×10^{-4} mol/L (0.24 g/L) respectively, which indicated that these PQP salts began to form detectable aggregates above these concentrations. The hydrodynamic radii of the aggregates from PQPCl-6 and PQPCl-14, R_h, were 28 nm and 77 nm, respectively (Figure 2-6).

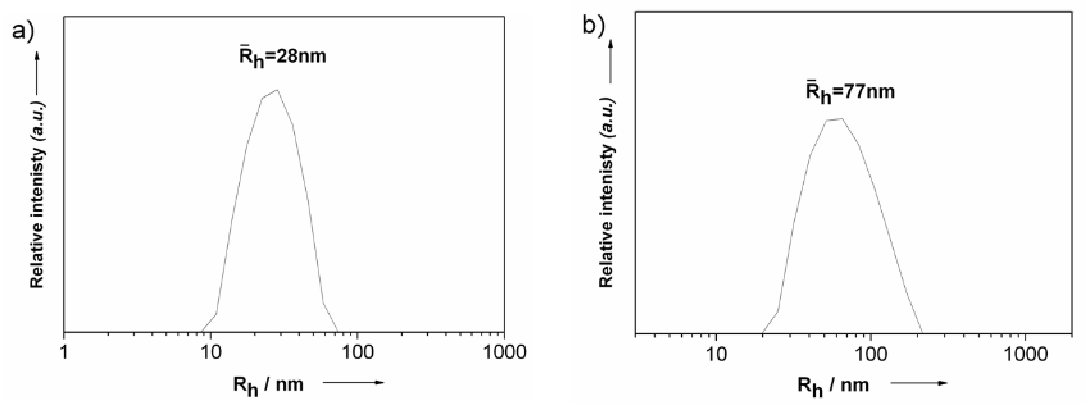

Figure 2-6. The intensity-weighted distribution of the aggregates formed by (a) PQPCl-6 ($7.3x10^{-4}$ mol/L in methanol) and (b) PQPCl-14 ($3.6x10^{-4}$ mol/L in methanol) obtained from the DLS measurements at 25 °C.

Evidence for the formation of the aggregates in methanol was additionally provided by using electron microscopy techniques. The aggregates could be transferred to surfaces[38, 39] by drop-casting methanolic solutions of PQPCl-6 and PQPCl-14 on substrates (silicon wafers or carbon covered copper grids) and removing the solvent quickly with a piece of filter paper (Figure 2-7). It should be noted that these aggregates were reproducibly formed, even on different substrate surfaces such as silicon, glass and highly ordered pyrolytic graphite (HOPG), which further proved that these aggregates were formed in solution but not during the solvent evaporation. Scanning electron microscopy (SEM) and transmission electron microscopy (TEM) images indicated that PQPCl-6 aggregated to fibers with a uniform width of *ca.* 40 nm (Figure 2-7a). In contrast to the cylinder-like fibers formed by PQPCl-6, PQPCl-14 self-assembled into ribbon-like aggregates with a width of 80 nm and lengths ranging from 0.5 to 2 μm (Figure 2-7b). The different thicknesses of the ribbons (Figure 2-7c) suggested that the ribbons were composed of overlapping sheets to form a layer-by-layer structure (so-called lamellar packing, see Figure 2-17). The occasionally twisted ribbons (Figure 2-7d) demonstrated that these aggregates were flexible. The morphological differences between PQPCl-6 and PQPCl-14 suggested a different packing mode for the two molecules, which was further supported by wide angle X-ray scattering (WAXS) measurements of the dried powders obtained from

their methanolic solutions.

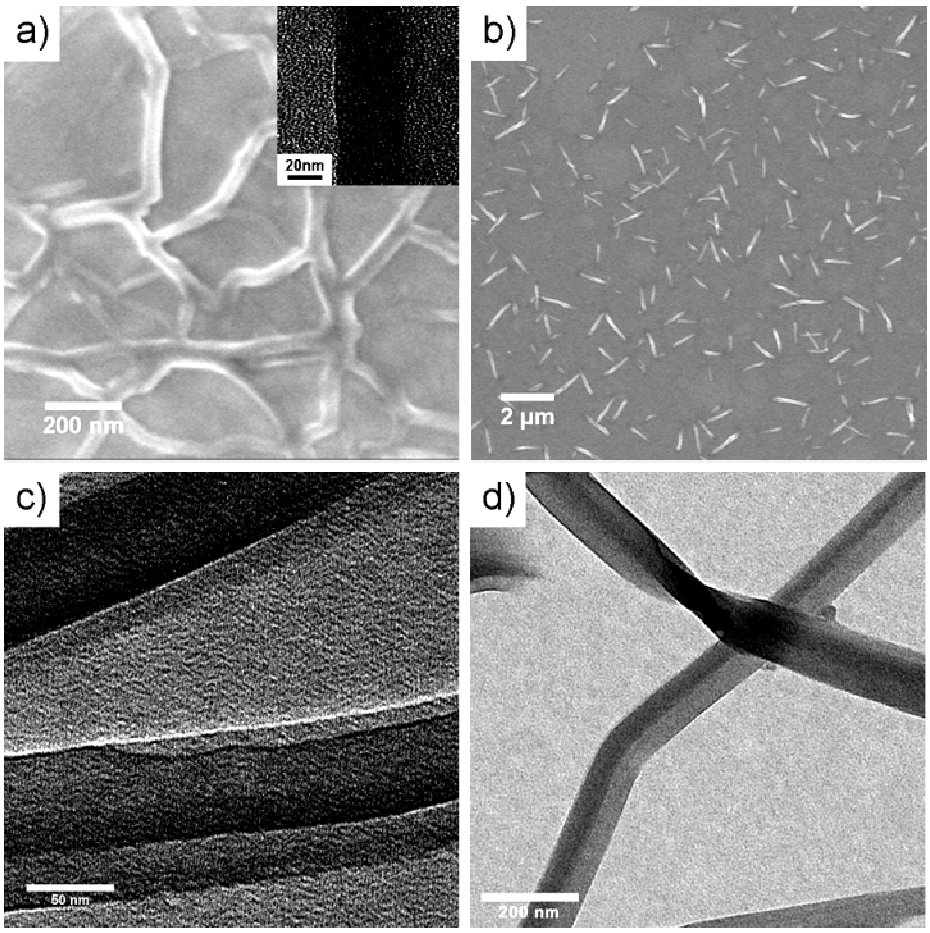

Figure 2-7. (a) SEM and TEM images (insert) of aggregates formed by PQPCl-6 ($1x10^{-3}$ mol/L in methanol, drop-cast on substrates); (b) SEM images of aggregates formed by PQPCl-14; (c) and (d) TEM images of aggregates formed by PQPCl-14 at different magnification ($1x10^{-3}$ mol/L in methanol, drop-cast on substrates).

The WAXS pattern of PQPCl-14 (Figure 2-8) showed intense reflections with d spacings of 40.1, 19.6 and 13.2 Å, which were characteristic of a lamellar structure.[40] Considering that the fully extended molecular length of PQPCl-14 was 28 Å (The MM2 force field was used to calculate the minimum-energy conformation during computer simulations.), each lamella sheet might consist of two interdigitated PQPCl-14 molecular layers (Figure 2-17). In contrast, PQPCl-6 did not adopt such a lamellar structure according to WAXS analysis (Figure 2-8). On the other hand, compared with PQPCl-14, PQPCl-6 exhibited a clear shift of its diffraction peaks to

larger angles in the range of 10 to 30°, suggesting a more condensed packing of the discotic molecular units.

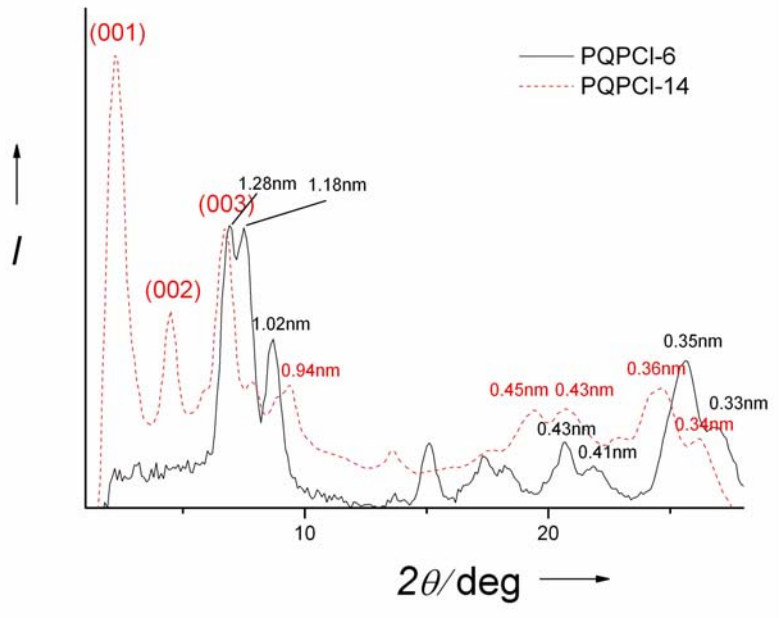

Figure 2-8. WAXS patterns of the dried powder of PQPCl-6 and PQPCl-14 obtained from their methanolic solutions.

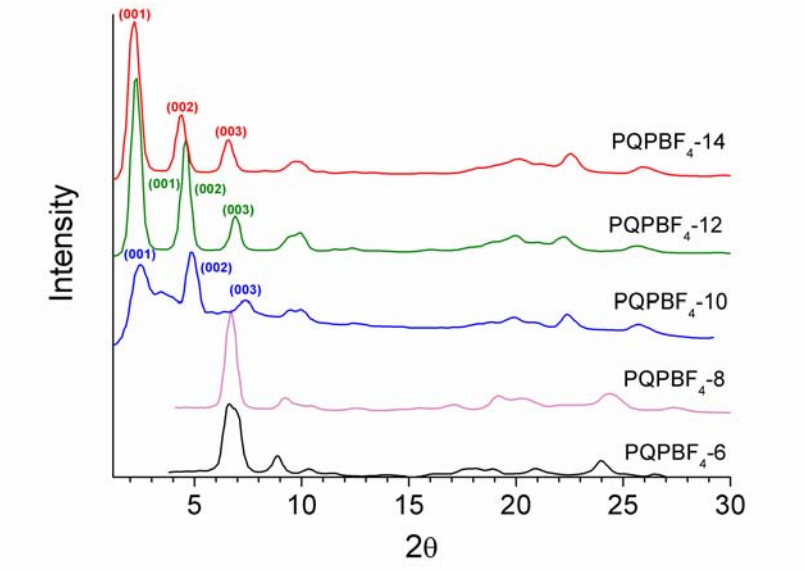

Figure 2-9. WAXS patterns of the dried powder of $PQPBF_4$-n (n = 6, 8, 10, 12, 14) obtained from their methanolic solutions.

In order to gain a more comprehensive understanding of the effect of the alkyl chain length on the self-assembly of PQP salts, the WAXS patterns of $PQPBF_4$ salts with different alkyl chains ($PQPBF_4$-6, **2-10b**; $PQPBF_4$-8, **2-11b**; $PQPBF_4$-10, **2-12b**;

$PQPBF_4$-12, **2-13b**; $PQPBF_4$-14, **2-13b**) were also compared. As shown in Figure 2-9, $PQPBF_4$-8 had a similar pattern to $PQPBF_4$-6 which indicated that they might adopt a similar molecular packing structure. Different from these two $PQPBF_4$ salts, the characteristic diffractions of lamellar stacking appeared in the WAXS patterns of $PQPBF_4$-n when their alkyl chain was longer than octyl (C10). This suggested that $PQPBF_4$-10, $PQPBF_4$-12 and $PQPBF_4$-14 could form layered structures like PQPCl-14. As observed in the case of PQPCl-6 and PQPCl-14, a morphology transformation of $PQPBF_4$-n could also occur when their alkyl chain changed from short chains (C6 and C8) to longer ones (C10, C12 and C14).

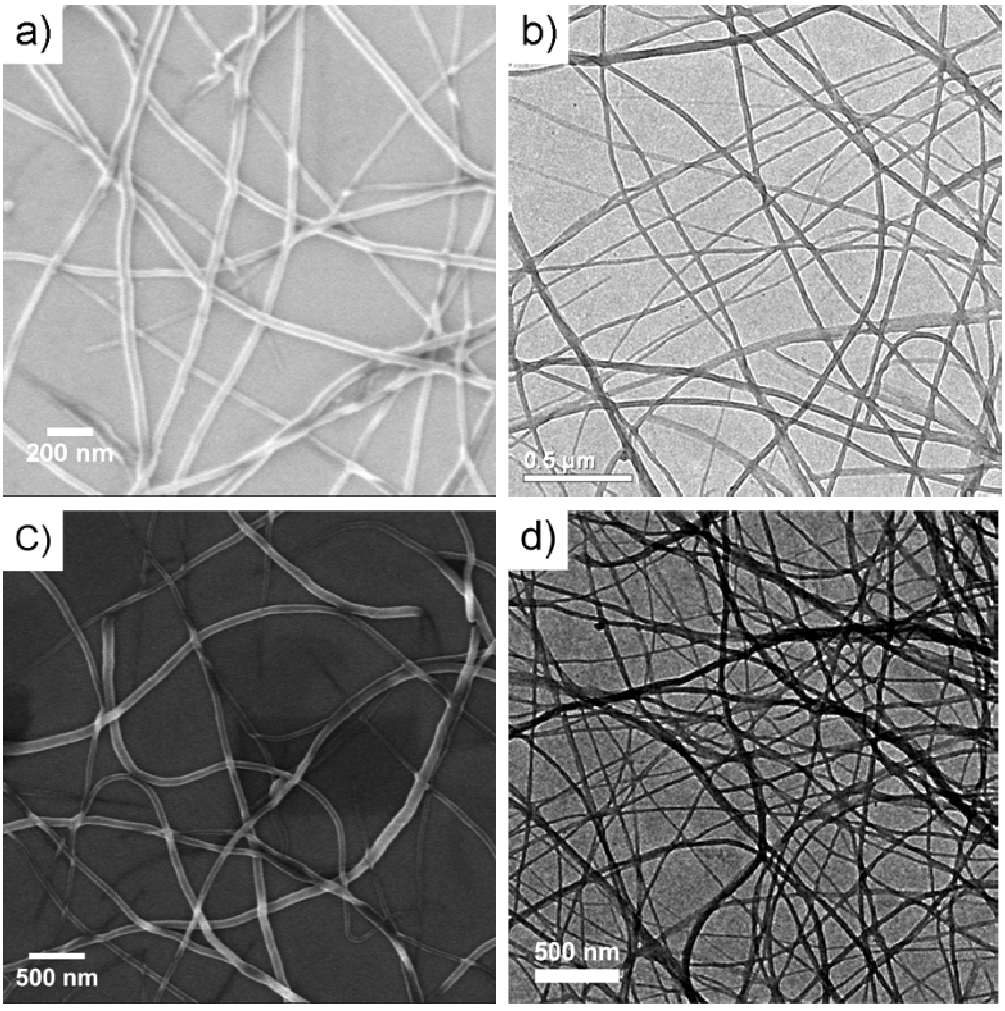

Figure 2-10. (a) SEM image and (b) TEM image of the aggregates formed by $PQPBF_4$-6 ($1x10^{-3}$ mol/L in methanol, drop-cast on substrates); (c) SEM image and (d) TEM image of the aggregates formed by $PQPBF_4$-8 ($1x10^{-3}$ mol/L in methanol, drop-cast on substrates).

Subsequently, the morphology of the aggregates from these $PQPBF_4$ salts was also studied with electron microscopy after drop-casting their methanolic solution on substrates (silicon wafers for SEM or carbon covered copper grids for TEM). A morphology change which was consistent with the results of the WAXS diffractions was observed. As shown in their electron microscopy images (Figure 2-10), $PQPBF_4$-6 and $PQPBF_4$-8 formed solid fibers which were similar to PQPCl-6. However, the fibrous structures for $PQPBF_4$-6 and $PQPBF_4$-8 seemed to be more separated and straight whereas the fibers from PQPCl-6 tended to form a network like structures.

The SEM images of $PQPBF_4$-10, $PQPBF_4$-12 (Figure 2-11) and $PQPBF_4$-14 (Figure 2-12) indicated that they also self-assembled into fiber-like aggregates with however shorter length and wider diameter. Interestingly, some of these aggregates were helical structures with varying pitches, which further confirmed their different packing behavior with $PQPBF_4$-6 and $PQPBF_4$-8.

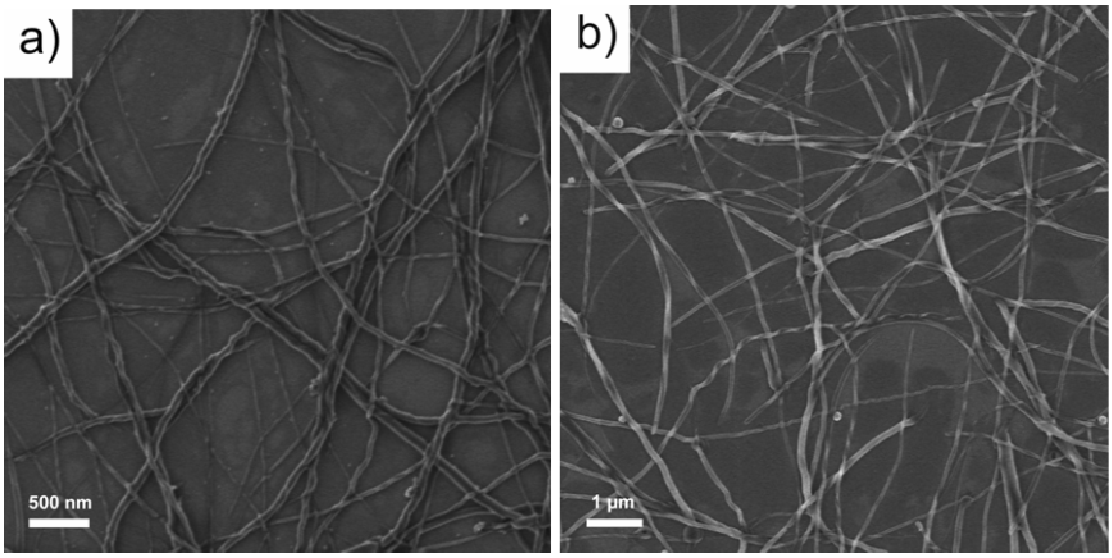

Figure 2-11. (a) SEM image of the aggregates formed by $PQPBF_4$-10($1x10^{-3}$ mol/L in methanol, drop-cast on a silicon wafer); (b) SEM image of the aggregates formed by $PQPBF_4$-12($1x10^{-3}$ mol/L in methanol, drop-cast on on a silicon wafer).

Among these three PQP salts mentioned above, the aggregates of $PQPBF_4$-14 were specified for a more detailed investigation since it contained the same tetradecyl

chain as PQPCl-14. Different from the ribbons obtained from PQPCl-14, relatively longer aggregates were formed from $PQPBF_4$-14 with a length of around 5 μm and a diameter ranging from 80 to 150 nm (Figure 2-12a, 2-12b). TEM characterization disclosed that many of the non-helical aggregates were actually nanotubes with a wall thickness of 40-60 nm and an inner diameter of 20-50 nm (Figure 2-12c, 2-12d). The different thickness of the tube walls (Figure 2-12c) implied that the tubes were also constructed *via* lamellar packing similar to the ribbons from PQPCl-14.

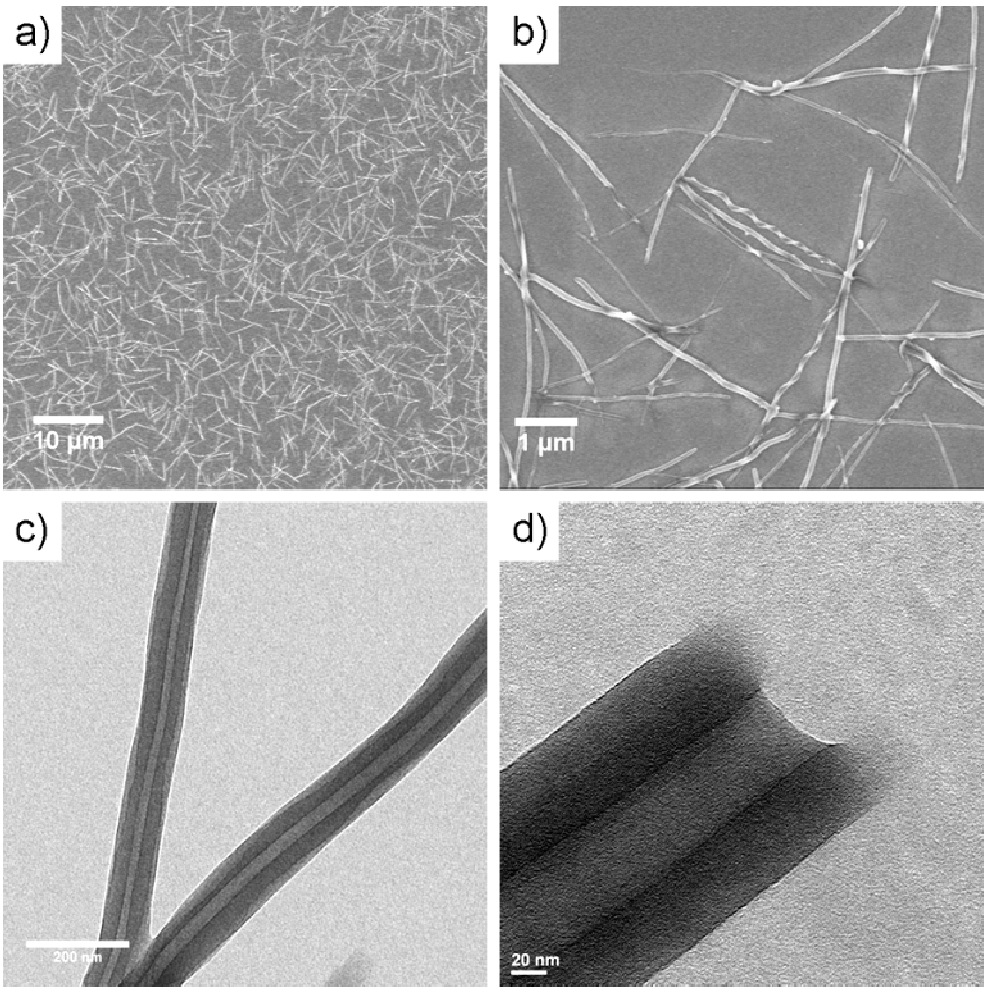

Figure 2-12. (a), (b) SEM and (c), (d) TEM images of the aggregates formed by $PQPBF_4$-14($1x10^{-3}$ mol/L in methanol, drop-cast on substrates).

The morphology change of PQP salts from fibers to layered aggregates such as ribbons and tubes could be explained by the packing parameter theory brought forwarded by Israelachivili.[41-44] This theory proposed that the morphology formed by an amphiphilic molecule was dependent upon its packing parameter, $P = v/(a_0 l_c)$,

where v was the volume of the hydrophobic chain, a_0 was the surface area of the hydrophobic core of the aggregate expressed per molecule in the aggregate (hereafter referred to as the area per molecule), and l_c was the chain length. If $P < 1/3$, spherical and ellipsoidal aggregates were favored morphologies; if $1/3 < P < 1/2$, the amphiphile tended to form cylindrical rods; if $1/2 < P \leq 1$, bilayer structures such as vesicles, tubes and lamellae were preferred (Figure 2-13).

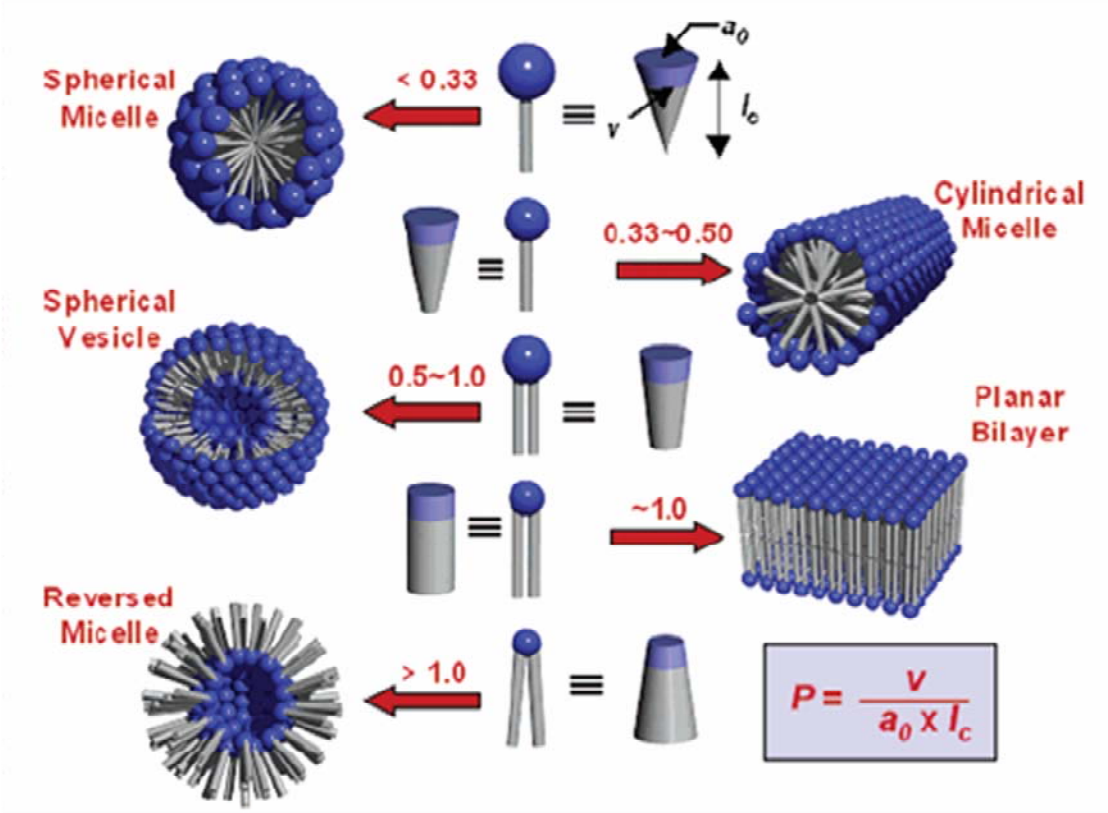

Figure 2-13. Various self-assembled morphologies depending on the critical packing parameter (P) of the amphiphilic molecules.

The decisive parameters in Israelachivili's theory were the aggregation number N, which determined the entropy, and the optimum surface area per molecule (at the hydrocarbon-water-interface) a_0, which itself was determined by the interplay between attractive and repulsive molecular interactions. The most likely aggregate was the one, which had the smallest aggregation number N (and thus the largest entropy), a molecular area a close to the optimum value a_0 and l smaller than the length of the stretched hydrocarbon chain. According to this, the ribbons from

PQPCl-14 or the tubes from $PQPBF_4$-14 had a larger aggregation number *N* than the fibers from PQPCl-6 or $PQPBF_4$-6. This corresponded to a smaller optimal surface area per molecule a_0 and an increase of the aggregation parameter *P*. Generally, for common surfactants, the tail length had no significant impact on the packing parameters, especially in the case of cylindrical and lamellar aggregates.[45, 46] However, in this work, the transition from fibers to layered structures such as ribbons and tubes was observed upon changing the hexyl chains to tetradecyl chains. The possible reason could be that the presence of the PAH part in the PQPs reduced the Coulombic repulsion between the positively charged molecules and enhanced their stacking by additional aromatic interactions. For example, strong π-π interactions between PQP molecules could be detected by electron diffraction analysis of the aggregates from both PQPCl-6 and PQPCl-14 (Figure 2-14).

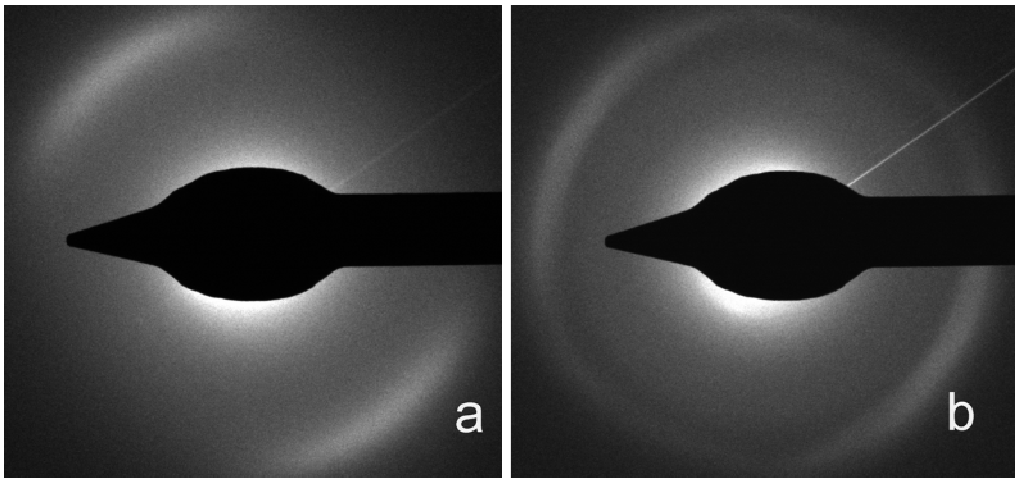

Figure 2-14. Electron diffraction images of the PQP aggregates ($1x10^{-3}$ mol/L in methanol, drop-cast on carbon film covered copper grids): (a) PQPCl-6; (b) PQPCl-14.

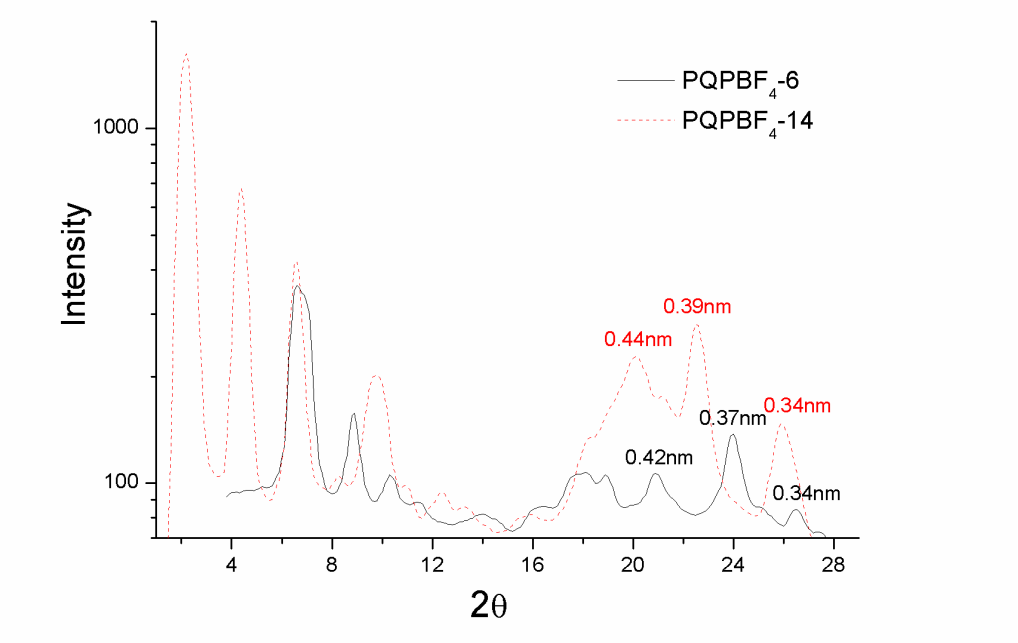

Figure 2-15. WAXS patterns of the dried powder of $PQPBF_4$-6 and $PQPBF_4$-14 obtained from methanolic solution.

The difference of the aromatic interaction between PQPX-6 and PQPX-14 could be identified from their WAXS patterns. Compared with PQPCl-6 and $PQPBF_4$-6, the less condensed, but even more ordered stacking of PQPCl-14 and $PQPBF_4$-14 which were obvious from their WAXS could be attributed to the increase in the length of tails (Figure 2-8 and Figure 2-15). The steric hindrance induced by the long alkyl chains probably prevented the aromatic parts from approaching each other.[13, 14] However, with the consideration that the packing parameter *P* of the ribbon was increased, the intramolecular interactions between these amphiphilic PQP molecules such as solvophobic effects and attractive interactions between the chains became more important in achieving lower interaction free energies and a smaller optimal surface area per molecule a_0.[42, 43] It is known that differences in substituent groups could significantly influence the aggregation behavior of polypeptides and conjugated polymers[47-51], and it is now evident that the same is true for the PQP salts described here.

2.3.2 The effect of counterions

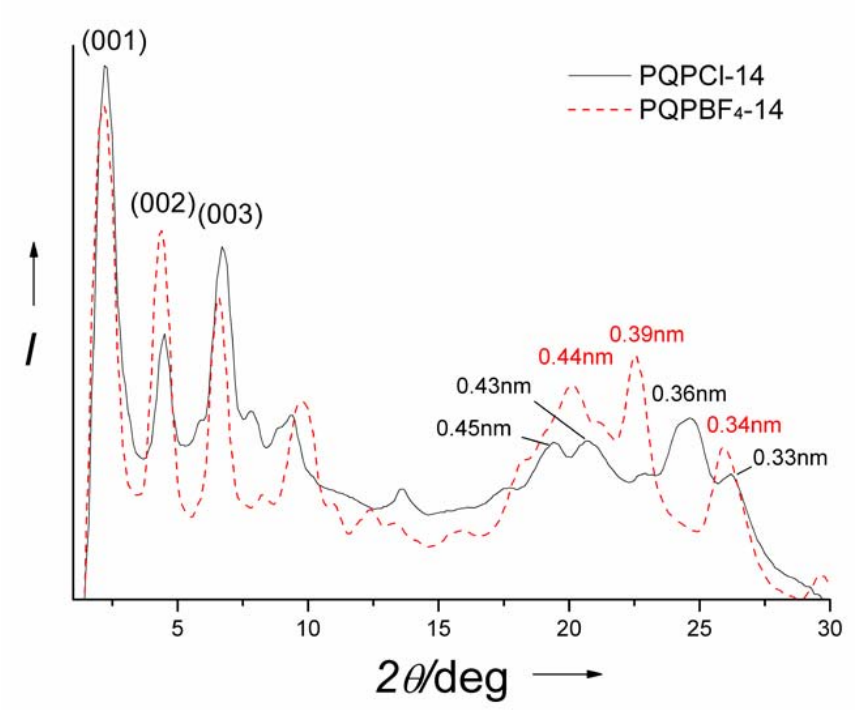

Figure 2-16. WAXS pattern of the dried powder of PQPCl-14 and $PQPBF_4$-14 obtained from the methanolic solution.

Besides the influence of the length of alkyl chain, changing the counterions of PQP salts also led to the alteration of the morphology formation for their aggregates. As shown in Figure 2-7 and Figure 2-12, the aggregation behavior of PQPX-14 was affected by varying the inorganic counterions. Although organic counterions have been previously shown to influence the self-assembly of amphiphiles[52-59], there is no previous example of purely inorganic counterions bringing about significant changes in morphology.

The effect of the counterion dependant change on the morphology of PQP salts was first investigated by comparing the WAXS patterns of PQPCl-14 and $PQPBF_4$-14 (Figure 2-16). Three sharp reflections, which were characteristic of lamellar stacking, appeared at the same positions in their WAXS patterns. This provided evidence that both the ribbons from PQPCl-14 and the tubes of $PQPBF_4$-14 were formed by similar lamellar structures as observed in their TEM images. However, their diffractions

between 10 and 30° were obviously different, suggesting the different packing motifs within lamellae:

The layered structure of the ribbon-shaped aggregates of PQPCl-14 was consistent with the stacking of the charged PAH head groups in a perfect face-to-face orientation with chloride anions (ionic radius = 1.21 Å in aqueous solution)[60] sandwiched between them (Figure 2-17). The helical and tubular aggregates of $PQPBF_4$-14 suggested that the replacement of the chloride anions with larger tetrafluoroborate ions (ionic radius = 2.30 Å in aqueous solution)[61] disrupted the perfect face-to-face alignment of adjacent PQP cations and caused them to adopt a slipped face-to-face orientation (Figure 2-17). Consequently, neighboring pairs of PQP cations were rotated with respect to one another along the axis of the aggregate and helically coiled structures resulted. Furthermore, additional stacking of the molecules along the axis of some helical structures would produce tubular aggregates in the end.[44]

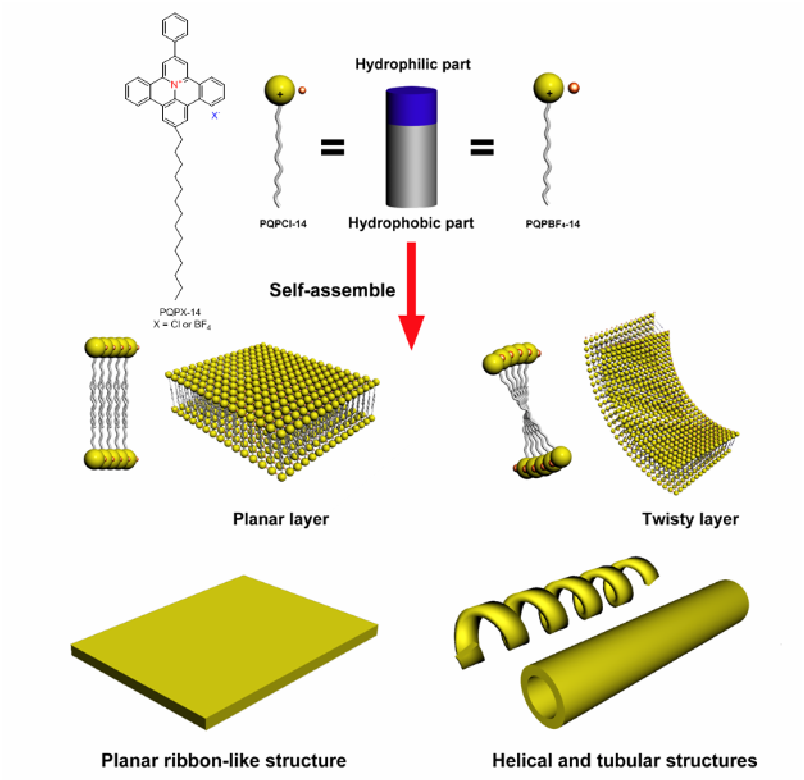

Figure 2-17. Representation showing a change in the counterion from Cl- to BF4- leading to a change from ribbons to helices and tubes.

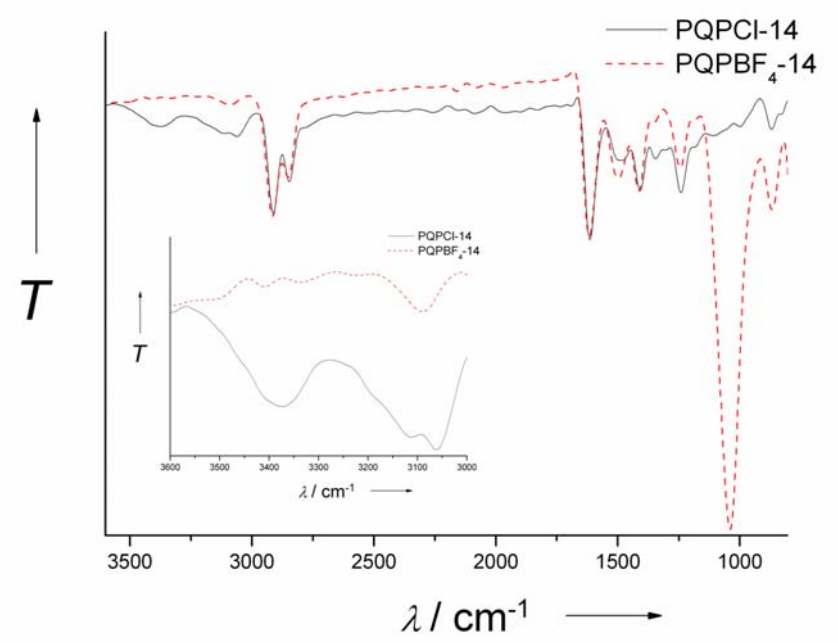

Figure 2-18. FTIR spectra of PQPCl-14 and $PQPBF_4$-14 and inset spectra is the 3000–3600 cm^{-1} region (r.t., pressed pellets with KBr).

The different molecular alignment in the aggregates of PQPCl-14 and $PQPBF_4$-14 was further supported by WAXS and Fourier transform infrared (FTIR) spectroscopy. The WAXS pattern of PQPCl-14 showed diffraction peaks at 0.45, 0.43, 0.36 and 0.34 nm, whereas the pattern of $PQPBF_4$-14 showed peaks at 0.44, 0.39 and 0.34 nm in the same region (Figure 2-16). Furthermore, the observation of weak bands at 3100 and 3350 cm^{-1} in the FTIR spectrum of PQPCl-14 and the virtual absence of analogous bands in the spectrum of $PQPBF_4$-14 (Figure 2-18) suggested the existence of hydrogen bonds between PQP molecules. Such intermolecular force has been found in ammonium salts and ionic liquids by experiments as well as theoretical calculation and was proved to be helpful for the stacking of the molecules[62, 63]. In this case, it might be derived from the interaction of anions and protons of PQP salts. The stronger hydrogen bond between PQPCl-14 could keep them in the perfect face to face position and result in the planar layered aggregates (Figure 2-17).

The WAXS patterns of PQPCl-6 and $PQPBF_4$-6 were consistent with an increase in distance between PQP cations (Figure 2-19) upon going from chloride (Cl-) to

tetrafluoroborate (BF_4-). However, aggregates of both PQP salts resulted in fibers (Figure 2-11 and Figure 2-10), indicating that the change of the counterions had no significant effect on the self-assembly of PQP with short alkyl chains (Figure 2-20).

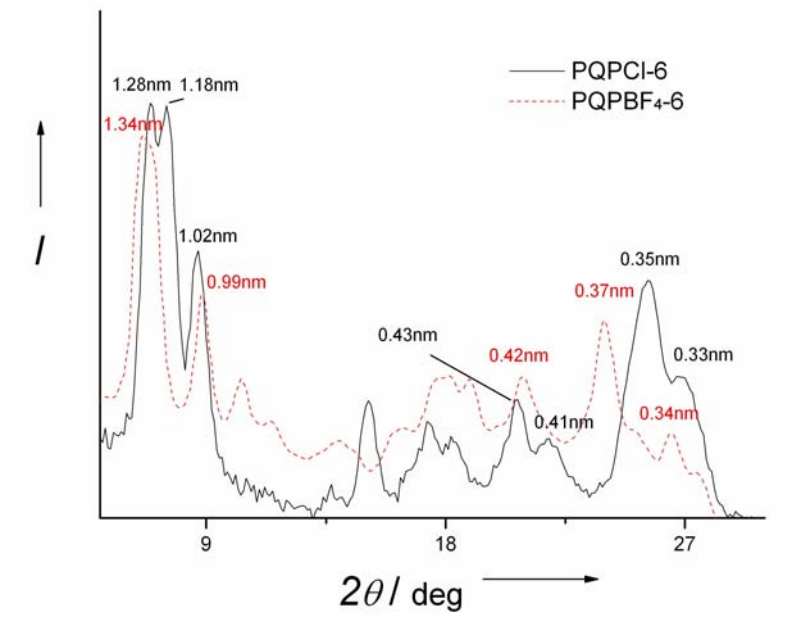

Figure 2-19. WAXS patterns of a dried powder of PQPCl-6 and $PQPBF_4$-6 obtained from methanolic solution

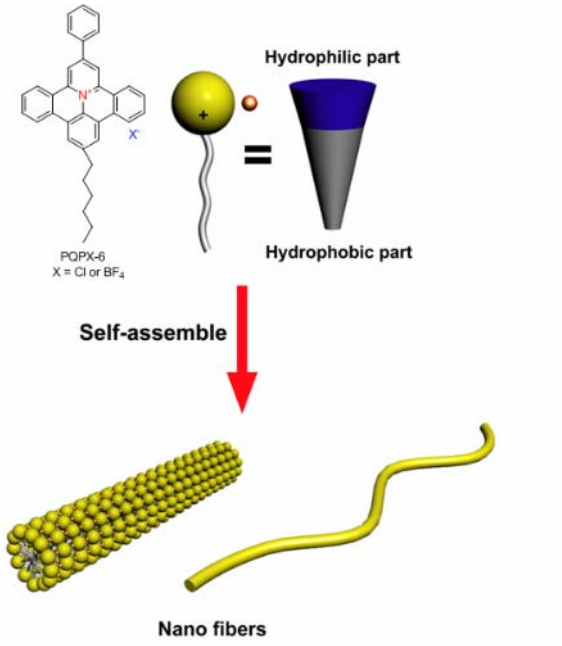

Figure 2-20. Aggregates of both PQPCl-6 and $PQPBF_4$-6 resulted in fibers.

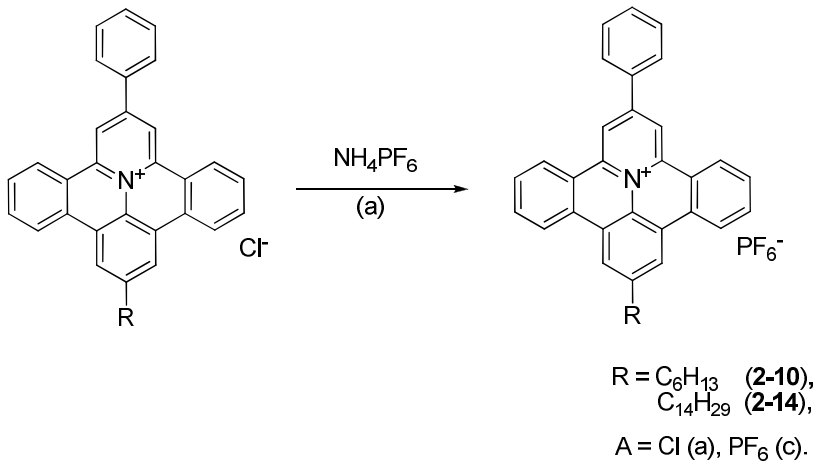

Scheme 2-7. Preparation of PQPPF$_6$-n; (a) methanol, filtration, r.t., yield = 98% (**2-10c**) and 96% (**2-14**c).

In the interest of comparing the effect of more counterions, PQPPF$_6$-6 **2-10c** and PQPPF$_6$-14 **2-14c** were prepared by ion exchange from PQPCl-6 and PQPCl-14 with ammonium hexafluorphosphate in methanol (Scheme 2-7). However, the resulting PQPPF$_6$-6 and PQPPF$_6$-14 had very low solubility in methanol and the concentration of the methanolic solution could not reach their critical aggregation concentration (CAC) as the PQP salts with chloride and tetrafluoroborate as counterions. Drop casting these diluted solution on a silicon wafer only resulted in crystallized structures (Figure 2-21).

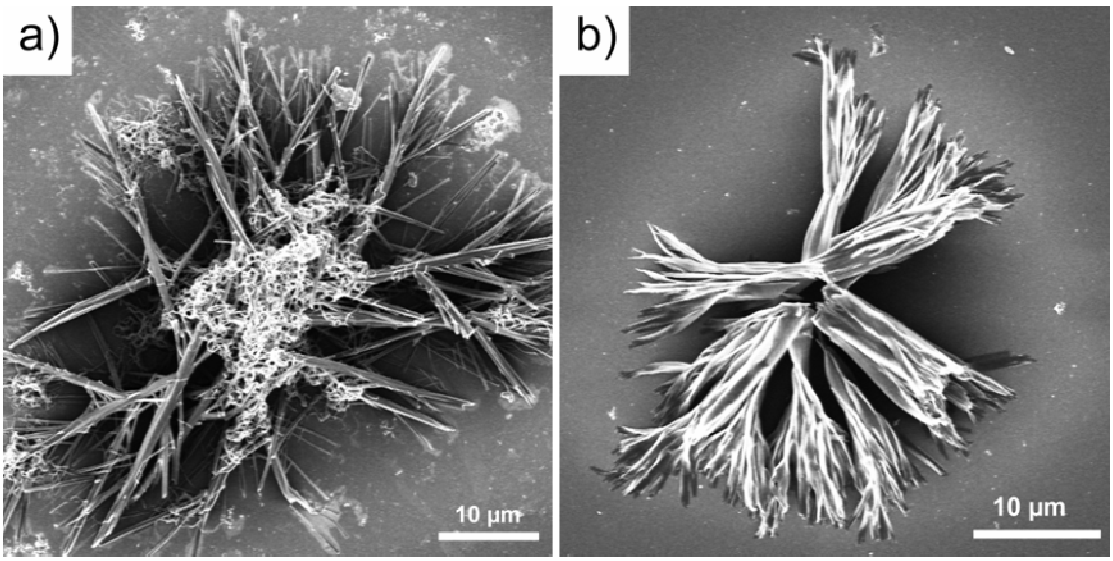

Figure 2-21. (a) SEM images of crystallized structures from PQPPF$_6$-6 and (b) PQPPF$_6$-14 ($2x10^{-4}$ mol/L in methanol, drop-cast on a silicon wafer).

2.3.3 The size and shape of aromatic cores

In order to explore the influence of the different aromatic core on the aggregation behavior of centrally charged PAHs, the self-assembly of the alkylated DBPQP salts (DBPQPBF$_4$-6 **2-21** and DBPQPBF$_4$-14 **2-22**) was subsequently investigated in a similar manner as alkylated PQP salts.

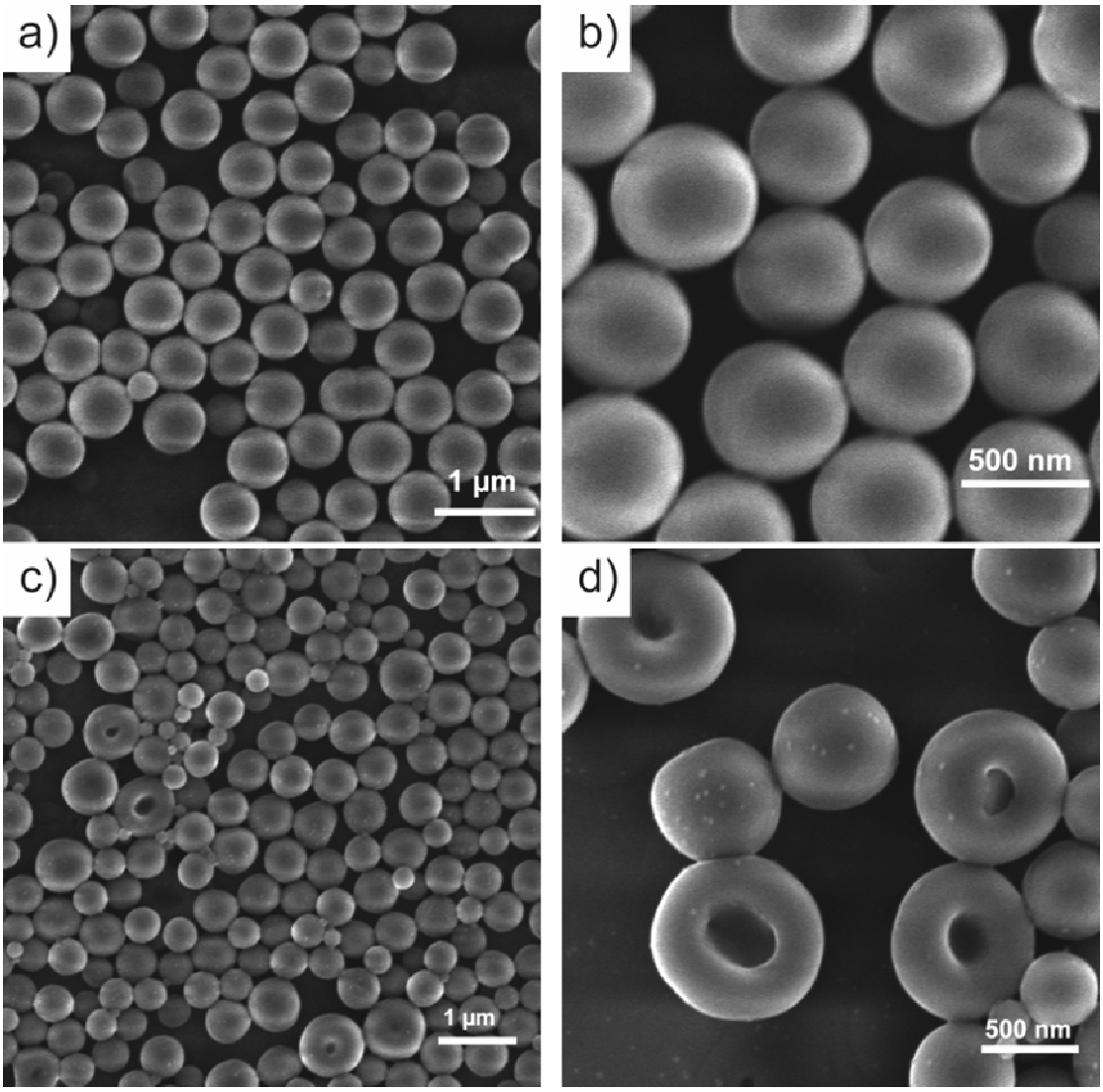

Figure 2-22. (a) and (b) SEM images of the aggregates formed by DBPQPBF$_4$-6 (1x10^{-3} mol/L in methanol, drop-cast on a silicon wafer); (c) and (d) SEM image of the aggregates formed by DBPQPBF$_4$-14 (1x10^{-3} mol/L in methanol, drop-cast on a silicon wafer).

The aggregates of these DBPQP salts could be directly observed by electron microscopy techniques after being transferred on the surface[38, 39] by drop-casting the

methanolic solution of DBPQPBF$_4$-6 and DBPQPBF$_4$-14 ($1x10^{-3}$ mol/L) on substrates (silicon wafers for SEM and carbon film covered copper grids for TEM) and removing the solvent quickly with a piece of filter paper.

The SEM images (Figure 2-22) indicated that both DBPQP salts aggregated into spherical aggregates. As shown in Figure 2-22a and b, the diameters of the aggregates formed by DBPQPBF$_4$-6 ranged from 200 to 600nm. The spheres of DBPQPBF$_4$-14 had wider diameter distribution which was between 150 and 800 nm (Figure 2-22c and d). The size of these spherical nanoscaled objects could not be correlated directly with molecular length of DBPQPBF$_4$-6 and DBPQPBF$_4$-14 (According to calculation, the extended molecular length of DBPQPBF$_4$-6 and DBPQPBF$_4$-14 were 20 and 28 Å respectively.[64]). Thereby, these objects could not be related to micelle-like structures, whose diameters were usually about twice the molecular length of the amphiphiles.[65] Furthermore, it was notable that some aggregates of DBPQPBF$_4$-14 had donut like structures which suggested these spheres were actually vesicles. This was probably due to the tetradecyl chain of DBPQPBF$_4$-14 being more flexible than the hexyl chain of DBPQPBF$_4$-6. Compared with the aggregates of DBPQPBF$_4$-6, the rigidity of the vesicles from DBPQPBF$_4$-14 decreased and these vesicles collapsed when they were transferred to silicon wafers.[38, 39]

Following TEM measurements offered more information about the internal structures of the aggregates from two DBPQP salts. Clearly, the spheres for DBPQPBF$_4$-6 and DBPQPBF$_4$-14 were all hollow vesicle structures (Figure 2-23). The wall thickness of aggregates from both DBPQPBF$_4$-6 and DBPQPBF$_4$-14 revealed a similar size of around 60 nm. However, compared with the vesicles of DBPQPBF$_4$-6, the spherical aggregates of DBPQPBF$_4$-14 were less stable under electron beam and their structures were easily decomposed during the TEM measurement (Figure 2-23b)[66, 67]. The instability of the aggregates from DBPQPBF$_4$-14 might also be induced by the longer and softer alkyl chains.

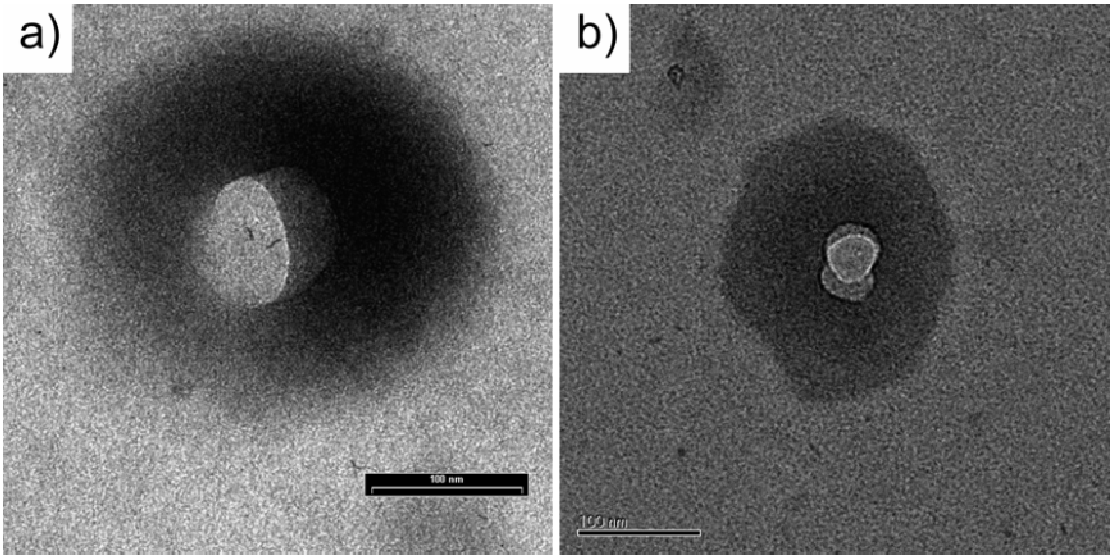

Figure 2-23. (a) TEM image of the aggregates of DBPQPBF$_4$-6 (1x10^{-3} mol/L in methanol, drop-cast on a carbon-film covered copper grid); (b) TEM image of the aggregates of DBPQPBF$_4$-14 (1x10^{-3} mol/L in methanol, drop-cast on a carbon-film covered copper grid).

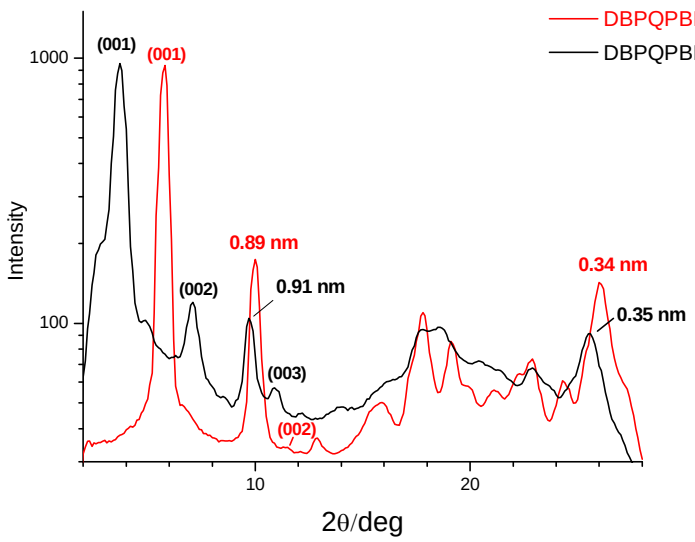

Figure 2-24. WAXS patterns of the dried powder of DBPQPBF$_4$-6 and DBPQPBF$_4$-14 obtained from methanolic solution.

In order to obtain more information about the molecular packing of two DBPQP salts, their WAXS patterns were compared in Figure 2-24. It turned out that both DBPQP salts exhibited the characteristic diffractions of lamellar packing. And this

suggested that all the vesicles of the PQP salts were formed by layered structures. Considering the length of the molecules mentioned above, the wall thickness of these vesicles fitted to approximately 15-18 bilayers of these DBPQP salts. These results indicated that the spherical aggregates were in fact so called multilayered vesicles (MLVs).[65]

According to Israelachivili's packing parameter theory[41-44] and the formation mechanism of MLVs[44, 68, 69], the packing parameters *P* of DBPQPBF$_4$-6 and DBPQPBF$_4$-14 were between 0.5 and 1. However, our previous research indicated that the packing parameter *P* of PQPBF$_4$-6, which had the same alkyl chain as DBPQPBF$_4$-6, was in the range of 0.33 to 0.5. The increase of packing parameter could be explained by the intermolecular interaction difference between these positively charged PAHs.[70] The additional dibenzo-structure of DBPQPBF$_4$-6 obviously extended its aromatic core. The positive charge of DBPQPBF$_4$-6 was thus expected to be more delocalized over the larger π-system with respect to PQPBF$_4$-6, thus resulting in the decrease of Coulombic repulsion between neighboring molecules. And the aromatic attraction between the PQP molecules could be enhanced accordingly.[3, 34] Therefore, the optimum surface area per molecule a_0 of DBPQPBF$_4$-6 decreased and its packing parameter *P* increased accordingly.

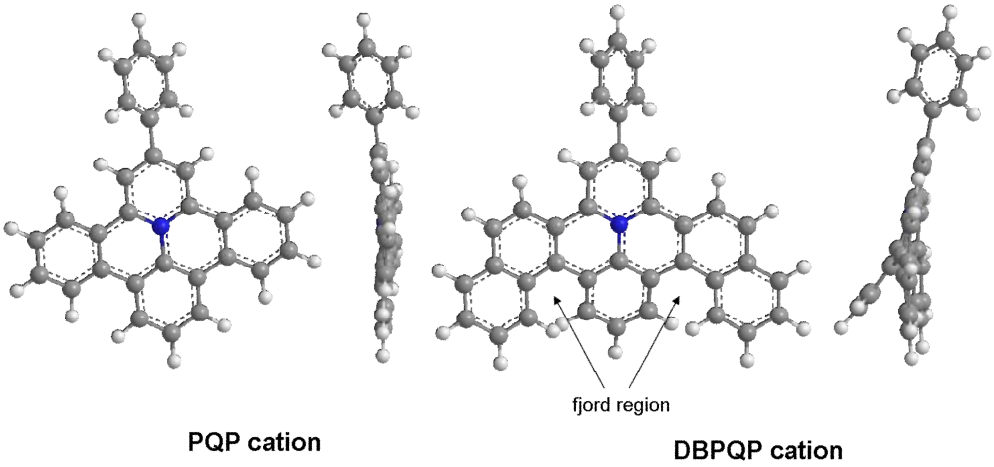

Figure 2-25. The simulated structures of PQP and DBPQP cations (optimized with MM2 method).

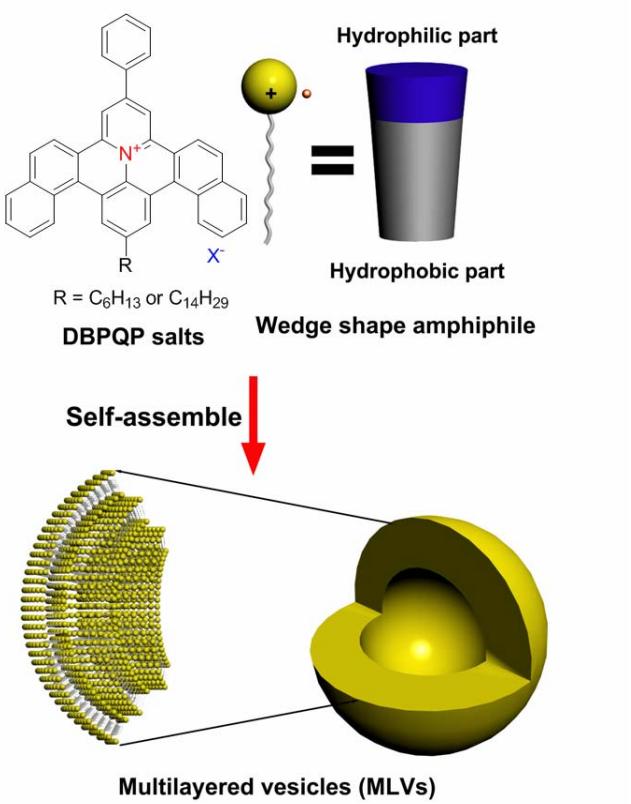

Figure 2-26. The formation of the MLVs from DBPQPBF$_4$-6 and DBPQPBF$_4$-14.

Another interesting fact was that different from the helical and tubular structures formed by PQPBF$_4$-14, the aggregates of DBPQPBF$_4$-14 were multilayered spherical vesicles even though they had similar packing parameters. The difference in the shape of their aggregates could be interpreted by the variation of the aromatic core structures. The two extended benzene rings not only caused the different symmetry of PQP and DBPQP but also made DBPQPBF$_4$ a non-planar molecule due to the existence of two fjord regions on it (Figure 2-25). As a result, the volume of the hydrophilic part of DBPQPBF$_4$-14 increased when it aggregated in solution and it became a so-called wedge-shaped amphiphile compared with PQPBF$_4$-14. The stacking of the wedge-shaped DBPQPBF$_4$-14 could lead to spontaneous curvature of the layered structures (Figure 2-26). Similar examples of the morphology control by adjusting the shape of molecules could also be found in study on the self-assembly of pyridinium salts and amphiphilic pyrelene dyes.[71-74]

There was no obvious difference between the vesicles formed by DBPQPBF$_4$-6

and DBPQPBF$_4$-14. That was to say, the different alkyl chains did not significantly affect the optimum surface area a_0 and packing parameter P of the two DBPQP salts, which had also been observed in the case of other vesicle forming surfactants.[29, 46]

2.4 Conclusions

In summary, a series of 2-phenyl-9-alkylbenzo[8,9]quinolizino-[4,5,6,7-*fed*]phenanthridinylium (PQP) salts were synthesized and characterized. Following the same synthetic concept, a class of unprecedented 2-phenyl-11-alkylnaphthacene[1,2]quinolizino[3,4,5,6-*def*]benzo[*i*]phenanthridinium tetrafluoroborates (DBPQPBF$_4$), which could be viewed as the extended derivates of PQP salts with two additional fused benzene rings, were also obtained in this work. The self-assembly behavior of these centrally charged PAHs were studied in methanolic solution and in the bulk. Interestingly, one-dimensional fibers with a uniform size distribution were obtained from the aggregation of PQPCl-6 and PQPBF$_4$-6 or PQPBF$_4$-8. And Increasing the alkyl chain length of the PQP salts reproducibly resulted in layered aggregates, while changing the counterion of the PQP salts from chloride (Cl-) to tetrafluoroborate (BF$_4$-) led to a change in the morphology of the aggregates from ribbons to helices and tubes. This could be ascribed to the different intermolecular orientations within layers which was induced by the different size of anions. For example, the face to face stacking of PQPCl-14 resulted in planar layered structures whereas the twisted stacking of PQPBF$_4$-14 gave rise to helical and tubular aggregates. Additionally, DBPQPBF$_4$-6 and DBPQPBF$_4$-14 could self-assemble into multilayered spherical vesicles. The curvature of their aggregates might be due to the unique symmetry and planarity of their aromatic parts. Various ion-containing aggregates from these amphiphilic aromatic molecules could be controllably obtained by this method. Recently, highly one-dimensional ionic conductivity from various ordered ionic imidazolium derivates was reported by T. Kato's group.[6, 75-79] On the other hand, G. C. Bazan *et al.* prepared light emitting diodes (LEDs) with controllable performance by changing the counterions of the cationic conjugated polymers.[80, 81] Therefore, these ordered aggregates from PQP salts

are expected to be useful in the fabrication of miniaturized devices such as biosensors and electrochromic devices and the study of their electronic properties is underway now.[82-86]

References

1. Katritzky, A. R.; Zakaria, Z.; Lunt, E.; Jones, P. G.; Kennard, O., *J. Chem. Soc.-Chem. Commun.* **1979**, (6), 268.
2. Katritzky, A. R.; Chermprapai, A.; Patel, R. C., *J. Chem. Soc.-Perkin Trans. 1* **1980**, (12), 2901.
3. Watson, M. D.; Fechtenkötter, A.; Müllen, K., *Chem. Rev.* **2001,** 101, (5), 1267.
4. Grimsdale, A. C.; Müllen, K., *Angew. Chem. Int. Ed.* **2005,** 44, (35), 5592.
5. Hoeben, F. J. M.; Jonkheijm, P.; Meijer, E. W.; Schenning, A., *Chem. Rev.* **2005,** 105, (4), 1491.
6. Kato, T.; Mizoshita, N.; Kishimoto, K., *Angew. Chem. Int. Ed.* **2006,** 45, (1), 38.
7. Meijer, E. W.; Schenning, A., *Nature* **2002,** 419, (6905), 353.
8. Bengs, H.; Closs, F.; Frey, T.; Funhoff, D.; Ringsdorf, H.; Siemensmeyer, K., *Liq. Cryst.* **1993,** 15, (5), 565.
9. Adam, D.; Schuhmacher, P.; Simmerer, J.; Haussling, L.; Siemensmeyer, K.; Etzbach, K. H.; Ringsdorf, H.; Haarer, D., *Nature* **1994,** 371, (6493), 141.
10. Würthner, F.; Thalacker, C.; Sautter, A.; Schartl, W.; Ibach, W.; Hollricher, O., *Chem.-Eur. J.* **2000,** 6, (21), 3871.
11. Cheng, X. H.; Jester, S. S.; Hoger, S., *Macromolecules* **2004,** 37, (19), 7065.
12. Hill, J. P.; Jin, W. S.; Kosaka, A.; Fukushima, T.; Ichihara, H.; Shimomura, T.; Ito, K.; Hashizume, T.; Ishii, N.; Aida, T., *Science* **2004,** 304, (5676), 1481.
13. Wu, J. S.; Fechtenkötter, A.; Gauss, J.; Watson, M. D.; Kastler, M.; Fechtenkötter, C.; Wagner, M.; Müllen, K., *J. Am. Chem. Soc.* **2004,** 126, (36), 11311.
14. Kastler, M.; Pisula, W.; Wasserfallen, D.; Pakula, T.; Müllen, K., *J. Am. Chem. Soc.* **2005,** 127, (12), 4286.
15. Pisula, W.; Kastler, M.; Wasserfallen, D.; Robertson, J. W. F.; Nolde, F.; Kohl, C.; Müllen, K., *Angew. Chem. Int. Ed.* **2006,** 45, (5), 819.
16. Kumar, S.; Wachtel, E. J.; Keinan, E., *J. Org. Chem.* **1993,** 58, (15), 3821.
17. Kumar, S.; Rao, D. S. S.; Prasad, S. K., *J. Mater. Chem.* **1999,** 9, (11), 2751.
18. Draper, S. M.; Gregg, D. J.; Madathil, R., *J. Am. Chem. Soc.* **2002,** 124, (14),

3486.

19. Gearba, R. I.; Lehmann, M.; Levin, J.; Ivanov, D. A.; Koch, M. H. J.; Barbera, J.; Debije, M. G.; Piris, J.; Geerts, Y. H., *Adv. Mater.* **2003,** 15, (19), 1614.
20. Gregg, D. J.; Fitchett, C. M.; Draper, S. M., *Chem. Commun.* **2006**, (29), 3090.
21. Buchardt, O.; Pedersen, C. L.; Svanholm, U., *Acta Chem. Scand.* **1969,** 23, (9), 3125.
22. Bello, A. M.; Kotra, L. P., *Tetrahedron Lett.* **2003,** 44, (52), 9271.
23. Lombard, R.; Stephan, J. P., *Bull. Soc. Chim. Fr.* **1958**, (11-1), 1458.
24. Pikus, A. L.; Feigelman, V. M.; Mezheritskii, V. V., *Zhurnal Org. Khimii* **1989,** 25, (12), 2603.
25. Dilthey, W., *Journal Fur Praktische Chemie-Leipzig* **1916,** 94, (2), 53.
26. Dilthey, W., *Berichte Der Deutschen Chemischen Gesellschaft* **1917,** 50, 1008.
27. Dilthey, W., *Journal Fur Praktische Chemie-Leipzig* **1917,** 95, (3/4), 107.
28. Gilchrist, T. L., *Heterocyclic Chemistry*. 3rd ed.; Prentice Hall: New Jersey, 1997.
29. Kunitake, T., *Angew. Chem. Int. Ed. Engl.* **1992,** 31, (6), 709.
30. Simpson, C. D.; Brand, J. D.; Berresheim, A. J.; Przybilla, L.; Rader, H. J.; Müllen, K., *Chem.-Eur. J.* **2002,** 8, (6), 1424.
31. Tomovic, Z.; Watson, M. D.; Müllen, K., *Angew. Chem. Int. Ed.* **2004,** 43, (6), 755.
32. Wasserfallen, D.; Kastler, M.; Pisula, W.; Hofer, W. A.; Fogel, Y.; Wang, Z. H.; Müllen, K., *J. Am. Chem. Soc.* **2006,** 128, (4), 1334.
33. Feng, X. L.; Wu, J. S.; Ai, M.; Pisula, W.; Zhi, L. J.; Rabe, J. P.; Müllen, K., *Angew. Chem. Int. Ed.* **2007,** 46, (17), 3033.
34. Wu, J. S.; Pisula, W.; Müllen, K., *Chem. Rev.* **2007,** 107, (3), 718.
35. Reichardt, C., *Chem. Rev.* **1994,** 94, (8), 2319.
36. Pisula, W.; Tomovic, Z.; Stepputat, M.; Kolb, U.; Pakula, T.; Müllen, K., *Chem. Mat.* **2005,** 17, (10), 2641.
37. Berne, B. J.; Pecora, R., *Dynamic Light Scattering: With Applications to Chemistry, Biology, and Physics*. Dover Publications: 2000.
38. Jonkheijm, P.; Hoeben, F. J. M.; Kleppinger, R.; van Herrikhuyzen, J.; Schenning,

A.; Meijer, E. W., *J. Am. Chem. Soc.* **2003,** 125, (51), 15941.

39. Yang, M.; Wang, W.; Yuan, F.; Zhang, X. W.; Li, J. Y.; Liang, F. X.; He, B. L.; Minch, B.; Wegner, G., *J. Am. Chem. Soc.* **2005,** 127, (43), 15107.
40. Ajayaghosh, A.; Varghese, R.; Praveen, V. K.; Mahesh, S., *Angew. Chem. Int. Ed.* **2006,** 45, (20), 3261.
41. Tanford, C., *J. Phys. Chem.* **1972,** 76, (21), 3020.
42. Israelachvili, J. N.; Mitchell, D. J.; Ninham, B. W., *Journal of the Chemical Society-Faraday Transactions Ii* **1976,** 72, 1525.
43. Israelachvili, J. N.; Mitchell, D. J.; Ninham, B. W., *Biochimica Et Biophysica Acta* **1977,** 470, (2), 185.
44. Shimizu, T.; Masuda, M.; Minamikawa, H., *Chem. Rev.* **2005,** 105, (4), 1401.
45. C. Tanford, *The Hydrophobic Effect*. Wiley-Interscience: New York, 1973.
46. Nagarajan, R., *Langmuir* **2002,** 18, (1), 31.
47. Rulkens, R.; Wegner, G.; Thurn-Albrecht, T., *Langmuir* **1999,** 15, (12), 4022.
48. Perahia, D.; Traiphol, R.; Bunz, U. H. F., *Macromolecules* **2001,** 34, (2), 151.
49. Wilson, J. N.; Steffen, W.; McKenzie, T. G.; Lieser, G.; Oda, M.; Neher, D.; Bunz, U. H. F., *J. Am. Chem. Soc.* **2002,** 124, (24), 6830.
50. Inouye, H.; Sharma, D.; Goux, W. J.; Kirschner, D. A., *Biophys. J.* **2006,** 90, (5), 1774.
51. Reches, M.; Gazit, E., *Phys. Biol.* **2006,** 3, (1), S10.
52. Oda, R.; Huc, I.; Homo, J. C.; Heinrich, B.; Schmutz, M.; Candau, S., *Langmuir* **1999,** 15, (7), 2384.
53. Oda, R.; Huc, I.; Schmutz, M.; Candau, S. J.; MacKintosh, F. C., *Nature* **1999,** 399, (6736), 566.
54. Berthier, D.; Buffeteau, T.; Leger, J. M.; Oda, R.; Huc, I., *J. Am. Chem. Soc.* **2002,** 124, (45), 13486.
55. Guan, Y.; Antonietti, M.; Faul, C. F. J., *Langmuir* **2002,** 18, (15), 5939.
56. Faul, C. F. J.; Antonietti, M., *Adv. Mater.* **2003,** 15, (9), 673.
57. Franke, D.; Vos, M.; Antonietti, M.; Sommerdijk, N.; Faul, C. F. J., *Chem. Mat.* **2006,** 18, (7), 1839.

58. Brizard, A.; Ahmad, R. K.; Oda, R., *Chem. Commun.* **2007**, (22), 2275.
59. Brizard, A.; Aime, C.; Labrot, T.; Huc, I.; Berthier, D.; Artzner, F.; Desbat, B.; Oda, R., *J. Am. Chem. Soc.* **2007,** 129, (12), 3754.
60. Dellamon.M; Senatore, L., *J. Phys. Chem.* **1970,** 74, (1), 205.
61. Hassel, O.; Kringstad, H., *Z. Anorg. Allg. Chem.* **1932,** 209, (3), 281.
62. Glazunov, V. P.; Mashkovsky, A. A.; Odinokov, S. E., *Journal of the Chemical Society-Faraday Transactions Ii* **1979,** 75, 629.
63. Dong, K.; Zhang, S. J.; Wang, D. X.; Yao, X. Q., *J. Phys. Chem. A* **2006,** 110, (31), 9775.
64. Shaik, S.; Shurki, A.; Danovich, D.; Hiberty, P. C., *Chem. Rev.* **2001,** 101, (5), 1501.
65. Li, Y. J.; Li, X. F.; Li, Y. L.; Liu, H. B.; Wang, S.; Gan, H. Y.; Li, J. B.; Wang, N.; He, X. R.; Zhu, D. B., *Angew. Chem. Int. Ed.* **2006,** 45, (22), 3639.
66. Williams, D. B.; Carter, C. B., *Transmission Electron Microscopy: A Textbook for Materials Science*. 1st ed.; Springer: 2004.
67. Fultz, B.; Howe, J., *Transmission Electron Microscopy and Diffractometry of Materials*. 3rd ed.; Springer: 2007.
68. Fendler, J. H., *Chem. Rev.* **1987,** 87, (5), 877.
69. Mueller, A.; O'Brien, D. F., *Chem. Rev.* **2002,** 102, (3), 727.
70. Wu, D. Q.; Zhi, L. J.; Bodwell, G. J.; Cui, G. L.; Tsao, N.; Müllen, K., *Angew. Chem. Int. Ed.* **2007,** 46, (28), 5417.
71. Haldar, J.; Aswal, V. K.; Goyal, P. S.; Bhattacharya, S., *J. Phys. Chem. B* **2001,** 105, (51), 12803.
72. Bhattacharya, S.; Nayak, S. K.; Chattopadhyay, S.; Banerjee, M.; Mukherjee, A. K., *J. Phys. Chem. B* **2001,** 105, (43), 22A.
73. Haldar, J.; Aswal, V. K.; Goyal, P. S.; Bhattacharya, S., *Angew. Chem. Int. Ed.* **2001,** 40, (7), 1228.
74. Zhang, X.; Chen, Z. J.; Würthner, F., *J. Am. Chem. Soc.* **2007,** 129, (16), 4886.
75. Ohtake, T.; Ogasawara, M.; Ito-Akita, K.; Nishina, N.; Ujiie, S.; Ohno, H.; Kato, T., *Chem. Mat.* **2000,** 12, (3), 782.

76. Yoshio, M.; Mukai, T.; Kanie, K.; Yoshizawa, M.; Ohno, H.; Kato, T., *Adv. Mater.* **2002,** 14, (5), 351.
77. Yoshio, M.; Mukai, T.; Ohno, H.; Kato, T., *J. Am. Chem. Soc.* **2004,** 126, (4), 994.
78. Kishimoto, K.; Suzawa, T.; Yokota, T.; Mukai, T.; Ohno, H.; Kato, T., *J. Am. Chem. Soc.* **2005,** 127, (44), 15618.
79. Kitamura, T.; Nakaso, S.; Mizoshita, N.; Tochigi, Y.; Shimomura, T.; Moriyama, M.; Ito, K.; Kato, T., *J. Am. Chem. Soc.* **2005,** 127, (42), 14769.
80. Yang, R. Q.; Wu, H. B.; Cao, Y.; Bazan, G. C., *J. Am. Chem. Soc.* **2006,** 128, (45), 14422.
81. Yang, R. Q.; Garcia, A.; Korystov, D.; Mikhailovsky, A.; Bazan, G. C.; Nguyen, T. Q., *J. Am. Chem. Soc.* **2006,** 128, 16532.
82. Binnemans, K., *Chem. Rev.* **2005,** 105, (11), 4148.
83. Gaylord, B. S.; Heeger, A. J.; Bazan, G. C., *Proc. Natl. Acad. Sci. U. S. A.* **2002,** 99, (17), 10954.
84. Liu, B.; Gaylord, B. S.; Wang, S.; Bazan, G. C., *J. Am. Chem. Soc.* **2003,** 125, (22), 6705.
85. Gong, X.; Wang, S.; Moses, D.; Bazan, G. C.; Heeger, A. J., *Adv. Mater.* **2005,** 17, (17), 2053.
86. Liu, B.; Bazan, G. C., *Proc. Natl. Acad. Sci. U. S. A.* **2005,** 102, (3), 589.

Chapter 3

Oxygen and Sulfur Containing Polycyclic Aromatic Hydrocarbons with Positive Charge: Synthesis and Characterization

In this chapter, the synthetic strategy toward a class of novel positively charged oxygen containing polycyclic aromatic hydrocarbons (PAHs), benzo[5,6]naphthaceno[1,12,11,10-*jklmna*]xanthylium (BNAX) salts and their analogs, positively charged sulfur containing benzo[5,6]naphthaceno[1,12,11,10-*jklmna*]thioxanthylium (BNATX) salts will be discussed. The photophysical properties and supramolecular behavior of the BNAX derivates will also be presented.

3.1 Introduction

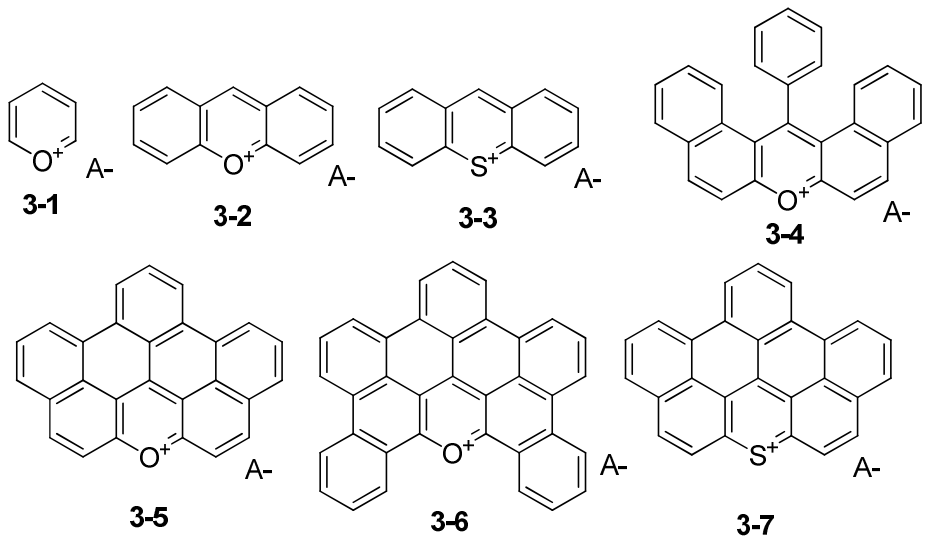

Scheme 3-1. Various oxygen or sulfur containing aromatic compounds with positive charge.

During the last decades, small oxygen or sulfur containing aromatic compounds with positive charge have received great attention of physicists and chemists both in theoretical study and in practical application due to their electron deficient nature. For example, pyrylium salts **3-1** are very reactive against nucleophilic agents and so they are important intermediates for the formation of a range of carbocyclic and other heterocyclic molecules.[1-5] Xanthylium salts **3-2** and thioxanthylium salts **3-3** are often studied as organic cations in physical chemistry.[6-11] An anion sensor based on dibenzoxanthylium cation **3-4** was also reported recently.[12] One can also expect that large oxygen and sulfur containing PAHs (having more than six fused aromatic rings)[13-15] with positive charge will show some different physical properties from their all-hydrocarbon PAH analogues. However, to the best of our knowledge, investigation on large oxygen or sulfur containing PAHs with positive charge has not been reported so far due to the synthetic difficulties.

Herein, we present the first synthesis and characterization of unprecedented large oxygen containing PAHs with positive charge, namely benzo[5,6]naphthaceno[1,12,11,10-*jklmna*]xanthylium salts (BNAX, **3-5**) and its alkylated derivates. In addition, the extended derivates of BNAX salts with additional two fused benzene rings, DBNAX salts **3-6**, were synthesized in this work. With a similar synthetic strategy, sulfur containing benzo[5,6]naphthaceno[1,12,11,10-*jklmna*]thioxanthylium salt (BNATX, **3-7**) was also developed by us.

The supramolecular chemistry of oxygen containing PAHs with positive charge (BNAX and DBNAX salts) was studied subsequently. Unique liquid crystal behavior was observed from di- (**3-25**) and tridodecyl (**3-27**) substituted BNAX salts. Both compounds formed columnar liquid crystalline phase and exhibited large unit cells in their 2D-WAXS patterns which could be attributed to the formation of dimer structures. Furthermore, mono alkylated BNAX (**3-24**) and DBNAX (**3-35**) salts showed aggregation behavior in solution, which was similar to the PQP derivates discussed in Chapter 2. Nano fibers with defined morphology could be obtained from

both compounds by simply drop-casting their methanolic solution on silicon wafers, and the mechanism of their self-assembly was also discussed.

3.2 Synthesis and characterization

The general synthetic route toward BNAX and BNATX derivates is shown in Scheme 3-2: Firstly, the starting dibenzo[*a*,*j*]xanthene or dibenzo[*a*,*j*]thioxanthene is oxidized into the corresponding dibenzo[*a*,*j*]xanthenylium or dibenzo[*a*,*j*]thioxanthenylium salts. Second, the planarization of the precursor by photocycliztaion leads to the target molecule. It is worthy to note that the structure of BNAX salt is mainly decided by the structure of the starting dibenzo[*a*,*j*]xanthene because the oxidization and photocyclization can barely change the aromatic skeletons. The variation of the dibenzo[*a*,*j*]xanthene such as attaching different functional groups on its periphery or extend its aromatic framework will enable us to obtain BNAX derivates with diversified structures.

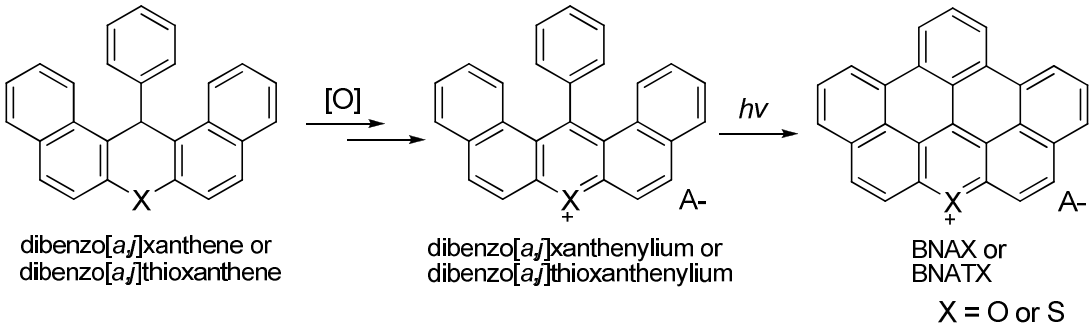

Scheme 3-2. The general synthetic route to BNAX and BNATX derivates.

3.2.1 Synthesis of benzo[5,6]naphthaceno[1,12,11,10-*jklmna*]-xanthylium (BNAX) salts

3.2.1.1 Synthesis of BNAX derivates with bromide as anion

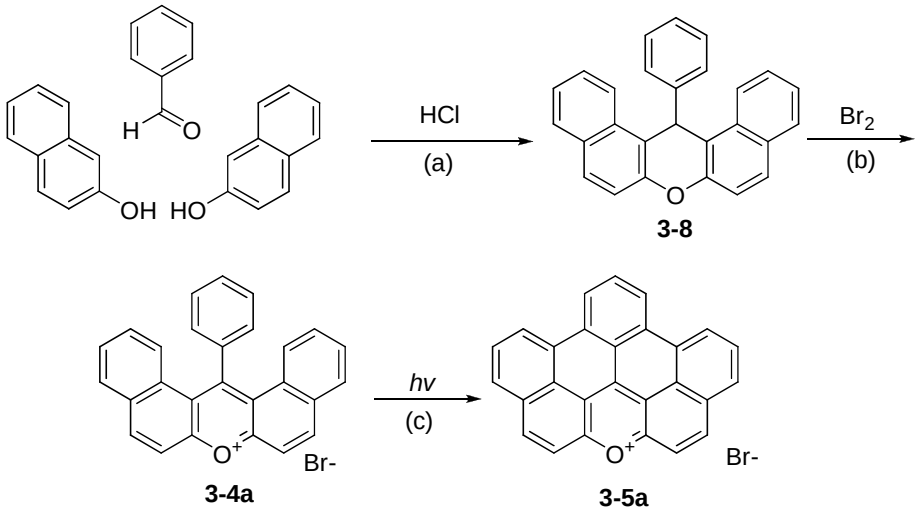

Scheme 3-3. Synthesis of benzo[5,6]naphthaceno[1,12,11,10-*jklmna*]xanthylium (BNAX) bromide; (a) concentrated hydrochloride acid (catalyst), glacial acetic acid, 100°C, 6 hours, yield = 60%; (b) diluted bromine (1 eq), glacial acetic acid, 120°C, 2 hours, yield = 85%; (c) acetonitrile or dichloromethane, r.t., *hυ*, *c.a.*24 hours, yield = 96%.

The first oxygen containing PAH cation synthesized in our work is benzo[5,6]naphthaceno[1,12,11,10-*jklmna*]xanthylium bromide (BNAXBr, **3-5a**). Its synthetic pathway is shown in Scheme 3-3: Claisen condensation between two equivalents of 2-naphtol and one equivalent of benzaldehyde with concentrated hydrochloride acid as the catalyst in glacial acetic acid resulted in 14-phenyl-14*H*-dibenzo[*a,j*]xanthene (**3-8**) with a yield of 60%.[16-19] The subsequent oxidization of **3-8** with a diluted acetic acid solution of bromine gave the undehydrogenated precursor, 14-phenyl-14-dibenzo[*a,j*]xanthenylium bromide (**3-4a**, yield = 85%).[20-22] Similar to the synthesis of PQP salts, the irradiation of the solution of **3-4a** (0.75 g/L in acetonitrile or dichloromethane) with 300 nm UV light for 24 hours and further recrystallization in methanol produced the target BNAXBr **3-5a** as needle-like purple crystals (yield = 96%). Further characterization of the product by MALDI-TOF MS spectrometry (only the cation part of **3-5a** could be detected in the normal model of MALDI-TOF/FD MS spectrometry) and ^{1}H NMR spectroscopy were in accordance with expectation (Figure 3-1 and Figure 3-2).

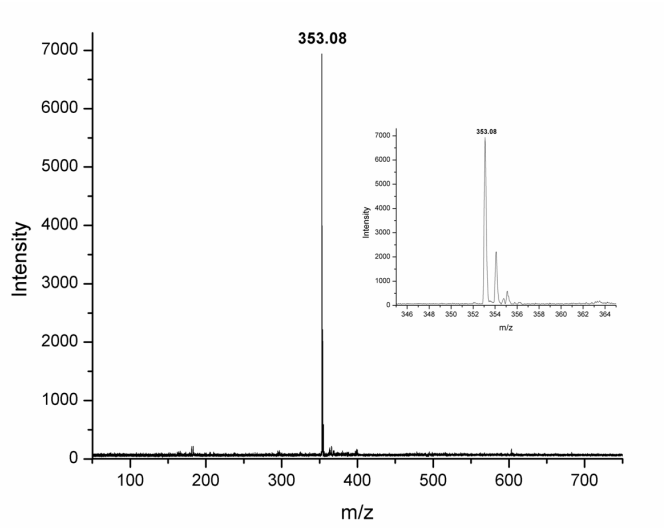

Figure 3-1. MALDI-TOF MS spectrum (TCNQ as matrix) of BNAX bromide **3-5a** (MW = 353 without anion).

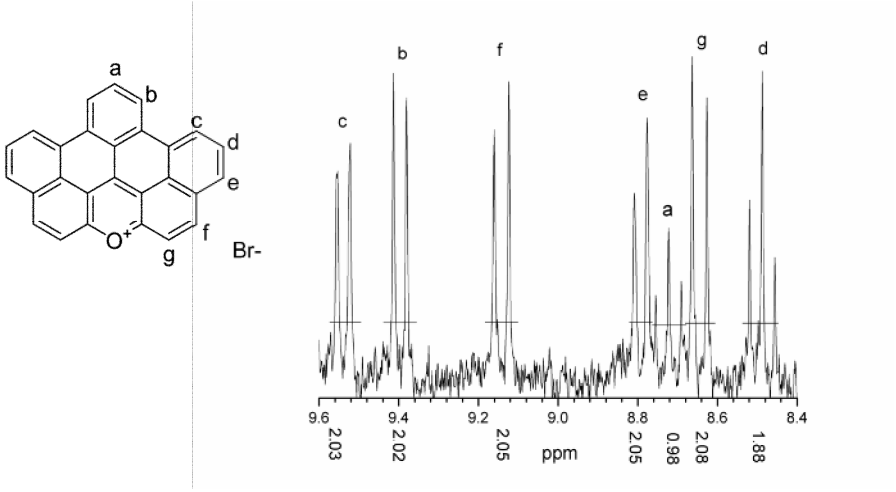

Figure 3-2. ^{1}H NMR spectrum of **3-5a** (r.t., 250MHz, CD_3OD : CD_2Cl_2 = 1 : 1, 1024 ns).

In order to obtain more BNAX derivates, which could enable us to further study their liquid crystal and self-assembly behavior, various alkylated BNAX bromides were synthesized by us with a modified route.

As shown in Scheme 3-4, mono- (**3-10**), di- (**3-11**) and tribromodibenzo[*a*,*j*]xanthene (**3-12**) were first synthesized from Claisen condensation of appropriate arylaldehyde (benzaldehyde or 4-bromobenzaldehyde) and naphtol (2-naphtol or 6-bromonaphthalen-2-ol) in good yields. Under Kumada coupling conditions with [1,1'-bis(diphenylphosphino)ferrocene]dichloropalladium(II)

dichloromethane ($PdCl_2(dppf)CH_2Cl_2$) as catalyst, Grignard reagents ($C_6H_{13}MgBr$ or $C_{12}H_{25}MgBr$) could couple with bromide substituted dibenzo[*a*,*j*]xanthene (**3-10**, **3-11** and **3-12**) to give the alkylated dibenzo[*a*,*j*]xanthene **3-13**, **3-14**, **3-15**, **3-16** and **3-17** in anhydrous THF. Subsequent oxidization of these alkylated dibenzo[*a*,*j*]xanthene in acetic acid with diluted bromine solution produced the corresponding alkylated 14-phenyl-14-dibenzo[*a*,*j*]xanthenylium bromides **3-18**, **3-19**, **3-20**, **3-21** and **3-22**. The final photocyclization of the alkylated dibenzo[*a*,*j*]xanthenylium bromides in acetic acid under 300 nm UV light resulted in alkylated BNAX bromides **3-23**, **3-24**, **3-25**, **3-26** and **3-27** as purple powders. All molecules were characterized by ^1H NMR, ^{13}C NMR spectroscopy as well as MALDI-TOF mass spectrometry.

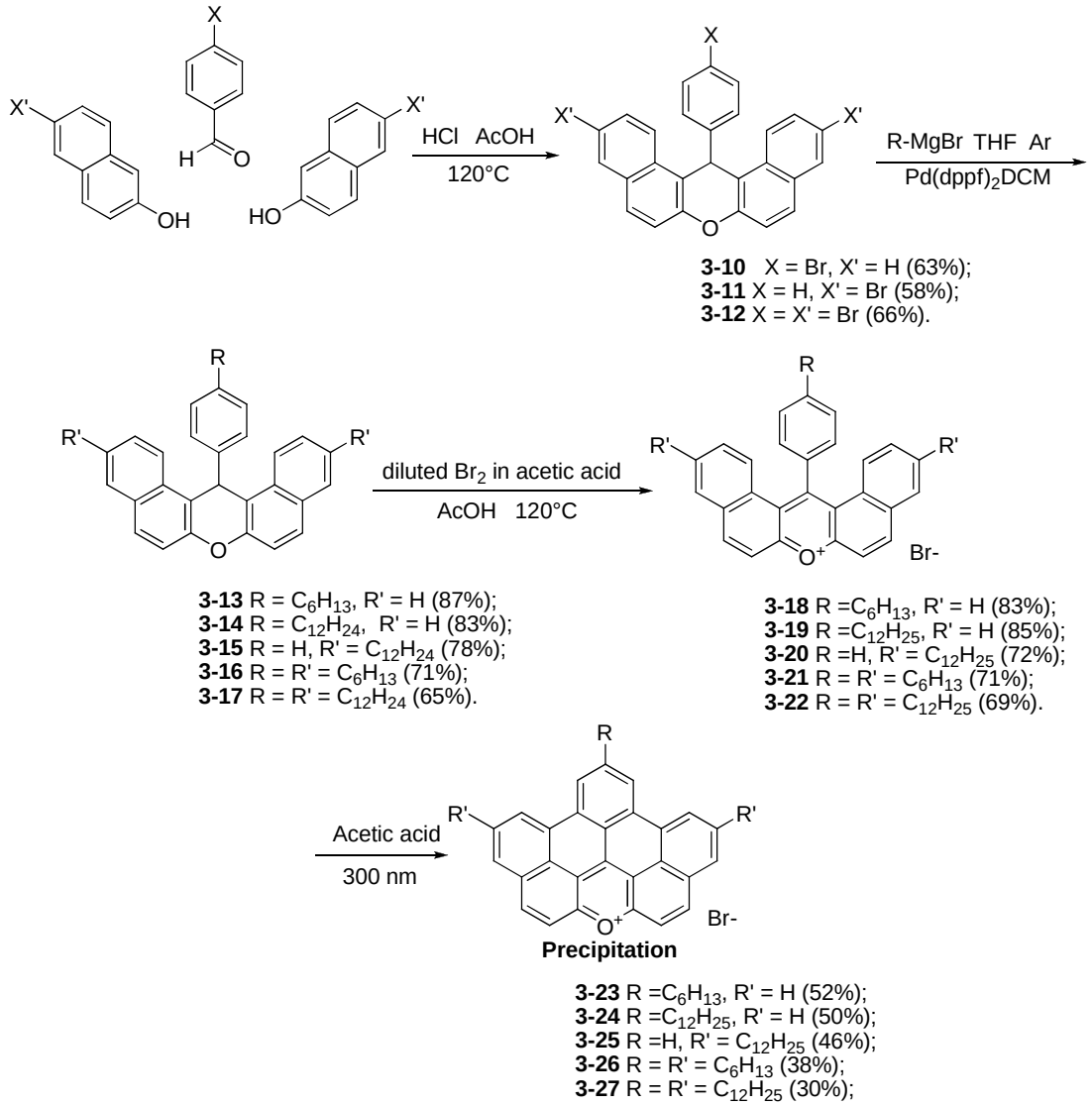

Scheme 3-4. Synthesis of various alkylated BNAX bromides.

One interesting fact about the photocyclization of the alkylated dibenzo[*a,j*]xanthenylium bromides was that acetic acid but not acetonitrile or dichloromethane could be used as the solvent for the photolysis dehydrogenation process. This was due to the product had very poor solubility in acetic acid and could precipitate right after the dehydrogenation. Therefore, using acetic acid for photocyclization could not only increase the yields of alkylated BNAX salts but also simplify their purification.

3.2.1.2 Synthesis of BNAX derivates with other anions

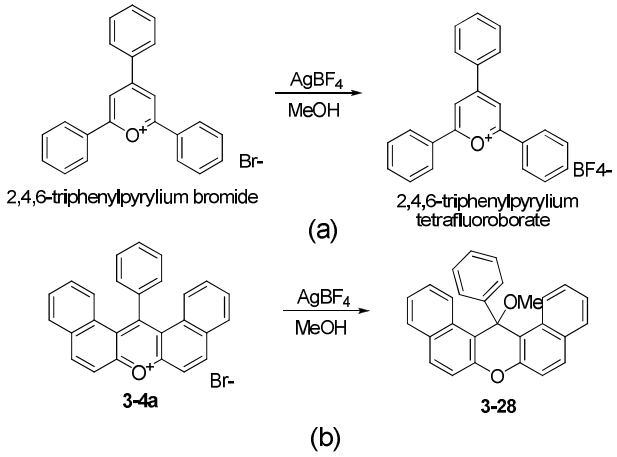

Scheme 3-5. The counterion exchange method of 2,4,6-triarylpyrylium salts (a) can not applied in the case of dibenzo[*a,j*]xanthenylium salts (b).

The limitation of the synthetic method to various BNAX bromides mentioned above is that their counterions are always bromide. Synthesis of BNAX derivates with other counterions such as tetrafluoroborate (BF_4-), perchlorate (ClO_4-) and hexafluorphosphate (PF_6-) is necessary for different purposes such as to stabilize the xanthenylium cations or to change their solubility in organic solvent. According to the literature[23, 24], the counterion exchange of small oxygen containing aromatic compound with positive charge such as 2,4,6-triphenylpyrylium bromide was performed in protic solvent including methanol and water. The significantly different solubility of starting silver tetrafluoroborate and resulting silver bromide was believed to be the driving force for the reaction (Scheme 3-5a).[24] However, the same procedure failed in the case of dibenzo[*a,j*]xanthenylium bromide **3-4a** (Scheme 3-5b): When

3-4a was dissolved in methanol, the red color of the solution faded in a short time (*ca.* 10 minutes). FD MS spectra of the resulting transparent solution (Figure 3-3) indicated that all the dibenzo[*a*,*j*]xanthenylium cation (m/z = 357) was consumed and a new compound whose molecular weight was 388 was produced instead. ^{1}H NMR spectroscopy confirmed the formation of 14-methoxy-14-phenyl-14H-dibenzo[*a*,*j*]xanthene **3-28** as only product in this reaction (Figure 3-4). Furthermore, the ion exchange of dehydrogenated BNAX bromide **3-5a** also failed due to its poor solubility in methanol and water.

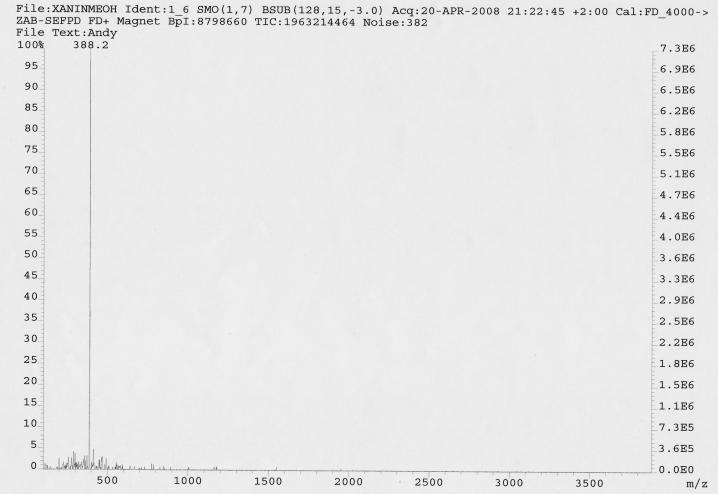

Figure 3-3. FD MS spectrum of the transparent solution from ion exchange of **3-4a** in methanol.

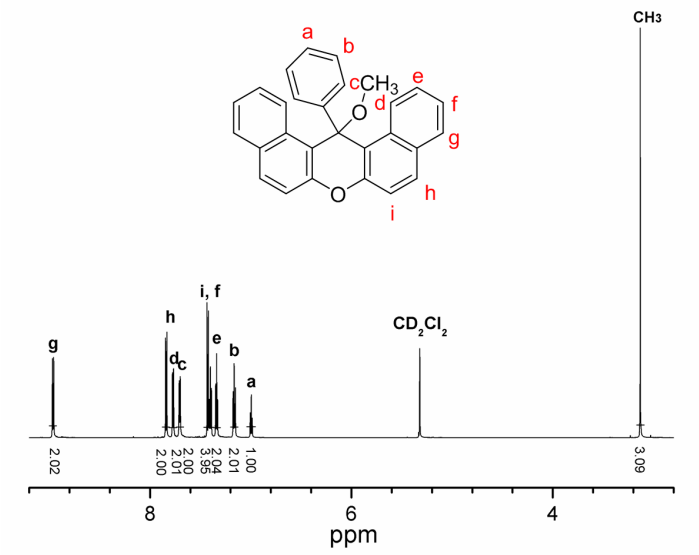

Figure 3-4. ^{1}H NMR spectrum of compound **3-28** (r.t., 700MHz, CD_2Cl_2).

Therefore, to develop a new method which can directly afford dibenzo[*a,j*]xanthenylium and BNAX salts with various counterions other than bromide is urgently required. Due to this, a stepwise synthetic precedure[25] was adopted in our research (Scheme 3-6). In this method, 14-phenyl-14*H*-dibenzo[*a,j*]xanthene **3-8** was firstly oxidized to 14-phenyl-14-hydroxy-dibenzo[*a,j*]xanthene **3-29** by PbO_2 in acetic acid at 100°C (yield = 95%). The treatment of **3-29** with inorganic acid in the mixture of acetic acid anhydride and toluene at 0°C resulted in 14-phenyl-dibenzo[*a,j*]xanthenylium salts **3-4** with anions from respective inorganic acids as red powder in nearly quantitative yields. Subsequent photocyclization of **3-4** produced corresponding BNAX salt **3-5** with different anions.

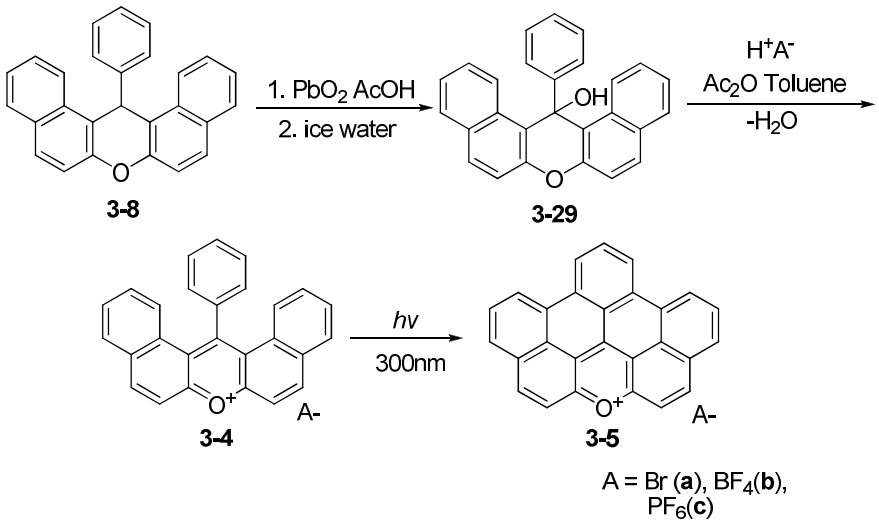

Scheme 3-6. Stepwise synthesis of dibenzo[*a,j*]xanthenylium and BNAX salts with different counterions.

3.2.2 Synthesis of dibenzo derivate of BNAX salts

In the pursuit of novel PAH molecules for material sciences, one of the most popular synthetic concepts is to enlarge the aromatic core.[26] For example, in the field of organic field-effect transistors, larger π-areas are expected to lead to improved mobilities since the charge-carrier mobility is in close relation to the size of the aromatic core.[27, 28] For photovoltaic applications a high extinction coefficient over a

broad range of the spectrum is a prerequisite, which can also be achieved by enlarging the aromatic core component.[29, 30] Moreover, such large disks are assumed to exhibit an improved self-ordering due to the extended π-area, which is another key feature to yield high performances in electronic devices. Due to these reasons, various extended all-hydrocarbon PAHs were synthesized by our group in the last years, and they not only showed interesting chemical and physical properties but also exhibited promising applications in material sciences.[31-34] In the field of heteroatom containing PAHs, the synthesis of large heteroatom containing PAHs with positive charge is still challenging. Herein, we report the synthesis of an unprecedented oxygen containing PAH with positive charge, DBNAX salts **3-6**. It can be regarded as the extended derivates of BNAX salts with additional two fused benzene rings and is the largest oxygen containing PAH with positive charge (having 35 conjugated aromatic carbon atoms) so far.

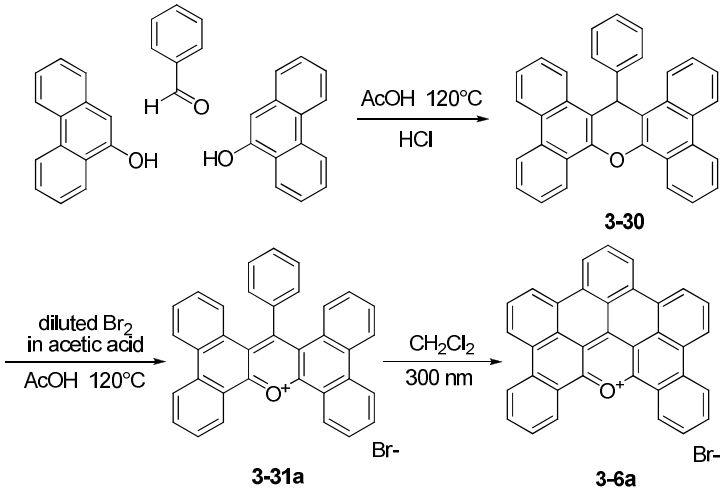

Scheme 3-7. Synthesis of DBNAX bromide **3-6a**.

The synthetic method for DBNAX bromide is shown in Scheme 3-7: Condensation reaction between 9-phenanthrenol and benzaldehyde in acetic acid gave 18-phenyl-18*H*-tetrabenzo[*a,c,h,j*]xanthene (**3-30**, yield = 48%) as white powders. The oxidization of tetrabenzo[*a,c,h,j*]xanthene **3-30** with diluted bromine solution in acetic acid at 120°C produced 18-phenyltetrabenzo[*a,c,h,j*]xanthenium bromide (**3-31a**, yield = 80%). The subsequent photocyclization of **3-31a** in dichloromethane resulted in the corresponding DBNAX bromide **3-6a** (yield = 85%) as purple needle

like crystals. Compound **3-6a** (MW = 453 without anion) was identified by MALDI TOF mass spectrometry firstly, proving the loss of 4 hydrogen atoms during the formation of 2 new carbon-carbon bonds, and the isotopic distribution, which was in agreement with simulated spectra (Figure 3-5a). Furthermore, it was interesting to note that even without any substituents which could improve the solubility in organic solvent, compound **3-6a** was still soluble enough in a mixed solvent (CD_3OD and CD_2Cl_2) to give well resolved ^1H NMR spectrum due to the positively charged aromatic core (Figure 3-5b).

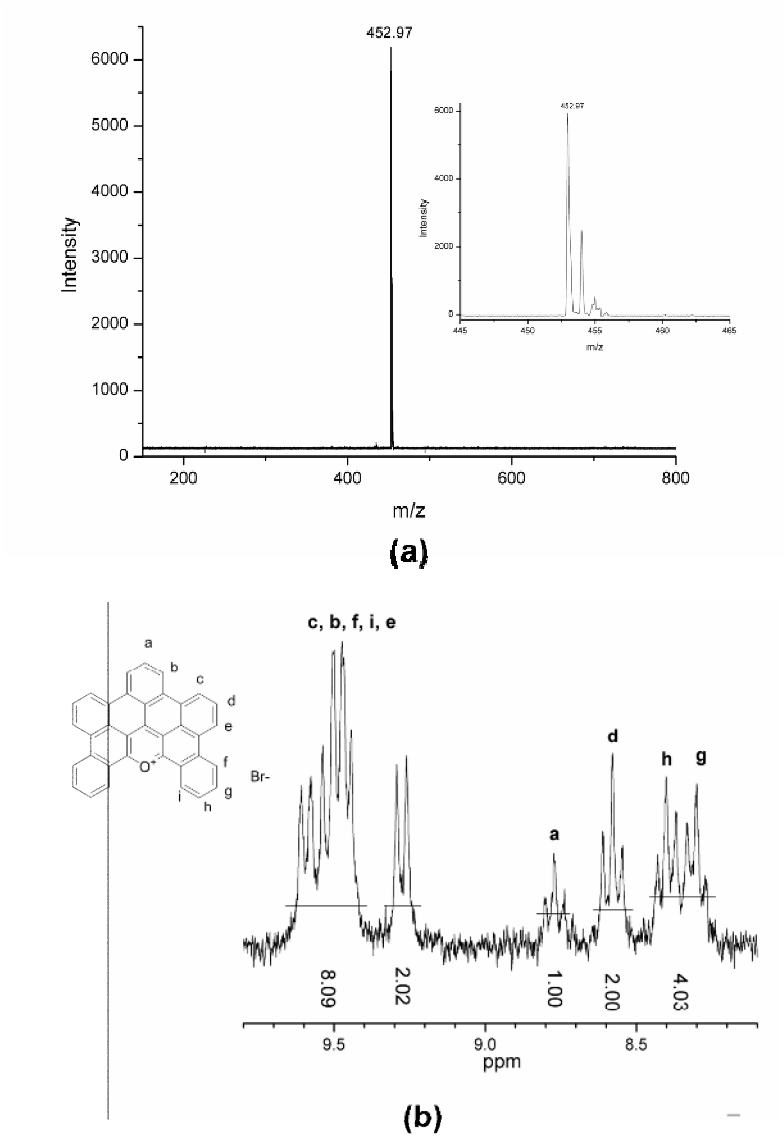

Figure 3-5. (a) MALDI TOF MS spectrum (with TCNQ as matrix) of DBNAX bromide **3-6a** (MW = 453 without anion) and (b) ^1H NMR spectrum (CD_3OD and CD_2Cl_2, r.t., 250MHz, 8500 ns) of **3-6a**.

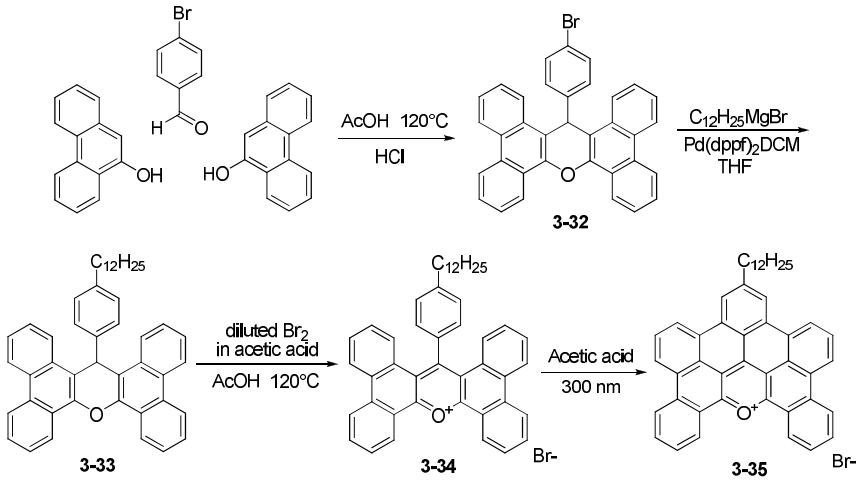

Scheme 3-8. Synthetic route toward 9-dodecyl-DBNAX bromide **3-35**.

In order to study the self-assembly behavior of DBNAX salt in solution, mono alkyl chain substituted DBNAX bromide was also synthesized in a similar method. As shown in Scheme 3-8, the condensation of 9-phenanthrenol and 4-brombenzaldhyde with acetic acid as solvent produced 18-(4-bromophenyl)-18*H*-tetrabenzo[*a,c,h,j*]xanthene (**3-32**) in a yield of 52%. The alkyl chain substituted tetrabenzo[*a,c,h,j*]xanthene **3-33**, could be derived from Kumada coupling of **3-32** and Grignard reagent in a yield of 70%. The oxidation of compound **3-33** with bromide in acetic acid resulted in 18-(4-dodecylphenyl)tetrabenzo[*a,c,h,j*]xanthenium bromide (**3-34**, yield = 76%) as red solid. The final photocyclization of **3-34** in acetic acid produced the target 9-dodecyl-DBNAX bromide **3-35** (yield = 42%) as purple precipitate. All molecules were characterized by ^{1}H NMR, ^{13}C NMR spectroscopy as well as MALDI-TOF mass spectrometry.

In the interest of getting DBNAX salts with different anions, stepwise oxidization of tetrabenzo[*a,c,h,j*]xanthene (**3-30**) was also applied in this work (Scheme 3-9): The oxidization of compound **3-30** with PbO_2 gave 18-phenyl-18*H*-tetrabenzo[*a,c,h,j*]xanthen-18-ol (**3-36**) in a yield of 93%. The succeeding treatment of **3-36** with tetrafluoroborate acid (48% in aqueous solution) produced 18-phenyltetrabenzo[*a,c,h,j*]xanthenium tetrafluoroborate (**3-33b**). Finally, DBNAX teterfluoroborate (DBNAX BF_4, **3-6b**) was obtained by photocyclization of **3-33b** in dichloromethane accordingly.

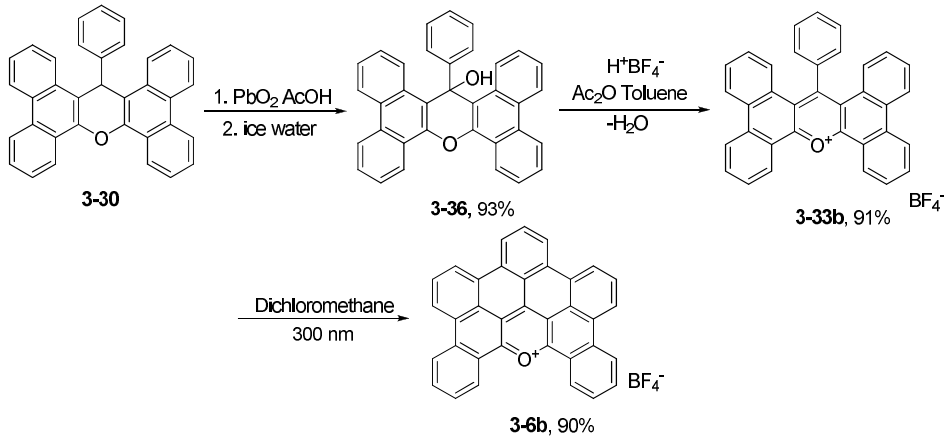

Scheme 3-9. Synthesis of DBNAX salt with tetrafluoroborate as anion.

To obtain a better understanding of the photocyclization to oxygen containing PAHs with positive charge, 2,3,4,5,6-pentaphenylpyrylium bromide **3-37** was also synthesized and irradiated with 300 nm UV. However, no dehydrogenated product but the starting material as well as decomposed product was detected by FD MS (not shown here) after continuous irradiation for several days. It was believed that the different structure of compound **3-33** and **3-37** caused the different results of their photolysis dehydrogenation. In the study of the photocyclization of stilbenes, it was concluded that steric hindrances could also greatly effect the photocyclization of stilbene derivatives.[35-39] Obviously, **3-37** which contained five free rotating phenyl rings required more energy to form planarized structure.

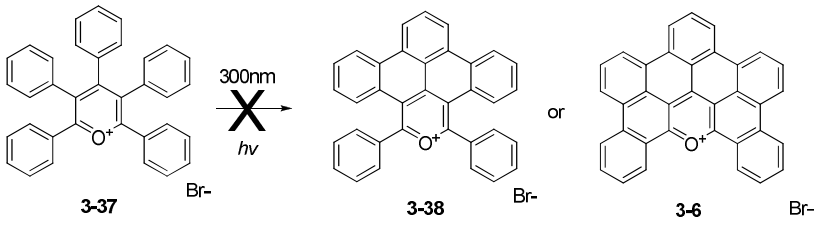

Scheme 3-10. Irradiation of 2,3,4,5,6-pentaphenylpyrylium salts **3-37** failed to give dehydrogenated product.

3.2.3 Synthesis of benzo[5,6]naphthaceno[1,12,11,10-*jklmna*]-thioxanthylium (BNATX) salts

As discussed in section 3.1, small sulfur containing aromatic compounds with

positive charge such as thiopyrylium and thioxanthylium salts are of great interest in the area of chemistry as well as physics.[11, 24, 40-50] Nevertheless, large sulfur containing PAHs with positive charge are still elusive. In this section, we present the synthesis and characterization of a novel sulfur containing PAH with positive charge on the aromatic core, benzo[5,6]naphthaceno[1,12,11,10-*jklmna*]thioxanthylium (BNATX, **3-7**) salts.

One of the most widely used method to prepare sulfur containing aromatic compounds with positive charge was the ion exchange of its pyrylium analog and sodium sulfide (Na_2S).[51, 52] For example, 2,4,6-triphenylthiapyrylium salt **3-39** could be obtained directly from 2,4,6-triphenylpyrylium salt and Na_2S in the mixed solvent of water and acetone.[46] However, this method could not be applied in the synthesis of dibenzo[*a*,*j*]thioxanthenylium derivates due to the high reactivity of dibenzo[*a*,*j*]xanthenylium salt **3-4** and protic solvent such as water and methanol (See section 3.2.1.2). Therefore, a synthetic route for BNATX salts with 14-phenyl-14*H*-dibenzo[*a*,*j*]thioxanthene (**3-40**) as intermediate was developed in this work:

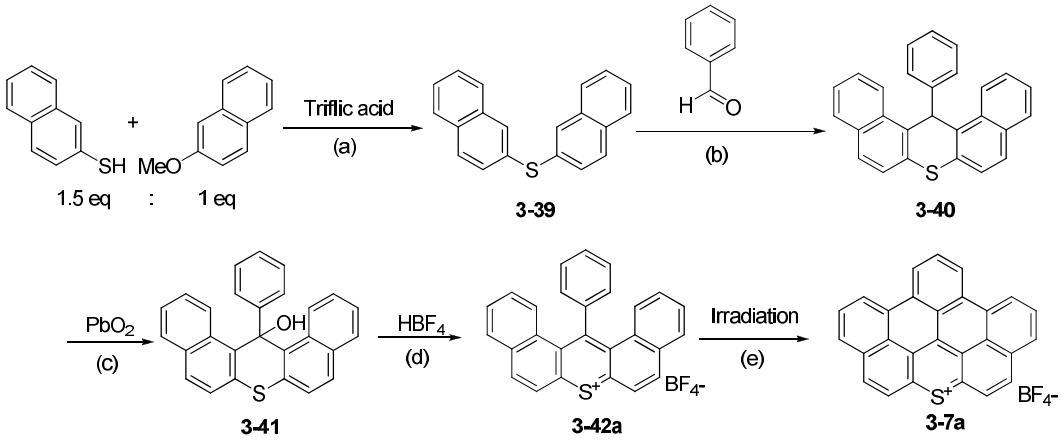

Scheme 3-11. Synthesis of BNTAX salt; (a) triflic acid (1 eq to 2-methoxynaphthalene), anhydrous toluene, refluxing, overnight, yield = 50%; (b) benzaldehyde (1 eq), acetic anhydride, 120°C, 6 hours, yield = 43%; (c) PbO_2 (1.5 eq), glacial acetic acid, 120°C, 3 hours, yield = 93%; (d) HBF_4 (48% in water, 5eq), acetic anhydride and toluene (3 : 1), -5°C, 30 minutes, yield = 80%; (e) dichloromethane, 300 nm, r.t., *c.a.* 16 hours, yield = 85%.

As shown in Scheme 3-11, the triflic acid catalyzed ether-sulfide exchange reaction[53] between 2-methoxynaphthalene and naphthalene-2-thiol gave dinaphthalen-2-ylsulfane (**3-39**) in a good yield. Condensation of **3-39** and benzaldehyde in acetic acid anhydride resulted in 14-phenyl-14*H*-dibenzo[*a,j*]thioxanthene (**3-40**). The subsequent oxidization of **3-40** with PbO_2 produced 14-phenyl-14*H*-dibenzo[a,j]thioxanthen-14-ol (**3-41**) as white powder. 14-Phenyldibenzo[*a,j*]thioxanthenium tetrafluoroborate (**3-42a**) was then obtained by adding tetrafluoroborate acid drop-wise to the solution of **3-41** under a ice-water bath. Irradiation of **3-42a** in dichloromethane under 300 nm UV light overnight gave benzo[5,6]naphthaceno[1,12,11,10-*jklmna*]thioxanthylium tetrafluoroborate (BNATX BF_4, **3-7a**) as purple needle like crystals. Further characterization of the product by MALDI-TOF MS spectrometry (TCNQ as matrix) and ^{1}H NMR spectroscopy were in accordance with expectation (Figure 3-6 and Figure 3-7).

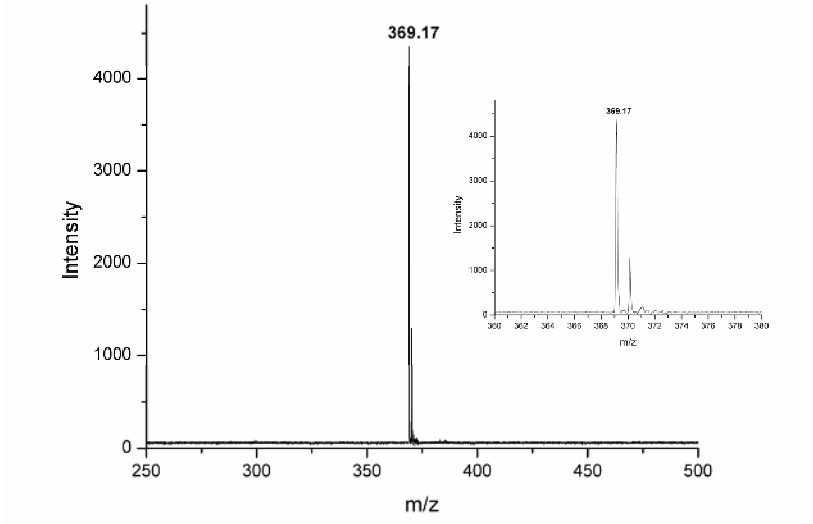

Figure 3-6. MALDI-TOF MS spectrum of compound **3-7a** (MW = 369 without anion).

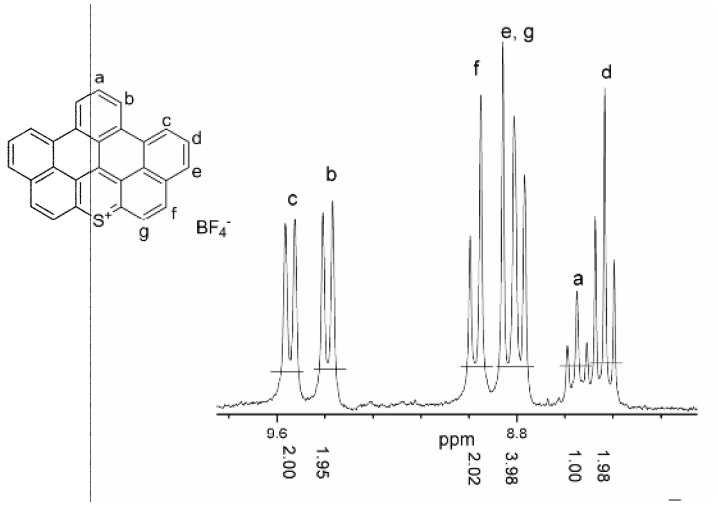

Figure 3-7. ^{1}H NMR spectrum of **3-7a** (r.t., 250MHz, CD_3OD : CD_2Cl_2 = 1 : 1, 8000 ns).

It was notable that in our initial work, the direct oxidization of dibenzo[*a*,*j*]thioxanthene **3-40** with diluted bromine failed to produce dibenzo[*a*,*j*]thioxanthenium bromide **3-42b** as expected (Scheme 3-12). FD MS spectra of the reaction mixture (not shown here) indicated that compound **3-40** was neither oxidized nor brominated even after very long reaction time (over 16 hours). F. D. Saeva *et al.* had concluded that the sulfur containing aromatic cation was more electron withdrawing than oxygen containing aromatic cation by comparing the redox potentials for 2,4,6-triphenylpyrylium and 2,4,6-triphenylthiapyrylium salts.[24] This would suggest that it needed stronger oxidizing agent to form sulfur containing aromatic cation. Therefore, only the two-step oxidization-dehydration process was used to synthesize dibenzo[*a*,*j*]thioxanthenium tetrafluoroborate **3-42a** in this method.

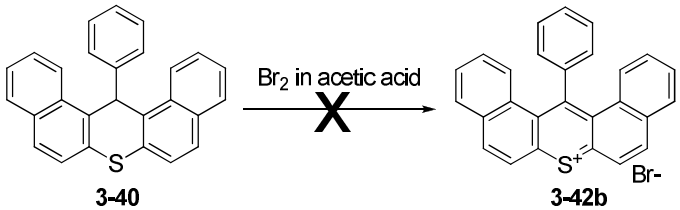

Scheme 3-12. Diluted bromine was unable to oxidize 14-phenyl-14*H*-dibenzo[*a*,*j*]thioxanthene

3.2.4 UV-vis absorption and fluorescence of BNAX and BNATX salts

Toward understanding the photophysical properties of BNAX and BNATX salts, the UV-vis absorption spectra of the dichloromethane solutions of dibenzo[*a*,*j*]xanthenylium **3-4a**, BNAXBr **3-5a** and BNATXBF$_4$ **3-7a** were compared in Figure 3-8. The basic absorption spectrum for **3-4a** was dominated by two major intense bands located at 509 (log ε = 4.63) and 310 nm (log ε = 4.72). In contrast, the absorption spectrum of dehydrogenated **3-5a** was rich and contained a number of bands, the most prominent being at 573 (log ε = 4.71), 435 (log ε = 4.16), 353 (log ε = 4.51) and 323 nm (log ε = 4.65). Furthermore, positively charged **3-7a** had three major bands which were at 600 (log ε = 4.31), 477 (log ε = 4.09) and 343 (log ε = 4.69), respectively. Compared with **3-5a**, the effect of sulfur atom in **3-7a** was to produce a hypochromic effect (i.e. a decrease in intensity, defined by IUPAC)[48] on the intensity of the absorption between 400 to 650 nm as well as an apparent red-shift in the maximum absorption (27 nm).

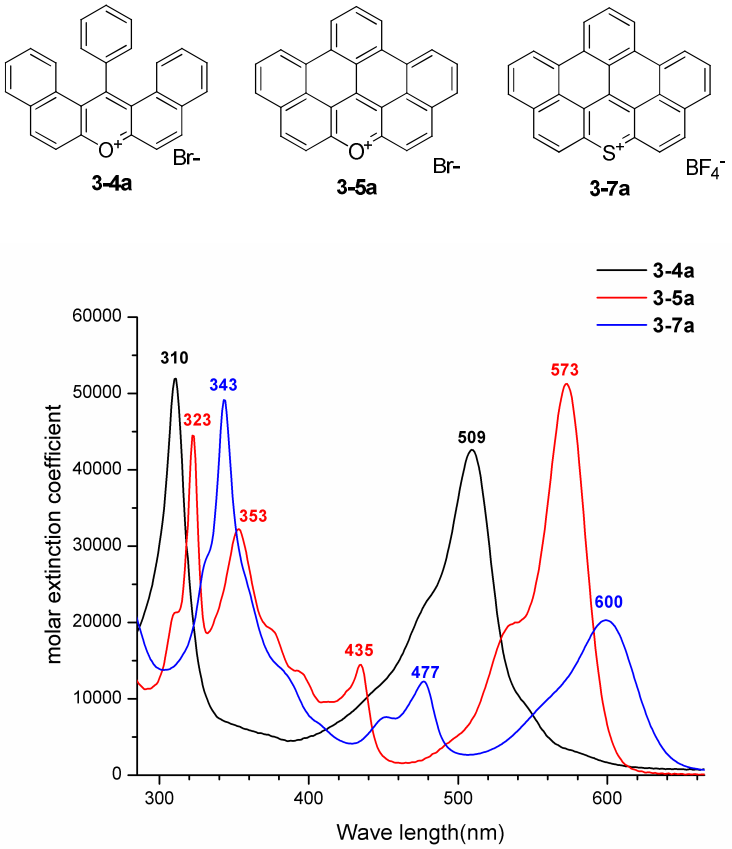

Figure 3-8. UV-vis absorption spectra of **3-4a** (black)**, 3-5a** (red) and **3-7a** (blue) in CH_2Cl_2, measured at room temperature.

The emission spectra of three compounds were also compared in this work. Fluorescence from **3-4a** could be observed in dichloromethane solution at 25 °C, though the dependence of the band shape on the excitation wavelength strongly supported that this was an artifact caused by minute traces of an impurity (not shown here).[54] As discussed in previous sections, compound **3-4a** was sensitive to water and photo irradiation. Therefore, such an impurity might be the addition product of **3-4a** with water in the environment as well as the dehydrogenated **3-5a** which was formed during the exciting process. By contrast, fluorescence from **3-5a** and **3-7a** were readily observed which were centred at 593 and 643 nm, respectively (Figure 3-9). The excitation and absorption spectra of **3-5a** as well as **3-7a** were in good agreement, and the small Stokes' shifts (SS) of 20 and 43 nm for each compound indicated a modest change in structure after relaxation from the initially produced Franck–Condon state.[54-56]

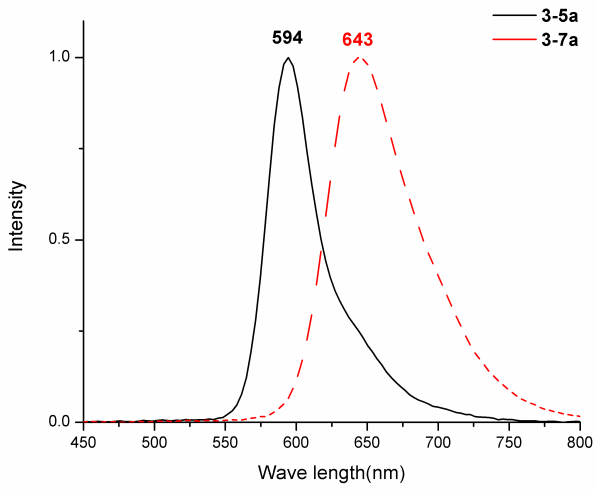

Figure 3-9. Fluorescence spectra of **3-5a** and **3-7a** in dichloromethane (r.t., excitated at 600 nm).

3.3 Supramolecular behavior of BNAX derivates

As mentioned in Chapter 1, the supramolecular chemistry of PAHs is significant for their applications. Ordered and controllable arrangement of PAHs can not only enhance their performance but also simplified the processing of organic devices.

However, to the best of our knowledge, such investigation on oxygen containing PAHs with positive charge is still absent. In this work, the liquid crystals from multi-alkyl substituted BNAX salts as well as the nanofibers formed by mono-alkyl substituted BNAX and DBNAX salts in solution were investigated and the results are presented here.

3.3.1 Discotic liquid crystalline from BNAX salts

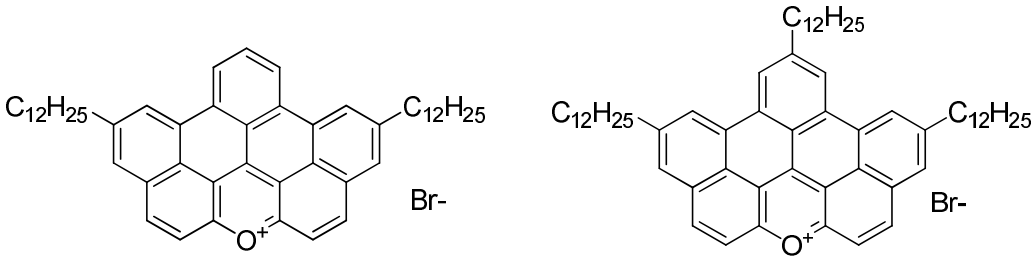

3-25 **3-27**

Scheme 3-13. Two BNAX salts used for liquid crystal behavior study.

With the help from Dr. W. Pisula, the supramolecular arrangement of the di- (**3-25**) and tridodecyl (**3-27**) substituted BNAX salts was investigated by using two-dimensional X-ray scattering experiments (2D-WAXS). For this propose, the extruded filaments were prepared from both compounds at 120 °C (Both compounds do not reveal any phase transition during DSC scans within a temperature range of -100 to 300 °C.).

At the temperature of 30 °C, the X-ray diffractions indicated for both compounds similar 2D patterns. As an example, the pattern of **3-27** was shown in Figure 3-10. The distribution of the reflections in the pattern was characteristic and could be separated into an equatorial and meridional plane. The equatorial small angle reflections were assigned to typical columnar structures assembled by the discotic molecules. These columnar stacks were well-aligned in the extrusion direction, whereby the positions of the reflections were related to a unit cell characteristic for the intercolumnar arrangement. In this case, a hexagonal cell with a parameter of 3.97 nm was derived. The equatorial distribution of the scattering intensities as a function of the scattering angle was shown in Figure 3-10c.

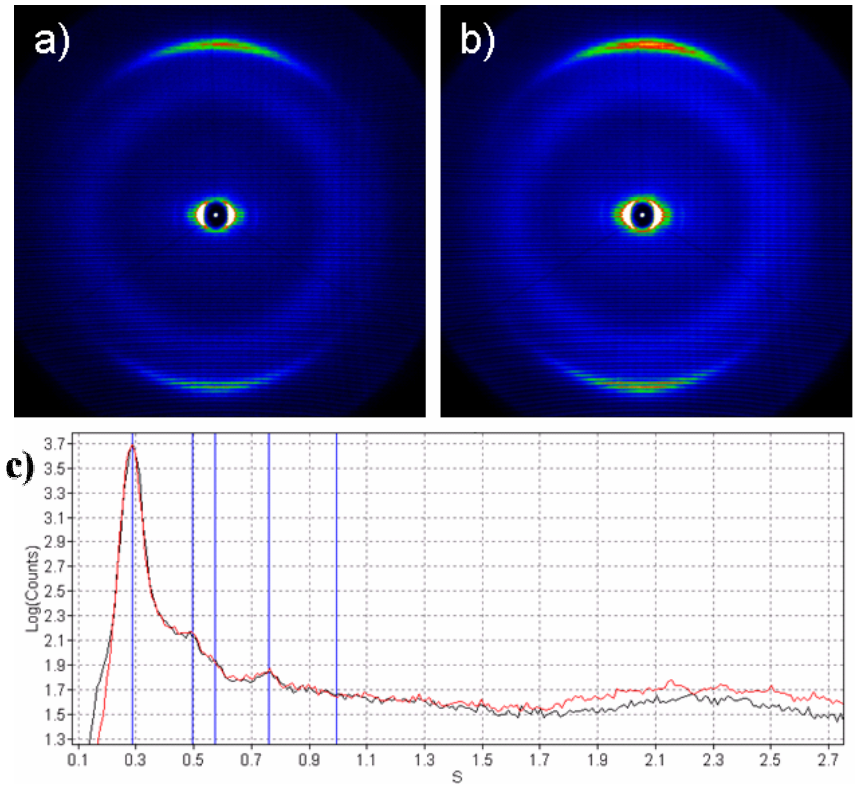

Figure 3-10. 2D-WAXS patterns of **3-27** at (a) 30 °C and (b) 150 °C, (c) equatorial distribution of the scattering intensities as a function of the scattering angle from the pattern recorded at 30 °C.

Interestingly, the parameter of the unit cell was almost twice larger than the simple molecular size (The fully stretched length of **3-27** was 2.2 nm which was simulated by MM2 method.). Considering the non-covalent intermolecular forces such as dipole-dipole, ionic, hydrophilic and hydrophobic interactions between the molecules which stacked in the columns, it was reasonable to assume that a kind of dimer structure was formed in the liquid crystal phase. Figure 3-3 displayed schematically the molecular shoulder-to-shoulder arrangement which was the most probable conformation of interacting **3-27** with each other because the repulsion of the cations could be reduced effectively by this way. Taking into account this dimer conformation and a minor intercolumnar repulsion, the large hexagonal unit cell of 3.97 nm was derived in a straightforward way.

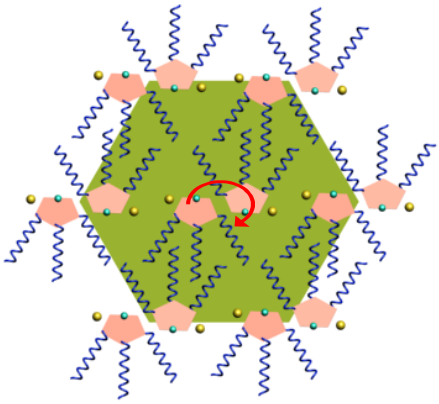

Figure 3-11. Schematic illustration of the dimer formation by a shoulder-to-shoulder arrangement of **3-27** and the corresponding hexagonal unit cell. The red arrow indicates the typical in-plane rotation of the dimer in the liquid crystalline phase.

The wide angle meridional reflections were attributed to a π-π stacking distance of 0.34 nm between individual dimers within the columnar structures. The dimers were packed in a non-tilted manner with their planes perpendicular to the columnar axis. The structural analysis suggested a columnar liquid crystalline phase for **3-27** due to the typical hexagonal unit cell, non-tilted stacked discs and finally the appearance of an amorphous halo, which could be explained by the disordered alkyl chains. Interestingly, the organisation and the corresponding dimensions of the liquid crystalline phase did not change at higher temperatures (Figure 3-10b, 150 °C) suggesting a pronounced stability of this state.

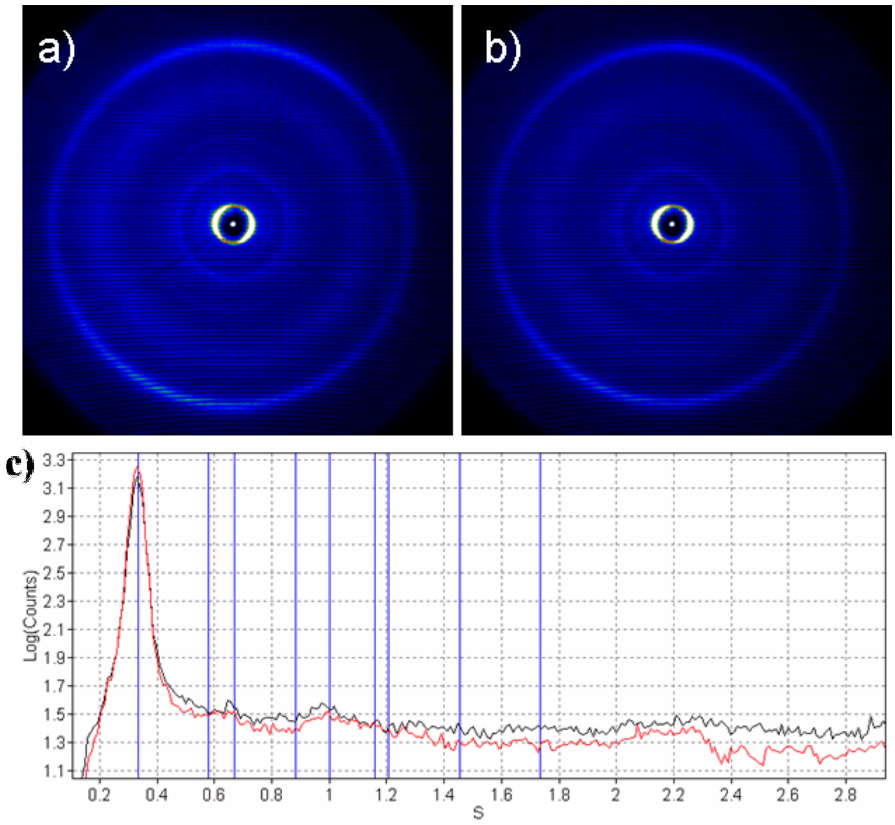

Figure 3-12. 2D-WAXS patterns of **3-25** at a) 30 °C and b) 150 °C, c) equatorial distribution of the scattering intensities as a function of the scattering angle from the pattern recorded at 30 °C.

The structural investigation of the didodecyl substituted BNAX salt **3-25** revealed a similar organization as described for **3-27** (Figure 3-12). Again, from the equatorial reflections a hexagonal unit cell with a slightly smaller parameter of 3.49 nm was determined. In this case, a dimer formation was also identified, whereby the slight decrease in the size of the unit cell could be explained by the substitution which only two instead of three dodecyl side chains, which influenced the intercolumnar distance. Furthermore, the intracolumnar non-tilted packing mode was identical to **3-27** with a π-π stacking distance of 0.34 nm. Therefore, compound **3-25** was characterised also as liquid crystalline, although it was just substituted by two dodecyl chains. The main difference between **3-25** and **3-27** was obvious from the meridional reflections contributed to π-stacking correlations. For **3-27** these reflections were more distinct, whereby for **3-25** they were more sharp, but more isotropic. The sharpness of the scattering intensities could be attributed to an enhanced π-π

interaction between dimers due to less disturbing side chains, while the isotropic shape of the reflections was due to the powder-like character of the material. Compound **3-27** was more waxy and could be therefore macroscopically better aligned leading to more distinct reflections.

3.3.2 Self-assembly of BNAX salts in solution

Besides the liquid crystalline behavior of alkylated BNAX salts, the self-assembly behavior of these amphiphilic molecules in solution was also investigated by us. The UV-vis spectra of mono-dodecyl substituted BNAX bromide **3-24** in different solvents were first compared in Figure 3-13. Its absorption spectrum in dichloromethane had four major bands at 576, 439, 357 and 327 nm respectively, whereas in methanol all the absorption peaks had a blue-shift, indicating that **3-24** had a different stacking behavior in its methanolic solution[57].

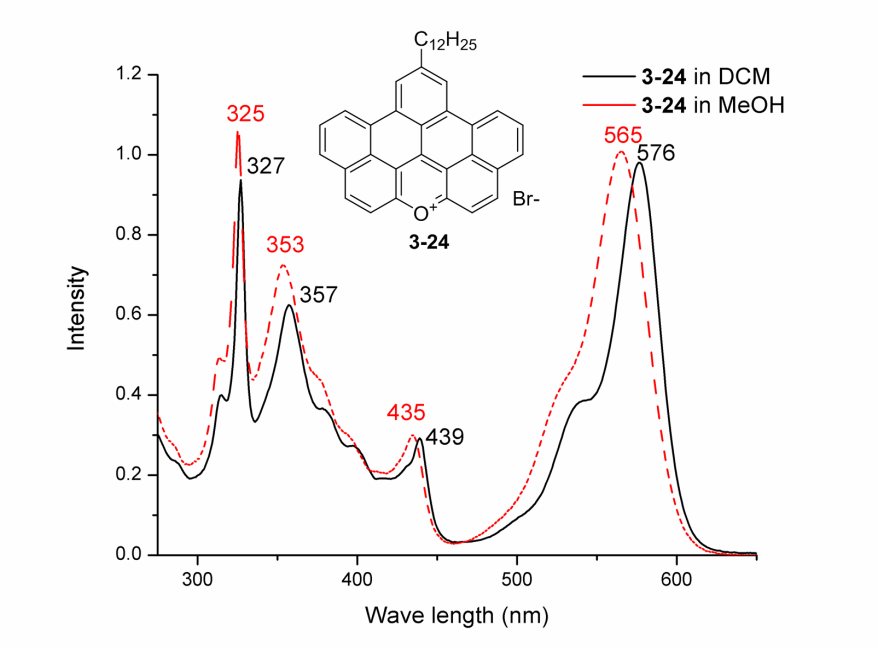

Figure 3-13. UV-vis spectra of **3-24** in dichloromethane (black) and methanol (red); 1 x 10^{-5} mol/l, r.t..

In order to further study the stacking behavior of **3-24** in different solvents, the morphology of the aggregates from **3-24** was observed by scanning electron microscopy (SEM) after drop-casting the solutions on silicon wafers. As shown in

Figure 3-14a and b, **3-24** formed a continuous film from its dichloromethane solution and no fine structures could be observed. Differently, fiber-like aggregates of **3-24** were formed from its methanolic solutions (Figure 3-14c and d). These nano fibers had a diameter of about 200 nm and the lengths are ranging from 1 to 2 µm. It was notable that the hydrophilic aromatic cation and the hydrophobic alkyl chain qualified **3-24** as an amphiphile. Compared with dichloromethane, methanol has stronger polarity and different solubility for the aromatic cation and alkyl chain of **3-24**. Therefore, amphiphile **3-24** could form ordered aggregates in methanol but not in dichloromethane.

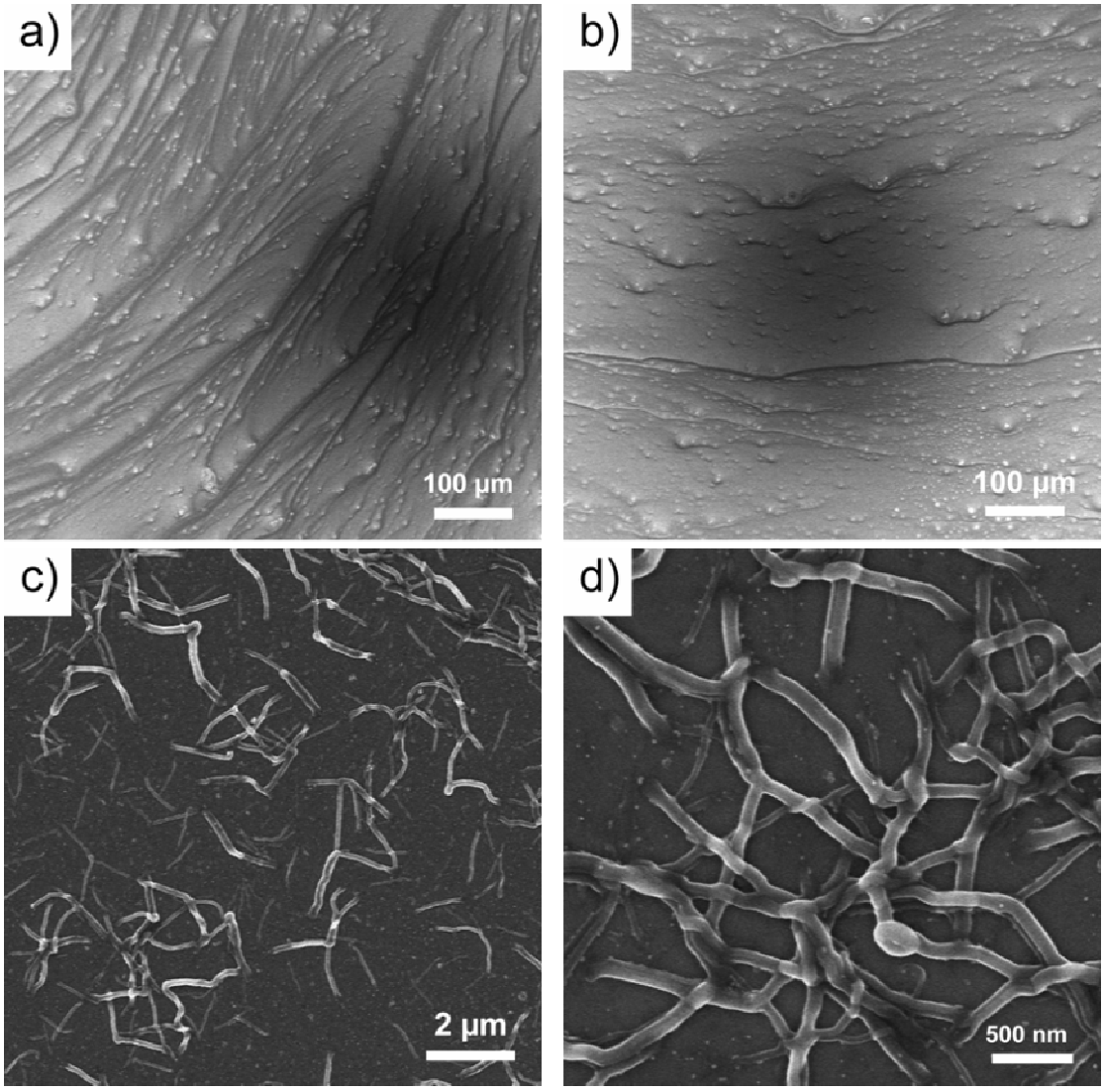

Figure 3-14. (a) and (b): SEM images of film formed by the dichloromethane solution of **3-24** (5×10^{-4} mol/l, drop-cast on a silicon wafer); (c) and (d): SEM images of nano fibers from

the methanolic solution of **3-24** (5×10^{-4} mol/l, drop-cast on a silicon wafer).

Furthermore, the self-assembly behavior of 9-dodecyl-DBNAX bromide **3-35**, which was the largest oxygen containing PAHs with positive charge, was also investigated in a similar manner. SEM images (Figure 3-15) indicated that drop-casting the methanolic solution of **3-35** on a silicon wafer also resulted in fiber like aggregates. Their diameters were ranging from 150 to 250 nm and the lengths are between 2.5 to 4 μm.

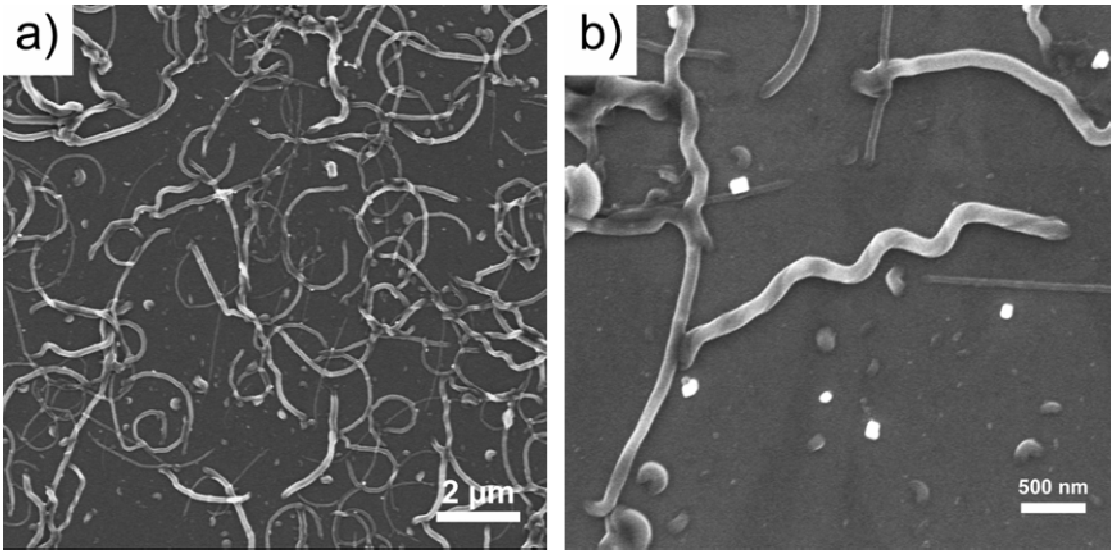

Figure 3-15. (a) and (b): SEM images of the aggregates from the methanolic solution of **3-35** (5×10^{-4} mol/l, drop-cast on a silicon wafer).

Interestingly, different from PQP and DBPQP discussed in Chapter 2, the morphology of the aggregates from **3-24** was similar to **3-35** although the latter compound was a dibenzo derivate of the former one. It should be noted that the morphology difference of the aggregates from PQP and DBPQP was due to the different symmetry and planarity of their aromatic core. PQP was a planar molecule whereas DBPQP became a non-planar one with the two extended benzene ring. However, according to the MM2 method simulated structures of BNAX and DBNAX cations (Figure 3-16), DBNAX cation still kept the planar structure as BNAX cation. Therefore, the effect of enlarged hydrophilic part was balanced out by the enhanced π-π interaction from larger aromatic core. As a result, DBNAX **3-35** still had a

packing mode close to BNAX **3-24** and both compounds could self-assemble into fiber like aggregates in their methanolic solution.

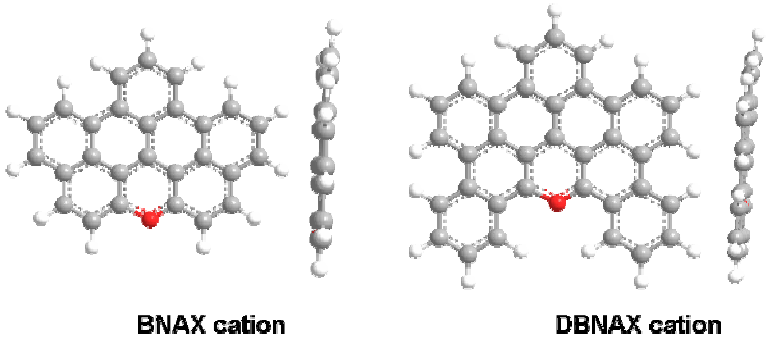

Figure 3-16. The simulated structures of BNAX and DBNAX cations (optimized with MM2 method).

3.4 Conclusion

In the summary, the synthetic strategy of positively charged oxygen containing BNAX salts and its dibenzo derivates, DBNAX salts were successfully developed by us. On the other hand, positively charged sulfur containing BNATX salts were also synthesized in this work. With our method, various BNAX salts with different alkyl chains could be obtained in moderated yields. And their supramolecular behavior were subsequently investigated. Liquid crystal behavior were observed from di- (**3-25**) and tridodecyl (**3-27**) substituted BNAX salts and both compounds exhibited large unit cell in their 2D-WAXS patterns which could be attributed to the formation of unique dimer structures. Furthermore, monododecyl substituted BNAX bromide **3-24** and DBNAX bromide **3-35** showed aggregation behavior in solutions. By drop casting their methanolic solution on silicon wafers, similar nano scaled fibers from both compounds can be observed. It is worthy to note that one reason which limited the application of xanthylium salts is their stability since they can easily react with nucleophilic reagents and are sensitive to irradiation.[58-60] However, BNAX and BNTAX salts reported here have impressive chemical stability. The UV-vis absorbance and fluorescence of the methanolic solution of BNAX and BNTAX salts kept unchanged for several months. Their FD mass and ^{1}H NMR spectra (not shown

here) also did not indicate the emergence of any new compounds or decomposition. Therefore, these oxygen/sulfur containing PAHs with positive charge which have different substituents as well as unique properties are expected to be used both as novel model compounds for theoretical studies[6-11] and as stable materials for organic devices such as ionic conductive layers of fuel cell[61] or chemical sensors[12] in the future.

References

1. Moghimi, A.; Rastegar, M. F.; Ghandi, M.; Taghizadeh, M.; Yari, A.; Shamsipur, M.; Yap, G. P. A.; Rahbarnoohi, H., *J. Org. Chem.* **2002,** 67, (7), 2065.
2. Gilchrist, T. L., *Heterocyclic Chemistry*. 3rd ed.; Prentice Hall: New Jersey, 1997.
3. Zimmermann, T., *J. Prakt. Chem.* **1994,** 336, (4), 303.
4. Comes, M.; Marcos, M. D.; Martinez-Manez, R.; Sancenon, F.; Soto, J.; Villaescusa, L. A.; Amoros, P.; Beltran, D., *Adv. Mater.* **2004,** 16, (20), 1783.
5. G.Harvey, R., *Polycyclic Aromatic Hydrocarbons*. Wiley-VCH: New York, 1997.
6. Dauben, H. J.; Wilson, J. D., *Chem. Comm.* **1968**, (24), 1629.
7. Khenkin, A. M.; Weiner, L.; Wang, Y.; Neumann, R., *J. Am. Chem. Soc.* **2001,** 123, (35), 8531.
8. Cozens, F. L.; Cano, M. L.; Garcia, H.; Schepp, N. P., *J. Am. Chem. Soc.* **1998,** 120, (23), 5667.
9. Hori, M.; Kataoka, T.; Shimizu, H.; Hsu, C. F.; Hasegawa, Y.; Eyama, N., *J. Chem. Soc.-Perkin Trans. 1* **1988**, (8), 2271.
10. Marcinek, A.; Rogowski, J.; Adamus, J.; Gebicki, J.; Platz, M. S., *J. Phys. Chem.* **1996,** 100, (32), 13539.
11. Heyes, D.; Menon, R. S.; Watt, C. I. F.; Wiseman, J.; Kubinski, P., *J. Phys. Org. Chem.* **2002,** 15, (10), 689.
12. Shamsipur, M.; Rouhani, S.; Mohajeri, A.; Ganjali, M. R.; Rashidi-Ranjbar, P., *Analytica Chimica Acta* **2000,** 418, (2), 197.
13. Fetzer, J. C., *Large (C> = 24) Polycyclic Aromatic Hydrocarbons: Chemistry and Analysis*. Wiley-Interscience: New York, 2000.
14. Fetzer, J. C., *Polycyclic Aromatic Compounds* **2002,** 22, (3-4), 321.
15. Fetzer, J. C., *Polycyclic Aromatic Compounds* **2007,** 27, (2), 143.
16. Claisen, L.; Claparede, A., *Ber. Deut. Chem. Ges.* **1887,** 14, 2460.
17. March, J., *Advanced Organic Chemistry, Reactions, Mechanisms and Structure*. 3rd ed.; John Wiley & Sons: 1985.
18. Carey, F. A., *Organic Chemistry*. 6th ed.; McGraw-Hill: New York, 2006.

19. Claisen, L., *Ber. Deut. Chem. Ges.* **1887,** 20, 665.
20. Werner, A., *Chem. Ber.* **1901,** 34, 3300.
21. McKinnon, D. M., *Can. J. Chem.* **1970,** 48, (21), 3388.
22. Katritzky, A. R.; Chermprapai, A.; Patel, R. C., *J. Chem. Soc.-Perkin Trans. 1* **1980**, (12), 2901.
23. Boldt, P.; Bruhnke, D.; Gerson, F.; Scholz, M.; Jones, P. G.; Bar, F., *Helv. Chim. Acta* **1993,** 76, (4), 1739.
24. Saeva, F. D.; Olin, G. R., *J. Am. Chem. Soc.* **1980,** 102, (1), 299.
25. Taljaard, B.; Goosen, A.; McCleland, C. W., *S. Afri. J. Chem.* **1987,** 40, (2), 139.
26. Wu, J. S.; Pisula, W.; Müllen, K., *Chem. Rev.* **2007,** 107, (3), 718.
27. van de Craats, A. M.; Stutzmann, N.; Bunk, O.; Nielsen, M. M.; Watson, M.; Müllen, K.; Chanzy, H. D.; Sirringhaus, H.; Friend, R. H., *Adv. Mater.* **2003,** 15, (6), 495.
28. Pisula, W.; Menon, A.; Stepputat, M.; Lieberwirth, I.; Kolb, U.; Tracz, A.; Sirringhaus, H.; Pakula, T.; Müllen, K., *Adv. Mater.* **2005,** 17, (6), 684.
29. van de Craats, A. M.; Warman, J. M., *Adv. Mater.* **2001,** 13, (2), 130.
30. Lemaur, V.; Da Silva Filho, D. A.; Coropceanu, V.; Lehmann, M.; Geerts, Y.; Piris, J.; Debije, M. G.; Van de Craats, A. M.; Senthilkumar, K.; Siebbeles, L. D. A.; Warman, J. M.; Bredas, J. L.; Cornil, J., *J. Am. Chem. Soc.* **2004,** 126, (10), 3271.
31. Simpson, C. D.; Brand, J. D.; Berresheim, A. J.; Przybilla, L.; Rader, H. J.; Müllen, K., *Chem.-Eur. J.* **2002,** 8, (6), 1424.
32. Tomovic, Z.; Watson, M. D.; Müllen, K., *Angew. Chem. Int. Ed.* **2004,** 43, (6), 755.
33. Wasserfallen, D.; Kastler, M.; Pisula, W.; Hofer, W. A.; Fogel, Y.; Wang, Z. H.; Müllen, K., *J. Am. Chem. Soc.* **2006,** 128, (4), 1334.
34. Feng, X. L.; Wu, J. S.; Ai, M.; Pisula, W.; Zhi, L. J.; Rabe, J. P.; Müllen, K., *Angew. Chem. Int. Ed.* **2007,** 46, (17), 3033.
35. Mattay, J.; Vondenhof, M., *Topics in Current Chemistry* **1991,** 159, 219.
36. Meier, H., *Angew. Chem. Int. Ed. Engl.* **1992,** 31, (11), 1399.
37. Ramamurthy, V.; Eaton, D. F.; Caspar, J. V., *Accounts Chem Res* **1992,** 25, (7),

299.

38. Whitten, D. G., *Accounts Chem Res* **1993,** 26, (9), 502.
39. Mohrschladt, R.; Schroeder, J.; Schwarzer, D.; Troe, J.; Vohringer, P., *J. Chem. Phys.* **1994,** 101, (9), 7566.
40. Maryanof.Be; Senkler, G. H.; Stackhou.J; Mislow, K., *J. Am. Chem. Soc.* **1974,** 96, (17), 5651.
41. Senkler, G. H.; Stackhou.J; Maryanof.Be; Mislow, K., *J. Am. Chem. Soc.* **1974,** 96, (17), 5648.
42. Stackhou.J; Maryanof.Be; Senkler, G. H.; Mislow, K., *J. Am. Chem. Soc.* **1974,** 96, (17), 5650.
43. Deangelis, F.; Doddi, G.; Ercolani, G., *J. Chem. Soc.-Perkin Trans. 2* **1987**, (5), 633.
44. Beddoes, R.; Heyes, D.; Menon, R. S.; Watt, C. I. F., *J. Chem. Soc.-Perkin Trans. 2* **1996**, (3), 307.
45. Alvaro, M.; Aprile, C.; Carbonell, E.; Ferrer, B. N.; Garcia, H., *Eur. J. Org. Chem.* **2006**, (11), 2644.
46. Branchi, B.; Doddi, G.; Ercolani, G., *J. Org. Chem.* **2005,** 70, (16), 6422.
47. Pau, J. K.; Kim, J. K.; Caserio, M. C., *J. Am. Chem. Soc.* **1978,** 100, (12), 3838.
48. Pau, J. K.; Ruggera, M. B.; Kim, J. K.; Caserio, M. C., *J. Am. Chem. Soc.* **1978,** 100, (13), 4242.
49. Barker, M. G., *Coord. Chem. Rev.* **1979,** 30, (DEC), 305.
50. Kapp, J.; Schade, C.; ElNahasa, A. M.; Schleyer, P. V., *Angew. Chem. Int. Ed. Engl.* **1996,** 35, (19), 2236.
51. Fischer, G. W.; Zimmermann, T., *Zeitschrift Fur Chemie* **1983,** 23, (4), 144.
52. Wizinger, R.; Ulrich, P., *Helv. Chim. Acta* **1956,** 39, (1), 207.
53. Radhakrishnan, K.; Lin, C. H., *Synlett* **2005**, (14), 2179.
54. Benniston, A. C.; Rewinska, D. B., *Org. Biomol. Chem.* **2006,** 4, (21), 3886.
55. Lakowicz, J. R., *Principles of Fluorescence Spectroscopy*. Plenum Press: New York, 1983.
56. Guilbault, G. G., *Practical Fluorescence*. Second Edition ed.; Marcel Dekker, Inc.:

New York, 1990.

57. D'Ilario, L.; Martinelli, A., *Modelling and Simulation in Materials Science and Engineering* **2006,** 14, (4), 581.
58. Dubois, A.; Canva, M.; Brun, A.; Chaput, F.; Boilot, J. P., *Synthetic Metals* **1996,** 81, (2-3), 305.
59. Dubois, A.; Canva, M.; Brun, A.; Chaput, F.; Boilot, J. P., *Applied Optics* **1996,** 35, (18), 3193.
60. Corma, A.; Garcia, H., *Topics in Catalysis* **1998,** 6, (1-4), 127.
61. Binnemans, K., *Chem. Rev.* **2005,** 105, (11), 4148.

Chapter 4

Versatile Synthesis of Nitrogen Containing PAHs with Positive Charge via Dibenzo[*a,j*]xanthenylium Salts

In this chapter, a novel synthetic pathway toward another kind of nitrogen containing PAHs with positive charge, dibenzo[*jk,mn*]naphtho[2,1,8-*fgh*]thebenidinium (DBNT) salts, will be presented. The self-assembly behavior of DBNT derivates will also be discussed.

4.1 Introduction

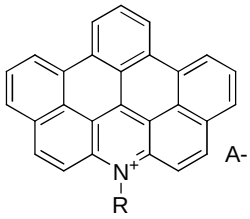

DBNT salts 4-1

Scheme 4-1. Dibenzo[*jk,mn*]naphtho[2,1,8-*fgh*]thebenidinium (DBNT, **4-1**) salts.

The incorporation of heteroatoms into the aromatic framework of PAHs cannot only influence their physical and chemical properties but also modify their supramolecular behavior.[1-7] This is one of the most widely used methods to obtain novel organic materials based on PAHs. However, the research work on heteroatom containing PAHs with positive charge is still rare, which is mainly due to the synthetic difficulties.[8-10] Dibenzo[*jk,mn*]naphtho[2,1,8-*fgh*]thebenidinium (DBNT, **4-1**) salts is one of the large nitrogen containing PAHs with positive charge (including 27 conjugated carbon atoms). The reported synthetic route toward its phenyl substituted derivate, 14-phenyl-dibenzo[*jk,mn*]naphtho[2,1,8-*fgh*]thebenidinium

hexafluorophosphate (PDBNTPF$_{6,}$ **4-5b**) took multi steps with a total yield of 1.9% and required strict dark environment in one step.[10] Therefore, the development of a versatile and efficient synthetic method to DBNT derivates is urgently required for the sake of investigating their properties and potential application in material sciences. Herein, starting from 14-phenyl-14-dibenzo[*a*,*j*]xanthenylium salts (**3**-**4**) as the key building blocks, we present a novel synthetic pathway toward DBNT salts. By this method, various DBNT derivates with different alkyl or alkylphenyl substituents on their nitrogen atoms (the 14 position of DBNT) were conveniently synthesized in two steps. The hydrophilic aromatic core and hydrophobic subsitutents (alkyl/alkylphenyl chains) composed of DBNT derivates as amphiphilic aromatic molecules. Due to the amphiphilic and aromatic interactions between the molecules, they could form one-dimensional (1D) nanofibers simply by drop-casting their methanolic solution on silicon wafers, and the morphology of the nanofibers exhibited an obvious dependence on the alkyl chain length of DBNT tecons.

4.2 Synthesis and characterization

4.2.1 Literature reported synthetic method toward DBNT salt

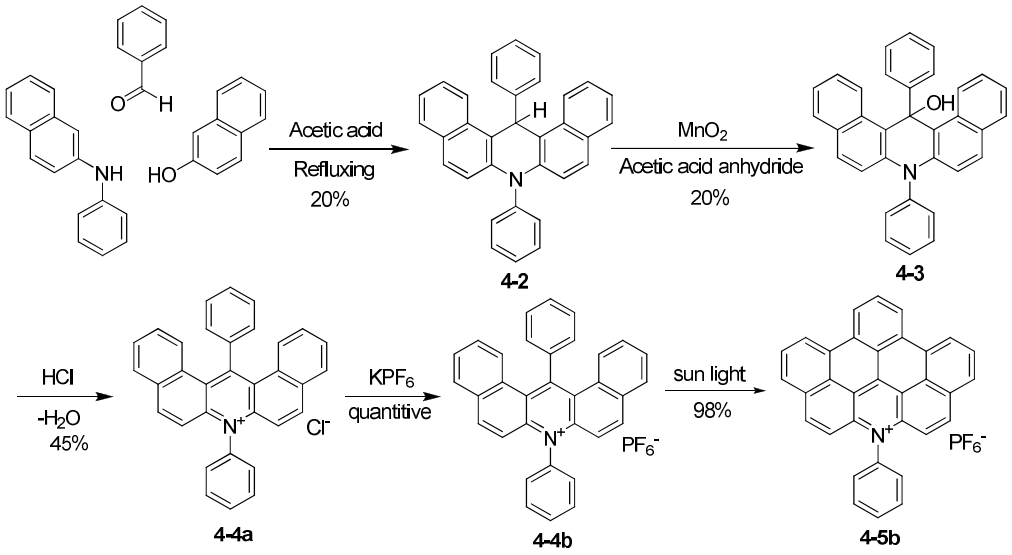

Scheme 4-2. Benniston's method to 14-phenyl-dibenzo[*jk*,*mn*]naphtho[2,1,8-*fgh*]-thebenidinium hexafluorophosphate (PDBNTPF$_{6,}$ **4-5b**).

Compound **4-5b**, which is the only DBNT salt reported so far, was synthesized by A. C. Benniston and his coworkers very recently.[10] The synthetic procedure used to prepare **4-5b** was adapted from the work previously reported by W. Dilthey *et al.*,[9] and its details are shown in Scheme 4-2.

Firstly, the condensation of N-phenyl-2-naphthylamine, benzaldehye and 2-naphthol in glacial acetic acid produced, after recrystallisation, 7,14-diphenyl-7,14-dihydrodibenzo[*a*,*j*]acridine (**4-2)** in a yield of 20%. Subsequent oxidation of compound **4-2** with manganese dioxide (MnO_2) gave the carbinol intermediate, 7,14-diphenyl-7,14-dihydrodibenzo[*a*,*j*]acridin-14-ol (**4-3**). This step had to be performed in the dark as the product was highly light-sensitive. According to Benniston *et al.*, the yields of **4-3** varied from 20 to 68% and the inconsistent yields were attributed to unwanted photodegradation during the reaction. The aromatization of **4-3** by HCl acidification generated 7-phenyl-14-phenyl-dibenz[*a*,*j*]acridinium cation with chloride as anion (**4-4a**, yield = 45%). Following ion exchange of **4-4a** with potassium hexafluorophosphate (KPF_6) and recrystallisation of the precipitate produced more stable 7-phenyl-14-phenyl-dibenz[*a*,*j*]acridinium hexafluorophosphate (**4-4b**). Irradiation of the air purged acetonitrile solution of **4-4b** with sun light resulted in the dehydrogenated product **4-5b** as red precipitate.

This synthetic route was obviously inefficient since the oxidation of **4-2** had to be strictly operated in the dark. Any unexpected exposure under light source caused the drastically decrease of the yield.[10] On the other hand, the substituted phenyl group on the nitrogen atoms of DBNT **4-1** was rigorously defined in the first step. It meant that any attempt to change the substituted groups must start from different 2-naphthylamines at the beginning, where the synthesis was both tedious and uneconomical. Accordingly, an alternative synthetic method was required to avoid these disadvantages and simplify the synthetic protocols.

4.2.2 New synthetic strategy for DBNT derivates

In our previous study on the synthesis of PQP salts, various nitrogen containing 1,2,4,6-tetraphenylpyridinium cations, which were the precursors of PQP salts, were obtained in nearly quantitative yields by the simple reaction between oxygen containing 2,4,6-triphenylpyrylium cations and anilines (See Chapter 2). And in the latter research of BNAX salts, oxygen containing 14-phenyl-14-dibenzo[*a*,*j*]xanthenylium cations (**3-4**) were synthesized by us in efficient methods with easily available starting materials (see Chapter 3). Therefore, in our mind, compound **3-4** could be viewed as the derivate of pyrylium salt with extended aromatic core. The same reaction between pyrylium salt and aniline could be expected for **3-4** and thus undehydrogenated precursors **4-4** could be produced in a novel approach. Accordingly, the synthesis of DBNT salts **4-1** could be simplified greatly.

In our work, the reaction between **3-4** and aniline in anhydrous THF under argon atmosphere did give compound **4-4** in moderate yields. However, as far as we know, the similar conversion from xanthenylium to corresponding acridinium have never been reported so far. In general, the reactions between xanthenylium salts and nucleophilic reagents mainly led to the addition reactions on their C-9 position (the carbon atom on the para position of oxygen atom, Scheme 4-3a).[11-20] The experimental results were consistent with molecular-orbital calculations of xanthenylium derivates.[20] In the case of **3-4**, such addition products of aniline in reaction mixture could also be detected by FD MS spectra (not shown). It was believed that the steric hindrance on the 14 position of **3-4** reduced the amount of addition products and enabled us to obtain **4-4** in reasonable yields.

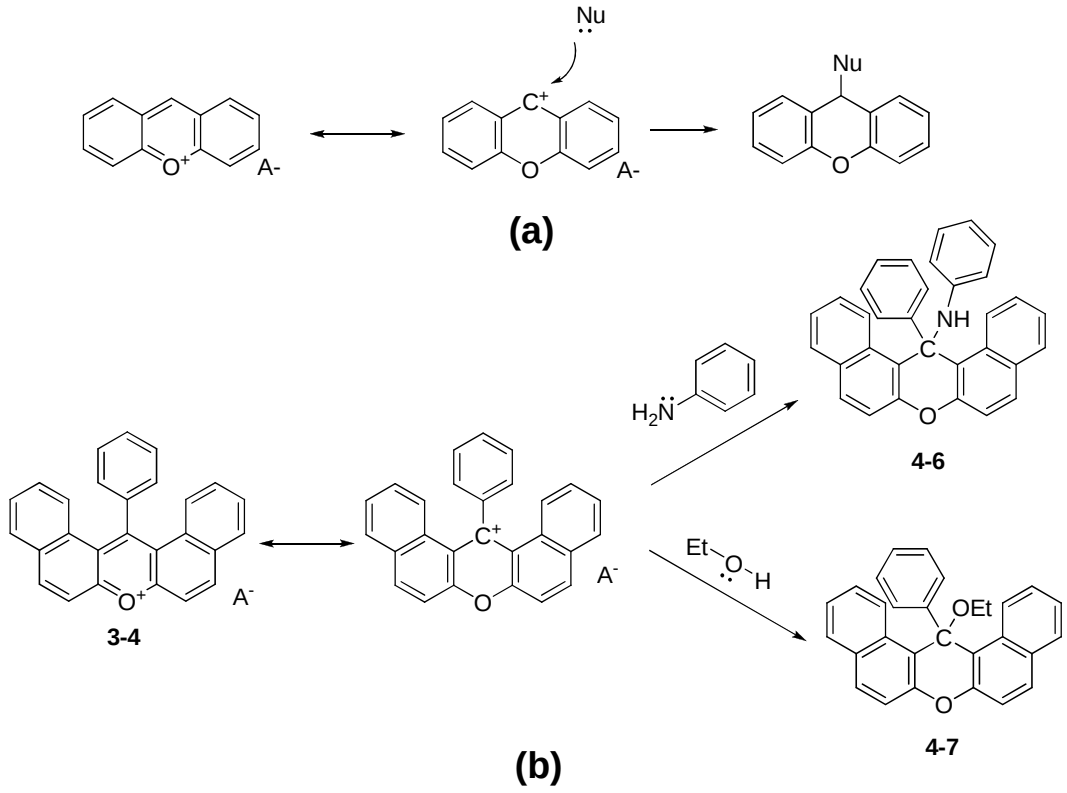

Scheme 4-3. (a) The literature reported reaction between xanthenylium derivates and nucleophilic reagents; (b) The side reaction of **3-4** and aniline and ethanol.

Another side reaction which could decrease the yield of **4-4** was the addition reaction between compound **3-4** and protic solvents such as water, methanol and ethanol (Scheme 4-3b). In our initial research on the synthesis of DBNT salts, ethanol was selected as the solvent for the reaction between **3-4b** and aniline because it was the most common solvent for the preparation of pyridinium salts from pyrylium salts.[8, 16] Whereas FD MS and ^{1}H NMR spectra of the resulting reaction mixture (Figure 4-1) indicated that the main product was from the addition reaction of **3-4b** and ethanol.

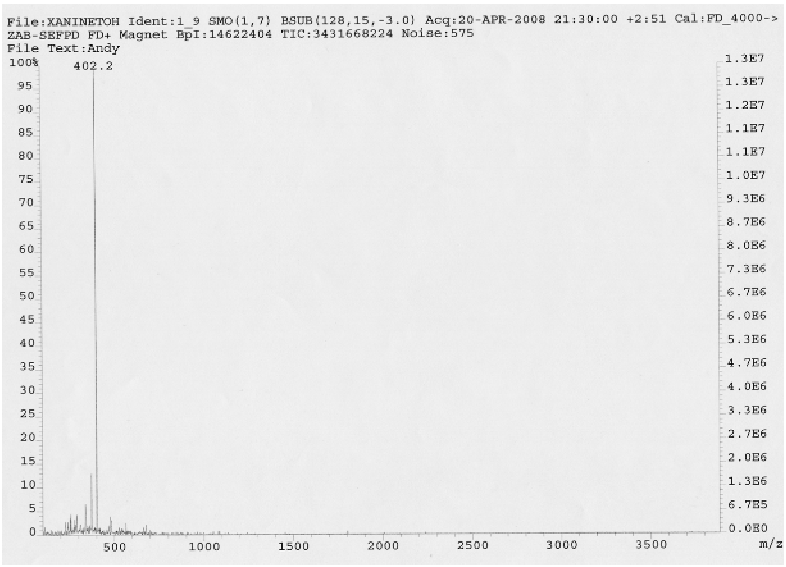

(a)

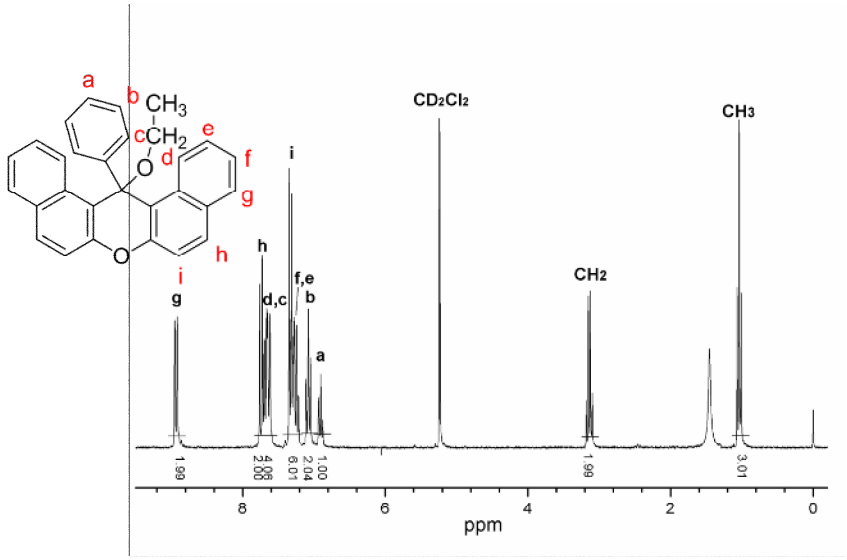

(b)

Figure 4-1. (a) FD MS spectrum of the addition product of **3-4b** and ethanol; (b) ^{1}H NMR specturm of the addition product of **3-4b** and ethanol (r.t., 250MHz, CD_2Cl_2).

Therefore, anhydrous tetrahydrofuran (THF) was chosen as the solvent for the reaction between **3-4** and aniline due to three reasons: first, THF was stable and would not react with **3-4**; secondly, it had moderate solubility for the starting materials; thirdly, the boiling point of THF was high enough to reach the reaction temperature for **4-4**.

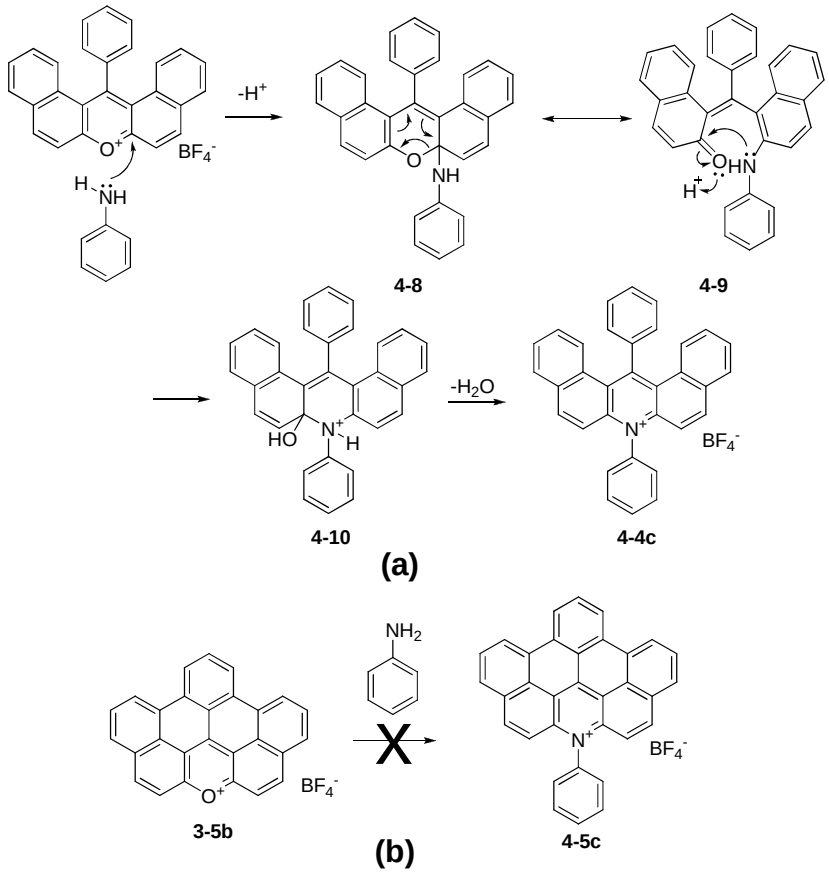

Scheme 4-4. (a) One possible synthetic mechanism of dibenzo[*a,j*]acridinium **4-4c**; (b) BNAX salt failed to react with aniline under the same condition.

A mechanism for the formation of dibenzo[*a,j*]acridinium **4-4** from dibenzo[*a,j*]xanthenylium **3-4** is proposed herein. As shown in Scheme 4-4, it might experience a nucleophilic C-2 opening/recyclization like 1,2,4,6-tetraphenylpyridinium (See Chapter 2). During that process, the first C-2 addition between **3-4** and aniline led to the ring opening product **4-9**. Subsequent intramolecular aldol condensation of **4-9** produced intermediate **4-10**, and the further dehydration reaction of the latter resulted in the recyclized product **4-4**. It was worthy to note that the FD MS spectra (not shown) indicated that the reaction between the BNAX tetrafluoroborate **3-5** and aniline under the same condition failed to give **4-5**, which might be due to the strong strain when opening the pyrylium ring of **3-5**. This result offered additional proof for our hypothesis regarding the formation of **4-4**.

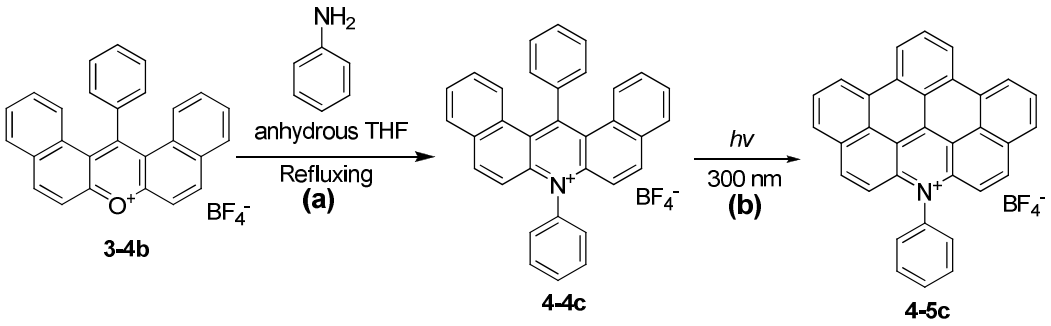

Scheme 4-5. Novel synthetic pathway toward DBNT salt **4-5c**; (a) aniline (1 eq), anhydrous THF, argon bubbling, refluxing, *c.a.* 6 hours, yield = 35%; (b) ethanol, r.t., *hυ*, *c.a.*24 hours, 80%.

With this method, the first DBNT salt synthesized by us was 14-phenyl-dibenzo[*jk*,*mn*]naphtho[2,1,8-*fgh*]thebenidinium tetrafluoroborate (PDBNTBF$_4$, **4-5c**). As shown in Scheme 4-5, the synthetic pathway of **4-5c** involved two steps: the reaction between **3-4b** and aniline gave the undehydrogenated precursors, **4-4c**. The subsequent photocyclization of **4-4c** produced corresponding DBNT salts **4-5c**. The characterization of the product by ^{1}H NMR spectroscopy as well as MALDI-TOF mass spectrometry showed coincidence with the expected structure (Figure 4-2).

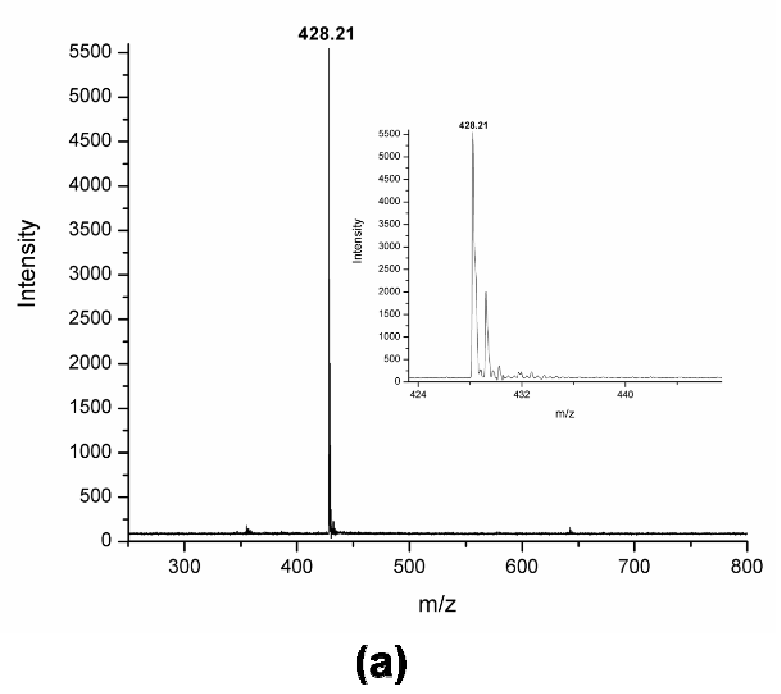

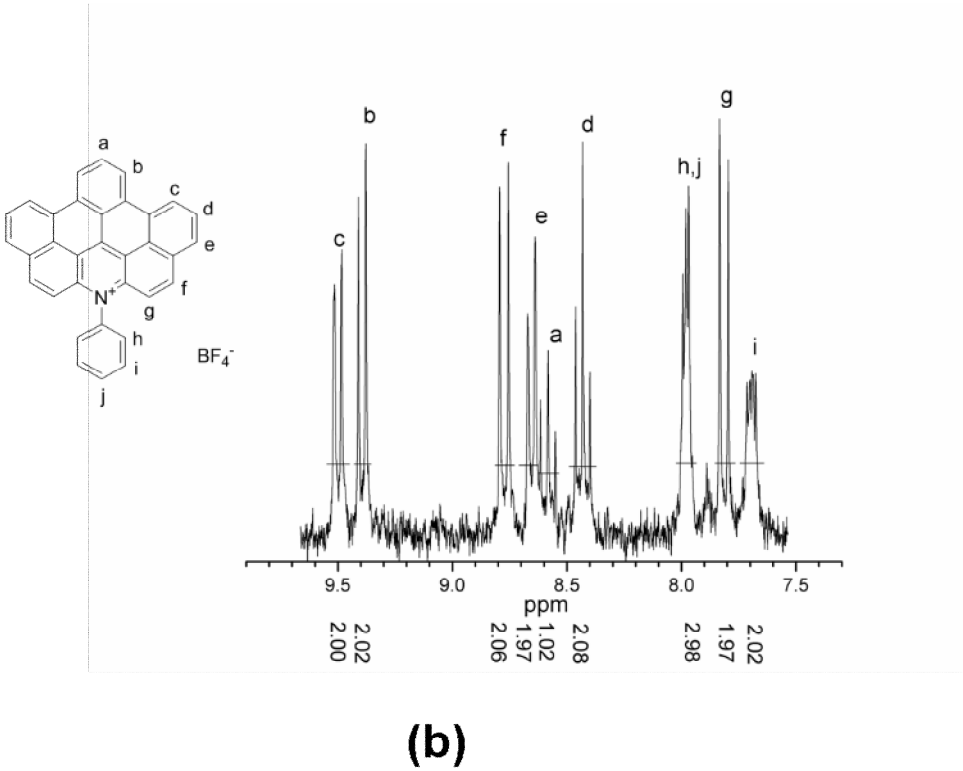

(b)

Figure 4-2. (a) MALDI TOF MS spectra of **4-5c** (MW = 428 without anion); (b) ^{1}H NMR of **4-5c** (r.t., 250MHz, CD_2Cl_2).

In our succeeding work, it turned out that dibenzo[*a,j*]xanthenylium **3-4** could react with anilines as well as amines in a similar manner. Therefore, this synthetic method could be applied to synthesize DBNT derivates with different substituents on their nitrogen atoms (the 14 position of DBNT) by simply using the same starting dibenzo[*a,j*]xanthenylium salt and different anilines/amines. Herein, DBNT derivates with various alkyl or phenyl alkyl chains: 14-hexyl-dibenzo[*jk,mn*]naphtho[2,1,8-*fgh*]thebenidinium bromide (**4-15a**), 14-dodecyl-dibenzo[*jk,mn*]naphtho[2,1,8-*fgh*]thebenidinium tetrafluoroborate (**4-16b**), 14-(4-hexylphenyl)-dibenzo[*jk,mn*]-naphtho[2,1,8-*fgh*]thebenidinium tetrafluoroborate (**4-17b**) and 14-(4-tetradecylphenyl)-dibenzo[*jk,mn*]naphtha[2,1,8-*fgh*]thebenidinium tetrafluoroborate (**4-18b**), were synthesized successfully with the two-step method. All molecules were characterized by ^{1}H and ^{13}C NMR spectroscopy, MALDI-TOF mass spectrometry as well as elemental analysis (Scheme 4-6):

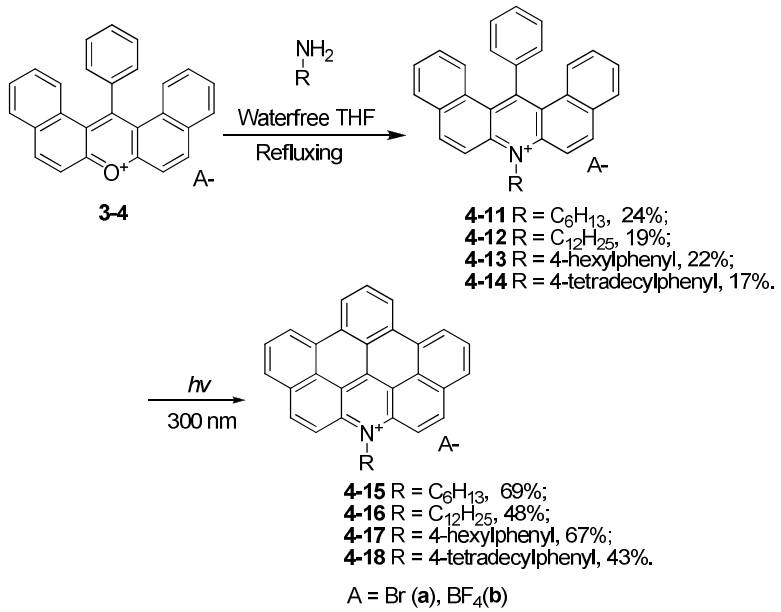

Scheme 4-6. Synthesis of various DBNT derivates with the two step method.

4.2.3 UV-vis absorption and fluorescence spectra of DBNT salts

In the interest of understanding the effect of shape and size of aromatic core on the physical properties of nitrogen containing PAHs with positive charge, the UV-vis absorption and fluorescence spectra of PQPBF$_4$-14 **2-14b** and DBNT **4-18b** in methanol were recorded and compared in Figure 4-3. Compared with **2-14b** (See the detailed description of the UV spectra of **2-14b** in Chapter 2), compound **4-18b** showed similar absorption bands among which the first main band was at 328 (log ε = 4.79), and the other two low energy bands were located at 416 (log ε = 4.34), and 507 nm (log ε = 4.63) respectively. The absorption maximum of **4-18b** (328 nm) showed a significant bathochromic shift with respect to the corresponding band of **2-14b** (305 nm). On the other hand, both molecules exhibited structureless emission peaks in their fluorescence spectra. Remarkably, the emission maximum at 535 nm for **4-18b** was red-shifted by 69 nm compared with **2-14b** (466 nm). The obvious difference of the absorbance and fluorescence spectra indicated a strong influence of the extension of the aromatic core size[21, 22] on their photophysical properties, which was similar to the other extended PAHs.[23, 24]

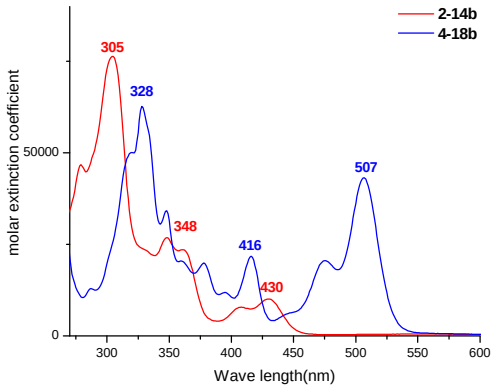

(a)

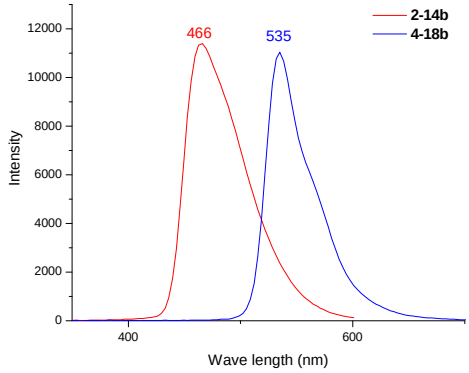

(b)

Figure 4-3. The UV-vis absorption (a) and fluorescence (b) of the different nitrogen containing PAHs with positive charge: **2-14b** (red) and **4-18b** (blue).

4.3 Self-assembly of DBNT salts

As shown in Chapter 2, we investigated the self-assembly behavior of alkylated PQP derivates in solution and obtained nanoscaled aggregates with different morphologies such as fibers and tubes by using PQP salts with different alkyl chains and counterions.[25] In order to obtain better understanding of the relationship between the aggregation of nitrogen containing PAHs with positive charge and the size of their aromatic cores, the self-assembly behavior of DBNT salts **4-15a** and **4-18b** in solution was investigated in a similar manner.

The morphology of the aggregates from these two DBNT salts was firstly studied by scanning electron microscopy (SEM) after drop-casting their methanolic solution

on silicon wafers. As shown in Figure 4-4a and b, compound **4-15a** formed fibrous aggregates and the diameters of these wirelike fibers were ranging from 150 to 200 nm, which was similar to the aggregates of PQP salt with hexyl chain and chloride as anion (compound **2-10a**). In the case of compound **4-18b** with longer alkyl chain and larger anion, aggregates with fibrous structures were also obtained. But it was interesting to note that their diameters were about 50 nm and some of them contained a helical structures (Figure 4-4c and d). Such helical structures were also observed for PQP salt with tetradecyl chain and tetrafluoroborate as anion (compound **2-14b**).

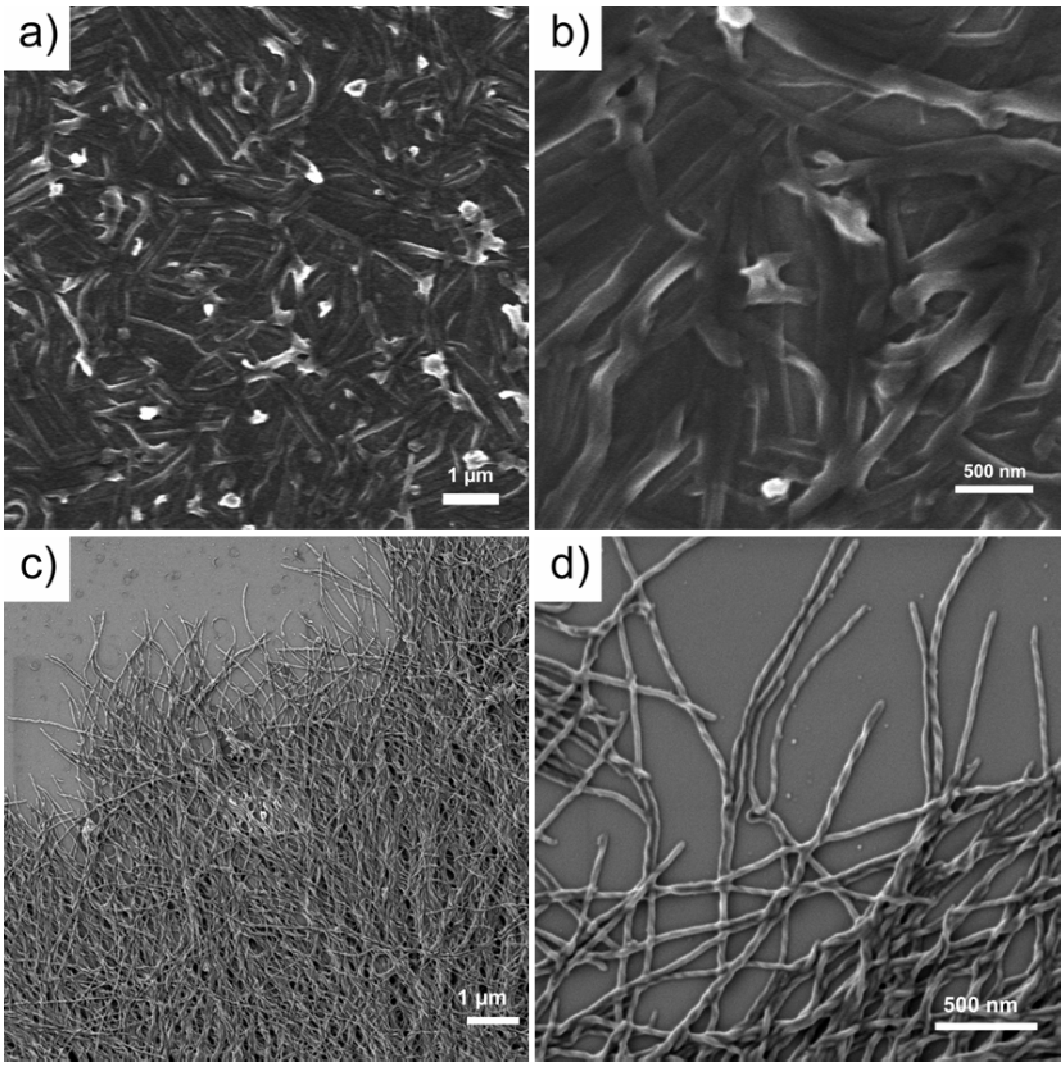

Figure 4-4. (a) and (b) SEM image of the aggregates formed by **4-15a**; and (c) and (d) SEM image of the aggregates formed by **4-18b**; ($1x10^{-3}$ mol/L in methanol, drop-cast on a silicon wafer).

The different morphology of aggregates from two compounds suggested that DBNT salts with different alkyl/alkylphenyl chain might also adopt different packing models, which was similar to previous description for PQP salts with different alkyl chains. Subsequent wide angle X-ray scattering (WAXS) measurements of the dry powder of **4-15a** and **4-18b** confirmed this hypothesis. As shown in Figure 4-5, the characteristic reflections of lamellar stacking (d spacings = 40.1, 19.6 and 13.2 Å) appeared in the WAXS patterns of compound **4-18b**, whereas such diffraction peaks could not be observed in the patterns of **4-15a**. Therefore, the morphology change of the aggregates form by **4-15a** and **4-18b** could be explained by the packing parameter theory brought forwarded by Israelachivili[26-29], as the case of PQP salts and other amphiphilic molecules[30-34]. With the increase of alkyl chain length, the increase of intramolecular interactions such as solvophobic effects and attractive interactions between the chains[27, 28] caused lower interaction free energies and a smaller optimal surface area per molecule a_0. As a result, the packing parameter P of **4-18b** increased in respect to **4-15a** and the lamellar aggregates formed accordingly. And their helically coiled shapes might also be caused by the twisted packing of molecules which was derived from the large tetrafluoroborate anion as PQP salt **2-14b**.[25]

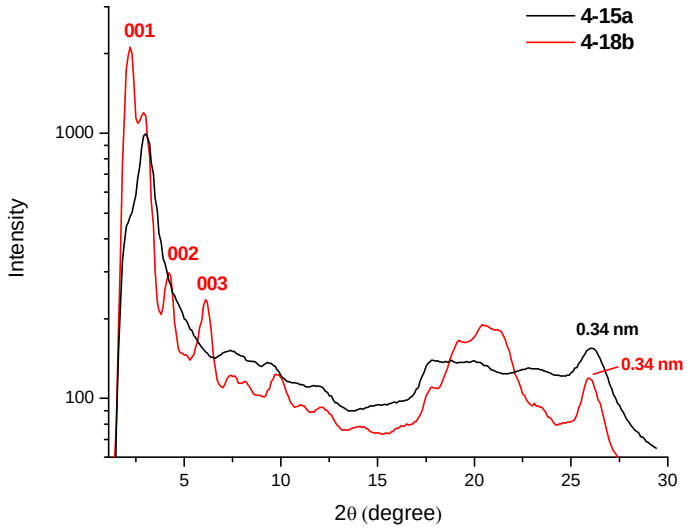

Figure 4-5. WAXS patterns of the dried powder of **4-15a** and **4-18b** obtained from their methanolic solutions.

It should be noted that DBNT cation contains 27 conjugated carbon atoms, which is larger than PQP cation (23 conjugated carbon atoms) but smaller than DBPQP cation (31 conjugated carbon atoms). Simulated structure of DBNT cation, **4-5** (optimized with MM2 method) indicates it is a planar molecule as PQP cation (Figure 4-6).

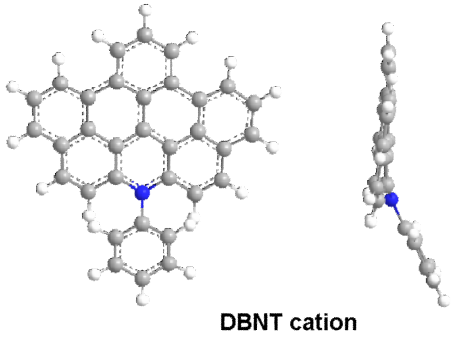

Figure 4-6. The simulated structure of DBNT cation (optimized with MM2 method).

Obviously, the similarity in the morphology of aggregates from PQP and DBNT salts indicated that both kinds of nitrogen containing PAHs with positive charge had similar self-assembly behavior since they both had planar aromatic cores. This result was similar to the case of BNAX and DBNAX discussed in Chapter 3. Combining with the results on the self-assembly study of PQP and BNAX derivates in Chapter 2 and 3, we could draw the conclusion that the governing effects on the morphology of the aggregates from these heteroatom containing PAHs with positive charge are the length of their alkyl chain, the size of their counterions and the symmetry/planarity of the aromatic core but not the size of their aromatic core. And this conclusion can be used as a guideline to design similar molecules with controllable self-assembly behavior in our future work.

4.4 Conclusion

In summary, we have developed a novel synthetic approach toward nitrogen containing DBNT salts. In this method, the undehydrogenated precursors, dibenzo[*a*,*j*]acridinium salts **4-4** could be produced directly from the reaction between dibenzo[*a*,*j*]xanthenylium derivates **3-4** and amine/aniline in reasonable yields.

Therefore, various DBNT salts with different substituents were successfully synthesized in this two-step method. By drop-casting their methanolic solutions on silicon wafers, two DBNT salts, **4-15a** and **4-18b** with different alkyl and alkylphenyl chain formed one dimension nanoscaled fibers with relatively different morphology. The former compound with hexyl chain aggregated into wirelike fibers, whereas the self-assembly of latter one which had tetradecylphenyl chain produced helical aggregates. The difference in their morphology was believed to be mainly due to their different hydrophobic substitutents.[25]

References

1. Bosdet, M. J. D.; Piers, W. E.; Sorensen, T. S.; Parvez, M., *Angew. Chem. Int. Ed.* **2007,** 46, (26), 4940.
2. Pieterse, K.; van Hal, P. A.; Kleppinger, R.; Vekemans, J.; Janssen, R. A. J.; Meijer, E. W., *Chem. Mat.* **2001,** 13, (8), 2675.
3. Bolger, J.; Gourdon, A.; Ishow, E.; Launay, J. P., *J. Chem. Soc.-Chem. Commun.* **1995**, (17), 1799.
4. Bolger, J.; Gourdon, A.; Ishow, E.; Launay, J. P., *Inorg. Chem.* **1996,** 35, (10), 2937.
5. Lemaur, V.; Da Silva Filho, D. A.; Coropceanu, V.; Lehmann, M.; Geerts, Y.; Piris, J.; Debije, M. G.; Van de Craats, A. M.; Senthilkumar, K.; Siebbeles, L. D. A.; Warman, J. M.; Bredas, J. L.; Cornil, J., *J. Am. Chem. Soc.* **2004,** 126, (10), 3271.
6. Barlow, S.; Zhang, Q.; Kaafarani, B. R.; Risko, C.; Amy, F.; Chan, C. K.; Domercq, B.; Starikova, Z. A.; Antipin, M. Y.; Timofeeva, T. V.; Kippelen, B.; Bredas, J. L.; Kahn, A.; Marder, S. R., *Chem.-Eur. J.* **2007,** 13, (12), 3537.
7. Kumar, S.; Rao, D. S. S.; Prasad, S. K., *J. Mater. Chem.* **1999,** 9, (11), 2751.
8. Katritzky, A. R.; Zakaria, Z.; Lunt, E.; Jones, P. G.; Kennard, O., *J. Chem. Soc.-Chem. Commun.* **1979**, (6), 268.
9. Dilthey, W.; Quint, F.; Heinen, J., *Journal Fur Praktische Chemie-Leipzig* **1939,** 152, (3/6), 49.
10. Benniston, A. C.; Rewinska, D. B., *Org. Biomol. Chem.* **2006,** 4, (21), 3886.
11. Awad, S. B.; Abdulmalik, N. F.; Abdou, S. E., *Bull. Chem. Soc. Jpn.* **1975,** 48, (7), 2200.
12. Abdulmalik, N. F.; Awad, S. B.; Sakla, A. B., *Bull. Chem. Soc. Jpn.* **1979,** 52, (11), 3431.
13. Abdulmalik, N. F.; Awad, S. B.; Sakla, A. B., *Helv. Chim. Acta* **1979,** 62, (6), 1872.
14. Koorts, J.; Taljaard, B.; Goosen, A., *South African Journal of Chemistry* **1987,** 40, (4), 237.

15. Katritzky, A. R.; Chermprapai, A.; Patel, R. C., *J. Chem. Soc.-Perkin Trans. 1* **1980**, (12), 2901.
16. Katritzky, A. R.; Zakaria, Z.; Lunt, E., *J. Chem. Soc.-Perkin Trans. 1* **1980**, (9), 1879.
17. Gilchrist, T. L., *Heterocyclic Chemistry*. 3rd ed.; Prentice Hall: New Jersey, 1997.
18. Deno, N. C.; Billups, W. E.; Bingman, J. S.; Lastomir.Rr; Whalen, R. G., *J. Org. Chem.* **1969,** 34, (10), 3207.
19. Hori, M.; Kataoka, T.; Shimizu, H.; Hsu, C. F.; Hasegawa, Y.; Eyama, N., *J. Chem. Soc.-Perkin Trans. 1* **1988**, (8), 2271.
20. Hori, M.; Kataoka, T., *Chemical & Pharmaceutical Bulletin* **1973,** 21, (6), 1282.
21. Reichardt, C., *Chem. Rev.* **1994,** 94, (8), 2319.
22. Pisula, W.; Tomovic, Z.; Stepputat, M.; Kolb, U.; Pakula, T.; Müllen, K., *Chem. Mat.* **2005,** 17, (10), 2641.
23. Yang, X. Y.; Dou, X.; Rouhanipour, A.; Zhi, L. J.; Rader, H. J.; Müllen, K., *J. Am. Chem. Soc.* **2008,** 130, (13), 4216.
24. Tomovic, Z.; Watson, M. D.; Müllen, K., *Angew. Chem. Int. Ed.* **2004,** 43, (6), 755.
25. Wu, D. Q.; Zhi, L. J.; Bodwell, G. J.; Cui, G. L.; Tsao, N.; Müllen, K., *Angew. Chem. Int. Ed.* **2007,** 46, (28), 5417.
26. Tanford, C., *J. Phys. Chem.* **1972,** 76, (21), 3020.
27. Israelachvili, J. N.; Mitchell, D. J.; Ninham, B. W., *Journal of the Chemical Society-Faraday Transactions Ii* **1976,** 72, 1525.
28. Israelachvili, J. N.; Mitchell, D. J.; Ninham, B. W., *Biochimica Et Biophysica Acta* **1977,** 470, (2), 185.
29. Shimizu, T.; Masuda, M.; Minamikawa, H., *Chem. Rev.* **2005,** 105, (4), 1401.
30. Rulkens, R.; Wegner, G.; Thurn-Albrecht, T., *Langmuir* **1999,** 15, (12), 4022.
31. Perahia, D.; Traiphol, R.; Bunz, U. H. F., *Macromolecules* **2001,** 34, (2), 151.
32. Wilson, J. N.; Steffen, W.; McKenzie, T. G.; Lieser, G.; Oda, M.; Neher, D.; Bunz, U. H. F., *J. Am. Chem. Soc.* **2002,** 124, (24), 6830.
33. Inouye, H.; Sharma, D.; Goux, W. J.; Kirschner, D. A., *Biophys. J.* **2006,** 90, (5),

1774.

34. Reches, M.; Gazit, E., *Phys. Biol.* **2006,** 3, (1), S10.

Chapter 5

Ionic Self-assembly of Nitrogen Containing Polycyclic Aromatic Hydrocarbons with Positive Charge

This chapter will describe the preparation of unique aromatic ionic complexes from nitrogen containing polycyclic aromatic hydrocarbon (PAHs) with positive charge through a novel ionic self-assembly (ISA) process. The self-assembly behavior of the resulting ionic complexes will also be discussed.

5.1 Introduction

5.1.1 Ionic self-assembly (ISA)

Noncovalent intermolecular interactions such as hydrogen bonding, van der Waals and aromatic interaction play critical roles in the biological world. Inspired by nature, similar principles are also applied in the construction of structures at the nanoscale in supramolecular chemistry.[1-6] Table 5-1 summarizes some of noncovalent intermolecular interactions, as well as some of their structure determining properties.

It is important to note that those interactions should be sufficiently strong (e.g., of the order of kT, k being the Boltzmann constant, and T is the absolute temperature) to provide sufficient stability, but not so strong that first contacts are irreversibly trapped; the self-optimization of the structures relies on the partial reversibility and the potential exploration of competing structural and energy states.

Table 5-1. Noncovalent intermolecular interactions for self-assembly

Type of interaction	Strength (kJ mol^{-1})	Range	Character
Van der Waals	<5	short	Non-selective, non-directional
H-bonding	5-65	short	Selective, directional
Coordination bonding	50-200	short	Directional
Amphiphilic	5-50	short	Non-selective
Ionic	50-250[a]	long	Non-selective
Aromatic interaction	0-50	short	Non-selective
Covalent	350	short	Irreversible

a. Dependent on solvent and ion solution; data are for organic media.

Among all the secondary interactions, ionic interactions which are also called Coulombic interactions have been largely underestimated in supramolecular chemistry. Although ionic interactions have been often used to build mesogenic amphiphilic salts, the concept of ionic self-assembly was first brought forward by M. Antonietti *et al*. in the beginning of this century.[7-12]

According to Antonietti, ionic self-assembly (ISA) is different from the simple Coulombic binding of salts. ISA is usually accompanied by a cooperative binding mechanism, *i.e.*, the first bonds stimulate further binding which propagate towards the final self-assembled structures. ISA is a very facile route to produce highly organized supramolecular materials from a variety of charged building blocks, by means of complexation with ionic surfactants.[8, 13]

In general, ISA is a technique that organizes multiply charged organic species by means of their association with oppositely charged counterions, with the latter (e.g., surfactants) being functionalized to have desirable properties. Hierarchical superstructures can then be generated in an ISA process, primarily through electrostatic interactions between charged surfactants and oppositely charged oligoelectrolytes. Usually, hydrophobic and hydrophilic interactions act as the secondary driving forces to promote self-organization. Additional interactions, such as

hydrogen bonding and π-π interactions can also be introduced to further stabilize and control the organization of the assemblies.

The construction of liquid-crystalline materials based on stepwise noncovalent interactions allows the properties of the new structures to be easily tuned through the careful choice of the alkyl volume fraction ("internal solvent") by simply exchanging the cation or anion in the assembly step without tedious synthetic operations. For example, introduction of double-tail surfactants, which enlarges the alkyl volume fraction within the materials, produces soft materials that display thermotropic liquid-crystalline materials from very rigid tectonic units. Thus, ISA has been successfully used to organize various types of charged oligomeric species, such as dyes, dendrimers, oligoanilines, inorganic polymetallic molecules, perylene derivatives, and coordination complexes, into well-ordered liquid-crystalline materials.

Standard commercially available charged surfactants have been often used in ISA research. However, studies on the ISA behavior of more elaborate amphiphilic molecules suitable to introduce new functionalities, such as π-π interactions, hydrogen bonding, chirality, or polymerizable groups inside the ionic self-assembled materials, has remained rare.[12, 14-19]

5.1.2 ISA of nitrogen containing PAHs with positive charge

Nitrogen containing PAHs with positive charge such as PQP salts are ideal building blocks for ionic self-assembly due to following reasons: (1) quaternary ammonium salts are most often used in the work of ISA because they are easily available from commercial sources or by convenient synthesis. In our work, the aromatic cation of PQP can also form ionic complexes with different organic anions; (2) in our previous research work, we have found that strong aromatic interactions between PQP molecules can exist besides ionic interaction.[20] These π-π interactions offer additional opportunities to obtain ionic complexes with new properties and functionalities for further applications;[21] (3) as we have shown in Chapter 2, the

morphology of the aggregations from the PQP derivates are affected by their inorganic anions.[20] Replacing the inorganic anions with organic anions are expected to enable us to obtain new morphologies and better control the self-assembly behavior of heteroatom containing PAHs with positive charge. Therefore, the ISA of heteroatom containing PAHs with positive charge is one of the most important goals in this work.

On the other hand, the ISA studies done by Antonietti *et al.* were mainly concentrated on the liquid crystal behavior of ionic complexes.[7-17, 19] In recent years, the solution behavior of functional organic molecules has attracted great attention of the chemists, physicists and material scientists who work in the field of supramolecular chemistry as well as organic electronic devices.[6, 22, 23] The self-assembled aggregates could be obtained from solution at relative low cost and is easy to be processed for device fabrication. The ionic complexes obtained by ISA method are also expected to form ordered aggregates. However, the investigation on the self-assembly behavior of such ionic complexes in solution as well as in the bulk is rarely reported so far.

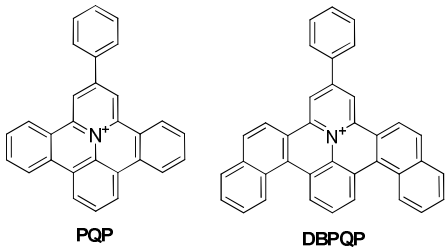

Figure 5-1. PQP and DBPQP cations used for ISA research.

In this work, centrally charged PAHs with different aromatic core, 2-phenyl-benzoquinolizino[4,5,6,7-*fed*]phenanthridinylium (PQP) and 2-phenyl-naphthacene[1,2]quinolizino[3,4,5,6-*def*]benzo[*i*]phenanthridinium (DBPQP) are chosen as cations (Figure 5-1), and commercially available anionic surfactants are used as anions. Various ionic complexes of them were successfully prepared by ISA method. These ionic complexes were characterized both by Fourier transform infrared (FTIR) spectroscopy[24, 25] and proton nuclear magnetic resonance (^{1}H NMR) spectroscopy. The self-assembly behavior of them was also studied by us with

scanning electron microscopy (SEM), wide angle X-ray scattering (WAXS) and dynamic light scattering (DLS). Various nanoscaled aggregates could be conveniently obtained by the drop-casting of the methanolic solution of these ionic complexes on surfaces and the morphologies of the aggregates exhibited obviously dependence on the cations as well as the anions.

5.2 ISA of PQP salts

5.2.1 ISA of PQP salts with anionic surfactants

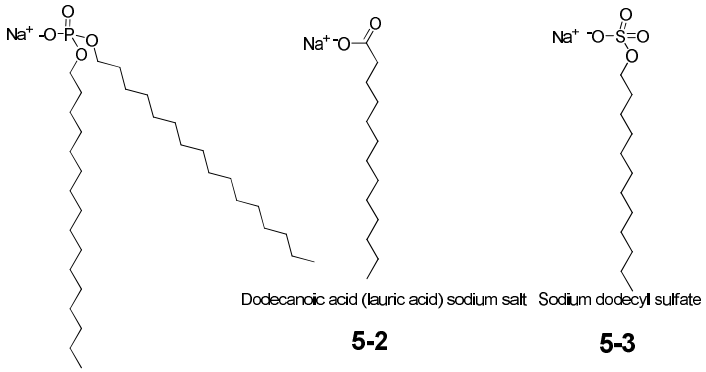

Figure 5-2. Various anionic surfactants intended to be used in our initial ISA research.

The first anion system investigated by us was commercially available anionic surfactants. Our initial intention was to use various anionic surfactants with different acid groups to complex with PQP and DBPQP cations like previous literature work[9]. Therefore, dihexadecyl phosphate (DHDP) sodium salt **5-1**, dodecanoic acid (lauric acid) sodium salt **5-2** and sodium dodecyl sulfate **5-3** (Figure 5-2) were chosen to complex with PQP cations firstly.

For the preparation of the ISA materials, a typical literature procedure was used in this work[9]: The methanolic solution of non-alkyl substituted PQP-BF_4 **2-3** was heated to reflux and then the aqueous or methanolic solution of equal equivalent of anionic surfactants (**5-1**, **5-2** or **5-3**) was added drop-wise within 30 minutes. After that the reaction mixture was cooled to room temperature, and the precipitated

complex was collected by centrifugation, washed with water to remove the inorganic salts and possible non-complexed precursors, and dried under vacuum.

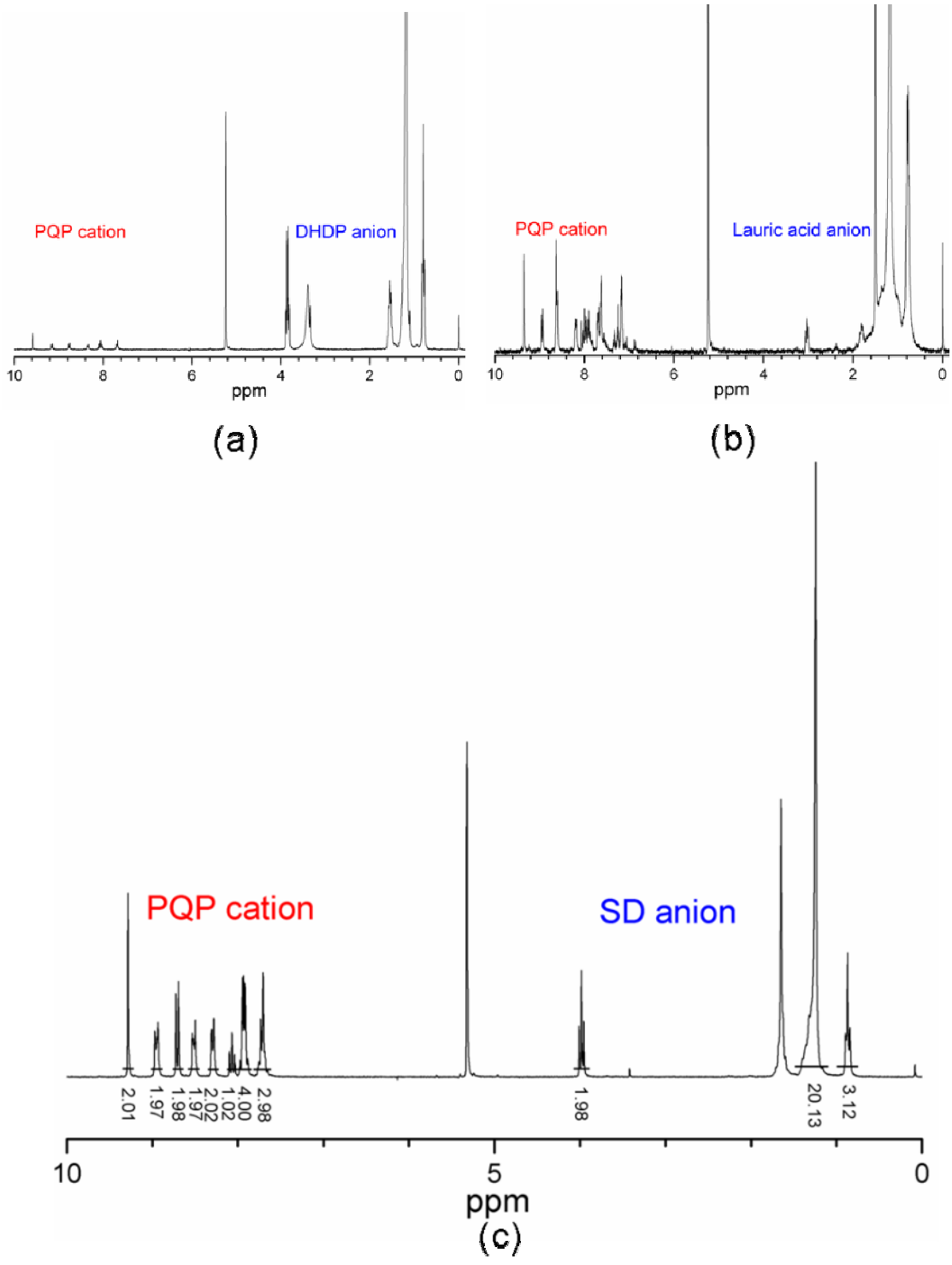

Figure 5-3. ^{1}H NMR spectra (250MHz, r.t., CD_2Cl_2) of ionic complexes derived from PQP cation and (a) DHDP anion; (b) Lauric acid anion; (c) Dodecyl sulfate (SD) anion.

The degree of ionic exchange of the complexes was firstly checked by ^{1}H NMR

spectroscopy. As shown in Figure 5-3, the proton signals from aromatic PQP cations and the alkyl chains of surfactant anioins could be clearly identified. By comparing their integral values, the degree of ion exchange could be decided. As shown in Figure 5-3a and b, it was obvious that DHDP **5-1** and lauric acid **5-2** anions failed to complex with PQP cations completely (charge ratio = 1 : 1) due to the unmatched integral values of the protons from cations and anions. Only sulfate anionic surfactant **5-3** could completely replace tetrafluoroborate anion of PQP salts (Figure 5-3c) which could be further confirmed by its FTIR spectra. According to Figure 5-4, the broad bands of the tetrafluoroborate anions (1043 and 1032 nm) disappeared in the FTIR spectrum of ionic complex **5-5**.

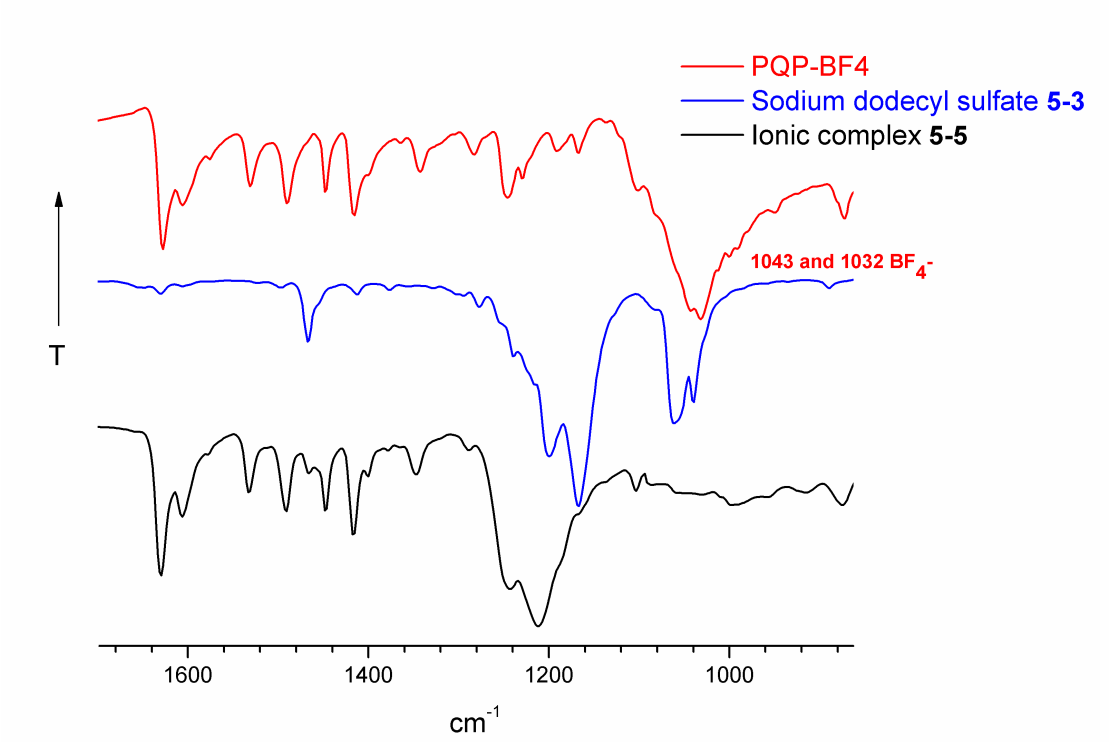

Figure 5-4. FTIR spectra of PQP-BF_4, sodium dodecyl sulfate **5-3** and ionic complex **5-5**.

These results were different from the literature description regarding the ionic exchange of ammonium salts which were able to complex completely with various phosphate as well as carboxylate salts such as **5-1** and **5-2**.[9] One possible explanation for the reactivity difference between ammonium and PQP cation was that the positive charge of PQP cation was mostly delocalized over the aromatic rings due to the

conjugation. As a result, the PQP cation was expected to show weak binding ability with respect to other ammonium salts, and only the anion salts from strong acids such as sulfates and sulfonates can complex with PQP cations completely.

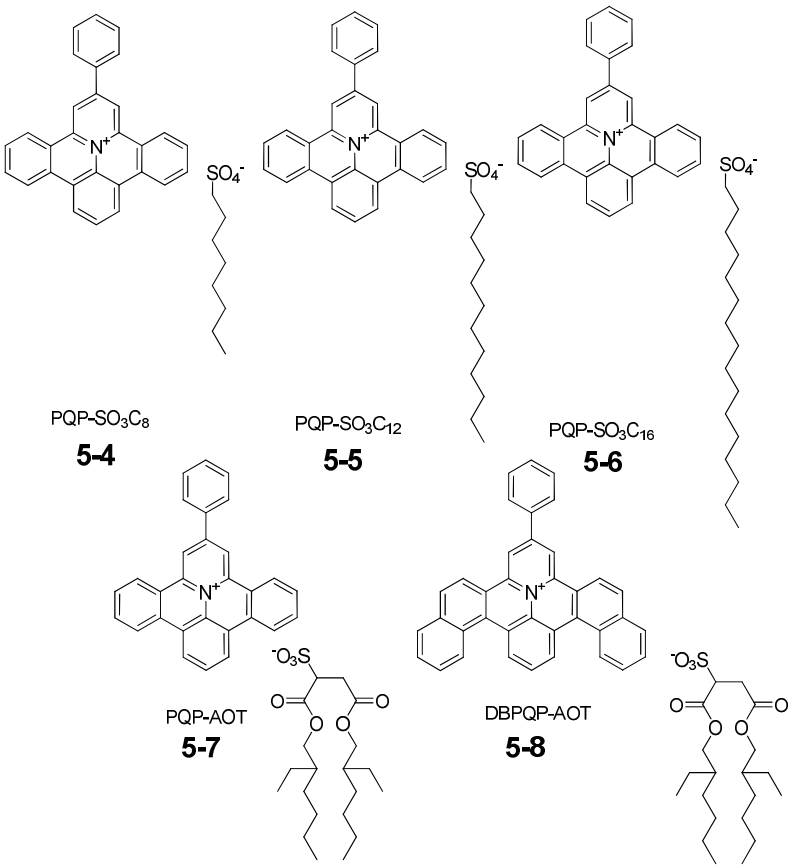

Figure 5-5. The ISA complexes obtained from PQP cations and various sulfate/sulfonate anions.

Therefore, in our succeeding work, various sulfate/sulfonate containing anionic surfactants with different tails were selected to complex with PQP and DBPQP cations. As shown in Figure 5-5, the resulting ionic complexes were 2-phenylbenzo[8,9]-quinolizino[4,5,6,7-*fed*]-phenanthridinylium octyl sulfate (PQP-SO_4C_8, **5-4**), 2-phenylbenzo[8,9]-quinolizino[4,5,6,7-*fed*]-phenanthridinylium sodium dodecyl sulfate (PQP-SO_4C_{12}, **5-5**) and 2-phenylbenzo[8,9]-quinolizino[4,5,6,7-*fed*]- phenanthridinylium hexadecyl sulfate (PQP-SO_4C_{16}, **5-6**), 2-phenylbenzo[8,9]-quinolizino[4,5,6,7-*fed*]-phenanthridinylium 1,4-bis(2-ethylhexyl)-sulfobutanedioate (PQP-AOT, **5-7**) and

2-phenyl-naphthacene[1,2]quinolizino[3,4,5,6-*def*]benzo[*i*]phenanthridinium 1,4-bis(2-ethylhexyl)-sulfobutanedioate (DBPQP-AOT, **5-8**), respectively. The ^{1}H NMR (Figure 5-6) and FTIR spectra of these ionic complexes confirmed that they are 1 : 1 (charge ration) adducts.

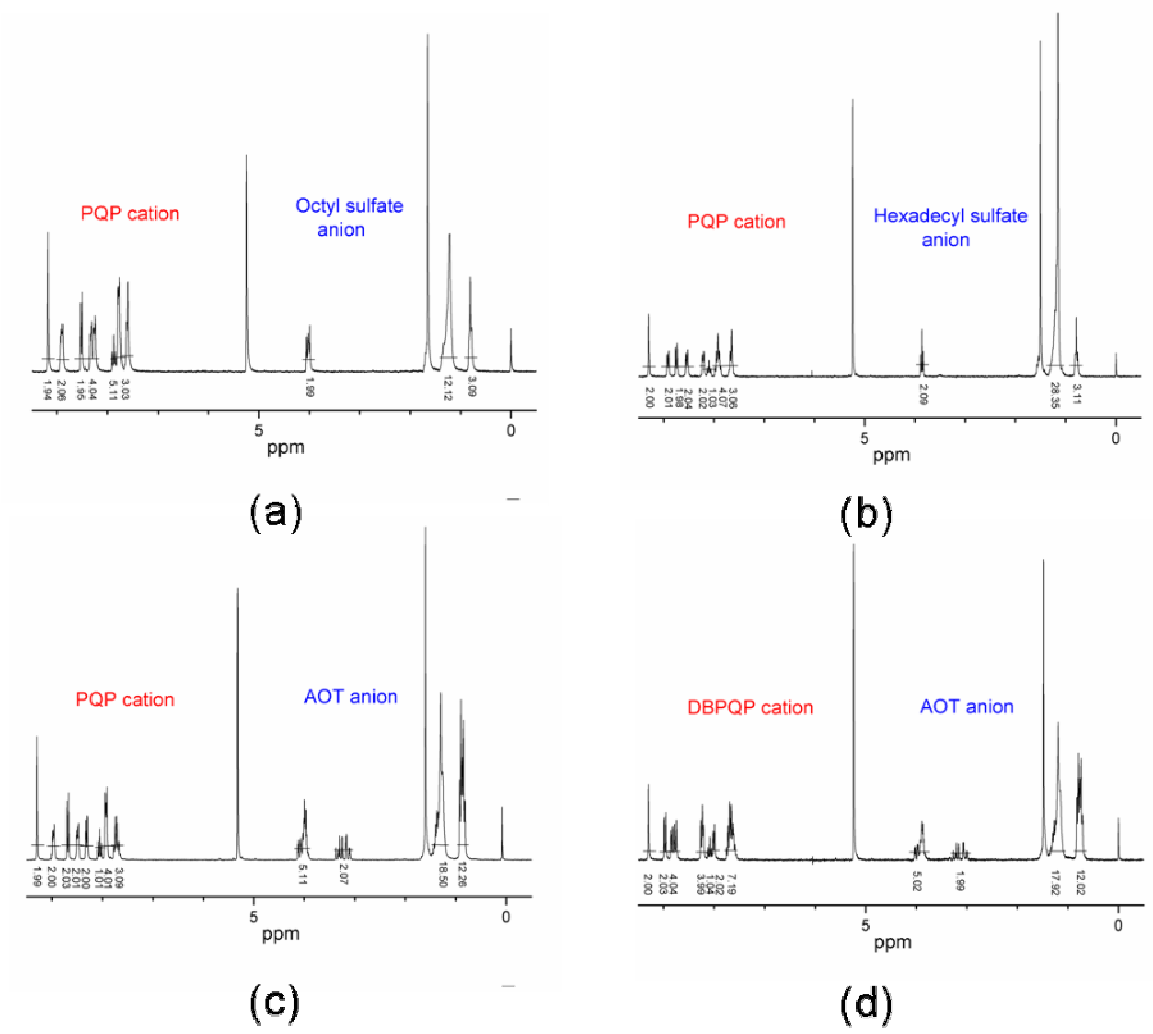

Figure 5-6. ^{1}H NMR spectra (250MHz, r.t., CD_2Cl_2) of ionic complexes: (a) PQP-SO_4C_8, **5-4**; (b) PQP-SO_4C_{16}, **5-6**; (c) PQP-AOT, **5-7**; (d) DBPQP-AOT, **5-8**.

In the interest of understanding the relationship between the chemical structures and the properties of the obtained ionic complexes, the self-assembly behavior of these complexes was investigated subsequently:

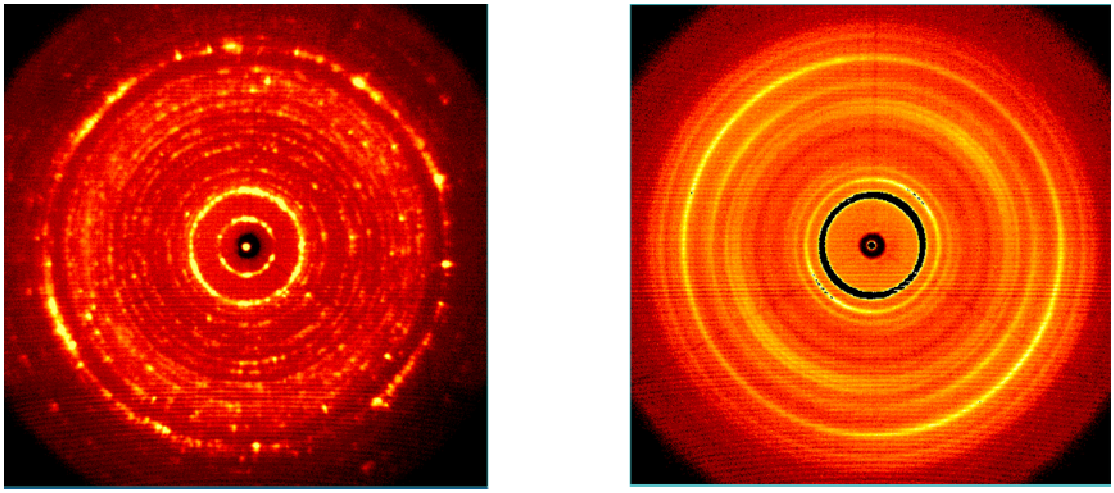

Figure 5-7. The WAXS patterns of the dried powder of (a) PQP-BF4 and (b) PQP-SO_4C_{12} obtained from their methanolic solutions.

To compare the stacking difference between PQP-BF_4 **2-3** and its ionic complexes, PQP-SO_4C_{12} **5-5**, their WAXS patterns were measured firstly. As shown in Figure 5-7a, **2-3** exhibited a highly crystalline structure with multiple diffraction peaks. In contrast, such diffraction peaks were not observed in the WAXS pattern of **5-5** (Figure 5-7b), which indicated the decrease of crystallinity. That was to say that ionic complex **5-5** did not have the ordered crystalline structures as **2-3** due to the flexible dodecyl chain of its anion.

It was worthy to note that **5-5** thus became an amphiphilic molecule after complexing with anionic surfactants, whereas **2-3** was a hydrophilic molecule. Similar to the alkylated PQP derivates discussed in Chapter 2, **5-5** and the other ionic complexes were expected to form ordered aggregates due to their amphiphilic nature. Therefore, the methanolic solutions ($1x10^{-3}$ mol/L) of PQP-SO_4C_8 **5-4**, PQP-SO_4C_{12} **5-5** and PQP-SO_4C_{16} **5-6** were drop-cast on silicon wafers and the morphology of the resulting aggregates were observed with SEM. Very interestingly, the aggregates from three ionic complexes showed totally different morphologies according to their SEM images (Figure 5-8): Compound **5-4**, which had the shortest alkyl tail (octyl chain) in three complexes, formed crystal-like rigid and short ribbons on the surface of silicon

wafer (Figure 5-8a and b). With the moderate length of alkyl chain (dodecyl chain), **5-5** self-assembled into scarf shape aggregates (Figure 5-8c and d). When the alkyl tail was increased to hexadecyl chain, the aggregates of **5-6** were remarkably to be the fibrous nanostructures (Figure 5-8e and f) which tended to stick with each other and formed network like structure. Additionally, the three kinds of aggregates also had different scale in their width (diameter) and length. The ribbons from **5-4** had the widths around 2.5 μm and lengths ranged from 5 to 8 μm. The lengths of the scrafs formed by **5-5** were hard to determine due to their flexed structures but their widths were about 1 to 2 μm. And the diameters of the fibers from **5-6** were of approximately 80 nm.

The morphology difference of the three ionic complexes could be obviously ascribed to the change of alkyl chain length of the anionic surfactants. The octyl sulfate anion of **5-4** had the shortest and least flexible alkyl chain. Therefore, the aggregates of **5-4** were closer to the crystalline phase than the ones from the other two complexes. Accordingly, **5-4** tended to form small and stiff crystalline-like structures. However, the hexadecyl chain in the case of **5-6** was very flexible and could offer enough hydrophobic interaction to drive it self-assemble into flexible aggregates. As a result, **5-6** was able to form extra long one-dimensional fibrous structures. The anion of compound **5-5** had a chain length between octyl and hexadecyl chains, and this made it form aggregates with the intermediated scarf-like structures.

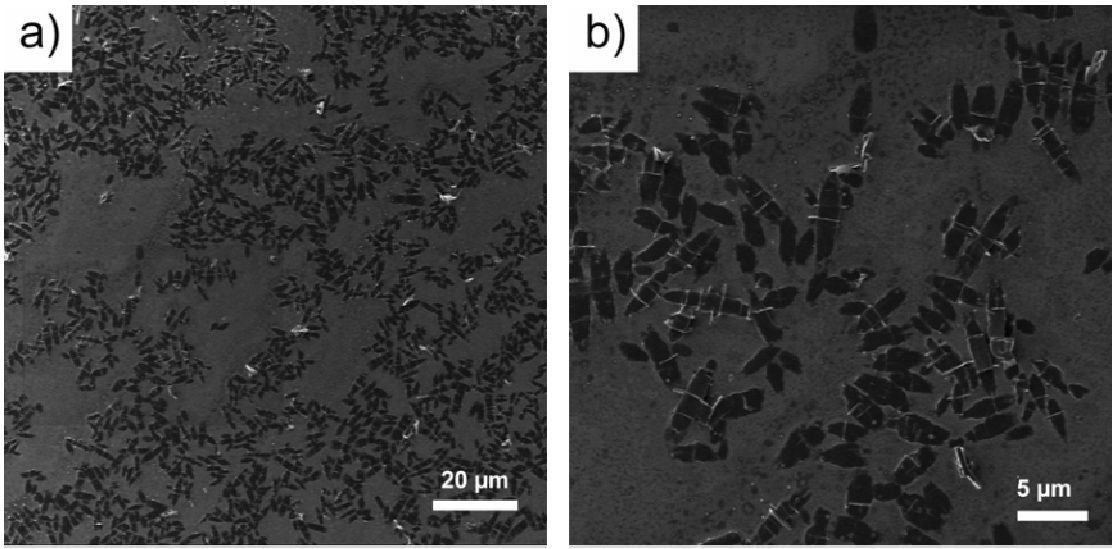

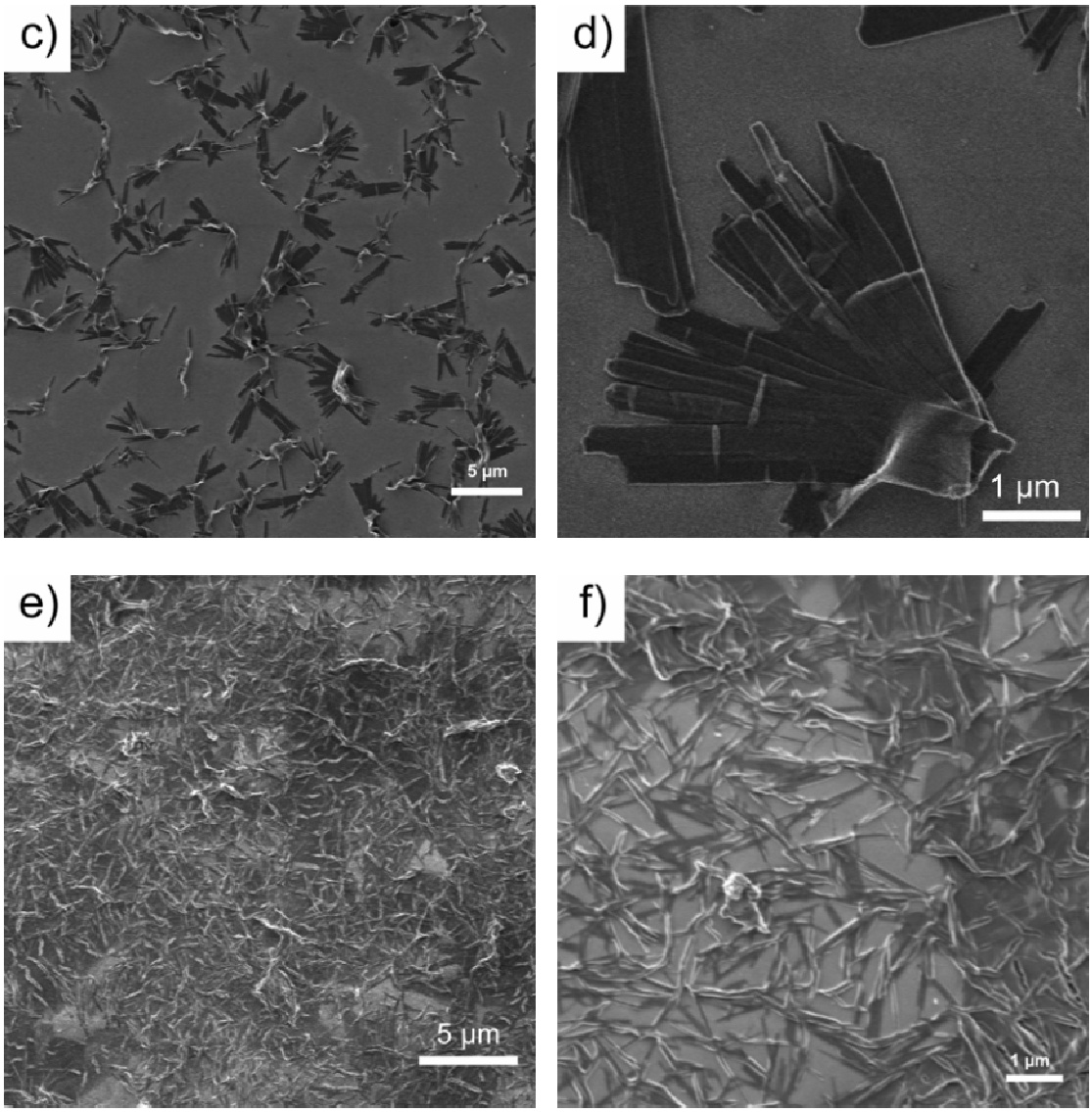

Figure 5-8. SEM images of aggregates obtained from the ionic complexes ($1x10^{-3}$ mol/L in methanol, drop-cast on silicon wafers): (a) and (b) PQP-SO_4C_8, **5-4**; (c) and (d) PQP-SO_4C_{12}, **5-5**; (e) and (f) PQP-SO_4C_{16}, **5-6**.

Besides changing the hydrophobic chain length of amphiphilic molecules, altering the number of its hydrophobic tails is also a typical strategy to modify the self-assembly behavior of amphiphiles.[23, 26] As we discussed in Chapter 2, for common surfactants such as pyridinium and sulfate salts, increasing the length of their alkyl chains could not result in obvious morphology changes of their aggregates in solution when the surfactant only had one alkyl chain.[27, 28] One of the most famous examples was reported by C. Tanford. In aqueous solution, he obtained similar

globular micelles from sulfate salts containing one alkyl chains with different length (from C6 to C20). Whereas it was reported that ammonium surfactants with two decyl chains (C10) could form bilayer vesicles in water.[26, 29] Compared with **5-4**, **5-5** and **5-6** in which the anions only had a single alkyl chain, the ionic complex with two alkyl chains such as PQP-AOT **5-7** was also expected to exhibit different aggregation behavior. Therefore, the self-assembly behavior of **5-7** was also studied by us. The SEM images indicated that drop-casting the methanolic solution of **5-7** ($1x10^{-3}$ mol/L) on silicon wafers could also result in nanoscaled aggregates. As shown in Figure 5-9, **5-7** formed knot-type nanofibers with the diameter around 80 nm, which was similar to the fibers formed by PQP-SO_4C_{16} **5-6**, thus indicating that for the aggregates formed by the ionic complexes, two short branched chains (AOT) and a single long straight alkyl chain (SO_4C_{16}) had a similar effect on their morphology.

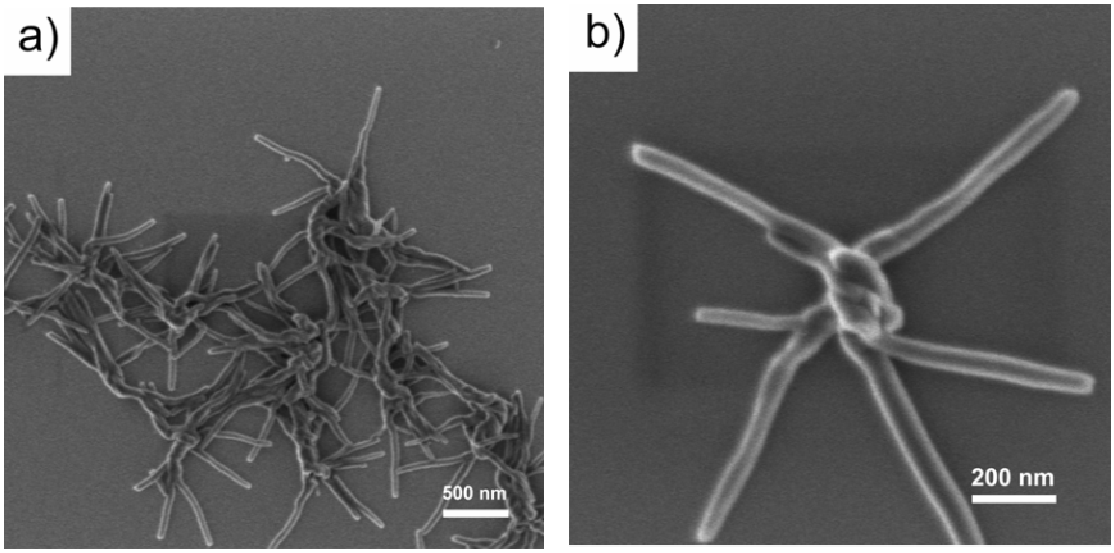

Figure 5-9. SEM images of aggregates from PQP-AOT ($1x10^{-3}$ mol/L in methanol, drop-cast on silicon wafers).

Although the morphology of the aggregates from the ionic complexes also exhibited a dependence on the length and number of their alkyl chains, these alkyl chains played a different role as compared with the alkyl chains of PQP salts mentioned in Chapter 2. In the case of alkyl chain containing PQP salts, DLS measurements indicated that their aggregates were formed in solution. Therefore, the

lengths of their alkyl chains resulted in different packing parameters *P* in methanol and then changed the morphologies of their aggregates from fibers to layered structures[26, 27]. Nevertheless, DLS measurements for the methanolic solutions of the ionic complexes did not detect the signals of aggregates even in a large range of concentrations (from $1x10^{-4}$ to $1x10^{-2}$ mol/L). These results indicated that these aggregates were in fact formed on the substrates during the solvent evaporation. Their formation was believed to experience a so-called cast assembly process, and similar behavior of aromatic molecules was also reported by W. Hu and his coworkers very recently[30]. Therefore, the morphology of the aggregates could not be simply explained with packing parameter theory and the crystalline property of the alkyl chain on their anions must be considered.

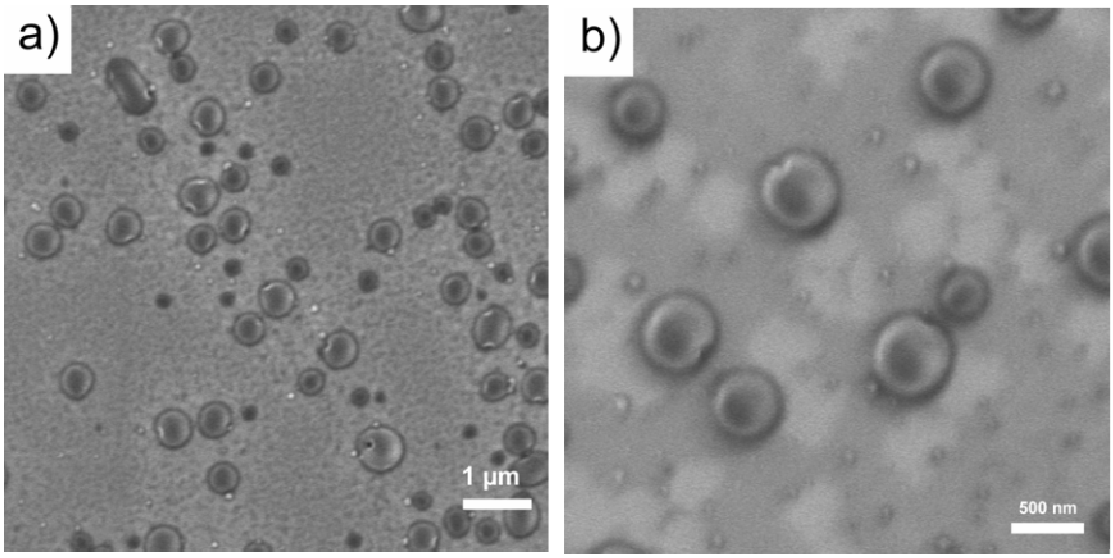

Figure 5-10. SEM images of aggregates from DBPQP-AOT ($1x10^{-3}$ mol/L in methanol, drop-cast on silicon wafers).

Additionally, different from PQP cation 2-3, DBPQP cation **2-20** was a non-planar cation. It was also used to complex with AOT anion and the self-assembly behavior of the resulting DBPQP-AOT **5-8** was investigated subsequently in this work. As shown in Figure 5-10, remarkable enough, spherical aggregates could be obtained by drop-casting the methanolic solution of **5-8** ($1x10^{-3}$ mol/L) on silicon wafers. Their diameters were ranging from 200 to 500 nm, which was similar to the

vesicles from the self-assembly of DBPQPBF$_4$-6 **2-21** and DBPQPBF$_4$-14 **2-22** discussed in Chapter 2. This result indicated that the shape of cation was still the governing effect which decided the morphology of the aggregates formed by ionic complexes.

5.3 Conclusion

In this work, various ionic complexes were derived by complexing PQP and DBPQP cations with different sulfate/sulfonate group containing anionic surfactants. The ionic complexes resulted from ISA exhibited unique self-assembly behavior which was controllable by the species and shape of cations and anions. Various aggregates such as nanofibers and spherical aggregates could be conveniently produced by drop-casting their methanolic solution in a defined manner. Besides the results presented here, the single crystalline and liquid crystalline behavior of the ionic complexes are under investigation with the help of V. Enkelmann and W. Pisula respectively. To understand the packing of the cation and anion of these ionic complexes could be very helpful to obtain the insight of intermolecular forces such as aromatic, amphiphilic and Coulombic interactions. These results are also of significant importance for fabrication of novel material molecules by ISA method.

References

1. Watson, M. D.; Fechtenkötter, A.; Müllen, K., *Chem. Rev.* **2001,** 101, (5), 1267.
2. Kato, T., *Science* **2002,** 295, (5564), 2414.
3. Lehn, J. M., *Science* **2002,** 295, (5564), 2400.
4. Whitesides, G. M.; Grzybowski, B., *Science* **2002,** 295, (5564), 2418.
5. Binnemans, K., *Chem. Rev.* **2005,** 105, (11), 4148.
6. Hoeben, F. J. M.; Jonkheijm, P.; Meijer, E. W.; Schenning, A., *Chem. Rev.* **2005,** 105, (4), 1491.
7. Camerel, F.; Strauch, P.; Antonietti, M.; Faul, C. F. J., *Chem.-Eur. J.* **2003,** 9, (16), 3764.
8. Faul, C. F. J.; Antonietti, M., *Adv. Mater.* **2003,** 15, (9), 673.
9. Guan, Y.; Zakrevskyy, Y.; Stumpe, J.; Antonietti, M.; Faul, C. F. J., *Chem. Commun.* **2003**, (7), 894.
10. Faul, C. F. J.; Antonietti, M.; Massa, W., *Acta Crystallogr. Sect. E.-Struct Rep. Online* **2004,** 60, O1769.
11. Guan, Y.; Yu, S. H.; Antonietti, M.; Bottcher, C.; Faul, C. F. J., *Chem.-Eur. J.* **2005,** 11, (4), 1305.
12. Franke, D.; Vos, M.; Antonietti, M.; Sommerdijk, N.; Faul, C. F. J., *Chem. Mat.* **2006,** 18, (7), 1839.
13. Faul, C. F. J., *Mol. Cryst. Liquid Cryst.* **2006,** 450, 255.
14. Wei, Z. X.; Laitinen, T.; Smarsly, B.; Ikkala, O.; Faul, C. F. J., *Angew. Chem. Int. Ed.* **2005,** 44, (5), 751.
15. Zhang, T. R.; Spitz, C.; Antonietti, M.; Faul, C. F. J., *Chem.-Eur. J.* **2005,** 11, (3), 1001.
16. Ozer, B. H.; Smarsly, B.; Antonietti, M.; Faul, C. F. J., *Soft Matter* **2006,** 2, (4), 329.
17. Zakrevskyy, Y.; Stumpe, J.; Faul, C. F. J., *Adv. Mater.* **2006,** 18, (16), 2133.
18. Camerel, F.; Ulrich, G.; Barbera, J.; Ziessel, R., *Chem.-Eur. J.* **2007,** 13, (8), 2189.
19. Kaper, H.; Franke, D.; Smarsly, B. M.; Faul, C. F. J., *Langmuir* **2007,** 23, (22),

11273.

20. Wu, D. Q.; Zhi, L. J.; Bodwell, G. J.; Cui, G. L.; Tsao, N.; Müllen, K., *Angew. Chem. Int. Ed.* **2007,** 46, (28), 5417.
21. Song, B.; Wang, Z. Q.; Chen, S. L.; Zhang, X.; Fu, Y.; Smet, M.; Dehaen, W., *Angew. Chem. Int. Ed.* **2005,** 44, (30), 4731.
22. Kastler, M.; Pisula, W.; Wasserfallen, D.; Pakula, T.; Müllen, K., *J. Am. Chem. Soc.* **2005,** 127, (12), 4286.
23. Shimizu, T.; Masuda, M.; Minamikawa, H., *Chem. Rev.* **2005,** 105, (4), 1401.
24. Thunemann, A. F.; Ruppelt, D.; Burger, C.; Müllen, K., *J. Mater. Chem.* **2000,** 10, (6), 1325.
25. Thunemann, A. F.; Kubowicz, S.; Burger, C.; Watson, M. D.; Tchebotareva, N.; Müllen, K., *J. Am. Chem. Soc.* **2003,** 125, (2), 352.
26. Kunitake, T., *Angew. Chem. Int. Ed.* **1992,** 31, (6), 709.
27. Tanford, C., *J. Phys. Chem.* **1972,** 76, (21), 3020.
28. Nagarajan, R., *Langmuir* **2002,** 18, (1), 31.
29. Kunitake, T.; Okahata, Y., *J. Am. Chem. Soc.* **1980,** 102, (2), 549.
30. Jiang, L.; Fu, Y. Y.; Li, H. X.; Hu, W. P., *J. Am. Chem. Soc.* **2008,** 130, (12), 3937.

Chapter 6

Summary and outlook

6.1 Summary of results

The results of present thesis: “Heteroatom Containing Polycyclic Aromatic Hydrocarbons with Positive Charge - Synthesis and Characterization” can be summarized as follows:

1. A series of 2-phenyl-benzo[8,9]quinolizino[4,5,6,7-*fed*]phenanthridinylium (PQP) salts with different alkyl chains and anions were synthesized in this work. The synthesis of the extended derivates of PQP salts with two fused benzene rings, 2-phenyl-naphthacene[1,2]quinolizino[3,4,5,6-*def*]benzo[*i*]phenanthridinium (DBPQP) tetrafluoroborate and its alkylated derivates, was also developed by us. The self-assembly behavior of these amphiphilic PAHs was subsequently investigated in methanolic solution as well as in the bulk. Interestingly, the aggregation of PQPCl-6 and $PQPBF_4$-6 or $PQPBF_4$-8 could produce one-dimensional nanofibers with a uniform size distribution. Furthermore, the PQP salts with longer alkyl chains (C10, C12 and C14) could self-assemble into layered aggregates, while changing the counterion of them from chloride (Cl-) to tetrafluoroborate (BF_4-) led to a change in the morphology of the aggregates from ribbons to helices and tubes. Additionally, multilayered spherical vesicles could be obtained from the self-assembly of $DBPQPBF_4$-6 and $DBPQPBF_4$-14 in methanol. All of these morphology changes could be ascribed to the changes in intermolecular interactions which resulting from the difference in the molecular structures such as aromatic cores, alkyl chains and counterions.

2. The synthetic strategy of oxygen containing PAHs with positive charge, benzo[5,6]naphthaceno[1,12,11,10-*jklmna*]xanthylium (BNAX) salts and its dibenzo

derivates, DBNAX salts were developed. With a similar method, sulfur containing benzo[5,6]naphthaceno[1,12,11,10-*jklmna*]thioxanthylium (BNATX) salts were also synthesized. Various BNAX salts with different alkyl chains could be obtained and their supramolecular behavior were subsequently investigated by us. A discotic liquid crystalline behavior was observed for di- (**3-25**) and tridodecyl (**3-27**) substituted BNAX salts and both compounds exhibited large unit cell in their 2D-WAXS patterns which could be attributed to the formation of dimer structures. By drop casting their methanolic solution on silicon wafers, similar nanoscaled fibers from monododecyl substituted BNAX bromide **3-24** and DBNAX bromide **3-35** could be observed.

3. A novel synthetic method toward nitrogen containing 14-phenyl-dibenzo[*jk,mn*]naphtho[2,1,8-*fgh*]thebenidinium (DBNT) salts was also developed. In this method, the undehydrogenated precursor of DBNT, dibenzoacridinium salt could be produced directly from the reaction between dibenzoxanthenylium derivates and amine/aniline in reasonable yields. Various DBNT salts with different alkyl and alkylphenyl chains on their nitrogen atom were synthesized in this two-step method. The self-assembly behavior of two alkylated DBNT salts, **4-15a** and **4-18b** was also studied in this work. Compound **4-15a** formed nanoscaled fibers and helical aggregates were obtained from **4-18b** in their methanolic solutions.

4. Various ionic complexes were derived by complexing PQP and DBPQP cations with different sulfate/sulfonate group containing anionic surfactants. The ionic complexes resulting from the ionic self-assembly (ISA) method exhibited self-assembly behavior which was controllable by the species and shape of cations and anions. Various aggreagtes such as nanofibers and spherical aggregates could be produced from their methanolic solution in a defined manner conveniently.

6.2 Outlook toward future work

As indicated in the title, the emphasis of the thesis was synthesis and characterization of heteroatom containing PAHs with positive charge. In this work,

various positively charged PAHs with nitrogen, oxygen and sulfur atoms on their aromatic framework were synthesized with versatile methods. The properties of the resulting molecules such as UV-vis absorption, fluorescence and suparmoelcular behavior was also studied. However, the study of their other properties such as electronic and optoelectronic behavior which is essential for their potential applications in material sciences is still absent and urgently required. Based on the present results, several extensions can be expected for the future work:

1. Doping PAHs with heteroatoms can influence their electronic nature without modifying the aromatic structure by substitutents.[1-3] Different from all-hydrocarbon PAHs, heteroatom containing PAHs with positive charge are acceptor molecules. Therefore, various charge transfer complexes (CT complexes) could be created by co-crystallization or mixing of such planar acceptors and other donors such as tetrathiafulvalene (TTF), tetramethyl tetraselena fulvalene (TMTSF) and HBCs in the future.

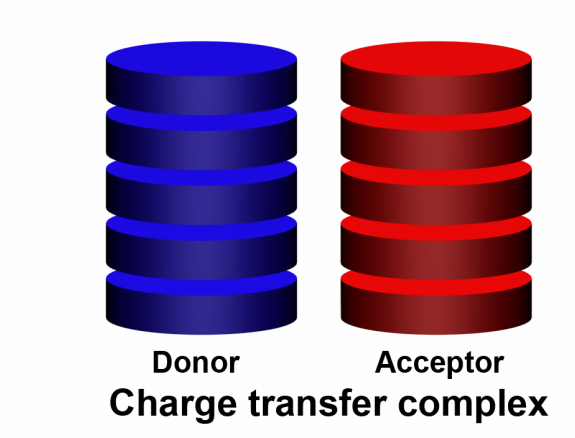

Figure 6-1. Structure of charge transfer complex.

2. One of the goals of molecular electronics is the development of ion-conductive materials. To be useful at a molecular level, this ion conductivity should be anisotropic, which means that the ion conductivity depends on the direction in which it is measured. As shown in previous chapters, heteroatom containing PAHs with positive charge could self-assemble into various ordered aggregates in a simple and repeatable manner. And multi-alkylated BNAX salts could also form ionic

discotic liquid crystals. Such aggregates and ionic liquid crystals are very promising candidates to design anisotropic ion-conductive materials because they not only have an anisotropic structural organization but also contain ions as charge carriers. Moreover, the long alkyl chains of the molecules can act as an insulating sheet for the ionconductive channel.[4-6] Therefore, construction of 1D ionic conducting materials based on these molecules is another object in our future work.

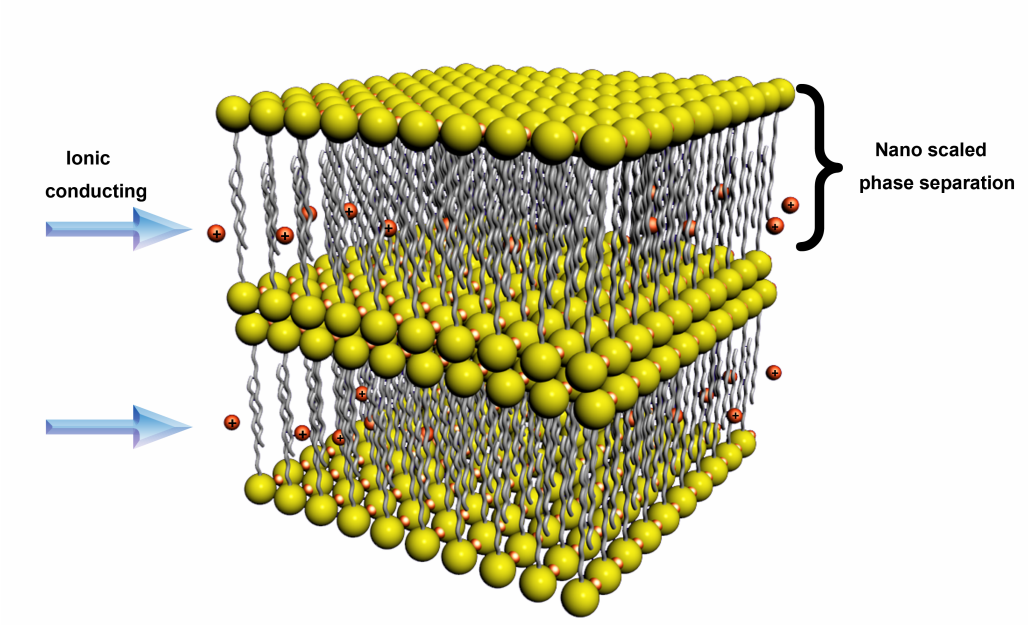

Figure 6-2. Illustration of the anisotropic ion conduction for self-organized ion conductive materials.

3. In Chapter 5, ionic self-assembly (ISA) of PQP cations with different anions turned out to be an effective approach to obtain ionic materials with controllable self-assembly behavior. Various ionic complexes based on PQP salts were successfully prepared by us with ISA method. These complexes exhibited unique self-assembly behavior and aggregates with diversified morphologies were obtained by drop-casting their solution on surfaces. The single crystalline as well as liquid crystalline behavior of these materials are also very important supramolecular properties and could help us to further understand the packing of these ionic complexes in the bulk. Now the research of these topics are underway with the help from V. Enkelmann and W. Pisula. Moreover, the preparation and properties of ISA

materials based on the other PAH molecules such as HBC derivates will also be studied in the future.

References

1. Adam, D.; Schuhmacher, P.; Simmerer, J.; Haussling, L.; Siemensmeyer, K.; Etzbach, K. H.; Ringsdorf, H.; Haarer, D., *Nature* **1994,** 371, (6493), 141.
2. Pieterse, K.; van Hal, P. A.; Kleppinger, R.; Vekemans, J.; Janssen, R. A. J.; Meijer, E. W., *Chem. Mat.* **2001,** 13, (8), 2675.
3. Ishi-i, T.; Yaguma, K.; Kuwahara, R.; Taguri, Y.; Mataka, S., *Org. Lett.* **2006,** 8, (4), 585.
4. Kato, T., *Science* **2002,** 295, (5564), 2414.
5. Binnemans, K., *Chem. Rev.* **2005,** 105, (11), 4148.
6. Kato, T.; Mizoshita, N.; Kishimoto, K., *Angew. Chem. Int. Edit.* **2006,** 45, (1), 38.

Chapter 7

Experiment part

General information

Chemicals:

All starting materials were obtained from commercial suppliers such as Aldrich, Acros, Fluka and Strem and used as received unless otherwise specified.

UV lamp for photocyclization:

Irradiations with an external UV source were performed with a Rayonet reactor (RPR-200) with 3000 Å lamps in quartz flasks.

NMR spectroscopy:

^{1}H and ^{13}C NMR spectra were recorded on Bruker DPX 250, Bruker AMX 300, Bruker DRX 500 or Bruker DRX 700 spectrometers with use of the solvent proton or carbon signal as an internal standard.

Mass spectrometry:

FD mass spectra were obtained on a VG Instruments ZAB 2-SE-FPD spectrometer. MALDI-TOF mass spectra were measured using a Bruker Reflex II-TOF spectrometer using a 337 nm nitrogen laser and 7,7,8,8-tetracyanoquinodimethane (TCNQ) as matrix.

UV/Vis spectroscopy:

UV/Vis spectra were recorded at room temperature on a Perkin-Elmer Lambda 9 spectrophotometer.

Fluorescence spectroscopy:

Fluorescence spectra were recorded on a SPEX-Fluorolog II (212) spectrometer.

Chromatography:

Preparative column chromatography was performed on silica gel form Merck with a particle size of 0.063-0.200 mm (Geduran Si 60) For analytical thin layer chromatography (TLC) silica gel coated substrates 60 F254 from Merck were used. Compounds were detected by fluorescence quenching at 254 nm and self-fluorescence at 366 nm.

Elemental analysis:

The Elemental Analysis was measured in Institut für Organische Chemie der Johannes Gutenberg-Universität Mainz for: C, H: Foss Heraeus vario EL.

Wide angle X-ray scattering:

A double graphite monochromator for the Cu-Kα radiation (λ=0.154 nm) was used for the WAXS experiments. SEM measurements were performed on a LEO 1530 field emission scanning electron microscope.

Electron microscopy:

SEM images were recorded by LEO 1530 Gemini field emission scanning electron microscope. TEM studies were conducted on a Philips Tecnai F20 electron microscope at an operating voltage of 200 kV. The sample was dissolved in methanol and the solution was dropped onto a copper grid covered with carbon film.

Fourier transform infrared:

Infrared (IR) spectra were recorded on Nicolet 730 FT-IR spectrophotometer using KBr pellet. DLS measurements were carried out on a laser light scattering spectrometer (BI-200SM) equipped with a digital correlator (BI-9000AT) at 514 nm.

Dynamic light scattering:

DLS measurements were carried out on a laser light scattering spectrometer (BI-200SM) equipped with a digital correlator (BI-9000AT) at 514 nm.

Single crystal analysis:

The single crystal analysis was preformed on a Nonius-KCCD diffractometer with Mp-Kα (λ=0.71923 Å, graphite monochromatized) at a temperature of 150 K. The structure were solved by direct methods (Shelxs) and refined on F with anisotropic temperature factors for all non-hydrogen atoms. The H atoms wre refined with fixed isotropic temperature factors in riding mode.

Synthesis:

PQP salts

1-(4-Alkylphenyl)-2,4,6-triphenylpyridinium salts:

2,4,6-triphenylpyrylium salt (2mmol) and 4-alkylaniline(2.2mmol) were added to 15ml absolute ethanol. The mixture was refluxed for 5 hours till the solution turned to transparent. After cooling the solution to room temperature, it was concentrated in *vacuo* to *c.a.* 3ml. The concentrated solution was poured to 400ml hexane then. After filtration, the solid was recrystallized from 20ml hexane to give the target pyridinium salts.

1-(4-Hexylphenyl)-2,4,6-triphenylpyridinium chloride (2-5a):

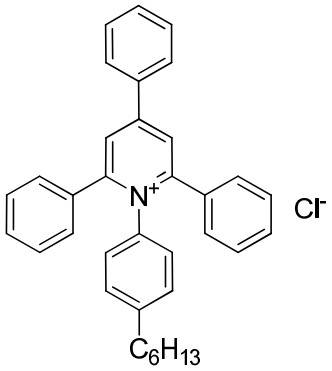

Pale yellow solid (yield = 90%), ^{1}H NMR (250MHz, CD_3OD, 25°C): δ(ppm) = 8.43 (s, 2H, aromatic), 8.10-8.07 (m, 2H, aromatic), 7.60-7.58 (m, 3H, aromatic), 7.36-7.24 (m, 10H, aromatic), 7.10-7.07 (d, 2H, ^{3}J(H,H)=7.5Hz, aromatic), 6.94-6.91 (d, 2H, ^{3}J(H,H)=7.5Hz, aromatic), 2.43-2.37 (t, 2H, ^{3}J(H,H)=7.5Hz, CH_2), 1.39-1.34 (m, 2H, CH_2), 1.22-1.00 (m, 6H, CH_2), 0.82-0.77 (t, 3H, CH_3); ^{13}C NMR (62.5MHz, CD_3OD, 25°C): d (ppm): 158.54, 146.83, 138.22, 135.37, 134.65, 133.77, 131.40, 131.09, 130.00, 129.73, 129.54,129.69, 126.87, 36.03, 32.74, 32.03, 29.31, 23.71, 14.45.

FD-MS (MW=468.67 without anion): m/z: 468.60.

Elemental analysis: Calculated. C 83.39%, H 6.80%, N 2.78%, Cl 7.03%; Found.

C 81.43%, H 6.94%, N 2.94%.

1-(4-Hexylphenyl)-2,4,6-triphenylpyridinium tetrafluoroborate (2-5b):

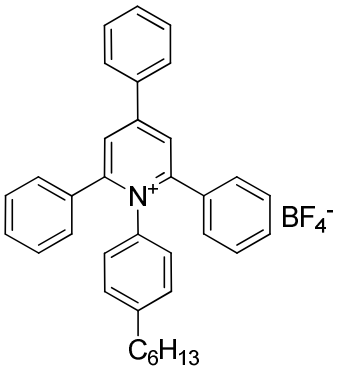

White powder (yield = 98%), ^{1}H NMR (250MHz, CD_2Cl_2, 25°C): δ(ppm) = 8.20 (s, 2H, aromatic), 7.96-7.93 (m, 2H, aromatic), 7.67-7.64 (m, 3H, aromatic), 7.35 (s, 10H, aromatic), 7.07-7.03 (d, 2H, ^{3}J(H,H)=10.0Hz, aromatic), 6.99-6.95 (d, 2H, ^{3}J(H,H)=10.0Hz, aromatic), 2.50-2.44 (t, 2H, ^{3}J(H,H)=7.5Hz, CH_2), 1.46-1.40 (m, 2H, CH_2), 1.29-1.07 (m, 6H, CH_2), 0.89-0.84 (t, 3H, CH_3); ^{13}C NMR (62.5MHz, CD_2Cl_2, 25°C): d (ppm): 157.88, 157.32, 146.07, 136.62, 134.50, 133.13, 132.95, 130.73, 130.30, 129.97, 129.48, 128.89, 128.64, 128.42, 126.51, 35.44, 31.87, 31.08, 28.52, 22.94, 14.19.

FD-MS (MW=468.67 without anion): m/z: 468.60.

Elemental analysis: Calculated. C 75.68%, H 6.17%, N 2.52%, B 1.95%, F 13.68%; Found. C 76.42%, H 6.92%, N 2.17%.

1-(4-Octylphenyl)-2,4,6-triphenylpyridinium tetrafluoroborate (2-6b):

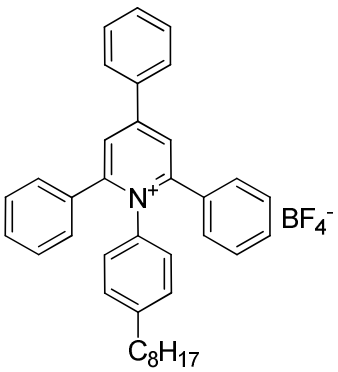

White powder (yield = 97%), ^{1}H NMR (250MHz, CD_2Cl_2, 25°C): δ(ppm) = 8.11

(s, 2H, aromatic), 7.88-7.85 (m, 2H, aromatic), 7.58-7.56 (m, 3H, aromatic), 7.31-7.26 (m, 10H, aromatic), 6.99-6.96 (d, 2H, ^{3}J(H,H)=7.5Hz, aromatic), 6.90-6.87 (d, 2H, ^{3}J(H,H)=7.5Hz, aromatic), 2.41-2.35 (t, 2H, ^{3}J(H,H)=7.5Hz, CH_2), 1.38-1.32 (t, 2H, ^{3}J(H,H)=7.5Hz, CH_2), 1.23-0.97 (m, 10H, CH_2), 0.84-0.78 (t, 3H, CH_3); ^{13}C NMR (62.5MHz, CD_2Cl_2, 25°C): d (ppm): 157.43, 156.86, 145.61, 136.21, 134.11, 132.72, 132.47, 130.26, 129.56, 129.02, 128.44, 128.22, 128.00, 126.09, 35.00, 31.77, 30.72, 28.47, 22.61, 13.80.

FD-MS (MW=496.72 without anion): m/z: 496.25.

Elemental analysis: Calculated. C 76.16%, H 6.56%, N 2.40%, B 1.85%, F 13.02%; Found. C 75.95%, H 7.34%, N 2.02%.

1-(4-Decylphenyl)-2,4,6-triphenylpyridinium tetrafluoroborate (2-7b):

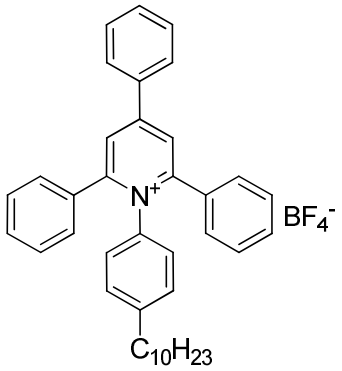

White powder (yield = 98%), ^{1}H NMR (250MHz, CD_2Cl_2, 25°C): δ(ppm) = 8.10 (s, 2H, aromatic), 7.87-7.84 (m, 2H, aromatic), 7.58-7.55 (m, 3H, aromatic), 7.31-7.21 (m, 10H, aromatic), 7.00-6.96 (d, 2H, ^{3}J(H,H)=10.0Hz, aromatic), 6.90-6.68 (d, 2H, ^{3}J(H,H)=10.0Hz, aromatic), 2.41-2.35 (t, 2H, ^{3}J(H,H)=7.5Hz, CH_2), 1.38-1.29 (m, 2H, CH_2), 1.18-0.97 (m, 14H, CH_2), 0.83-0.78 (t, 3H, CH_3); ^{13}C NMR (62.5MHz, CD_2Cl_2, 25°C): d (ppm): 149.95, 146.05, 142.29, 134.39, 134.34, 132.13, 131.12, 130.06, 129.02, 128.21, 126.50, 124.76, 123.81, 123.58, 123.41, 118.25, 36.17, 31.85, 31.43, 29.62, 29.53, 29.43, 29.32, 29.28, 22.62, 13.80.

FD-MS (MW=524.78 without anion): m/z: 524.11.

Elemental analysis: Calculated. C 76.34%, H 7.23%, N 2.28%, B 1.76%, F

12.39%; Found. C 75.46%, H 6.57%, N 2.58%.

1-(4-Dodecylphenyl)-2,4,6-triphenylpyridinium tetrafluoroborate (2-8b):

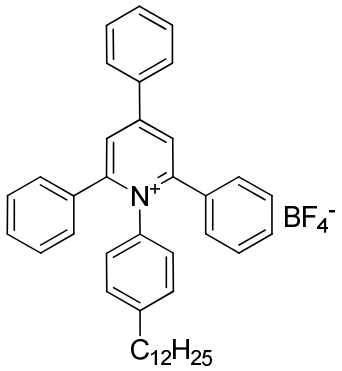

White powder (yield = 98%), ^{1}H NMR (250MHz, CD_2Cl_2, 25°C): δ(ppm) = 8.10 (s, 2H, aromatic), 7.88-7.84 (m, 2H, aromatic), 7.57-7.55 (m, 3H, aromatic), 7.32-7.21 (m, 10H, aromatic), 7.01-6.98(d, 2H, ^{3}J(H,H)=7.5Hz, aromatic), 6.89-6.86 (d, 2H, ^{3}J(H,H)=7.5Hz, aromatic), 2.41-2.35 (t, 2H, ^{3}J(H,H)=7.5Hz, CH_2), 1.40-1.32 (m, 2H, CH_2), 1.26-0.98 (m, 18H, CH_2), 0.82-0.77 (t, 3H, CH_3); ^{13}C NMR (250MHz, CD_2Cl_2, 25°C): d (ppm): 157.86, 157.21, 145.96, 136.68, 134.67, 133.21, 132.79, 130.64, 130.22, 130.03, 129.42, 128.83, 128.70, 128.47, 126.66, 37.60, 35.41, 31.95, 31.38, 29.64, 29.54, 29.45, 29.37, 22.94, 22.73, 13.92.

FD-MS (MW=552.83 without anion): m/z: 552.80.

Elemental analysis: Calculated. C 76.99%, H 7.25%, N 2.19%, B 1.69%, F 11.88%; Found. C 76.70%, H 7.12%, N 1.70%.

1-(4-Tetradecylphenyl)-2,4,6-triphenylpyridinium chloride (2-9a):

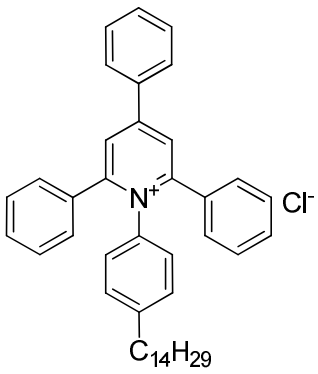

Pale yellow solid (yield = 88%), ^{1}H NMR (250MHz, CD_3OD, 25°C): δ(ppm) =

8.45 (s, 2H, aromatic), 8.13-8.09 (m, 2H, aromatic), 7.63-7.60 (m, 3H, aromatic), 7.39-7.28 (m, 10H, aromatic), 7.13-7.09 (d, 2H, ^{3}J(H,H)=7.5Hz, aromatic), 6.96-6.93 (d, 2H, ^{3}J(H,H)=7.5Hz, aromatic), 2.45-2.39 (t, 2H, ^{3}J(H,H)=7.5Hz, CH_2), 1.41-1.35 (t, 2H, ^{3}J(H,H)=7.5Hz, CH_2), 1.01-1.23 (m, 22H, CH_2), 0.85-0.81 (t, 3H, CH_3); ^{13}C NMR (62.5MHz, CD_3OD, 25°C): d (ppm): 158.52, 146.81, 138.23, 135.38, 134.66, 133.76, 131.38, 131.08, 131.02, 130.04, 129.74, 129.69, 129.53, 126.88, 121.36, 36.02, 33.13, 32.09, 30.83, 30.53, 29.66, 23.79, 14.49.

FD-MS (MW=580.88 without anion): m/z: 580.84.

Elemental analysis: Calculated. C 83.80%, H 8.18%, N 2.27%, 5.75%; Found. C 81.63%, H 8.45%, N 2.41%.

1-(4-Tetradecylphenyl)-2,4,6-triphenylpyridinium tetrafluoroborate (2-9b):

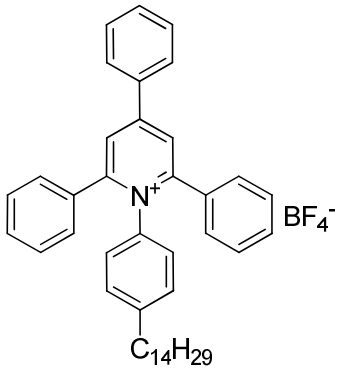

White powder (yield = 95%), ^{1}H NMR (250MHz, CD_3OD, 25°C): δ(ppm) = 8.45 (s, 2H, aromatic), 8.12-8.09 (m, 2H, aromatic), 7.63-7.60 (m, 3H, aromatic), 7.39-7.26 (m, 10H, aromatic), 7.13-7.09(d, 2H, ^{3}J(H,H)=7.5Hz, aromatic), 6.96-6.93 (d, 2H, ^{3}J(H,H)=7.5Hz, aromatic), 2.45-2.39 (t, 2H, ^{3}J(H,H)=7.5Hz, CH2), 1.42-1.36 (t, 2H, ^{3}J(H,H)=7.5Hz, CH_2), 1.23-1.02 (m, 22H, CH_2), 0.84-0.82 (t, 3H, CH_3); ^{13}C NMR (62.5MHz, CD_3OD, 25°C): d (ppm): 158.56, 158.51, 146.80, 138.23, 135.42, 134.69, 133.73, 131.36, 131.06, 131.02, 130.03, 129.73, 129.68, 129.52, 126.89, 36.02, 33.13, 32.08, 30.83, 30.53, 29.66, 23.79, 14.48.

FD-MS (MW=580.88 without anion): m/z: 580.95.

Elemental analysis: Calculated. C 77.35%, H 7.55%, N 2.10%, B 1.62%, F

11.38%; Found. C 77.35%, H 7.63%, N 2.19%.

2-Phenyl-9-alkylbenzoquinolizino[4,5,6,7-*fed*]phenanthridinylium salts (PQP salts):

Method A (Direct synthesis):

2g 1-(4-alkylphenyl)-2,4,6-triphenylpyridinium salts was dissolved in 200ml absolute ethanol. The ethanolic solution was irradiated at 300nm wavelength. After 72 hours, the solid product was filtered off. The filtrate was concentrated in vacuo to give a 2nd corp. The combined solid was recrystallized in ethanol to give the PQP salts.

2-Phenyl-9-hexylbenzo[8,9]quinolizino[4,5,6,7-*fed*]phenanthridinylium chloride (PQPCl-6, 2-10a):

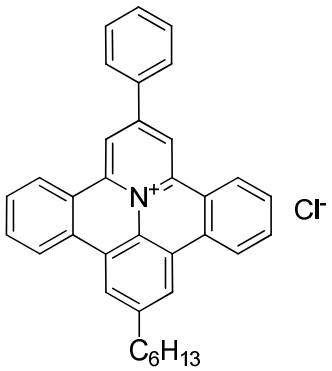

Yellow powder (yield = 47%), ^{1}H NMR (250MHz, CD_3OD, 25°C): δ(ppm) = 9.35 (s, 2H, aromatic), 8.96-8.93 (d, 2H, ^{3}J(H,H)=7.5Hz, aromatic), 8.69-8.65 (d, 4H, ^{3}J(H,H)=10Hz, aromatic), 8.27-8.25 (m, 2H, aromatic), 7.98-7.92 (t, 2H, ^{3}J(H,H)=7.5Hz, aromatic), 7.88-7.82 (d, 2H, ^{3}J(H,H)=7.5Hz, aromatic), 7.70 (s, 3H, aromatic), 2.97-2.91 (t, 2H, ^{3}J(H,H)=7.5Hz, CH2),1.78-1.75 (m, 2H, CH_2), 1.38-1.31 (m, 6H, CH_2), 0.90-0.84 (t, 3H, CH_3); ^{13}C NMR (62.5MHz, CD_3OD, 25°C): d (ppm): 151.01, 147.14, 143.89, 136.00, 135.31, 133.11, 132.01, 131.10, 130.36, 129.70, 127.40, 127.97, 126.13, 125.27, 124.97, 124.73, 119.28, 37.14, 32.93, 32.75, 30.35, 23.79, 14.48.

MALDI-TOF-MS (MW=464.64 without anion): m/z: 464.04.

Elemental analysis: Calculated. C 84.06%, H 6.05%, N 2.80%, Cl 7.09%; Found.

C 82.28%, H 5.05%, N 2.94%.

2-Phenyl-9-hexylbenzo[8,9]quinolizino[4,5,6,7-*fed*]phenanthridinylium tetrafluoroborate (PQPBF$_4$-6, 2-10b):

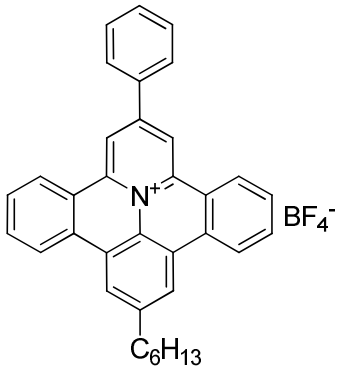

Yellow powder (yield = 66%), ^{1}H NMR (250MHz, CD_2Cl_2, 25°C): δ(ppm) = 9.31 (s, 2H, aromatic), 8.89-8.86 (d, 2H, ^3J(H,H)=7.5Hz, aromatic), 8.69-8.67 (d, 4H, ^3J(H,H)=7.5Hz, aromatic), 8.20-8.16 (m, 2H, aromatic), 8.10-8.04 (t, 2H, ^3J(H,H)=7.5Hz, aromatic), 8.00-7.94 (t, 2H, ^3J(H,H)=7.5Hz, aromatic), 7.76-7.73 (d, 3H, ^3J(H,H)=7.5Hz, aromatic), 3.11-3.05 (t, 2H, ^3J(H,H)=7.5Hz, CH_2),1.90-1.84 (m, 2H, CH_2), 1.52-1.32 (m, 6H, CH_2), 0.95-0.89 (t, 3H, CH_3); ^{13}C NMR (62.5MHz, CD_2Cl_2, 25°C): d (ppm): 150.37, 146.50, 142.69, 134.86, 134.71, 132.58, 131.58, 130.50, 129.40, 128.61, 126.89, 126.24, 125.17, 124.21, 123.97, 123.82, 118.61, 36.60, 32.04, 31.82, 29.42, 22.97, 14.21.

MALDI-TOF-MS (MW=464.64 without anion): m/z: 464.27.

Elemental analysis: Calculated. C 76.23%, H 5.48%, N 2.54%, B 1.96%, F 13.78%; Found. C 76.20%, H 5.88%, N 2.48%.

2-Phenyl-9-octylbenzo[8,9]quinolizino[4,5,6,7-*fed*]phenanthridinylium tetrafluoroborate (PQPBF$_4$-8, 2-11b):

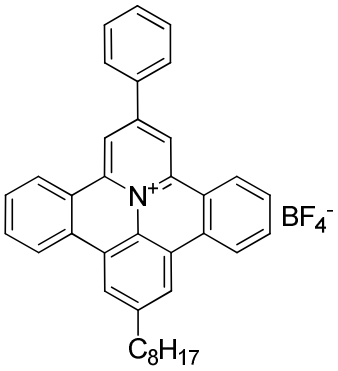

Yellow powder (yield = 64%), ^{1}H NMR (250MHz, CD_2Cl_2, 25°C): δ(ppm) = 9.26 (s, 2H, aromatic), 8.83-8.80 (d, 2H, ^{3}J(H,H)=7.5Hz, aromatic), 8.64-8.62 (m, 4H, aromatic), 8.12-8.09 (m, 2H, aromatic), 8.04-7.98 (t, 2H, ^{3}J(H,H)=7.5Hz, aromatic), 7.94-7.88 (t, 2H, ^{3}J(H,H)=7.5Hz, aromatic), 7.69-7.66 (d, 3H, ^{3}J(H,H)=7.5Hz, aromatic), 3.06-3.00 (t, 2H, ^{3}J(H,H)=7.5Hz, CH_2), 1.84-1.79 (m, 2H, CH_2), 1.38-1.22 (m, 10H, CH_2), 0.82-0.78 (t, 3H, CH_3); ^{13}C NMR (62.5MHz, CD_2Cl_2, 25°C): d (ppm): 150.39, 146.51, 142.72, 134.86, 134.73, 132.59, 131.58, 130.51, 129.41, 128.60, 126.90, 125.17, 124.22, 123.98, 123.83, 118.63, 36.60, 32.23, 31.86, 29.82, 29.76, 29.62, 23.04, 14.23.

MALDI-TOF-MS (MW=492.69 without anion): m/z: 492.17.

Elemental analysis: Calculated. C 76.69%, H 5.91%, N 2.42%, B 1.87%, F 13.11%; Found. C 76.40%, H 6.94%, N 1.96%.

2-Phenyl-9-decylbenzo[8,9]quinolizino[4,5,6,7-*fed*]phenanthridinylium tetrafluoroborate (PQPBF$_4$-10, 2-12b):

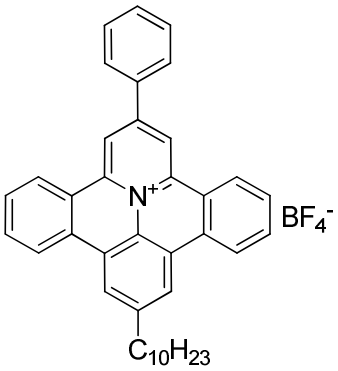

Yellow powder (yield = 63%), ^{1}H NMR (250MHz, CD_2Cl_2, 25°C): δ(ppm) = 9.28 (s, 2H, aromatic), 8.85-8.82 (d, 2H, ^{3}J(H,H)=7.5Hz, aromatic), 8.67-8.64 (d, 4H,

^{3}J(H,H)=7.5Hz, aromatic), 8.13-8.09 (m, 2H, aromatic), 8.06-8.00 (t, 2H, ^{3}J(H,H)=7.5Hz, aromatic), 7.96-7.90 (t, 2H, ^{3}J(H,H)=7.5Hz, aromatic), 7.70-7.67 (d, 3H, ^{3}J(H,H)=7.5Hz, aromatic), 3.08-3.02 (t, 2H, ^{3}J(H,H)=7.5Hz, CH_2),1.85-1.80 (m, 2H, CH_2), 1.36-1.19 (m, 14H, CH_2), 0.79-0.76 (t, 3H, CH_3); ^{13}C NMR (62.5MHz, CD_2Cl_2, 25°C): d (ppm): 150.45, 146.53, 142.77, 134.88, 134.80, 132.60, 131.60, 130.53, 129.49, 128.62, 126.91, 126.33, 125.23, 124.27, 124.03, 123.86, 118.69, 36.63, 32.29, 31.88, 29.98, 29.87, 29.76, 29.71, 23.06, 14.25.

MALDI-TOF-MS (MW=520.74 without anion): m/z: 520.90.

Elemental analysis: Calculated. C 76.85%, H 6.61%, N 2.30%, B 1.77%, F 12.47%; Found. C 76.43%, H 5.74%, N 2.53%.

2-Phenyl-9-dodecylbenzo[8,9]quinolizino[4,5,6,7-*fed*]phenanthridinylium tetrafluoroborate (PQPBF$_4$-12, 2-13b):

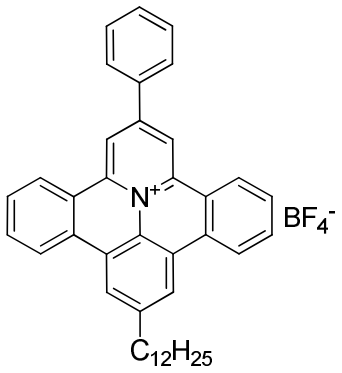

Yellow powder (yield = 62%), ^{1}H NMR (250MHz, CD_2Cl_2, 25°C): δ(ppm) = 9.29 (s, 2H, aromatic), 8.92-8.89 (d, 2H, ^{3}J(H,H)=7.5Hz, aromatic), 8.64-8.58 (d, 4H, ^{3}J(H,H)=7.5Hz, aromatic), 8.23 (m, 2H, aromatic), 7.92-7.89 (t, 2H, ^{3}J(H,H)=7.5Hz, aromatic), 7.85-7.82 (t, 2H, ^{3}J(H,H)=7.5Hz, aromatic), 7.69-7.66 (d, 3H, ^{3}J(H,H)=7.5Hz, aromatic), 2.93-2.87 (t, 2H, ^{3}J(H,H)=7.5Hz, CH_2),1.76 (m, 2H, CH_2), 1.35-1.20 (m, 18H, CH_2), 0.83-0.78 (t, 3H, CH_3); ^{13}C NMR (62.5MHz, CD_2Cl_2, 25°C): d (ppm): 149.70, 145.96, 141.97, 134.34, 133.95, 132.15, 131.16, 130.00, 128.62, 128.24, 126.56, 125.49, 124.51, 123.59, 123.33, 123.19, 117.99, 36.06, 31.85, 31.36, 29.59, 29.43, 29.33, 29.29, 22.62, 13.81.

MALDI-TOF-MS (MW=548.80 without anion): m/z: 548.15.

Elemental analysis: Calculated. C 77.48%, H 6.66%, N 2.20%, B 1.70%, F 11.96%; Found. C 76.87%, H 6.58%, N 2.25%.

2-Phenyl-9-tetradecylbenzo[8,9]quinolizino[4,5,6,7-*fed*]phenanthridinylium chloride (PQPCl-14, 2-14a):

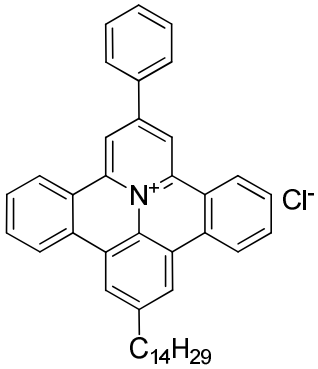

Yellow powder (yield = 41%), ^{1}H NMR (250MHz, CD_3OD, 25°C): δ(ppm) = 9.53 (s, 2H, aromatic), 9.10-9.06 (d, 2H, ^{3}J(H,H)=7.5Hz, aromatic), 8.85-8.82 (d, 4H, ^{3}J(H,H)=7.5Hz, aromatic), 8.31-8.29 (m, 2H, aromatic), 8.06-8.00(t, 2H, ^{3}J(H,H)=7.5Hz, aromatic), 7.95-7.89 (d, 2H, ^{3}J(H,H)=7.5Hz, aromatic), 7.72-7.69 (d, 3H, ^{3}J(H,H)=7.5Hz, aromatic), 3.11-3.04 (t, 2H, ^{3}J(H,H)=7.5Hz, CH_2),1.89-1.84 (m, 2H, CH_2), 1.48-1.19 (m, 22H, CH_2), 0.84-0.79 (t, 3H, CH_3); ^{13}C NMR (62.5MHz, CD_3OD, 25°C): d (ppm): 151.07, 147.15, 143.96, 136.02, 135.31, 133.08, 132.00, 131.09, 130.43, 129.70, 128.00, 127.48, 126.19, 125.33, 125.02, 124.76, 119.34, 37.10, 33.12, 32.71, 30.81, 30.77, 30.61, 30.52, 23.78, 14.48.

MALDI-TOF-MS (MW=576.85 without anion): m/z: 576.36.

Elemental analysis: Calculated. C 84.35%, H 7.57%, N 2.29%, Cl 5.79%; Found. C 85.39%, H 8.21%, N 2.14%.

2-Phenyl-9-tetradecylbenzo[8,9]quinolizino[4,5,6,7-*fed*]phenanthridinylium tetrafluoroborate (PQPBF_4-14, 2-14b):

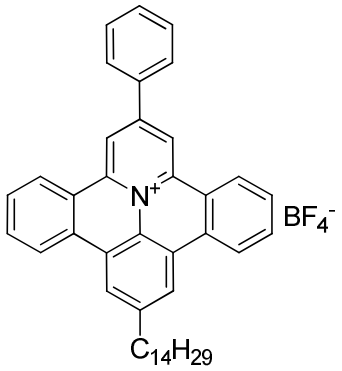

Yellow powder (yield = 59%), ^{1}H NMR (250MHz, CD_3OD, 25°C): δ(ppm) = 9.56 (s, 2H, aromatic), 9.12-9.09 (d, 2H, ^{3}J(H,H)=7.5Hz, aromatic), 8.88-8.85 (d, 4H, ^{3}J(H,H)=7.5Hz, aromatic), 8.33-8.29 (m, 2H, aromatic), 8.06-8.02 (t, 2H, ^{3}J(H,H)=5Hz, aromatic), 7.96-7.91 (d, 2H, ^{3}J(H,H)=5Hz, aromatic), 7.72-7.69 (d, 3H, ^{3}J(H,H)=7.5Hz, aromatic), 3.17-3.07 (t, 2H, ^{3}J(H,H)=7.5Hz, CH_2),1.90-1.84 (m, 2H, CH_2), 1.47-1.19 (m, 22H, CH_2), 0.84-0.79 (t, 3H, CH_3); ^{13}C NMR (62.5MHz, CD_2Cl_2, 25°C): d (ppm): 150.55, 146.80, 142.81, 135.19, 134.79, 132.99, 132.01, 130.85, 129.49, 129.08, 127.40, 126.33, 125.35, 124.44, 124.17, 124.04, 118.83, 36.90, 32.69, 32.20, 30.43, 30.28, 30.18, 30.13, 23.46, 14.65.

MALDI-TOF-MS (MW=576.85 without anion): m/z: 576.24.

Elemental analysis: Calculated. C 77.82%, H 6.99%, N 2.11%, B 1.63%, F 11.96%; Found. C 77.05%, H 6.92%, N 2.25%.

Method B (Ion exchange):

1mmol 2-phenyl-9-alkylbenzo[8,9]quinolizino[4,5,6,7-*fed*]phenanthridinylium chloride (PQPCl-n) was dissolved in 25ml methanol. The methanolic solution was heated to reflux and then the aqueous solution of NH_4PF_6 (1.2 mmol in 10 ml water) was added dropwise. The resulting yellow precipitate was filtrated and washed with water to give $PQPPF_6$-n.

2-Phenyl-9-hexylbenzo[8,9]quinolizino[4,5,6,7-*fed*]phenanthridinylium tetrafluoroborate ($PQPPF_6$-6, 2-10c):

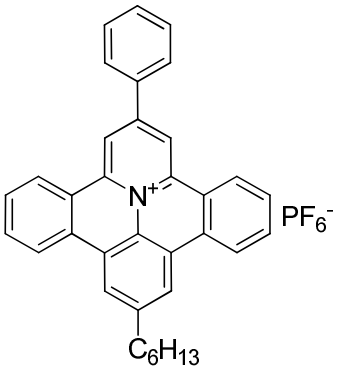

Yellow powder (yield = 100%), ^{1}H NMR (250MHz, CD_2Cl_2, 25°C): δ(ppm) = 9.27 (s, 2H, aromatic), 8.85-8.81 (d, 2H, ^{3}J(H,H)=10Hz, aromatic), 8.66-8.63 (d, 4H, ^{3}J(H,H)=7.5Hz, aromatic), 8.13-8.10 (m, 2H, aromatic), 8.05-7.99 (t, 2H, ^{3}J(H,H)=7.5Hz, aromatic), 7.95-7.89 (t, 2H, ^{3}J(H,H)=7.5Hz, aromatic), 7.69-7.66 (d, 3H, ^{3}J(H,H)=7.5Hz, aromatic), 3.07-3.01 (t, 2H, ^{3}J(H,H)=7.5Hz, CH_2),1.85-1.79 (m, 2H, CH_2), 1.43-1.30 (m, 6H, CH_2), 0.87-0.81 (t, 3H, CH_3); ^{13}C NMR (62.5MHz, CD_2Cl_2, 25°C): d (ppm): 150.43, 146.50, 142.78, 134.85, 134.70, 132.56, 131.54, 130.50, 129.53, 128.63, 126.91, 126.30, 125.24, 124.28, 124.06, 123.89, 118.74, 36.63, 32.04, 31.84, 29.42, 22.97, 14.22.

Elemental analysis: Calculated. C 68.96%, H 4.96%, N 2.30%, P 5.08%, F 18.70%; Found. C 68.96%, H 4.84%, N 2.51%.

2-Phenyl-9-tetradecylbenzo[8,9]quinolizino[4,5,6,7-*fed*]phenanthridinylium tetrafluoroborate (PQPPF$_6$-14, 2-14c):

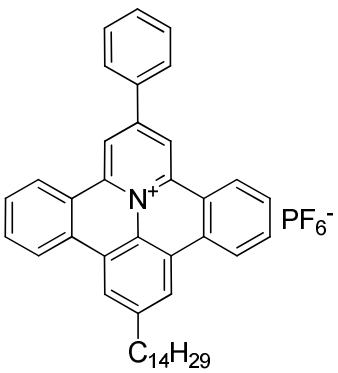

Yellow powder (yield = 99%), ^{1}H NMR (250MHz, CD_3OD, 25°C): δ(ppm) = 9.60 (s, 2H, aromatic), 9.15-9.12 (d, 2H, ^{3}J(H,H)=7.5Hz, aromatic), 8.93-8.89 (d, 4H, ^{3}J(H,H)=7.5Hz, aromatic), 8.34-8.30 (m, 2H, aromatic), 8.09-8.03 (t, 2H,

^{3}J(H,H)=7.5Hz, aromatic), 7.98-7.92 (d, 2H, ^{3}J(H,H)=7.5Hz, aromatic), 7.74-7.67 (m, 3H, aromatic), 3.15-3.09 (t, 2H, ^{3}J(H,H)=7.5Hz, CH_2),1.89-1.83 (m, 2H, CH_2), 1.50-1.22 (m, 22H, CH_2), 0.84-0.79 (t, 3H, CH_3); ^{13}C NMR (62.5MHz, CD_2Cl_2, 25°C): d (ppm): 150.81, 146.92, 143.15, 135.26, 135.20, 132.99, 131.99, 130.93, 129.89, 129.08, 127.37, 126.73, 125.62, 124.67, 124.45, 124.27, 119.12, 37.04, 32.72, 32.30, 30.49, 30.30, 30.19, 30.15, 23.48, 14.67.

Elemental analysis: Calculated. C 71.55%, H 6.42%, N 1.94%, P 4.29%, F 15.79; Found. C 71.24%, H 6.41%, N 1.94%.

DBPQP salts

2,6-Di(naphthalen-2-yl)-4-phenylpyrylium tetrafluoroborate (2-16):

Under argon atmosphere, BF_3-OEt_2 (9.838 mmol, 1.25 mL) was added to a mixture of benzaldehyde (4.919 mmol, 522 mg) and 2-acetylnaphthalene (9.838 mmol, 1.672 g) in anhydrous toluene (4 mL). The solution was refluxed for 2 h. After cooling to room temperature, acetone (3 mL) was added and the dark red solution was poured into 100 mL of ether. The red precipitate was filtered, washed with ether, recrystallized in tetrahydrofuran and dried under vacuum.

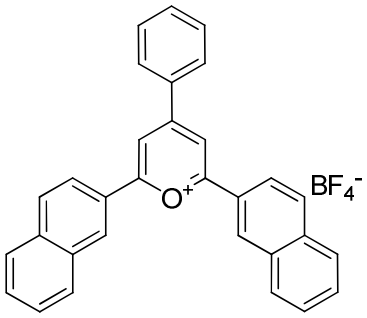

Red powder, (yield = 34%), ^{1}H NMR (250MHz, CD_2Cl_2, 25°C): δ(ppm) = 8.95 (s, 2H, aromatic), 8.66 (s, 2H, aromatic), 8.28-8.10 (m, 8H, aromatic), 7.94-7.91 (d, 2H, ^{3}J(H,H)=7.5Hz, aromatic), 7.72-7.62 (m, 7H, aromatic); ^{13}C NMR (62.5MHz, CD_2Cl_2, 25°C): d (ppm): 137.23, 133.79, 132.36, 131.58, 131.35, 131.25, 130.30, 129.77, 129.10, 128.90, 126.42, 123.02, 116.00, 115.57, 112.47, 111.93, 105.50.

MALDI-TOF-MS (MW=409.16 without anion): m/z: 409.40.

Elemental analysis: Calculated. C 75.02%, H 4.26%, O 3.22%, B 2.18%, F 15.31%; Found. C 74.24%, H 4.52%.

1-(4-Alkylphenyl)-2,6-di(naphthalen-2-yl)-4-phenylpyridinium tetrafluoroborate:

2,6-Di(naphthalen-2-yl)-4-phenylpyrylium tetrafluoroborate (2mmol) and 4-alkylaniline(2.2mmol) were added to 15ml absolute ethanol. The mixture was refluxed for 16 hours till the solution turned to transparent. After cooling the solution to room temperature, it was concentrated in vacuo to ca. 3ml. The concentrated solution was poured to 400ml hexane then. After filtration, the solid was recrystallized from 20ml hexane to give the target pyridinium salts.

2,6-Di(naphthalen-2-yl)-1,4-diphenylpyridinium tetrafluoroborate (2-17):

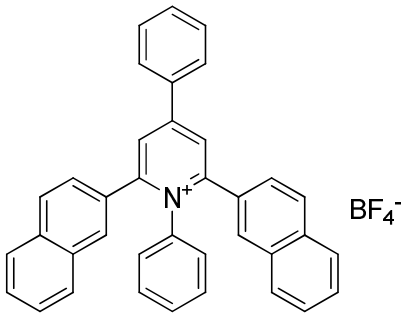

Yellow powder, (yield = 97%), ^{1}H NMR (250MHz, CD_2Cl_2, 25°C): δ(ppm) = 8.25 (s, 2H, aromatic), 8.00 (s, 2H, aromatic), 7.94-7.90 (m, 2H, aromatic), 7.83-7.79 (m, 2H, aromatic), 7.76-7.72 (m, 2H, aromatic), 7.67-7.63 (d, 2H, ^{3}J(H,H)=10Hz, aromatic), 7.59-7.56 (m, 3H, aromatic), 7.52-7.47 (m, 4H, aromatic), 7.26-7.22 (m, 4H, aromatic), 7.04-7.01 (m, 3H, aromatic); ^{13}C NMR (62.5MHz, CD_2Cl_2, 25°C): d (ppm): 157.94, 157.31, 134.58, 133.67, 132.97, 132.71, 130.98, 130.57, 130.45, 130.31, 129.60, 129.53, 128.98, 128.89, 128.73, 128.65, 128.09, 127.76, 126.95, 125.76, 125.32.

MALDI-TOF-MS (MW=484.21 without anion): m/z: 484.24.

Elemental analysis: Calculated. C 77.77%, H 4.59%, N 2.45%, B 1.89%, F 13.36%; Found. C 78.56%, H 4.92%, N 3.23%.

1-(4-Hexylphenyl)-2,6-di(naphthalen-2-yl)-4-phenylpyridinium tetrafluoroborate (2-18):

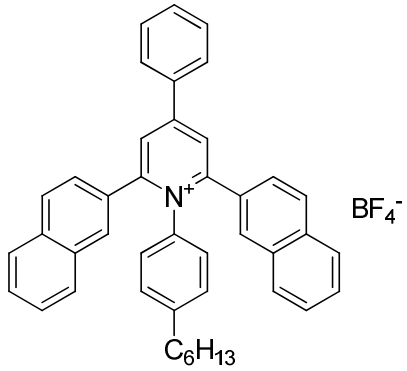

Yellow powder, (yield = 94%), ^{1}H NMR (250MHz, CD_2Cl_2, 25°C): δ(ppm) = 8.24 (s, 2H, aromatic), 7.99 (s, 2H, aromatic), 7.94-7.90 (m, 2H, aromatic), 7.83-7.79 (m, 2H, aromatic), 7.75-7.71 (m, 2H, aromatic), 7.65-7.56 (m, 5H, aromatic), 7.52-7.45 (m, 4H, aromatic), 7.24-7.19 (m, 2H, aromatic), 7.11-7.07 (d, 2H, ^{3}J(H,H)=10Hz, aromatic), 6.82-6.79 (d, 2H, ^{3}J(H,H)=7.5Hz, aromatic), 2.30-2.24 (t, 2H, ^{3}J(H,H)=7.5Hz, CH_2), 1.27-1.15 (m, 2H, CH_2), 1.04-0.96 (m, 4H, CH_2), 0.86-0.81 (m, 2H, CH_2), 0.75-0.69 (t, 3H, ^{3}J(H,H)=7.5Hz, CH_3); ^{13}C NMR (62.5MHz, CD_2Cl_2, 25°C): d (ppm): 157.77, 157.40, 146.12, 136.69, 134.62, 133.67, 132.93, 130.98, 130.57, 130.31, 129.58, 128.99, 128.77, 128.62, 128.57, 128.07, 127.73, 126.91, 125.80, 35.36, 31.79, 30.91, 28.42, 22.84, 14.19.

MALDI-TOF-MS (MW=568.30 without anion): m/z: 568.37.

Elemental analysis: Calculated. C 78.78%, H 5.84%, N 2.14%, B 1.65%, F 11.59%; Found. C 78.62%, H 5.70%, N 2.10%.

1-(4-Tetradecylphenyl)-2,6-di(naphthalen-2-yl)-4-phenylpyridinium tetrafluoroborate (2-19):

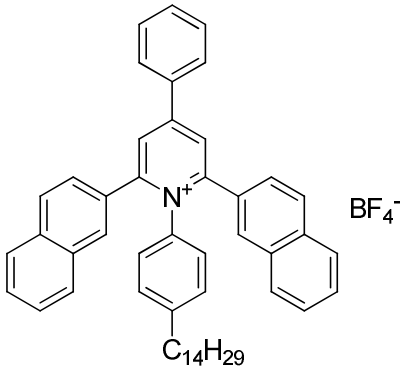

Yellow powder, (yield = 92%),[1]H NMR (250MHz, CD_2Cl_2, 25°C): δ(ppm) = 8.25 (s, 2H, aromatic), 8.00 (s, 2H, aromatic), 7.95-7.91 (m, 2H, aromatic), 7.84-7.80 (m, 2H, aromatic), 7.75-7.71 (m, 2H, aromatic), 7.65-7.56 (m, 5H, aromatic), 7.53-7.46 (m, 4H, aromatic), 7.24-7.19 (m, 2H, aromatic), 7.11-7.07 (d, 2H, ^3J(H,H)=10Hz, aromatic), 6.83-6.80 (d, 2H, ^3J(H,H)=7.5Hz, aromatic), 2.31-2.25 (t, 2H, ^3J(H,H)=7.5Hz, CH_2), 1.28-1.16 (m, 2H, CH_2), 1.06-0.78 (m, 22H, CH_2), 0.76-0.70 (t, 3H, ^3J(H,H)=7.5Hz, CH_3); ^{13}C NMR (62.5MHz, CD_2Cl_2, 25°C): d (ppm): 157.85, 157.45, 146.22, 136.72, 134.66, 133.71, 132.98, 131.08, 130.67, 130.30, 129.62, 129.09, 128.87, 128.67, 128.60, 128.11, 127.74, 126.96, 125.90, 35.40, 32.55, 31.89, 31.04, 30.93, 30.50, 30.11, 29.43, 28.50, 22.89, 14.23.

MALDI-TOF-MS (MW=680.43 without anion): m/z: 680.71.

Elemental analysis: Calculated. C 79.78%, H 7.09%, N 1.82%, B 1.41%, F 9.90%; Found. C 80.36%, H 7.43%, N 2.23%.

2-Phenyl-naphthacene[1,2]quinolizino[3,4,5,6-*def*]benzo[*i*]phenanthridinium tetrafluoroborate (DBPQPBF_4, 2-20):

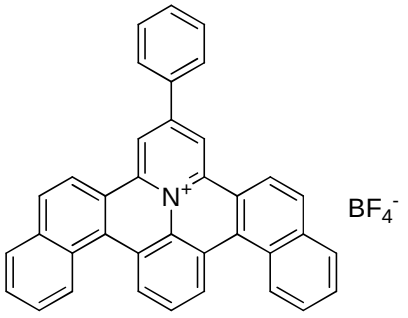

Orange powder, (yeild= 71%), ^{1}H NMR (700MHz, CD_2Cl_2, 25°C): δ(ppm) =

9.12 (s, 2H, aromatic), 8.94-8.93 (d, 2H, ^{3}J(H,H)=7.0Hz, aromatic), 8.79-8.78 (d, 2H, ^{3}J(H,H)=7.0Hz, aromatic), 8.57-8.55 (d, 2H, ^{3}J(H,H)=14.0Hz, aromatic), 8.15-8.14 (d, 2H, ^{3}J(H,H)=7.0Hz, aromatic), 8.08-8.05 (m, 3H, aromatic), 7.95-7.94 (d, 2H, ^{3}J(H,H)=7.0Hz, aromatic), 7.69-7.67 (t, 2H, ^{3}J(H,H)=7.0Hz, aromatic), 7.64-7.60 (m, 4H, aromatic), 7.57-7.55 (t, 1H, ^{3}J(H,H)=7.0Hz, aromatic); ^{13}C NMR (62.5MHz, CD_2Cl_2, 25°C): d (ppm): 148.25, 144.68, 141.40, 136.40, 133.69, 133.49, 132.73, 130.65, 130.33, 129.88, 129.12, 129.05, 128.63, 128.40, 127.65, 126.95, 123.30, 121.15, 118.30.

MALDI-TOF-MS (MW=480.58 without anion): m/z: 480.20.

Elemental analysis: Calculated. C 78.32%, H 3.91%, N 2.47%, B 1.91%, F 13.39%; Found. C 78.48%, H 3.13%, N 1.84%.

2-Phenyl-11-hexyl-naphthacene[1,2]quinolizino[3,4,5,6-*def*]benzo[*i*]phenanthridinium tetrafluoroborate (DBPQPBF$_4$-6, 2-21):

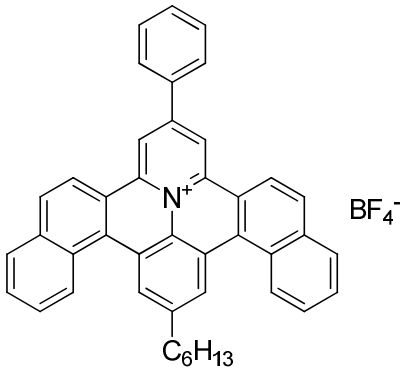

Orange powder, (yeild= 57%), ^{1}H NMR (700MHz, CD_2Cl_2, 25°C): δ(ppm) = 9.23 (s, 2H, aromatic), 8.92-8.91 (d, 2H, ^{3}J(H,H)=7.0Hz, aromatic), 8.87 (s, 2H, aromatic), 8.66-8.64 (d, 2H, ^{3}J(H,H)=14.0Hz, aromatic), 8.24-8.23 (d, 2H, ^{3}J(H,H)=7.0Hz, aromatic), 8.12-8.11 (d, 2H, ^{3}J(H,H)=7.0Hz, aromatic), 8.06-8.04 (d, 2H, ^{3}J(H,H)=14.0Hz, aromatic), 7.78-7.72 (m, 4H, aromatic), 7.65-7.63 (t, 2H, ^{3}J(H,H)=7.0Hz, aromatic), 7.60-7.58 (t, 1H, ^{3}J(H,H)=7.0Hz, aromatic), 3.02-3.00 (t, 2H, ^{3}J(H,H)=7.0Hz, CH_2), 1.80-1.76 (m, 2H, CH_2), 1.42-1.38 (m, 2H, CH_2), 1.32-1.24 (m, 4H, CH_2), 0.83-081 (t, 3H, ^{3}J(H,H)=7.0Hz, CH_3); ^{13}C NMR (62.5MHz, CD_2Cl_2, 25°C): d (ppm): 149.72, 144.54, 141.40, 136.25, 132.49, 132.35, 130.50,

130.44, 129.72, 129.04, 128.61, 128.41, 128.11, 126.87, 123.19, 120.76, 118.60, 116.51, 36.27, 32.04, 31.70, 29.37, 23.03, 14.23.

MALDI-TOF-MS (MW=564.74 without anion): m/z: 564.51.

Elemental analysis: Calculated. C 79.27%, H 5.26%, N 2.15%, B 1.66%, F 11.66%; Found. C 78.73%, H 5.20%, N 2.21%.

2-Phenyl-11-tetradecyl-naphthacene[1,2]quinolizino[3,4,5,6-*def*]benzo[*i*]phenanthridinium tetrafluoroborate (DBPQPBF_4-14):

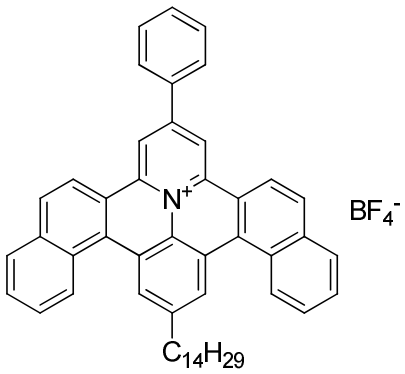

Orange powder, (yeild= 33%), ^{1}H NMR (250MHz, CD_2Cl_2, 25°C): δ(ppm) = 9.18 (s, 2H, aromatic), 8.86-8.82 (d, 2H, ^3J(H,H)=10.0Hz, aromatic), 8.79 (s, 2H, aromatic), 8.64-8.60 (d, 2H, ^3J(H,H)=10.0Hz, aromatic), 8.21-8.17 (d, 2H, ^3J(H,H)=10.0Hz, aromatic), 8.12-8.09 (d, 2H, ^3J(H,H)=7.5Hz, aromatic), 8.02-8.98 (d, 2H, ^3J(H,H)=10.0Hz, aromatic), 7.75-7.56 (m, 7H, aromatic), 3.00-2.94 (t, 2H, ^3J(H,H)=7.5Hz, CH_2), 1.78-1.73 (m, 2H CH_2), 1.36-1.16 (m, 22H, CH_2), 0.80-074 (t, 3H, ^3J(H,H)=7.5Hz, CH_3); ^{13}C NMR (62.5MHz, CD_2Cl_2, 25°C): d (ppm): 150.11, 144.90, 141.75, 136.62, 135.29, 132.88, 132.74, 130.87, 130.82, 130.09, 129.40, 129.01, 128.94, 128.77, 127.22, 123.58, 121.16, 118.99, 36.64, 32.67, 32.12, 30.40, 30.25, 30.10, 25.69, 24.15, 23.44, 22.44, 14.63.

MALDI-TOF-MS (MW=676.39 without anion): m/z: 676.68.

Elemental analysis: Calculated. C 80.20%, H 6.60%, N 1.83%, B 1.42%, F 9.95%; Found. C 80.57%, H 7.36%, N 2.18%.

BNAX salts

General method to dibenzo[*a,j*]xanthene:

Claisen condensation:

To a solution of appropriate arylaldehyde (benzaldehyde or 4-bromobenzaldehyde, 50mmol) and naphtol (2-naphtol or 6-bromonaphthalen-2-ol, 100mmol) in glacial acetic acid (40 ml), concentrated HCl (1ml) was added dropwise. The solution was heated with oil bath to 100°C and kept at this temperature until crystallization took place. When the solution was cooled to room temperature, the precipitated product was filtered with suction and recrystallized from glacial acetic acid to give the target compound.

14-Phenyl-14*H*-dibenzo[*a,j*]xanthene (3-8)

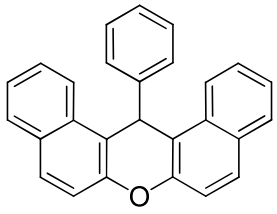

White needles (Yield=60%), ^{1}H NMR (250MHz, CD_2Cl_2, 25°C): δ(ppm) = 8.33-8.29 (d, 2H, ^{3}J(H,H)=10.0Hz, aromatic), 7.77-7.71 (t, 4H, ^{3}J(H,H)=7.5Hz, aromatic), 7.53-7.30 (m, 8H, aromatic), 7.10-7.04 (t, 2H, ^{3}J(H,H)=7.5Hz, aromatic), 6.95-6.89 (t, 1H, ^{3}J(H,H)=7.5Hz, aromatic), 6.42 (s, 1H, CH); ^{13}C NMR (62.5MHz, CD_2Cl_2, 25°C): d (ppm): 148.40, 145.04, 131.10, 130.89, 128.73, 128.62, 128.28, 128.03, 126.63, 126.28, 124.14, 122.43, 117.77, 116.96, 37.83.

FD-MS (MW=358.44): m/z: 358.67.

Elemental analysis: Calculated. C 90.47%, H 5.06% O 4.66%; Found. C 90.35%, H 5.12%.

14-(4-Bromophenyl)-14*H*-dibenzo[*a,j*]xanthene (3-10)

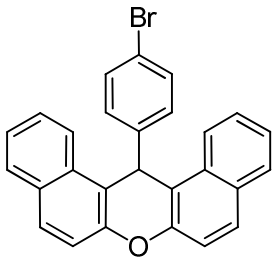

White needles. (Yield=63%), ^{1}H NMR (250MHz, CD_2Cl_2, 25°C): δ(ppm) = 8.25-8.22 (d, 2H, ^{3}J(H,H)=7.5Hz, aromatic), 7.78-7.72 (t, 4H, ^{3}J(H,H)=7.5Hz, aromatic), 7.54-7.48 (t, 2H, ^{3}J(H,H)=7.5Hz, aromatic), 7.48-7.31 (m, 6H, aromatic), 7.20-7.17 (d, 2H, ^{3}J(H,H)=7.5Hz, aromatic), 6.394 (s, 1H, CH); ^{13}C NMR (62.5MHz, CD_2Cl_2, 25°C): d (ppm): 149.37, 145.00, 132.28, 131.91, 131.84, 130.67, 129.91, 129.64, 127.72, 125.20, 123.17, 120.91, 118.72, 117.32, 38.22.

FD-MS (MW=437.34): m/z: 436.15.

Elemental analysis: Calculated. C 74.15%, H 3.92%, Br 18.27%, O 3.66%; Found. C 73.77%, H 3.92%.

3,11-Dibromo-14-phenyl-14*H*-dibenzo[*a,j*]xanthene (3-11)

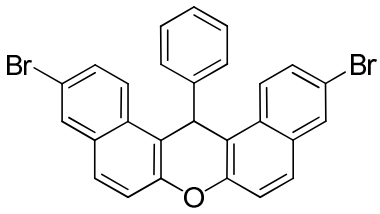

White needles (Yield=58%), ^{1}H NMR (250MHz, CD_2Cl_2, 25°C): δ(ppm) = 8.16-8.12 (d, 2H, ^{3}J(H,H)=10.0Hz, aromatic), 7.90-7.89 (d, 2H, ^{3}J(H,H)=2.5Hz, aromatic), 7.65-7.61 (d, 2H, ^{3}J(H,H)=10.0Hz, aromatic), 7.58-7.54 (d, 2H, ^{3}J(H,H)=10.0Hz, aromatic), 7.42-7.36 (t, 4H, ^{3}J(H,H)=7.5Hz, aromatic), 7.10-7.04 (t, 2H, ^{3}J(H,H)=7.5Hz, aromatic), 6.96-6.90 (t, 1H, ^{3}J(H,H)=7.5Hz, aromatic), 6.27 (s, 1H, CH); ^{13}C NMR (62.5MHz, CD_2Cl_2, 25°C): d (ppm): 149.00, 144.93, 132.66, 131.10, 130.38, 130.17, 128.99, 128.51, 128.44, 127.10, 124.81, 119.52, 118.54, 117.51, 38.43.

FD-MS (MW=516.24): m/z: 514.02.

Elemental analysis: Calculated. C 62.82%, H 3.12%, Br 30.96%, O 3.10%; Found. C 61.69%, H 2.82%.

3,11-Dibromo-14-(4-bromophenyl)-14*H*-dibenzo[*a,j*]xanthene (3-12)

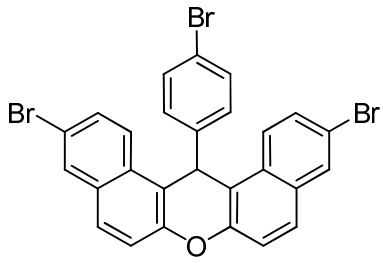

White needles (Yield=66%), ^{1}H NMR (250MHz, CD_2Cl_2, 25°C): δ(ppm) = 8.09-8.06 (d, 2H, ^{3}J(H,H)=7.5Hz, aromatic), 7.91-7.90 (d, 2H, ^{3}J(H,H)=2.5Hz, aromatic), 7.66-7.63 (d, 2H, ^{3}J(H,H)=7.5Hz, aromatic), 7.58-7.54 (d, 2H, ^{3}J(H,H)=10.0Hz, aromatic), 7.42-7.38 (d, 2H, ^{3}J(H,H)=10.0Hz, aromatic), 7.26-7.16 (m, 4H, aromatic), 6.28 (s, 1H, CH); ^{13}C NMR (62.5MHz, CD_2Cl_2, 25°C): d (ppm): 148.62, 143.54, 132.25, 131.63, 130.78, 130.10, 129.70, 129.63, 128.33, 124.18, 121.00, 119.11, 118.22, 116.52, 37.44.

FD-MS (MW=595.13): m/z: 593.53.

Elemental analysis: Calculated. C 54.49%, H 2.54%, Br 20.28%, O 2.69%; Found. C 53.74%, H 2.86%.

Kumada coupling for alkylated dibenzoxanthene

Appropriate brom-dibenzoxanthene (10 mmol), [1,1'-Bis(diphenylphosphino)ferrocene]dichloropalladium(II) dichloromethane, ($PdCl_2$(dppf)CH_2Cl_2, 5 mol% per Br), anhydrous THF (100 ml) were added in a 250 ml Shlenck round bottom bottle. The mixture was degassed by two *freeze-pump-thaw* cycles. Grignard reagent (2 mol per Br) was added to the bottle slowly. The mixture was stirred at 60 °C for 18 h under argon atmosphere and then cooled to room temperature. Methanol (20 ml) was added to quench the reaction. The mixture was extracted with dichloromethane (200ml x 3). The organic phase was washed with water (100ml x 2), dried over $MgSO_4$ and concentrated under reduced pressure. The

residue was purified by column chromatography (silica gel, PE/DCM) to give the alkylated dibenzoxanthene.

14-(4-Hexylphenyl)-14*H*-dibenzo[*a,j*]xanthene (3-13)

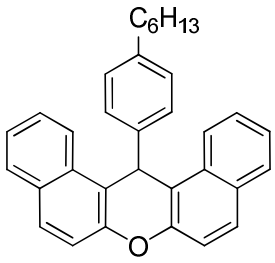

Needle like crystal (PE : DCM = 6 : 1, yield=87%), ^{1}H NMR (250MHz, CD_2Cl_2, 25°C): δ(ppm) = 8.34-8.30 (d, 2H, ^{3}J(H,H)=10.0Hz, aromatic), 7.78-7.70 (t, 4H, ^{3}J(H,H)=10.0Hz, aromatic), 7.54-7.48 (t, 2H, ^{3}J(H,H)=7.5Hz, aromatic), 7.42 (s, 1H, aromatic), 7.39-7.31 (m, 5H, aromatic), 6.91-6.87 (t, 2H, ^{3}J(H,H)=5.0Hz, aromatic), 6.39 (s, 1H, CH), 2.33-2.27 (t, 2H, ^{3}J(H,H)=7.5Hz, CH_2), 1.35-1.30 (m, 2H, CH_2), 1.11 (m, 6H, CH_2), 0.72-0.69 (t, 3H, CH_3); ^{13}C NMR (62.5MHz, CD_2Cl_2, 25°C): d (ppm): 148.53, 142.31, 141.33, 131.22, 131.00, 128.71, 128.37, 127.89, 126.70, 124.22, 124.11, 122.58, 117.88, 117.30, 37.50, 35.30, 31.55, 31.23, 29.02, 22.45, 13.72.

MALDI-TOF-MS (MW=442.59): m/z: 442.30.

Elemental analysis: Calculated. C 89.55%, H 6.83%, O 3.61%; Found. C 89.84%, H 7.31%.

14-(4-Dodecylphenyl)-14*H*-dibenzo[*a,j*]xanthene (3-14)

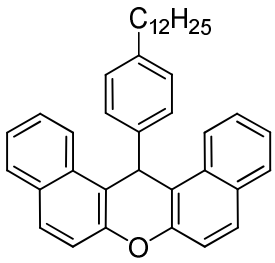

Transparent liquid (PE : DCM = 7 : 1, yield=83%), ^{1}H NMR (250MHz, CD_2Cl_2, 25°C): δ(ppm) = 8.32-8.29 (d, 2H, ^{3}J(H,H)=7.5Hz, aromatic), 7.77-7.71 (t, 4H,

^{3}J(H,H)=7.5Hz, aromatic), 7.53-7.47 (t, 2H, ^{3}J(H,H)=7.5Hz, aromatic), 7.41 (s, 1H, aromatic), 7.38-7.30 (m, 5H, aromatic), 6.90-6.86 (t, 2H, ^{3}J(H,H)=5.0Hz, aromatic), 6.38 (s, 1H, CH), 2.32- 2.26(t, 2H, ^{3}J(H,H)=7.5Hz, CH_2), 1.32 (m, 2H, CH_2), 1.13-1.10 (m, 18H, CH_2), 0.80-0.75 (t, 3H, CH_3); ^{13}C NMR (62.5MHz, CD_2Cl_2, 25°C): d (ppm): 148.63, 142.42, 141.44, 131.32, 131.11, 128.82, 128.47, 128.00, 126.81, 124.33, 122.68, 117.99, 117.40, 37.60, 35.41, 31.95, 31.38, 29.64, 29.54, 29.45, 29.37, 22.73, 13.92.

MALDI-TOF-MS (MW=526.77): m/z: 526.41.

Elemental analysis: Calculated. C 88.93%, H 8.04%, O 3.04%; Found. C 89.56%, H 6.98%.

3,11-Didodecyl-14-phenyl-14*H*-dibenzo[*a,j*]xanthene (3-15)

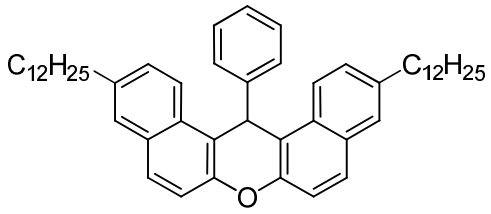

White powder (PE : DCM = 8 : 1, yield=78%), ^{1}H NMR (250MHz, CD_2Cl_2, 25°C): δ(ppm) = 8.21-8.18 (d, 2H, ^{3}J(H,H)=7.5Hz, aromatic), 7.65-7.62 (d, 2H, ^{3}J(H,H)=7.5Hz, aromatic), 7.51 (s, 1H, aromatic), 7.44-7.41 (d, 2H, ^{3}J(H,H)=7.5Hz, aromatic), 7.36-7.32 (d, 4H, ^{3}J(H,H)=10.0Hz, aromatic), 7.08-7.02 (t, 2H, ^{3}J(H,H)=7.5Hz, aromatic), 6.93-6.87 (t, 2H, ^{3}J(H,H)=7.5Hz, aromatic), 6.35 (s, 1H, CH), 2.67-2.61 (t, 4H, ^{3}J(H,H)=7.5Hz, CH_2), 1.57-1.54 (m, 4H, CH_2), 1.31-1.08 (m, 36H, CH_2), 0.80-0.75 (t, 6H, CH_3); ^{13}C NMR (62.5MHz, CD_2Cl_2, 25°C): d (ppm): 148.45, 145.83, 139.45, 131.59, 129.92, 128.79, 128.67, 128.55, 127.70, 126.74, 122.81, 118.19, 117.41, 38.49, 36.05, 32.30, 31.78, 30.05, 29.97, 29.90, 29.73, 23.07, 14.25.

MALDI-TOF-MS (MW=695.09): m/z: 694.41

Elemental analysis: Calculated. C 88.13%, H 9.57%, O 2.30%; Found. C 87.99%,

H 9.46%.

3,11-Dihexyl-14-(4-hexylphenyl)-14*H*-dibenzo[*a,j*]xanthene (3-16)

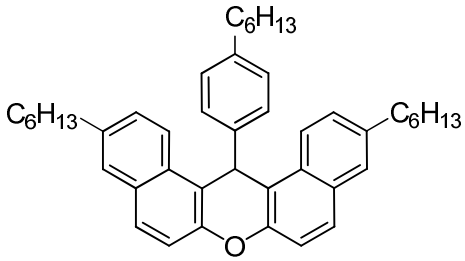

Transparent oil like liquid (PE : DCM = 9 : 1, yield=71%), ^{1}H NMR (250MHz, CD_2Cl_2, 25°C): δ(ppm) = 8.22-8.19 (d, 2H, ^{3}J(H,H)=7.5Hz, aromatic), 7.66-7.62 (d, 2H, ^{3}J(H,H)=10.0Hz, aromatic), 7.52 (s, 2H, aromatic), 7.36-7.30 (m, 6H, aromatic), 6.90-6.86 (d, 2H, ^{3}J(H,H)=10.0Hz, aromatic), 6.33 (s, 1H, CH), 2.68- 2.62 (t, 4H, ^{3}J(H,H)=5.0Hz, CH_2), 2.33-2.27 (t, 2H, ^{3}J(H,H)=7.5Hz, CH_2), 1.61-1.56 (m, 4H, CH_2), 1.23-1.11 (m, 20H, CH_2), 0.82-0.69 (m, 9H, CH_3); ^{13}C NMR (62.5MHz, CD_2Cl_2, 25°C): d (ppm): 148.45, 143.03, 141.68, 139.40, 131.59, 129.94, 128.77, 128.63, 128.32, 127.69, 122.87, 118.20, 117.63, 38.06, 36.07, 35.76, 32.14, 32.01, 31.76, 31.69, 29.44, 23.00, 22.90, 14.24, 14.16.

MALDI-TOF-MS (MW=610.42): m/z: 610.91.

3,11-Didodecyl-14-(4-dodecylphenyl)-14*H*-dibenzo[*a,j*]xanthene (3-17)

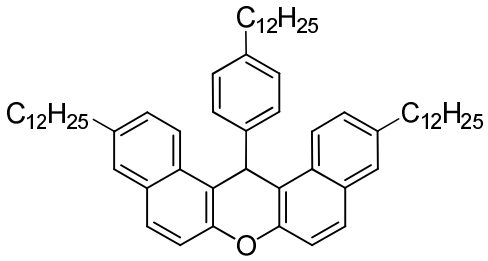

Transparent oil like liquid (PE : DCM = 9 : 1, yield=65%), ^{1}H NMR (250MHz, CD_2Cl_2, 25°C): δ(ppm) = 8.19-8.16 (d, 2H, ^{3}J(H,H)=7.5Hz, aromatic), 7.62-7.59 (d, 2H, ^{3}J(H,H)=7.5Hz, aromatic), 7.49 (s, 2H, aromatic), 7.33-7.27 (m, 6H, aromatic), 6.86-6.83 (d, 2H, ^{3}J(H,H)=7.5Hz, aromatic), 6.30 (s, 1H, CH), 2.65-2.58 (t, 4H, ^{3}J(H,H)=7.5Hz, CH_2), 2.29-2.23 (t, 2H, ^{3}J(H,H)=7.5Hz, CH_2), 1.55-1.52 (m, 4H,

CH_2), 1.29-1.07 (m, 56H, CH_2), 0.77-0.71 (m, 9H, CH_3); ^{13}C NMR (62.5MHz, CD_2Cl_2, 25°C): d (ppm): 147.89, 142.46, 141.13, 138.86, 131.02, 129.37, 128.21, 128.07, 128.03, 127.75, 127.14, 122.30, 117.64, 117.07, 37.49, 35.50, 35.19, 31.75, 31.23, 31.17, 29.49, 29.46, 29.42, 29.35, 29.18, 22.51, 13.70.

MALDI-TOF-MS (MW=862.42): m/z: 862.61.

Xanthenylium derivates with bromide as anion

To the appropriate 14-phenyl-14*H*-dibenzo[*a*,*j*]xanthene derivates (20 mmol) in glacial acetic acid (300 ml) at 100 °C was added dropwise bromine (20 mmol) in acetic acid (30 ml). The solution was kept at this temperature for 1 hour. When the solution was cooled to room temperature, the precipitated solid was filtered with suction and recrystallized from glacial acetic acid to give the product.

14-Phenyl-14-dibenzo[*a,j*]xanthenylium bromide (3-4a)

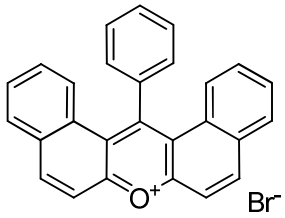

Reddish orange crystals with a golden glimmer (Yield = 85%), ^{1}H NMR (250MHz, CD_2Cl_2, 25°C): δ(ppm) = 8.78-8.74 (d, 2H, ^3J(H,H)=10.0Hz, aromatic), 8.27-8.13 (m, 4H, aromatic), 7.90-7.69 (m, 5H, aromatic), 7.53-7.50 (m, 2H, aromatic), 7.43-7.36 (m, 2H, aromatic), 7.20-7.17 (d, 2H, ^3J(H,H)=7.5Hz, aromatic); ^{13}C NMR (62.5MHz, CD_2Cl_2, 25°C): d (ppm): 167.55, 159.75, 147.73, 138.88, 133.14, 132.78, 132.42, 132.05, 131.00, 130.04, 129.63, 128.66, 126.75, 122.58, 117.73.

MALDI-TOF-MS (MW=357.42 without anion): m/z: 357.11.

14-(4-Hexylphenyl)dibenzo[*a,j*]xanthenylium bromide (3-18)

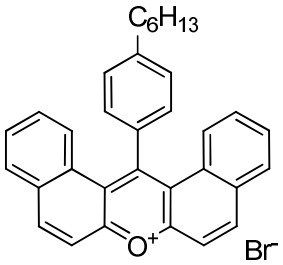

Reddish orange crystals with a golden glimmer (Yield = 83%), ^{1}H NMR (250MHz, CD_2Cl_2, 25°C): δ(ppm) = 8.76-8.73 (d, 2H, ^{3}J(H,H)=7.5Hz, aromatic), 8.25-8.21 (d, 2H, ^{3}J(H,H)=10.0Hz, aromatic), 8.15-8.11 (d, 2H, ^{3}J(H,H)=10.0Hz, aromatic), 7.74-7.62 (m, 4H, aromatic), 7.39-7.34 (m, 4H, aromatic), 7.24-7.20 (d, 2H, ^{3}J(H,H)=10.0Hz, aromatic), 2.91-2.85 (t, 2H, ^{3}J(H,H)=7.5Hz, CH_2), 1.80-1.75 (m, 2H, CH_2), 1.38-1.35 (m, 6H, CH_2), 0.91-0.85 (t, 3H, CH_3); ^{13}C NMR (62.5MHz, CD_2Cl_2, 25°C): d (ppm): 167.55, 159.33, 147.82, 147.03, 135.52, 132.77, 132.36, 131.56, 130.26, 129.54, 129.20, 128.27, 126.22, 122.44, 117.36, 35.88, 31.69, 31.42, 28.65, 22.68, 13.87.

MALDI-TOF-MS (MW=441.22, without anion): m/z: 441.44.

14-(4-Dodecylphenyl)dibenzo[*a,j*]xanthenium bromide (3-19)

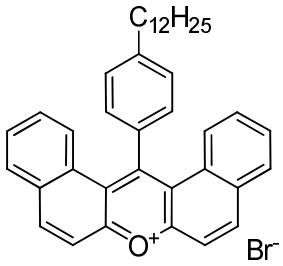

Reddish orange crystals with a golden glimmer (Yield = 85%), ^{1}H NMR (250MHz, CD_2Cl_2, 25°C): δ(ppm) = 8.77-8.74 (d, 2H, ^{3}J(H,H)=7.5Hz, aromatic), 8.26-8.22 (d, 2H, ^{3}J(H,H)=10.0Hz, aromatic), 8.16-8.13 (d, 2H, ^{3}J(H,H)=7.5Hz, aromatic), 7.88-7.49 (m, 6H, aromatic), 7.42-7.35 (m, 4H, aromatic), 7.25-7.22 (d, 2H, ^{3}J(H,H)=10.0Hz, aromatic), 2.92-2.86 (t, 2H, ^{3}J(H,H)=7.5Hz, CH_2), 1.82-1.73 (m, 2H, CH_2), 1.40-1.20 (m, 6H, CH_2), 0.82-0.76 (t, 3H, CH_3); ^{13}C NMR (62.5MHz, CD_2Cl_2, 25°C): d (ppm): 160.89, 159.92, 147.48, 139.49, 137.14, 133.21, 132.82, 132.00, 130.71, 129.98, 128.91, 128.71, 126.64, 117.78, 114.03, 36.32, 32.32, 30.13, 30.06,

30.03, 29.76, 29.42, 23.07, 21.35, 14.26.

MALDI-TOF-MS (MW=525.32 without anion): m/z: 525.37.

3,11-Didodecyl-14-phenyldibenzo[*a,j*]xanthenium bromide (3-20)

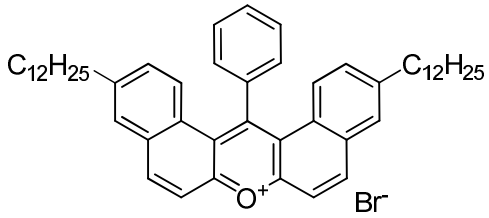

Red solid (Yield = 72%), ^{1}H NMR (250MHz, CD_2Cl_2, 25°C): δ(ppm) = 8.73-8.70 (d, 2H, ^{3}J(H,H)=7.5Hz, aromatic), 8.24-8.21 (d, 2H, ^{3}J(H,H)=7.5Hz, aromatic), 7.91-7.85 (m, 5H, aromatic), 7.51-7.49 (s, 2H, aromatic), 7.26-7.03 (m, 4H, aromatic), 2.76-2.70 (t, 4H, ^{3}J(H,H)=7.5Hz, CH_2), 1.49 (m, 4H, CH_2), 1.82 (m, 36H, CH_2), 0.81-0.77 (m, 6H, CH_3); ^{13}C NMR (62.5MHz, CD_2Cl_2, 25°C): d (ppm): 149.33, 146.21, 139.21, 134.17, 133.74, 133.24, 132.88, 132.34, 129.24, 129.06, 128.96, 128.25, 128.08, 127.97, 127.25, 124.29, 121.15, 36.52, 32.77, 32.08, 30.54, 30.50, 30.40, 30.21, 23.56, 23.51, 14.83, 14.74.

MALDI-TOF-MS (MW=693.50 without anion): m/z: 693.31.

3,11-Dihexyl-14-(4-hexylphenyl)dibenzo[*a,j*]xanthenium bromide (3-21)

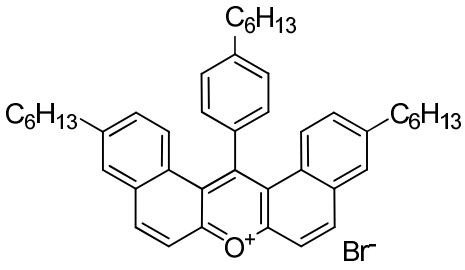

Red solid (Yield = 71%), ^{1}H NMR (250MHz, CD_2Cl_2, 25°C): δ(ppm) = 8.73-8.71 (d, 2H, ^{3}J(H,H)=5.0Hz, aromatic), 8.30-8.27 (d, 2H, ^{3}J(H,H)=7.5Hz, aromatic), 7.95-7.92 (d, 2H, ^{3}J(H,H)=7.5Hz, aromatic), 7.67-7.63 (d, 2H, ^{3}J(H,H)=10.0Hz, aromatic), 7.44-7.39 (s, 2H, aromatic), 7.23-7.13 (m, 4H, aromatic), 2.93-2.87 (t, 4H, CH_2), 2.76-2.70 (m, 2H, CH_2), 1.82 (m, 4H, CH_2), 1.40-1.27 (m, 20H,

CH_2), 0.82 (m, 9H, CH_3); ^{13}C NMR (62.5MHz, CD_2Cl_2, 25°C): d (ppm): 159.25, 148. 25, 147.63, 145.29, 133.28, 132.80, 131.72, 131.29, 128.40, 127.74, 127.48, 127.36, 123.55, 120.02, 117.36, 36.15, 35.58, 31.85, 31.68, 31.55, 31.12, 29.10, 28.72, 22.87, 22.64, 14.04, 13.94.

MALDI-TOF-MS (MW=609.41 without anion): m/z: 609.55.

3,11-Didodecyl-14-(4-dodecylphenyl)dibenzo[*a,j*]xanthenium bromide (3-22)

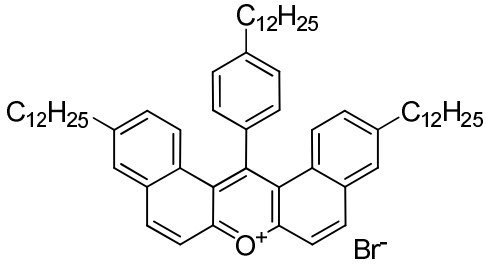

Red solid (Yield = 69%), ^1H NMR (250MHz, CD_2Cl_2, 25°C): δ(ppm) = 8.70-8.67 (d, 2H, ^3J(H,H)=7.5Hz, aromatic), 8.22-8.19 (d, 2H, ^3J(H,H)=7.5Hz, aromatic), 7.91-7.87 (d, 2H, ^3J(H,H)=10.0Hz, aromatic), 7.65-7.63 (d, 2H, ^3J(H,H)=7.5Hz, aromatic), 7.38-7.35 (s, 2H, aromatic), 7.23-7.09 (m, 4H, aromatic), 2.93-2.87 (t, 4H, CH_2), 2.76-2.70 (m, 2H, CH_2), 1.83-1.78 (m, 4H, CH_2), 1.49-1.10 (m, 56H, CH_2), 0.79-0.77 (m, 9H, CH_3); ^{13}C NMR (62.5MHz, CD_2Cl_2, 25°C): d (ppm): 157.75, 147.10, 146.08, 143.71, 134.03, 131.82, 131.42, 130.28, 130.01, 126.93, 126.83, 126.55, 126.05, 122.17, 119.05, 34.01, 33.68, 32.50, 31.53, 30.17, 29.95, 28.05, 27.97, 27.69, 27.46, 27.33, 21.02, 12.98.

MALDI-TOF-MS (MW=861.69 without anion): m/z: 861.52.

BNAX derivates with bromide as anion

0.1 mmol 14-Phenyl-14-dibenzo[*a,j*]xanthenylium bromide (or its alkylated derivates) was dissolved in 200ml acetic acid. After the solution was irradiated at 300nm wavelength for 24 hours, the solid product was filtered off. The filtrate was concentrated in vacuo to give a 2nd corp. The combined solid was recrystallized in methanol to give the fused benzo[5,6]naphthaceno[1,12,11,10-*jklmna*]xanthylium

(BNAX) bromide (or its alkylated derivates).

Benzo[5,6]naphthaceno[1,12,11,10-*jklmna*]xanthylium bromide (3-5a)

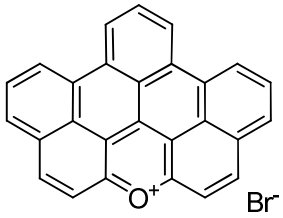

Purple needle-like crystal (Yield = 96%), ^{1}H NMR (250MHz, CD_2Cl_2&CD_3OH, 25°C): δ(ppm) = 9.68-9.65 (d, 2H, ^{3}J(H,H)=7.5Hz, aromatic), 9.54-9.50 (d, 2H, ^{3}J(H,H)=10.0Hz, aromatic), 9.28-9.25(d, 2H, ^{3}J(H,H)=7.5Hz, aromatic), 8.91-8.88 (d, 2H, ^{3}J(H,H)=7.5Hz, aromatic), 8.82-8.73 (m, 3H, aromatic), 8.60-8.54 (t, 2H, ^{3}J(H,H)=7.5Hz, aromatic).

MALDI-TOF-MS (MW=353.10 without anion): m/z: 353.08.

7-Hexyl-benzo[5,6]naphthaceno[1,12,11,10-*jklmna*]xanthylium bromide (3-23)

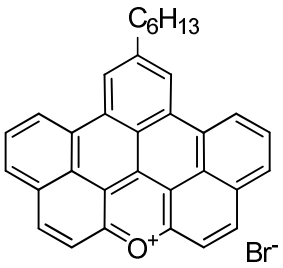

Purple powder (Yield = 52%), ^{1}H NMR (250MHz, CD_2Cl_2, 25°C): δ(ppm) = 9.13-9.10 (d, 2H, ^{3}J(H,H)=7.5Hz, aromatic), 8.95-8.92 (d, 2H, ^{3}J(H,H)=7.5Hz, aromatic), 8.69 (s, 2H, aromatic), 8.60-8.57 (d, 2H, ^{3}J(H,H)=7.5Hz, aromatic), 8.33-8.29 (d, 2H, ^{3}J(H,H)=10.0Hz, aromatic), 8.27-8.21 (t, 2H, ^{3}J(H,H)=7.5Hz, aromatic), 1.93-1.90 (t, 2H, CH_2), 1.87-1.42 (m, 8H, CH_2), 1.39-1.37 (t, 3H, CH_3); ^{13}C NMR (62.5MHz, CD_2Cl_2, 25°C): d (ppm): 161.59, 158.73, 148.52, 139.95, 138.63, 135.66, 135.03, 134.75, 134.18, 134.07, 129.77, 126.40, 123.77, 117.84, 37.42, 37.39, 35.03, 28.26, 18.93, 18.58.

MALDI-TOF-MS (MW=437.19 without anion): m/z: 437.35.

7-Dodecyl-benzo[5,6]naphthaceno[1,12,11,10-*jklmna*]xanthylium bromide (3-24)

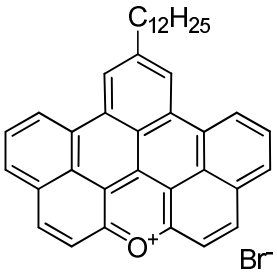

Purple powder (Yield = 50%), ^{1}H NMR (250MHz, CD_2Cl_2, 25°C): δ(ppm) = 9.35-9.32 (d, 2H, ^{3}J(H,H)=7.5Hz, aromatic), 9.05-9.02 (d, 2H, ^{3}J(H,H)=7.5Hz, aromatic), 8.96 (s, 2H, aromatic), 8.70-8.67 (d, 2H, ^{3}J(H,H)=7.5Hz, aromatic), 8.49-8.46 (d, 2H, ^{3}J(H,H)=7.5Hz, aromatic), 8.39-8.33 (t, 2H, ^{3}J(H,H)=7.5Hz, aromatic), 1.95-1.89 (t, 2H, CH_2), 1.49-1.15 (m, 20H, CH_2), 0.78-0.73 (t, 3H, CH_3); ^{13}C NMR (62.5MHz, CD_2Cl_2, 25°C): d (ppm): 161.67, 158.53, 148.44, 139.68, 138.61, 135.54, 135.23, 134.70, 134.20, 134.09, 129.79, 126.42, 123.74, 117.85, 37.50, 37.45, 35.22, 32.48, 30.56, 28.35, 18.86, 18.47.

MALDI-TOF-MS (MW=521.28 without anion): m/z: 521.33.

Elemental analysis: Calculated. C 77.86%, H 6.20%, Br 13.28%, O 2.66%; Found. C 77.06%, H 6.13%.

4,10-Didodecyl-benzo[5,6]naphthaceno[1,12,11,10-*jklmna*]xanthylium bromide (3-25)

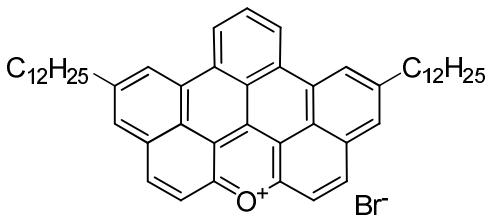

Purple powder (Yield = 46%), ^{1}H NMR (250MHz, CD_2Cl_2&CD_3OH, 25°C): δ(ppm) = 9.40-9.36 (m, 4H, aromatic), 9.09-9.05 (d, 2H, ^{3}J(H,H)=10.0Hz, aromatic),

8.67-8.57 (m, 5H, aromatic), 1.96-1.89 (t, 4H, CH_2), 1.50-1.15 (m, 40H, CH_2), 0.79-0.73 (t, 6H, CH_3); ^{13}C NMR (62.5MHz, CD_2Cl_2, 25°C): d (ppm): 161.59, 158.47, 148.30, 139.62, 138.55, 135.48, 135.17, 134.67, 134.16, 134.05, 129.73, 126.36, 123.70, 117.77, 36.48, 32.70, 32.02, 30.49, 30.45, 30.36, 30.16, 23.50, 23.44, 14.73, 14.52.

MALDI-TOF-MS (MW=689.47 without anion): m/z: 689.58.

4,7,10-Trihexyl-benzo[5,6]naphthaceno[1,12,11,10-*jklmna*]xanthylium bromide (3-26)

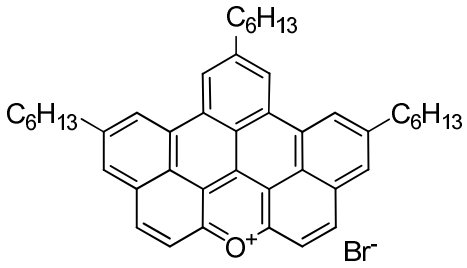

Purple solid (Yield = 38%), ^1H NMR (250MHz, CD_2Cl_2, 25°C): δ(ppm) = 9.30-9.25 (m, 4H, aromatic), 9.14-9.10 (d, 2H, ^3J(H,H)=10.0Hz, aromatic), 8.55-8.47 (m, 4H, aromatic), 1.99-1.93 (t, 4H, CH_2), 1.90-1.82 (t, 2H, CH_2), 1.65-1.58 (m, 4H, CH_2), 1.48-1.22 (m, 20H, CH_2), 0.82-0.71 (m, 9H, CH_3); ^{13}C NMR (62.5MHz, CD_2Cl_2, 25°C): d (ppm): 161.45, 158.37, 147.85, 139.44, 138.49, 136.27, 135.06, 134.46, 133.90, 133.81, 129.54, 126.25, 123.36, 117.30, 34.23, 34.19, 31.91, 31.87, 31.80, 31.66, 31.60, 24.91, 16.95, 15.90.

MALDI-TOF-MS (MW=605.38 without anion): m/z: 605.44.

4,7,10-Tridodecyl-benzo[5,6]naphthaceno[1,12,11,10-*jklmna*]xanthylium bromide (3-27)

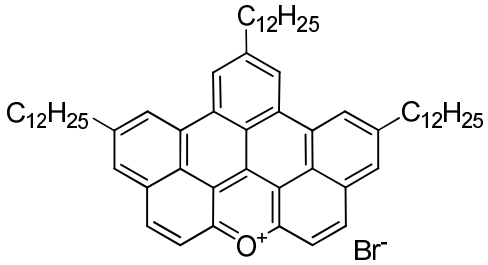

Purple solid (Yield = 30%), ^{1}H NMR (250MHz, CD_3OD&CD_2Cl_2 = 1 : 1, 25°C): δ(ppm) = 9.43-9.36 (m, 4H, aromatic), 9.28-9.24 (d, 2H, ^{3}J(H,H)=10.0Hz, aromatic), 8.70-8.62 (m, 4H, aromatic), 2.06-1.98 (t, 4H, CH_2), 1.95-1.87 (t, 2H, CH_2), 1.70-1.65 (m, 4H, CH_2), 1.53-1.28 (m, 56H, CH_2), 0.89-0.74 (m, 9H, CH_3); ^{13}C NMR (62.5MHz, CD_2Cl_2, 25°C): d (ppm): 161.42, 158.33, 147.89, 139.38, 138.52, 136.21, 135.00, 134.48, 133.95, 133.89, 129.53, 126.17, 123.41, 117.35, 33.68, 32.75, 31.57, 30.43, 29.69, 29.44, 27.96, 27.90, 27.73, 27.65, 27.53, 20.84, 11.85.

MALDI-TOF-MS (MW=857.66 without anion): m/z: 857.81.

Xanthenylium derivates with other anions

Synthesis of dibenzo[*a,j*]xanthene-ol

14-Phenyl-14*H*-dibenzo[*a,j*]xanthene (5.6 mmol) and lead dioxide (PbO_2, 2 g; 8.4 mmol) in a glacial acetic acid (50 ml) was stirred while heating on a oil bath at 120°C for 3 hours. The cooled mixture was poured onto crushed ice, and the solid residue was recrystallized from aqueous acetone to give the corresponding 14-phenyl-14*H*-dibenzo[*a,j*]xanthen-14-ol.

14-Phenyl-14*H*-dibenzo[*a,j*]xanthen-14-ol (3-29)

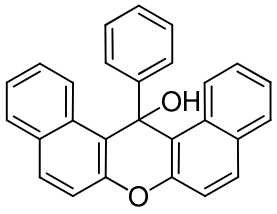

White powder, (yield=95%), ^{1}H NMR (250MHz, CD_2Cl_2, 25°C): δ(ppm) = 8.95-8.91 (d, 2H, ^{3}J(H,H)=10.0Hz, aromatic), 7.76-7.72 (d, 2H, ^{3}J(H,H)=10.0Hz, aromatic), 7.69-7.62 (m, 4H, aromatic), 7.35-7.31 (d, 2H, ^{3}J(H,H)=10.0Hz, aromatic), 7.29-7.22 (m, 4H, aromatic), 7.11-7.05 (t, 2H, ^{3}J(H,H)=7.5Hz, aromatic), 6.93-6.87 (t, 1H, ^{3}J(H,H)=7.5Hz, aromatic), 3.12 (s, 1H, OH); ^{13}C NMR (62.5MHz, CD_2Cl_2, 25°C): d (ppm): 132.57, 131.80, 131.70, 129.89, 129.49, 128.17, 127.94, 127.73, 127.53, 127.41, 126.94, 126.86, 125.93, 124.89, 124.81, 118.31.

MALDI-TOF-MS (MW=374.13): m/z: 374.21.

Dehydration of xanthene-ol

14-Phenyl-14*H*-dibenzo[*a*,*j*]xanthen-14-ol (5 mmol) in acetic anhydride (15 mL) and toluene (5 mL) was cooled and treated with inorganic acid (ca. 25 mmol) until no further precipitation occurred. The cooled solution was filtered and washed with anhydrous ether to yield the 14-phenyl-14-dibenzo[*a*,*j*]xanthenylium salts.

14-Phenyl-14-dibenzo[*a*,*j*]xanthenylium tetrafluoroborate (3-4b)

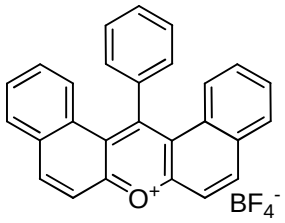

Dark red crystals with a golden glimmer (Yield = 92%), ^{1}H NMR (250MHz, CD_2Cl_2, 25°C): δ(ppm) = 8.78-8.74 (d, 2H, ^{3}J(H,H)=10.0Hz, aromatic), 8.25-8.21 (d, 2H, ^{3}J(H,H)=10.0Hz, aromatic), 8.16-8.12(d, 2H, ^{3}J(H,H)=10.0Hz, aromatic), 7.91-7.81 (m, 3H, aromatic), 7.75-7.69 (t, 2H, ^{3}J(H,H)=7.5Hz, aromatic), 7.48-7.36 (m, 4H, aromatic), 7.17-7.14 (d, 2H, ^{3}J(H,H)=7.5Hz, aromatic); ^{13}C NMR (62.5MHz, CD_2Cl_2, 25°C): d (ppm): 167.30, 159.95, 147.70, 138.67, 133.20, 132.73, 132.40, 132.10, 130.90, 130.08, 129.43, 128.60, 126.73, 122.56, 117.72.

MALDI-TOF-MS (MW=357.13 without anion): m/z: 357.20.

14-Phenyl-14-dibenzo[*a*,*j*]xanthenylium hexafluorophosphate (3-4c)

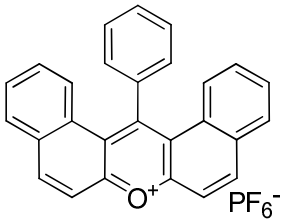

Dark red crystals with a golden glimmer (Yield = 95%), ^{1}H NMR (250MHz, CD_2Cl_2, 25°C): δ(ppm) = 8.75-8.71 (d, 2H, ^{3}J(H,H)=10.0Hz, aromatic), 8.21-8.17 (d, 2H, ^{3}J(H,H)=10.0Hz, aromatic), 8.13-8.10(d, 2H, ^{3}J(H,H)=7.5Hz, aromatic),

7.90-7.82 (m, 3H, aromatic), 7.74-7.68 (t, 2H, ^{3}J(H,H)=7.5Hz, aromatic), 7.46-7.35 (m, 4H, aromatic), 7.16-7.12 (d, 2H, ^{3}J(H,H)=10.0Hz, aromatic); ^{13}C NMR (62.5MHz, CD_2Cl_2, 25°C): d (ppm): 167.51, 159.90, 147.64, 138.61, 133.15, 132.73, 132.40, 132.06, 130.91, 130.08, 129.41, 128.59, 126.67, 122.55, 117.60.

MALDI-TOF-MS (MW=357.13 without anion): m/z: 357.18.

BNAX derivates with other anions

Benzo[5,6]naphthaceno[1,12,11,10-*jklmna*]xanthylium tetrafluoroborate (3-5b)

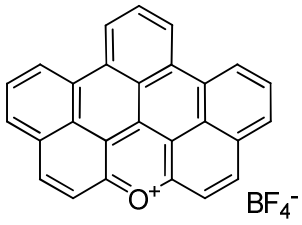

Purple needle-like crystal (Yield = 96%), ^{1}H NMR (250MHz, CD_2Cl_2&CD_3OH, 25°C): δ(ppm) = 9.48-9.45 (d, 2H, ^{3}J(H,H)=7.5Hz, aromatic), 9.32-9.29 (d, 2H, ^{3}J(H,H)=7.5Hz, aromatic), 9.12-9.09(d, 2H, ^{3}J(H,H)=7.5Hz, aromatic), 8.75-8.71 (d, 2H, ^{3}J(H,H)=10.0Hz, aromatic), 8.63-8.56 (m, 3H, aromatic), 8.45-8.39 (t, 2H, ^{3}J(H,H)=7.5Hz, aromatic).

MALDI-TOF-MS (MW=353.39 without anion): m/z: 353.20.

Elemental analysis: Calculated. C 73.67%, H 2.98%, B 2.46%, F 17.26%, O 3.63%; Found. C 73.91%, H 4.54%.

Benzo[5,6]naphthaceno[1,12,11,10-*jklmna*]xanthylium hexafluorophosphate (3-5c)

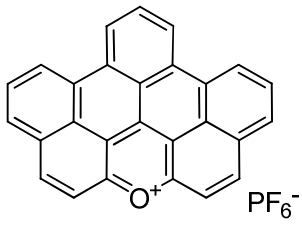

Purple needle-like crystal (Yield = 96%), ^{1}H NMR (250MHz, CD_2Cl_2&CD_3OH, 25°C): δ(ppm) = 9.46-9.43 (d, 2H, ^{3}J(H,H)=7.5Hz, aromatic), 9.30-9.27 (d, 2H, ^{3}J(H,H)=7.5Hz, aromatic), 9.10-9.07(d, 2H, ^{3}J(H,H)=7.5Hz, aromatic), 8.73-8.70 (d, 2H, ^{3}J(H,H)=7.5Hz, aromatic), 8.61-8.54 (m, 3H, aromatic), 8.43-8.37 (t, 2H, ^{3}J(H,H)=7.5Hz, aromatic).

MALDI-TOF-MS (MW=353.39 without anion): m/z: 353.33.

Elemental analysis: Calculated. C 65.07%, H 2.63%, P 6.22%, F 22.87%, O 3.21%; Found. C 63.58%, H 4.99%.

DBNAX salts

Tetrabenzo[*a,c,h,j*]xanthene

To a solution of appropriate benzaldehyde (50mmol) and 9-hydroxyphenanthren (100mmol) in glacial acetic acid (40 ml) concentrated HCl (1ml) was added drop wise. The solution was heated with oil bath to 120°C and kept at this temperature until crystallization took place. When the solution was cooled to room temperature, the precipitated product was filtered with suction and recrystallized from glacial acetic acid to give products.

18-Phenyl-18*H*-tetrabenzo[*a,c,h,j*]xanthene (3-30)

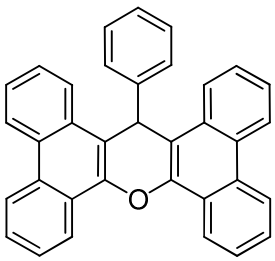

White powders (Yield=48%), ^{1}H NMR (700MHz, D-DMSO, 25°C): δ(ppm) = 8.93-8.91 (t, 4H, ^{3}J(H,H)=7.0Hz, aromatic), 8.87-8.86 (d, 2H, ^{3}J(H,H)=7.0Hz, aromatic), 8.84-8.83 (d, 2H, ^{3}J(H,H)=7.0Hz, aromatic), 7.94-7.92 (t, 4H, ^{3}J(H,H)=7.0Hz, aromatic), 7.86-7.84 (t, 2H, ^{3}J(H,H)=7.0Hz, aromatic), 7.77-7.74 (m, 4H, aromatic), 7.66-7.64 (t, 2H, ^{3}J(H,H)=7.0Hz, aromatic), 7.14-7.12 (t, 2H,

^{3}J(H,H)=7.0Hz, aromatic), 6.98-6.96 (t, 1H, ^{3}J(H,H)=7.0Hz, aromatic), 6.76 (s, 1H, CH); ^{13}C NMR (62.5MHz, D-DMSO, 25°C): d (ppm): 144.98, 143.26, 130.11, 129.35, 128.34, 128.16, 127.74, 127.61, 127.39, 126.35, 125.55, 124.19, 124.06, 123.35, 123.13, 122.04, 117.79, 114.55.

MALDI-TOF-MS (MW=458.56): m/z: 458.51.

18-(4-Bromophenyl)-18*H*-tetrabenzo[*a,c,h,j*]xanthene (3-31)

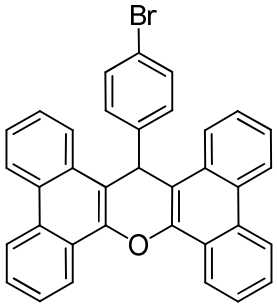

White powders (Yield=52%), ^{1}H NMR (700MHz, D-DMSO, 25°C): δ(ppm) = 8.93-8.92 (d, 4H, ^{3}J(H,H)=7.0Hz, aromatic), 8.89-8.88 (d, 2H, ^{3}J(H,H)=7.0Hz, aromatic), 8.81-8.80 (d, 2H, ^{3}J(H,H)=7.0Hz, aromatic), 7.95-7.93 (t, 4H, ^{3}J(H,H)=7.0Hz, aromatic), 7.87-7.85 (t, 2H, ^{3}J(H,H)=7.0Hz, aromatic), 7.77-7.75 (t, 2H, ^{3}J(H,H)=7.0Hz, aromatic), 7.71-7.70 (d, 2H, ^{3}J(H,H)=7.0Hz, aromatic), 7.68-7.66 (t, 2H, ^{3}J(H,H)=7.0Hz, aromatic), 7.34-7.33 (d, 2H, ^{3}J(H,H)=7.0Hz, aromatic), 6.78 (s, 1H, CH); ^{13}C NMR (62.5MHz, D-DMSO, 25°C): d (ppm): 144.34, 143.27, 131.26, 130.29, 130.17, 129.17, 127.83, 127.76, 127.63, 127.44, 125.64, 124.08, 123.97, 123.40, 123.15, 122.07, 119.55, 114.01, 35.97.

MALDI-TOF-MS (MW=537.46): m/z: 537.45.

Kumada coupling for alkylated tetrabenzoxanthene

Appropriate bromo-tetrabenzoxanthene (10 mmol), [1,1'-Bis(diphenylphosphino)ferrocene]dichloropalladium(II) dichloromethane, ($PdCl_2$(dppf)CH_2Cl_2, 5 mol% per Br), anhydrous THF (100 ml) were added in a 250 ml Shlenck round bottom bottle. The mixture was degassed by two *freeze-pump-thaw* cycles. Grignard reagent (2 mol per Br) was added to the bottle slowly. The mixture

was stirred at 60 °C for 18 h under argon atmosphere and then cooled to room temperature. Methanol (20 ml) was added to quench the reaction. The mixture was extracted with dichloromethane (200ml x 3). The organic phase was washed with water (100ml x 2), dried over $MgSO_4$ and concentrated under reduced pressure. The residue was purified by column chromatography (silica gel, PE/DCM) to give the alkylated dibenzoxanthene.

18-(4-Dodecylphenyl)-18*H*-tetrabenzo[*a,c,h,j*]xanthene (3-32)

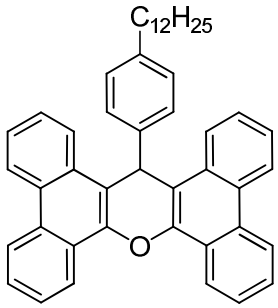

White powders (PE : DCM = 7 : 1, yield=70%), ^{1}H NMR (250MHz, D-DMSO, 25°C): δ(ppm) = 8.80-8.77 (d, 2H, ^3J(H,H)=7.5Hz, aromatic), 8.61-8.59 (d, 2H, ^3J(H,H)=5.0Hz, aromatic), 8.58-8.56 (d, 2H, ^3J(H,H)=5.0Hz, aromatic), 8.41-8.38 (d, 2H, ^3J(H,H)=7.5Hz, aromatic), 7.77-7.57 (m, 6H, aromatic), 7.51-7.45 (t, 2H, ^3J(H,H)=7.5Hz, aromatic), 7.43-7.40 (d, 2H, ^3J(H,H)=7.5Hz, aromatic), 6.86-6.83 (d, 2H, ^3J(H,H)=7.5Hz, aromatic), 6.34 (s, 1H, CH), 2.28-2.22 (t, 2H, ^3J(H,H)=7.5Hz, CH_2), 1.28-1.06 (m, 20H, CH_2), 0.78-0.73 (m, 3H, CH_3);^{13}C NMR (62.5MHz, CD_2Cl_2, 25°C): d (ppm): 145.10, 142.93, 142.58, 131.66, 131.07, 129.41, 129.33, 128.29, 128.17, 128.10, 126.15, 126.05, 124.41, 124.23, 123.68, 123.45, 115.37, 38.71, 36.37, 32.90, 32.31, 30.59, 30.48, 30.39, 30.32, 23.68, 14.88.

MALDI-TOF-MS (MW=626.89): m/z: 626.95.

Tetrabenzoxanthenium with bromide as anion

To the appropriate 14-phenyl-14*H*-tetrabenzo[*a,c,h,j*]xanthene derivtes (0.3mmol) in glacial acetic acid (200 ml) at 120 °C was added dropwise bromine (0.3 mmol) in acetic acid (3 ml). The solution was kept at this temperature for 1 hour. When the

solution was cooled to room temperature, the precipitated product was filtered with suction and recrystallized from glacial acetic acid to give reddish orange crystals with a golden glimmer.

18-Phenyltetrabenzo[*a,c,h,j*]xanthenium bromide (3-33a)

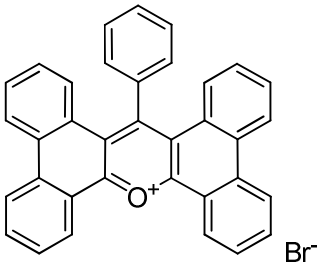

Reddish orange crystals with a golden glimmer (Yield = 80%), ^{1}H NMR (700MHz, CD_2Cl_2, 25°C): δ(ppm) = 9.27-9.26 (d, 2H, ^{3}J(H,H)=7.0Hz, aromatic), 8.91-8.90 (d, 2H, ^{3}J(H,H)=7.0Hz, aromatic), 8.85-8.84 (d, 2H, ^{3}J(H,H)=7.0Hz, aromatic), 8.24-8.22 (t, 2H, ^{3}J(H,H)=7.0Hz, aromatic), 8.10-8.08 (t, 2H, ^{3}J(H,H)=7.0Hz, aromatic), 7.89-7.91 (t, 1H, ^{3}J(H,H)=7.0Hz, aromatic), 7.81-7.78 (m, 4H, aromatic), 7.55-7.54 (d, 2H, ^{3}J(H,H)=7.0Hz, aromatic), 7.27 (s, 4H, aromatic); ^{13}C NMR (62.5MHz, D-DMSO, 25°C): d (ppm): 166.55, 160.89, 150.31, 139.42, 138.87 137.99, 134.38, 133.57, 132.65, 132.29, 131.79, 131.01, 130.19, 128.88, 128.08, 127.01, 126.69, 125.17, 121.21.

MALDI-TOF-MS (MW=457.16 without anion): m/z: 457.22.

18-(4-Dodecylphenyl)tetrabenzo[*a,c,h,j*]xanthenium bromide (3-34)

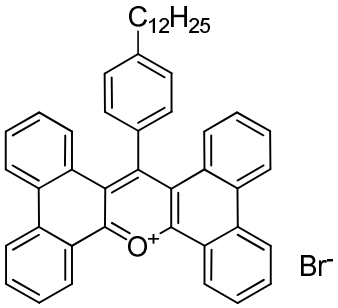

Reddish orange crystals with a golden glimmer (Yield = 76%), ^{1}H NMR (500MHz, CD_2Cl_2, 25°C): δ(ppm) = 9.15-9.13 (d, 2H, ^{3}J(H,H)=10.0Hz, aromatic),

8.78-8.76 (d, 2H, ^3J(H,H)=10.0Hz, aromatic), 8.71-8.69 (d, 2H, ^3J(H,H)=10.0Hz, aromatic), 8.18-8.15 (t, 2H, ^3J(H,H)=7.5Hz, aromatic), 8.04-8.01 (t, 2H, ^3J(H,H)=7.5Hz, aromatic), 7.72-7.69 (t, 2H, ^3J(H,H)=7.5Hz, aromatic), 7.53-7.51 (d, 2H, ^3J(H,H)=10.0Hz, aromatic), 7.34-7.32 (d, 2H, ^3J(H,H)=10.0Hz, aromatic), 7.24-7.16 (m, 6H, aromatic), 2.84-2.81 (t, 2H, ^3J(H,H)=7.5Hz, CH_2), 1.75-1.72 (m, 2H, CH_2), 1.36-1.21 (m, 18H, CH_2), 0.82-0.79 (t, 3H, CH_3); ^{13}C NMR (125MHz, CD_2Cl_2, 25°C): d (ppm): 166.63, 161.05, 150.47, 139.60, 138.95 138.06, 134.53, 133.61, 132.73, 132.46, 131.98, 131.12, 130.37, 129.06, 128.26, 127.11, 126.81, 125.34, 121.28, 38.50, 34.56, 34.08, 32.37, 32.31, 32.17, 32.03, 25.35, 16.57.

MALDI-TOF-MS (MW=625.35 without anion): m/z: 625.41.

Photocyclization of tetrabenzoxanthenylium salts

0.05 mmol 14-phenyl-14-tetrabenzo[*a,c,h,j*]xanthenylium derivate was dissolved in 200ml water free dichloromethane. After the solution was irradiated at 300nm wavelength for 24 hours, the solid product was filtered off. The filtrate was concentrated in vacuo to give a 2nd corp. The combined solid was recrystallized in methanol to give the fused DBNAX salts.

DBNAX bromide (3-6a)

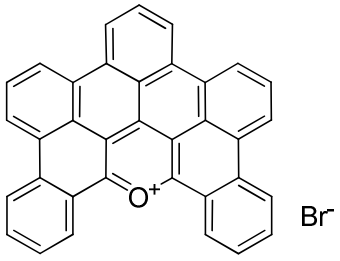

Puple powder (Yield=85%), ^{1}H NMR (250MHz, CD_3OD : CD_2Cl_2 = 1 : 1, 25°C): δ(ppm) = 9.61-9.44 (m, 8H, aromatic), 9.29-9.26 (d, 2H, ^3J(H,H)=7.5Hz, aromatic), 8.80-8.74 (t, 1H, ^3J(H,H)=7.5Hz, aromatic), 8.61-8.55 (t, 2H, ^3J(H,H)=7.5Hz, aromatic), 8.42-8.37 (t, 2H, ^3J(H,H)=7.5Hz, aromatic), 8.33-8.27 (t, 2H, ^3J(H,H)=7.5Hz, aromatic).

MALDI-TOF-MS (MW=453.13 without anion): m/z: 452.97.

Elemental analysis: Calculated. C 78.81%, H 3.21%, Br 14.98%, O 3.00%; Found. C 77.96%, H 4.08%.

9-Dodecyl-DBNAX bromide (3-35)

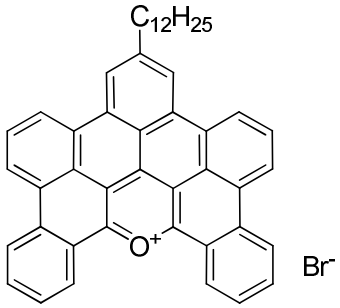

Purple powder (Yield = 42%), ^{1}H NMR (700MHz, $C_2D_2Cl_4$, 25°C): δ(ppm) = 8.86-8.80 (d, 4H, ^{3}J(H,H)=42.0Hz, aromatic), 8.65 (s, 4H, aromatic), 8.35 (s, 2H, aromatic), 8.15-8.13 (t, 2H, ^{3}J(H,H)=7.0Hz, aromatic), 7.96-7.91 (m, 4H, aromatic), 2.76-2.74 (t, 2H, CH_2), 1.72-1.70 (m, 2H, CH_2), 1.37-1.23 (m, 18H, CH_2), 0.85-0.83 (t, 3H, CH_3); ^{13}C NMR (125MHz, D-DMSO, 25°C): d (ppm): 151.89, 134.45, 133.51, 132.88, 132.10, 129.46, 129.36, 126.93, 125.91, 125.66, 125.34, 124.20, 124.10, 124.04, 123.16, 119.92, 116.75, 116.06, 109.25, 31.14, 29.85, 29.10, 29.03, 28.98, 28.82, 28.56, 21.90, 13.73.

MALDI-TOF-MS (MW=621.32 without anion): m/z: 621.50.

Synthesis of teterbenzoxanthene-ol

18-Phenyl-18*H*-tetrabenzo[*a,c,h,j*]xanthene (0.6 mmol) and lead dioxide (PbO_2, 0.2 g; 0.8 mmol) in a glacial acetic acid (250 ml) was stirred while heating on a oil bath at 120°C for 3 hours. The cooled mixture was poured onto crushed ice, and the solid residue was recrystallized from aqueous acetone to give the corresponding 14-phenyl-14*H*-dibenzo[*a,j*]xanthen-14-ol.

18-Phenyl-18*H*-tetrabenzo[*a,c,h,j*]xanthen-18-ol (3-36)

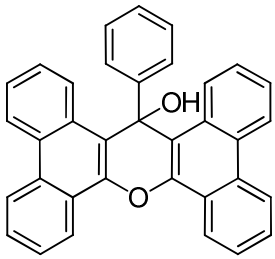

White powder, (yield=93%), ^{1}H NMR (250MHz, D-DMSO, 25°C): δ(ppm) = 9.00-8.96 (m, 2H, aromatic), 8.75-8.72 (d, 2H, ^{3}J(H,H)=7.5Hz, aromatic), 8.69-8.65 (d, 2H, ^{3}J(H,H)=10.0Hz, aromatic), 8.59-8.55 (t, 2H, ^{3}J(H,H)=5.0Hz, aromatic), 7.76-7.70 (d, 2H, ^{3}J(H,H)=7.5Hz, aromatic), 7.67-7.61 (d, 2H, ^{3}J(H,H)=7.5Hz, aromatic), 7.56-7.53 (d, 2H, ^{3}J(H,H)=7.5Hz, aromatic), 7.50 (s, 1H, OH), 7.29-7.26 (m, 4H, aromatic), 6.98-6.92 (t, 2H, ^{3}J(H,H)=7.5Hz, aromatic), 6.78-6.74 (t, 1H, ^{3}J(H,H)=5.0Hz, aromatic); ^{13}C NMR (62.5MHz, CD_2Cl_2, 25°C): d (ppm): 148.13, 141.07, 131.13, 129.75, 128.85, 128.74, 128.58, 128.08, 127.59, 127.33, 126.57, 126.26, 125.30, 124.15, 123.31, 123.10, 116.78, 72.70.

MALDI-TOF-MS (MW=474.55): m/z: 474.26.

14-Phenyl-14-tetrabenzo[*a,c,h,j*]xanthenylium tetrafluoroborate (3-33b)

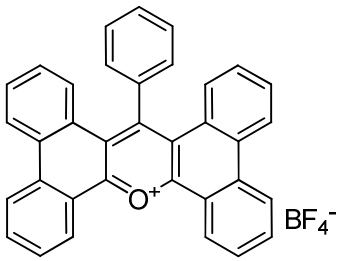

Dark red crystals with a golden glimmer (Yield = 91%), ^{1}H NMR (700MHz, CD_2Cl_2, 25°C): δ(ppm) = 9.28-9.27 (d, 2H, ^{3}J(H,H)=7.0Hz, aromatic), 8.92-8.91 (d, 2H, ^{3}J(H,H)=7.0Hz, aromatic), 8.86-8.85 (d, 2H, ^{3}J(H,H)=7.0Hz, aromatic), 8.25-8.23 (t, 2H, ^{3}J(H,H)=7.0Hz, aromatic), 8.11-8.09 (t, 2H, ^{3}J(H,H)=7.0Hz, aromatic), 7.90-7.92 (t, 1H, ^{3}J(H,H)=7.0Hz, aromatic), 7.82-7.79 (m, 4H, aromatic), 7.55-7.54 (d, 2H, ^{3}J(H,H)=7.0Hz, aromatic), 7.28 (s, 4H, aromatic); ^{13}C NMR (62.5MHz, CD_2Cl_2, 25°C): d (ppm): 166.61, 161.02, 150.42, 139.55, 138.90 138.01, 134.47, 133.59, 132.68, 132.43, 131.92, 131.10, 130.32, 129.01, 128.18, 127.06, 126.77, 125.30,

121.22.

MALDI-TOF-MS (MW=457.16 without anion): m/z: 457.21.

DBNAX tetrafluoroborate (3-6b)

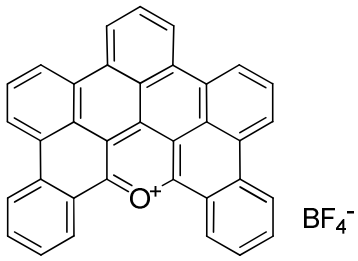

Puple powder (Yield=90%), ^{1}H NMR (250MHz, CD_3OD : CD_2Cl_2 = 1 : 1, 25°C): δ(ppm) = 9.62-9.45 (m, 8H, aromatic), 9.30-9.27 (d, 2H, ^{3}J(H,H)=7.5Hz, aromatic), 8.81-8.75 (t, 1H, ^{3}J(H,H)=7.5Hz, aromatic), 8.62-8.56 (t, 2H, ^{3}J(H,H)=7.5Hz, aromatic), 8.42-8.37 (t, 2H, ^{3}J(H,H)=7.5Hz, aromatic), 8.33-8.27 (t, 2H, ^{3}J(H,H)=7.5Hz, aromatic).

MALDI-TOF-MS (MW=453.13 without anion): m/z: 453.26.

Elemental analysis: Calculated. C 77.80%, H 3.17%, B 2.00%, F 14.06%, O 2.96%; Found. C 77.74%, H 4.01%.

BNATX salts

Dinaphthalen-2-ylsulfane (3-39)

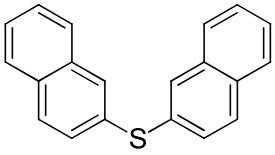

Under argon atmosphere, the solution of 2-methoxynaphthalene (10 mmol), naphthalene-2-thiol (15 mmol) and triflic acid (10 mmol) in toluene (100 mL) was heated to reflux and the progress of the reaction was monitored by TLC. After the completion of the reaction (overnight), the reaction mixture was cooled to r.t. and poured into 5% NaOH and extracted with Et_2O (50 mL). The organic extracts were washed with 5% NaOH and brine and dried over MgSO4, and the solvent was

removed in vacuo. The resulting crude product was purified by column chromatography (PE : DCM = 5 : 1).

White crystal (yield = 50%), ^{1}H NMR (250MHz, CD_2Cl_2, 25°C): δ(ppm) = 7.79-7.64 (m, 8H, aromatic), 7.42-7.33 (m, 6H, aromatic); ^{13}C NMR (62.5MHz, CD_2Cl_2, 25°C): d (ppm): 132.80, 132.02, 131.31, 128.71, 127.82, 127.56, 126.65, 126.31, 125.62, 125.22.

FD-MS (MW = 286.08): m/z: 286.30.

14-Phenyl-14*H*-dibenzo[*a,j*]thioxanthene (3-40)

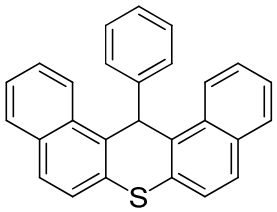

To a solution of benzaldehyde (50mmol) in acetic anhydride (40 ml), dinaphthalen-2-ylsulfane (50mmol) was added slowly. The solution was heated with oil bath to 120°C and kept at this temperature for 6 hours. When the solution was cooled to room temperature, the solvent was removed by rotate evaporation. The solid residue was dissolved in DCM and washed with brine (100 ml x 2). The organic layer was dried over $MgSO_4$ and the solvent was removed in vacuo. The resulting crude product was purified by column chromatography (PE : DCM = 6 : 1).

White crystal (yield = 43%), ^{1}H NMR (250MHz, CD_2Cl_2, 25°C): δ(ppm) = 8.53-8.49 (d, 2H, ^{3}J(H,H)=10.0Hz, aromatic), 7.87-7.84 (d, 2H, ^{3}J(H,H)=7.5Hz, aromatic), 7.75-7.71 (d, 2H, ^{3}J(H,H)=10.0Hz, aromatic), 7.64-7.58 (t, 2H, ^{3}J(H,H)=7.5Hz, aromatic), 7.53-7.43 (m, 4H, aromatic), 7.29 (s, 1H, CH), 6.97-6.93 (m, 3H, aromatic), 6.84-6.71 (m, 2H, aromatic); ^{13}C NMR (62.5MHz, CD_2Cl_2, 25°C): d (ppm): 140.93, 133.29, 132.81, 132.07, 129.49, 128.47, 128.13, 127.76, 127.74, 126.87, 125.88, 125.59, 122.75, 40.16.

FD-MS (MW = 374.11): m/z: 374.25.

14-Phenyl-14*H*-dibenzo[*a,j*]thioxanthen-14-ol (3-41)

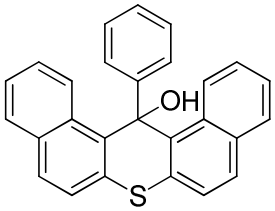

14-Phenyl-14*H*-dibenzo[*a,j*]thioxanthene (5.6 mmol) and lead dioxide (PbO_2, 2 g; 8.4 mmol) in a glacial acetic acid (50 ml) was stirred while heating on a oil bath at 120°C for 3 hours. The cooled mixture was poured onto crushed ice, and the solid residue was recrystallized from aqueous acetone to give the corresponding 14-phenyl-14*H*-dibenzo[*a,j*]thioxanthen-14-ol. The resulted product was directly used as starting material for next step without further purification.

White powder (yield = 93%);

FD-MS (MW = 390.11): m/z: 390.28.

14-Phenyldibenzo[*a,j*]thioxanthenium tetrafluoroborate (3-42a)

14-Phenyl-14*H*-dibenzo[*a,j*]thioxanthen-14-ol (5 mmol) in acetic anhydride (15 mL) and toluene (5 mL) was cooled and treated with fluoroboric acid (ca. 25 mmol) until no further precipitation occurred. The cooled solution was filtered and washed with anhydrous ether to yield the 14-phenyl-14-dibenzo[*a,j*]thioxanthenylium tetrafluoroborate as red powder. The resulted product was directly used as starting material for photocyclization without further purification.

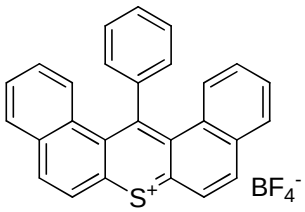

Red powder (yield = 80%);

MALDI-TOF-MS (MW = 373.10 without anion): m/z: 373.12.

Benzo[5,6]naphthaceno[1,12,11,10-*jklmna*]thioxanthylium tetrafluoroborate (3-7)

0.1 mmol 14-Phenyl-14-dibenzo[*a*,*j*]thioxanthenylium tetrafluoroborate was dissolved in 200ml dichloromethane. After the solution was irradiated at 300nm wavelength for 24 hours, the solid product was filtered off. The filtrate was concentrated in vacuo to give a 2nd corp. The combined solid was recrystallized in methanol to give the fused benzo[5,6]naphthaceno[1,12,11,10-*jklmna*]thioxanthylium (BNTAX) tetrafluoroborate.

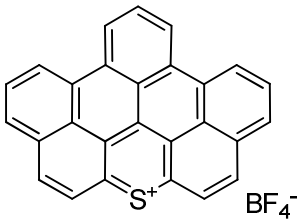

Purple powder (yield = 85%), ^{1}H NMR (250MHz, CD_2Cl2, 25°C): δ(ppm) = 9.57-9.54 (d, 2H, ^{3}J(H,H)=7.5Hz, aromatic), 9.45-9.41 (d, 2H, ^{3}J(H,H)=10.0Hz, aromatic), 8.96-8.92 (d, 2H, ^{3}J(H,H)=10.0Hz, aromatic), 8.85-8.77 (t, 4H, ^{3}J(H,H)=10.0Hz, aromatic), 8.63-8.57 (t, 1H, ^{3}J(H,H)=7.5Hz, aromatic), 8.54-8.48 (t, 2H, ^{3}J(H,H)=7.5Hz, aromatic).

MALDI-TOF-MS (MW = 369.07): m/z: 369.17.

Elemental analysis: Calculated. C 71.08%, H 2.87%, B 2.35%, F 16.66%, S 7.03%; Found. C 71.14%, H 3.04%, S 6.88.

PDBNT salts

7,14-Diphenyldibenzo[*a,j*]acridinium derivates

All the aniline/amine were dried according to handbook procedure before use. 14-Phenyl-14-dibenzo[*a,j*]xanthenylium salt (2mmol) and appropriate aniline/amine (2.2mmol) were added to 15ml anhydrous THF. The mixture was refluxed for 5 hours till the solution turned to transparent. After cooling the solution to room temperature, it was concentrated in vacuo to ca. 3ml. The concentrated solution was poured to 400ml hexane then. After filtration, the solid was recrystallized from 20ml hexane to give the target 7,14-diphenyldibenzo[*a,j*]acridinium salts.

7,14-Diphenyldibenzo[*a,j*]acridinium tetrafluoroborate (4-4c)

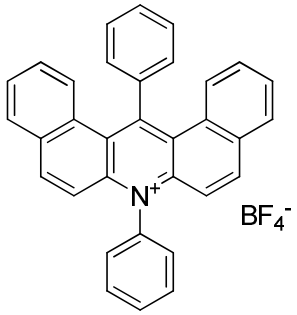

Golden yellow needles (Yield = 35%). ^{1}H NMR (250MHz, CD_2Cl_2, 25°C): δ(ppm) = 8.50-8.46 (d, 2H, ^{3}J(H,H)=10.0Hz, aromatic), 8.20-8.16 (d, 2H, ^{3}J(H,H)=10.0Hz, aromatic), 8.05-8.03 (m, 3H, aromatic), 8.00-7.76 (m, 7H, aromatic), 7.67-7.40 (m, 8H, aromatic). ^{13}C NMR (62.5MHz, CD_2Cl_2, 25°C): d (ppm): 143.00, 140.81, 140.29, 138.72, 132.61, 131.93, 131.62, 131.58, 130.95, 130.04, 129.30, 129.23, 129.02, 128.91, 128.25, 127.93, 125.10.

MALDI-TOF-MS (MW=432.17 without anion): m/z: 432.26.

Elemental analysis: Calculated. C 76.32%, H 4.27% B 2.08%, F 14.63%, N 2.70%; Found. C 76.88%, H 3.92% N 2.52%.

7-Hexyl-14-phenyldibenzo[*a,j*]acridinium bromide (4-11a)

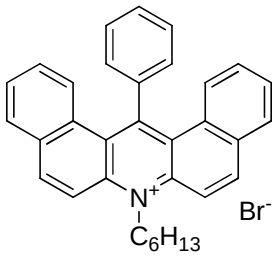

Golden yellow powder (Yield = 24%). ^{1}H NMR (250MHz, CD_2Cl_2, 25°C): δ(ppm) = 8.41-8.37 (d, 2H, ^{3}J(H,H)=10.0Hz, aromatic), 8.11-8.07 (d, 2H, ^{3}J(H,H)=10.0Hz, aromatic), 8.00-7.95 (m, 3H, aromatic), 7.89-7.66 (m, 7H, aromatic), 7.58-7.36 (m, 3H, aromatic), 5.07-5.03 (t, 2H, ^{3}J(H,H)=5.0Hz, CH_2), 3.11-3.07 (m, 2H, CH_2), 1.47-1.12 (m, 6H, CH_2), 0.81-0.77 (m, 3H, CH_3); ^{13}C NMR (62.5MHz, CD_2Cl_2, 25°C): d (ppm): 143.45, 141.20, 140.71, 139.10, 133.06, 132.37, 132.02, 132.98, 131.25, 130.50, 129.71, 129.60, 127.93, 31.52, 29.54, 27.34, 22.77, 14.11.

MALDI-TOF-MS (MW=440.24 without anion): m/z: 440.30.

Elemental analysis: Calculated. C 76.15%, H 5.81% Br 15.35%, N 2.69%; Found. C 75.53%, H 6.43% N 2.52%.

7-Dodecyl-14-phenyldibenzo[*a,j*]acridinium tetrafluoroborate (4-12b)

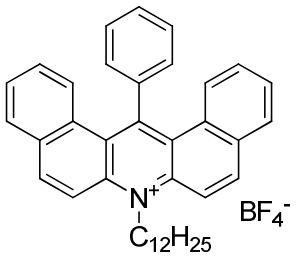

Golden yellow powder (Yield = 19%). ^{1}H NMR (250MHz, CD_2Cl_2, 25°C): δ(ppm) = 8.45-8.41 (d, 2H, ^{3}J(H,H)=10.0Hz, aromatic), 8.15-8.11 (d, 2H, ^{3}J(H,H)=10.0Hz, aromatic), 8.07-8.00 (m, 3H, aromatic), 7.94-7.76 (m, 7H, aromatic), 7.62-7.41 (m, 3H, aromatic), 5.09-5.05 (t, 2H, ^{3}J(H,H)=5.0Hz, CH_2), 3.12-3.08 (m, 2H, CH_2), 1.50-1.11 (m, 18H, CH_2), 0.82-0.78 (m, 3H, CH_3); ^{13}C NMR (62.5MHz, CD_2Cl_2, 25°C): d (ppm): 143.25, 141.00, 140.53, 138.97, 132.96, 132.27, 131.89, 132.78, 131.07, 130.32, 129.55, 129.45, 127.73, 32.82, 31.75, 31.23, 30.34, 29.54, 27.34, 25.08, 22.77, 14.11.

MALDI-TOF-MS (MW=524.33 without anion): m/z: 524.45.

Elemental analysis: Calculated. C 76.59%, H 6.92% B 1.77%, F 12.43%, N 2.29%; Found. C 75.78%, H 6.55% N 2.49%.

14-Phenyl-7-(4-hexylphenyl)dibenzo[*a,j*]acridinium tetrafluoroborate (4-13b)

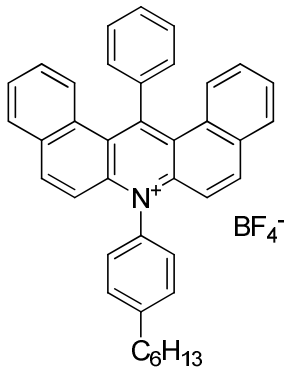

Golden yellow powder (Yield = 22%). ^{1}H NMR (250MHz, CD_2Cl_2, 25°C): δ(ppm) = 8.44-8.40 (d, 2H, ^{3}J(H,H)=10.0Hz, aromatic), 8.13-8.09 (d, 2H, ^{3}J(H,H)=10.0Hz, aromatic), 7.94-7.92 (m, 3H, aromatic), 7.90-7.62 (m, 7H, aromatic), 7.55-7.30 (m, 7H, aromatic), 2.97-2.91 (t, 2H, CH_2), 1.91-1.78 (m, 2H, CH_2), 1.46-1.31 (m, 6H, CH_2), 0.95-0.98 (m, 3H, CH_3). ^{13}C NMR (62.5MHz, CD_2Cl_2, 25°C): d (ppm): 143.05, 140.87, 140.35, 138.80, 132.68, 131.99, 131.68, 131.70, 131.01, 130.10, 129.38, 129.70, 129.12, 128.97, 128.35, 127.97, 125.15, 35.44, 31.87, 31.08, 28.52, 22.94, 14.19.

MALDI-TOF-MS (MW=516.27 without anion): m/z: 516.35.

Elemental analysis: Calculated. C 77.62%, H 5.68% B 1.79%, F 12.59%, N 2.32%; Found. C 75.49%, H 5.47% N 2.42%.

14-Phenyl-7-(4-tetradecylphenyl)dibenzo[a,j]acridinium tetrafluoroborate (4-14b)

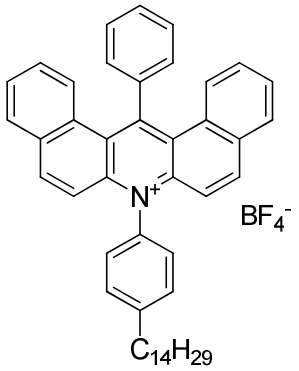

Golden yellow powder (Yield = 17%). ^{1}H NMR (250MHz, CD_2Cl_2, 25°C): δ(ppm) = 8.43-8.39 (d, 2H, ^{3}J(H,H)=10.0Hz, aromatic), 8.12-8.08 (d, 2H, ^{3}J(H,H)=10.0Hz, aromatic), 7.93-7.91 (m, 3H, aromatic), 7.89-7.61 (m, 7H, aromatic), 7.54-7.29 (m, 7H, aromatic), 2.96-2.91 (t, 2H, CH_2), 1.91-1.78 (m, 2H, CH_2), 1.46-1.16 (m, 22H, CH_2), 0.88-0.85 (m, 3H, CH_3). ^{13}C NMR (62.5MHz, CD_2Cl_2, 25°C): d (ppm): 143.06, 140.85, 140.37, 138.81, 132.66, 131.97, 131.66, 131.68, 130.92, 130.05, 129.32, 129.68, 129.10, 128.95, 128.33, 127.92, 125.10, 36.05, 33.11, 32.11, 30.85, 30.56, 29.62, 23.79, 14.49.

MALDI-TOF-MS (MW=628.39 without anion): m/z: 628.51.

Elemental analysis: Calculated. C 78.87%, H 7.04% B 1.51%, F 10.62%, N 1.96%; Found. C 77.17%, H 7.07% N 1.97%.

Photocyclization

1 mmol 7,14-diphenyldibenzo[*a,j*]acridinium derivates was dissolved in 200ml absolute ethanol. The ethanolic solution was irradiated at 300nm wavelength. After 72 hours, the solid product was filtered off. The filtrate was concentrated in vacuo to give a 2nd corp. The combined solid was recrystallized in ethanol to give the PDBNT salts.

14-Phenyl-dibenzo[*jk,mn*]naphtho[2,1,8-*fgh*]thebenidinium tetrafluoroborate (4-5c)

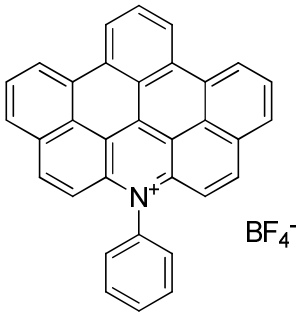

Golden red needles (Yield = 85%), ^{1}H NMR (250MHz, CD_2Cl_2, 25°C): δ(ppm) = 9.35-9.32 (d, 2H, ^{3}J(H,H)=7.5Hz, aromatic), 9.18-9.15 (d, 2H, ^{3}J(H,H)=7.5Hz, aromatic), 8.82-8.78 (d, 2H, ^{3}J(H,H)=10.0Hz, aromatic), 8.68-8.65 (d, 2H, ^{3}J(H,H)=7.5Hz, aromatic), 8.40-8.34 (t, 3H, ^{3}J(H,H)=7.5Hz, aromatic), 8.08-8.06 (t, 3H, ^{3}J(H,H)=2.5Hz, aromatic), 7.88-7.84 (m, 4H, aromatic); ^{13}C NMR (62.5MHz, CD_2Cl_2, 25°C): d (ppm): 148.50, 140.49, 139.55, 133.92, 133.41, 132.13, 131.65, 130.19, 130.15, 129.89, 128.14, 127.09, 124.18, 122.59, 118.66, 117.17.

MALDI-TOF-MS (MW=428.14 without anion): m/z: 428.21.

Elemental analysis: Calculated. C 76.92%, H 3.52% B 2.10%, F 14.25%, N 2.72%; Found. C 76.95%, H 3.72% N 2.61%.

14-Hexyl-dibenzo[*jk,mn*]naphtho[2,1,8-*fgh*]thebenidinium bromide (4-15a)

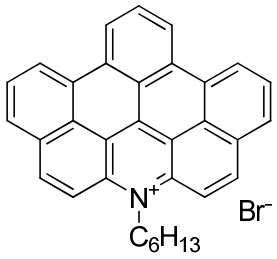

Golden red powder (Yield = 69%), ^{1}H NMR (250MHz, CD_2Cl_2, 25°C): δ(ppm) = 8.49-8.46 (d, 2H, ^{3}J(H,H)=7.5Hz, aromatic), 8.27-8.24 (d, 2H, ^{3}J(H,H)=7.5Hz, aromatic), 8.16-8.09 (m, 4H, aromatic), 7.79-7.73 (m, 6H, aromatic), 7.36-7.32 (m, 1H, ^{3}J(H,H)=5.0Hz, aromatic), 5.16-5.12 (t, 2H, ^{3}J(H,H)=5.0Hz, CH_2), 3.15-3.10 (m, 2H, CH_2), 1.50-1.18 (m, 6H, CH_2), 0.83-0.80 (m, 3H, CH_3); ^{13}C NMR (62.5MHz, CD_2Cl_2, 25°C): d (ppm): 142.60, 139.89, 138.15, 137.31, 133.78, 131.11, 129.56, 128.55, 126.13, 122.88, 120.99, 116.59, 113.44, 110.75, 104.62, 32.31, 30.03, 29.97,

29.74, 23.07, 14.26.

MALDI-TOF-MS (MW=428.14 without anion): m/z: 428.21.

Elemental analysis: Calculated. C 76.74%, H 5.07% Br 15.47%, N 2.71%; Found. C 77.24%, H 4.53% N 2.49%.

14-Dodecyl-dibenzo[*jk,mn*]naphtho[2,1,8-*fgh*]thebenidinium tetrafluoroborate (4-16b)

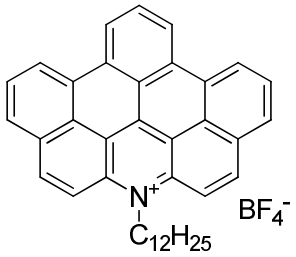

Golden red powder (Yield = 48%), ^{1}H NMR (250MHz, CD_2Cl_2, 25°C): δ(ppm) = 8.46-8.43 (d, 2H, ^{3}J(H,H)=7.5Hz, aromatic), 8.24-8.21 (d, 2H, ^{3}J(H,H)=7.5Hz, aromatic), 8.13-8.04 (m, 4H, aromatic), 7.79-7.73 (m, 6H, aromatic), 7.33-7.29 (m, 1H, ^{3}J(H,H)=5.0Hz, aromatic), 5.14-5.10 (t, 2H, ^{3}J(H,H)=5.0Hz, CH_2), 2.04-2.02 (m, 2H, CH_2), 1.76-1.71 (m, 2H, CH_2), 1.48-1.32 (m, 18H, CH_2), 0.81-0.79 (m, 3H, CH_3); ^{13}C NMR (62.5MHz, CD_2Cl_2, 25°C): d (ppm): 142.51, 139.80, 138.06, 137.22, 133.70, 131.03, 129.48, 128.45, 126.04, 122.79, 120.91, 116.50, 113.35, 110.66, 104.53, 32.28, 31.36, 30.23, 29.85, 29.64, 29.29, 22.62, 14.31.

MALDI-TOF-MS (MW=520.30 without anion): m/z: 520.11.

Elemental analysis: Calculated. C 77.10%, H 6.30% B 1.78%, F 12.51%, N 2.31%; Found. C 77.29%, H 6.11% N 2.53%.

14-(4-Hexylphenyl)-dibenzo[*jk,mn*]naphtho[2,1,8-*fgh*]thebenidinium tetrafluoroborate (4-17b)

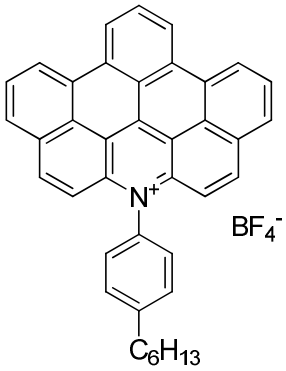

Golden red powder (Yield = 67%), ^{1}H NMR (250MHz, CD_2Cl_2, 25°C): δ(ppm) = 9.41-9.38 (d, 2H, ^{3}J(H,H)=7.5Hz, aromatic), 9.29-9.26 (d, 2H, ^{3}J(H,H)=7.5Hz, aromatic), 8.74-8.70 (d, 2H, ^{3}J(H,H)=10.0Hz, aromatic), 8.61-8.59 (d, 2H, ^{3}J(H,H)=7.5Hz, aromatic), 8.53-8.47 (t, 1H, ^{3}J(H,H)=7.5Hz, aromatic), 8.42-8.36 (t, 2H, ^{3}J(H,H)=7.5Hz, aromatic), 7.85-7.74 (m, 4H, aromatic), 7.55-7.52 (d, 2H, ^{3}J(H,H)=7.5Hz, aromatic); 2.94-2.88 (t, 2H, ^{3}J(H,H)=7.5Hz, CH_2), 1.84-1.76 (m, 2H, CH_2), 1.46-1.35 (m, 6H, CH_2), 0.94-0.89 (m, 3H, CH_3); ^{13}C NMR (62.5MHz, CD_2Cl_2, 25°C): d (ppm): 148.41, 140.40, 139.51, 133.89, 133.36, 132.09, 131.61, 130.15, 130.11, 129.86, 128.09, 127.07, 124.10, 122.53, 118.59, 117.11, 36.27, 32.13, 31.74, 29.48, 23.05, 14.29.

MALDI-TOF-MS (MW=512.24 without anion): m/z: 512.22.

Elemental analysis: Calculated. C 78.14%, H 5.04% B 1.80%, F 12.68%, N 2.34%; Found. C 77.94%, H 4.83% N 2.25%.

14-(4-Tetradecylphenyl)-dibenzo[*jk*,*mn*]naphtho[2,1,8-*fgh*]thebenidinium tetrafluoroborate (4-18b)

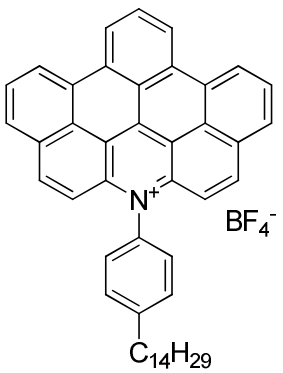

Golden red powder (Yield = 43%), ^{1}H NMR (250MHz, CD_2Cl_2, 25°C): δ(ppm) =

9.05-9.01 (d, 2H, ^{3}J(H,H)=7.5Hz, aromatic), 8.84-8.81 (d, 2H, ^{3}J(H,H)=7.5Hz, aromatic), 8.69-8.65 (d, 2H, ^{3}J(H,H)=10.0Hz, aromatic), 8.52-8.49 (d, 2H, ^{3}J(H,H)=7.5Hz, aromatic), 8.26-8.20 (t, 1H, ^{3}J(H,H)=7.5Hz, aromatic), 8.17-8.11 (t, 2H, ^{3}J(H,H)=7.5Hz, aromatic), 7.84-7.78 (m, 4H, aromatic), 7.59-7.55 (d, 2H, ^{3}J(H,H)=10.0Hz, aromatic); 2.99-2.93 (t, 2H, ^{3}J(H,H)=7.5Hz, CH_2), 1.91-1.85 (m, 2H, CH_2), 1.54-1.21 (m, 22H, CH_2), 0.85-0.83 (m, 3H, CH_3). ^{13}C NMR (62.5MHz, CD_2Cl_2, 25°C): d (ppm): 148.70, 140.69, 139.78, 134.18, 133.55, 132.33, 131.81, 130.40, 130.60, 130.08, 128.33, 127.38, 124.39, 122.81, 118.92, 117.41, 37.11, 33.15, 32.73, 30.92, 30.70, 30.65, 29.88, 22.98, 14.55,

MALDI-TOF-MS (MW=624.36 without anion): m/z: 624.42.

Elemental analysis: Calculated. C 79.32%, H 6.51% B 1.52%, F 10.68%, N 1.97%; Found. C 79.72%, H 6.22% N 1.95%.